

OPTIMAL VARIABLE SPEED LIMIT CONTROL FOR MIXED TRAFFIC FLOWS IN A
CONNECTED AND AUTONOMOUS VEHICLE ENVIRONMENT

by

Miao Yu

A dissertation submitted to the faculty of
The University of North Carolina at Charlotte
in partial fulfillment of the requirements
for the degree of Doctor of Philosophy in
Infrastructure And Environmental Systems

Charlotte

2018

Approved by:

Dr. Wei Fan

Dr. Martin Kane

Dr. Miguel Pando

Dr. David Weggel

Dr. Jay Wu

Dr. Jing Yang

ABSTRACT

MIAO YU. Optimal variable speed limit control for mixed traffic flows in a connected and autonomous vehicle environment. (Under the direction of DR. WEI FAN)

Traffic demand grows rapidly over the past decades around the world, which leads to severe traffic congestion problems. Congestion has numerous negative effects, such as wasting time of drivers and passengers, increasing delays, decreasing travel time reliability, wasting fuel, and increasing air pollution and greenhouse gas (GHG) emission. In addition, when congestion occurs, the variation in speeds and headways between vehicles might lead to longer queues, longer travel time on the highways, higher accident possibilities and more frustrated drivers. In conclusion, traffic congestion is detrimental to the operational efficiency as well as travelers' safety.

In order to relieve highway congestion, the departments of transportation (DOT) have been seeking new ways to satisfy the increasing demand and make full use of the infrastructure resources. Thus, some ad hoc traffic management strategies have been developed and deployed by the DOTs so that the existing roadway resources can be fully optimized. Among different types of traffic management strategies, active traffic management (ATM) is a scheme that can be used for relieving congestion and improving traffic flow on the highways. Among these ATM strategies, variable speed limit (VSL) control has been implemented around the world (e.g., Germany, the United Kingdom, and the United States). VSL control systems are deployed to relieve freeway congestion, improve safety, and/or reduce the emission of greenhouse gases and fuel consumption under different situations.

Moreover, with the development of emerging technologies, various novel methods on the basis of the intelligent transportation systems have been developed in

recent years. Connected autonomous vehicle (CAV) belongs to such technology. The CAVs integrate vehicle-to-vehicle (V2V), vehicle-to-infrastructure (V2I) and infrastructure-to-vehicle (I2V) communication into control systems. The existing research efforts proved that enhanced performances could be achieved using CAV technologies.

The research intends to systematically develop a VSL control framework in a CAV environment, in which the V2V, V2I, I2V, and platooning technologies are integrated with the VSL control. In addition, mixed traffic flows (including trucks and cars) are taken into account in the developed VSL control models. The policies (such as left-lane truck restriction policy) that are used to reduce the impacts of trucks on cars and CAV technologies (e.g., vehicle platooning) integrated with VSL control are explored. Multi-objective optimization models are formulated. In terms of the discrete speed limit values in the real world, discrete optimization techniques, such as genetic algorithm (GA) and tabu search (TS), are employed to solve the optimization control models. Different scenarios are designed to compare the control results. Sensitivity analyses are presented, and comprehensive characteristics underlying the VSL control are discussed in detail. Summary and conclusions are made, and further research directions are also given.

ACKNOWLEDGMENTS

I would first like to express my deepest gratitude to my advisor, Professor Wei Fan, for his guidance, patience, and support throughout my graduate studies at the University of North Carolina at Charlotte. He has truly served as a mentor to me; over the years, he has presented me with challenging problems that helped me develop my technical skills, but also consistently welcomed and encouraged me to develop my own research questions.

I also would like to thank the other members of the Ph.D. committee: Professor Martin Kane, Professor Miguel Pando, Professor David Weggel, Professor Jay Wu, and Professor Jing Yang. I would like to thank them for their interesting and useful comments on the manuscript of this dissertation. And I am also grateful to the professors here in North Carolina, who taught me a lot during my Ph.D. study.

I would like to thank Professor Honghai Zhang for his help in my life and study. I am also greatly to all my friends who have made my life in the U.S. enjoyable.

Finally, but most importantly, my gratitude goes to my family. I want to especially thank my wife Ni Fang. Without her support, encouragement, patience, and unwavering love, this dissertation would not have been possible. I am also grateful to my parents, Hanbiao Wang and Ping Wu, and my sister, Chenyan Yu, who have made all of these possible and always encourage me to pursue my goals.

DEDICATION

To my dear wife and parents and those who helped me over the years.

TABLE OF CONTENTS

LIST OF TABLES	x
LIST OF FIGURES	xi
LIST OF ABBREVIATIONS	xiv
CHAPTER 1: INTRODUCTION	1
1.1. Problem Statement	1
1.2. Objectives	5
1.3. Expected Contributions	5
1.4. Dissertation Overview	6
CHAPTER 2: LITERATURE REVIEW	11
2.1. Introduction	11
2.2. Theoretical Background of Freeway Speed Control	12
2.3. VSL Control Algorithm	20
2.4. VSL Practices and Evaluations	41
2.5. Connected Autonomous Vehicles and VSL Control	52
2.6. Calibration of Microscopic Traffic Simulation Models	59
2.7. Summary	71
CHAPTER 3: VSL CONTROL MODELS	72
3.1. Introduction	72
3.2. Traffic Flow Model	73
3.3. METANET and VSL Control	76
3.4. CTM and VSL Control	99
3.5. Connected and Autonomous Vehicles	108
3.6. VSL Control for Multiple Bottlenecks	116

3.7. Integrated Control System	119
3.8. Objective Function and Constraints	120
3.9. Summary	131
CHAPTER 4: PROPOSED SOLUTION ALGORITHMS	132
4.1. Introduction	132
4.2. Sequential Quadratic Programming (SQP)	134
4.3. Tabu Search Algorithm	136
4.4. Genetic Algorithm	142
4.5. Summary	147
CHAPTER 5: CASE STUDIES	148
5.1. Introduction	148
5.2. Hypothetical Freeway Segment	148
5.3. Real World Freeway Segment	153
5.4. Summary	155
CHAPTER 6: CALIBRATION OF MICROSCOPIC TRAFFIC SIMULATION MODELS USING METAHEURISTIC ALGORITHMS	156
6.1. Introduction	156
6.2. Calibration Methods	159
6.3. Numerical Results	165
6.4. Summary	173
CHAPTER 7: NUMERICAL RESULTS	175
7.1. Introduction	175
7.2. VSL Control at A Lane Drop Bottleneck	175
7.3. VSL Control for Mixed Traffic Flows	193
7.4. Combined VSL Control and Truck Lane Restriction	209
7.5. VSL Control in a CAV Environment	228

7.6. VSL Control and CAV Platooning	248
7.7. Summary	259
CHAPTER 8: SUMMARY AND CONCLUSIONS	260
8.1. Introduction	260
8.2. Summary and Conclusions	261
8.3. Directions for Future Research	265
REFERENCES	267

LIST OF TABLES

TABLE 2.1: Summary of Literature Review on MPC-based VSL Control	26
TABLE 2.2: Summary of Literature Review on VSL Control based on Local Feedback	30
TABLE 2.3: Summary of Literature Review on VSL Control based on Optimization Algorithm	35
TABLE 2.4: Summary of the Practice of VSL Control in the United States	50
TABLE 2.5: Summary Literature Review on VSL and CAV	58
TABLE 2.6: Summary of Literature on the Calibration of Microscopic Traffic Simulation Models	69
TABLE 6.1: Car-following Parameters in VISSIM	165
TABLE 6.2: Comparison between GA and TS Methods	173
TABLE 7.1: Summary of Simulated Scenarios ($N_c=5$)	183
TABLE 7.2: Total Value of Travel Time Only and Total Value of Speed Variation Only	191
TABLE 7.3: Summary of Simulated Results	197
TABLE 7.4: Summary of Control Results	217
TABLE 7.5: Computation Results of the CTM at Each Bottleneck	232
TABLE 7.6: The IDM's Parameter Value	233
TABLE 7.7: Simulation Scenarios and Descriptions	235
TABLE 7.8: Performance Comparison under Different Scenarios	238
TABLE 7.9: Simulation Outputs with Different Communication Range	247
TABLE 7.10: Simulation Scenarios and Descriptions	249
TABLE 7.11: Performance Comparison under Different Scenarios	251
TABLE 7.12: Simulation Outputs with Difference Updating Frequency	258

LIST OF FIGURES

FIGURE 1.1: Research Structure	10
FIGURE 2.1: Fundamental Diagram	13
FIGURE 2.2: VSL Control and Flow-Density Diagram (Zackor 1991)	14
FIGURE 2.3: Hegyi et al.'s Model for VSL Control and Flow-Density Diagram (Hegyi et al. 2004)	15
FIGURE 2.4: Expectations of the VSL Impact on Flow-Density Diagram (Papageorgiou et al. 2008)	16
FIGURE 2.5: Flow-Density Diagram under the Impact of VSL Control (Khondaker and Kattan 2015a)	17
FIGURE 3.1: An Illustration for the METANET Model	73
FIGURE 3.2: Fundamental Diagram and Cell i	75
FIGURE 3.3: Illustration of VSL at A Lane Drop Bottleneck	78
FIGURE 3.4: Illustration of the VSL Control and Truck Lane Restrictions	89
FIGURE 3.5: Illustration of VSL Control and Truck Lane Restriction on Segment i	90
FIGURE 3.6: An Illustration of A Freeway Stretch with Multiple Bottlenecks	102
FIGURE 3.7: FD and the Demand and Supply Lines	103
FIGURE 3.8: FD with Capacity Drops at the m -th Bottleneck for Two Vehicle Classes	104
FIGURE 3.9: Traffic Regimes for Two Vehicle Classes	104
FIGURE 3.10: Control Framework for CAVs to Form and Maintain Platoons	113
FIGURE 3.11: Illustration of a CAV That Joins to Form a Platoon on the Freeway	114
FIGURE 3.12: Illustration of the Headways of CAVs	115
FIGURE 3.13: An Illustration of Multiple Bottlenecks under Different Conditions	118
FIGURE 3.14: Speed and Deceleration Rate with and without VSL Control	122
FIGURE 4.1: SQP Based Solution Framework for the VSL Control	135

FIGURE 4.2: A Tabu Search Based Solution Framework for the VSL Control	141
FIGURE 4.3: Illustration of GA Procedure and the Proposed Chromosome Structure at Time Interval k	144
FIGURE 4.4: A Genetic Algorithm Based Solution Framework for the VSL Control	146
FIGURE 5.1: Hypothetical Freeway Stretch with One On-Ramp and Off-Ramp	149
FIGURE 5.2: Demand Profiles	149
FIGURE 5.3: Case Study and VSL Signs	150
FIGURE 5.4: A Hypothetical Freeway Stretch with One On-Ramp and Off-Ramp	152
FIGURE 5.5: Demand Profiles	152
FIGURE 5.6: (a) Map of the Case Study; and (b) Truck Percentage vs. Study Period	154
FIGURE 6.1: GA Calibration Process	161
FIGURE 6.2: TS Calibration Process	163
FIGURE 6.3: I-5 (a) Map of the Case Study from the PeMS, (b) VISSIM Model	167
FIGURE 6.4: Truck Percentage vs. Time throughout the Study Period	168
FIGURE 6.5: Values of Objective Function during the Optimization Period	169
FIGURE 6.6: Flow Profiles for Field Measurement and Simulation Outputs Comparison between GA and TS	171
FIGURE 7.1: Sensitivity Analyses for the Tabu Algorithm	179
FIGURE 7.2: Sensitivity Analyses for the Weight of Total Travel Time	181
FIGURE 7.3: Flow, Density, and Speed Profiles	184
FIGURE 7.4: Optimal VSL Values for VSL Control during Each Time Interval	185
FIGURE 7.5: Speed Profiles on Each Segment at $k=68\text{min}$	186
FIGURE 7.6: VSL Control Performances vs. VSV	187
FIGURE 7.7: Objective Function and the Number of VSL Control Segments	192
FIGURE 7.8: Sensitivity Analysis for the Weight of Total Speed Variation	195
FIGURE 7.9: Objective Function Values of the SQP and GA vs. Iterations	199

FIGURE 7.10: Speed Contours on Each Segment without and with VSL Control	201
FIGURE 7.11: Optimal Speed Limit Scheme for the VSL Control on Each Segment	203
FIGURE 7.12: Flow and Density without and with VSL Control	205
FIGURE 7.13: Driver Compliance Rates and Control Performances	207
FIGURE 7.14: Truck Percentage vs. Objective Function and Its Components	209
FIGURE 7.15: Comparison between the Simulation Data and Prediction Results in the TR and NTR Lanes on Segment <i>L4</i>	213
FIGURE 7.16: Scenario 3	219
FIGURE 7.17: Scenario 8	221
FIGURE 7.18: Scenario 9	222
FIGURE 7.19: VSL Profiles Optimized by the SA and GA	223
FIGURE 7.20: (a) TTT vs. Truck Percentage. (b) TSD vs. Truck Percentage. (c) TSV vs. Truck Percentage	226
FIGURE 7.21: Speed Profiles at Each Loop Detector	230
FIGURE 7.22: Information about the Freeway Stretch	230
FIGURE 7.23: Deployment of VSL Signs	230
FIGURE 7.24: Contour of Speed Limit under Scenario 4	239
FIGURE 7.25: Flow Profiles at Each Bottleneck	241
FIGURE 7.26: Simulation Performances vs. Penetration Rate	244
FIGURE 7.27: Speed Profiles without VSL Control	253
FIGURE 7.28: Speed profile under Scenario 6	253
FIGURE 7.29: Efficiency Measurements vs. Penetration Rate	255

LIST OF ABBREVIATIONS

ACC	adaptive cruise control
ATM	active traffic management
AV	autonomous vehicle
CACC	cooperate adaptive cruise control
CAV	connected autonomous vehicle
CTM	cell transmission model
CV	connected vehicle
FD	fundamental diagram
GA	genetic algorithm
GHG	greenhouse gas
I2V	infrastructure to vehicle
ML	managed lane
MPC	model predictive control
RM	ramp metering
TS	tabu search
TSD	total speed difference
TSV	total speed variation
TTT	total travel time
V2V	vehicle to vehicle
V2I	vehicle to infrastructure
VSL	variable speed limit

CHAPTER 1: INTRODUCTION

1.1. Problem Statement

Traffic demand grows rapidly over the past decades around the world, which leads to severe traffic congestion problems. The Highway Capacity Manual (HCM 2010) defines the traffic congestion as a situation in areas when the traffic demand exceeds the capacity of the highway systems, and it is faced by many travelers on a daily basis particularly during the peak hour periods. Nowadays, traffic congestion has been getting worse. For example, congestion occurs on more roads, affects more trips in the transportation system, wastes more travel time, and extends more times of a day than that in the past (FHWA 2004). Generally speaking, congestion has numerous negative effects, such as wasting the time of drivers and passengers, increasing delays, decreasing travel time reliability, wasting fuel, and increasing air pollution and greenhouse gas (GHG) emission. In addition, when congestion occurs, the variation in speeds and headways between vehicles might lead to longer queues, longer travel time on the highways, increased possibility of accidents and more frustrated drivers. In conclusion, traffic congestion is detrimental to the operational efficiency as well as travelers' safety.

Due to the limited budget, it is impossible to expand current or build new roadway networks. In order to address this issue and relieve highway congestions, the local, state, and federal departments of transportation (DOT) have been seeking new ways to satisfy the increasing demand and make full use of the infrastructure resources. Thus, some ad hoc traffic management strategies have been developed and deployed by

the DOTs so that the existing roadway resources can be fully utilized. Among many traffic management strategies, active traffic management (ATM) is a scheme that can be used for relieving congestion and improving traffic flow on the highways (Mirshahi et al. 2007). Typically, the ATM includes managed lanes (ML), variable speed limit (VSL), route guidance (RG), and ramp metering (RM), which makes use of the automatic system and human interventions to manage traffic demand, improve the efficiency of high systems, and enhance safety of highway users. ATM seeks to relieve the congestion through controlling both the mainstream and ramp demands. It has been verified that the ATM systems can be implemented to improve the level of safety and maximize freeway throughput (Mirshahi et al. 2007). Among these ATM strategies, VSL control has been widely implemented around the world (including Germany, the United Kingdom, and the United States) and has been suggested by the Federal Highway Administration (FHWA) as the next step in addressing the U.S. freeway congestion problems (Mirshahi et al. 2007). VSL control systems are deployed to relieve freeway congestions, improve safety, and/or reduce the emission of greenhouse gases and fuel consumption under different situations. For example, VSL systems implemented on freeways aim to suppress shockwaves at both non-recurrent and recurrent freeway bottlenecks and relieve adverse weather impact on freeways (Katz et al. 2017). VSL control can also be used to reduce the possibility of secondary accidents on freeways by displaying a lower speed limit when there is an incident on the freeway. VSL systems have been employed in the work zone as well so that a smoother flow of traffic between the upstream and downstream sections can be achieved (Katz et al. 2017).

VSL control strategies have been studied by a lot of researchers in which different types of objective functions were developed (e.g., minimizing total travel time, maximizing total travel distance, and minimizing GHG emissions and fuel consumption). Existing approaches used by the researchers can be classified into four categories: model predictive model (MPC), local feedback theory, shock wave theory, and optimization algorithm. Among these approaches, MPC has been the most widely used approach since it was first adopted by Hegyi et al. to address the VSL control problem in 2005. In addition, the traffic flow models that have been employed include, but are not limited to, the METANET model, cell transmission model (CTM), Lighthill-Whitham-Richard (LWR) model, and three-phase traffic theory. Even though numerous promising results have been achieved, there are still a lot of problems that need to be addressed. One of the problems is the driver compliance rate. According to the existing studies, with low driver compliance rate, the control results might not be good enough. Besides, heavy vehicles are not taken into account when developing a VSL control model in most of the existing studies. It has been verified that the driver behaviors of passenger cars can be negatively affected by the presence of different percentages of trucks traveling on the freeways (van Lint et al. 2008). As such, a VSL control framework that accounts for heavy vehicles should be developed.

Moreover, with the development of emerging technologies, various novel methods on the basis of the intelligent transportation systems have been developed in recent years. Typically, such new methods aim to increase the efficiency of the transportation system, rather than building more roads. One of the representative technologies is the driving-assistant system. Such a system can comfort drivers by

performing driving task, which is also beneficial to freeway efficiency as well as the safety. Connected autonomous vehicle (CAV) belongs to such technology. One of the applications of the CAV technologies is the cooperative adaptive cruise control (CACC) system. The CACC system is an improved technique that integrates vehicle-to-vehicle (V2V) wireless communication with the adaptive cruise control (ACC) system to obtain enhanced performances, including improved traffic flow, reduced fuel consumption, and enhanced safety. Furthermore, the CACC system can also integrate vehicle-to-infrastructure (V2I) and infrastructure-to-vehicle (I2V) communication into the control systems. The introduction of the cooperative systems will generate several benefits including increased capacity (Shladover et al. 2012). The CAV technologies are more efficient in many ways than the existing intelligent transportation systems (ITS).

The research intends to systematically develop a VSL control framework in a CAV environment, in which the V2V, V2I, and platoon technologies are integrated with the VSL control. In addition, heavy vehicles (such as trucks) are taken into account in the developed VSL control models. Some policies and technologies (such as left-lane truck restriction policy, ACC and CACC equipped vehicles, and truck platoons) that are used to reduce the impacts of trucks on passenger cars are explored. A multi-objective optimization model is built. In terms of the discrete speed limit values in the real world, discrete optimization techniques, such as genetic algorithm (GA) and tabu search (TS), are employed to solve the optimization control models. Different scenarios are designed to compare the control results. Sensitivity analyses are presented and comprehensive characteristics underlying the VSL control are discussed in details. Summary and conclusions are made and further research directions are also given.

1.2. Objectives

The goal of this research is to develop a comprehensive VSL control framework in a CAV environment which belongs to a proof-of-concept study. The proposed work in this research is intended to fulfill the following objectives:

1. To develop a VSL control framework that takes mixed traffic flows into account. Discrete optimization algorithms, such as GA, are adopted to solve the developed VSL control problems. In addition, the VSL control results under left-lane truck lane restriction policy are also assessed;
2. To systematically assess the VSL control performances in a CAV environment. VSL control strategies integrated with different types of CAV technologies (such as V2V and V2I) are developed;
3. To explore VSL control results with a different number of control segments, different truck percentages, and different penetration of CAVs. The efficiency of the control systems and the level of safety under different control scenarios are also evaluated;
4. To select a real-world freeway corridor to examine the developed control strategies so that the gaps between the theoretical research and the application of the developed VSL control can be bridged.

1.3. Expected Contributions

In order to relieve the growing freeway congestion and make full use of the freeway resources, one of the most effective ATM strategies, i.e., VSL, is studied in this study. A lot of promising results of VSL have been achieved; however, there are still a lot

of problems which need to be addressed when developing an effective VSL control system. Moreover, the development of CAV technologies provides added benefits to the control systems, which might help achieve enhanced VSL control performances. The expected contributions from this research are summarized as follows:

1. Ability to develop VSL control strategy for mixed traffic flows. Such strategies can also be integrated with different heavy-vehicle based managed lane policies;
2. Ability to systematically developed and apply discrete optimization algorithms to solve the control models and produce quality solutions for the VSL control;
3. Ability to evaluate the performances of VSL control in a CAV environment;
4. Ability to account for different levels of CAV technologies, such as V2V, V2I, and platoon cars;
5. Ability to relieve the real world freeway congestion problems by using the developed VSL control strategies.

1.4. Dissertation Overview

The dissertation will be structured as shown in Figure 1.1. In this chapter, the significance and motivation of the VSL control have been discussed, followed by the description of study objectives and expected contributions.

Chapter 2 presents a comprehensive review of the current state-of-the-art and state-of-the-practice of VSL control. Previous approaches that have been adopted to solve the VSL control problems are classified into four categories: (1) model predict control;

(2) local feedback approach; (3) optimal control approach; (4) shock wave theory. In addition, the applications of the VSL control around the world are also reviewed. Finally, in this chapter, since a real-world freeway corridor is selected, calibration methods that have been developed and used to calibrate the microscopic traffic simulation models are also reviewed and presented in this chapter.

Chapter 3 presents VSL control models formulated in this dissertation, including the traffic flow models, objective function and constraints, car-following characteristics of CAVs, and the integrated control system. The METANET and CTM are used to predict traffic states on the freeways. Since the accuracy of the traffic flow models (e.g., METANET) can be affected by the presence of heavy vehicles on the roadways, researchers typically consider mixed traffic flows by converting other classes of vehicles to the passenger car equivalents (PCE). As such, the method to compute the PCE value with VSL control is introduced in this chapter. Based on the PCE value, the effective density, flow, and speed are computed. A modified METANET and CTM are developed in which the equilibrium traffic data (such as equilibrium flow and equilibrium density) are considered. A multi-objective function which aims to minimize the total speed variation (TSV) between the control speeds and detected speeds at the most upstream and downstream detectors, total speed difference (TSD) between the control speeds and real speeds, and the total travel time (TTT) on the selected freeway stretch are established. The VSL control strategies with different CAV technologies including V2V, V2I, and platooning cars are also developed. Since a real-world freeway stretch that contains more than one bottlenecks is selected to examine the developed control strategies, the VSL

control for multiple bottlenecks is also discussed in this chapter. The control objectives and constraints are also included.

Chapter 4 discusses the proposed solution framework for the VSL control in this research. An effective method (i.e., sequential quadratic programming (SQP)) which has been used to solve the nonlinearly constrained optimization problems and two metaheuristic algorithms including the GA and TS, are proposed to find an optimal set of speed limit values during every control time period. Note that, the SQP algorithm is used as a benchmark to examine the solution quality of the GA and TS.

Chapter 5 describes case studies (including both hypothetical and real-world freeway stretches) used in this study. The detailed information about the case studies (e.g., demand at the on-ramp and mainline and truck percentage) is also presented.

Chapter 6 discusses the calibration of the microscopic traffic simulation model on the basis of the selected real-world case study. The corresponding traffic data from the Caltrans Performance Measurement System (PeMS) are collected. The data include the number of vehicles, flow and speed, positions of detectors on the freeways, average travel time, the percentage of trucks, and locations of on- and off-ramps. By using the collected data, the calibration is conducted. The objective function is defined to minimize the difference between the simulated and field traffic data (e.g., flow and speed). To obtain a good calibration result, different metaheuristic algorithms and warm start methods (using the solutions obtained from one algorithm as a starting point for another algorithm) are introduced and tested. Finally, the parameter set with the best performance (e.g., with the least objective function value) is used to examine the performance of the developed VSL control systems.

Chapter 7 describes the results of the developed VSL control models in detail. The simulation outputs with a different number of control segments are explored. The relationships between the control performances and driver compliance rates as well as truck percentages are discussed. Additionally, this chapter also presents the details of the VSL control by using the real world freeway corridor selected and calibrated parameters in Chapter 6. The control results under different scenarios with different technologies including V2V, V2I, and platooning cars are assessed. In addition, different penetration rates of CAVs and communication distances are explored in this chapter as well. The control performances including average flow, speed and density, speed variation, number of stops, average delay, queues, and emission of greenhouse gas are compared under different scenarios. Potential impacts of the introduction of new technologies on the mobility, efficiency, and environments are presented through different comparisons.

Chapter 8 concludes the dissertation with a summary of the developed control models, solution approaches, and numerical results. Suggestions for future research directions are also provided.

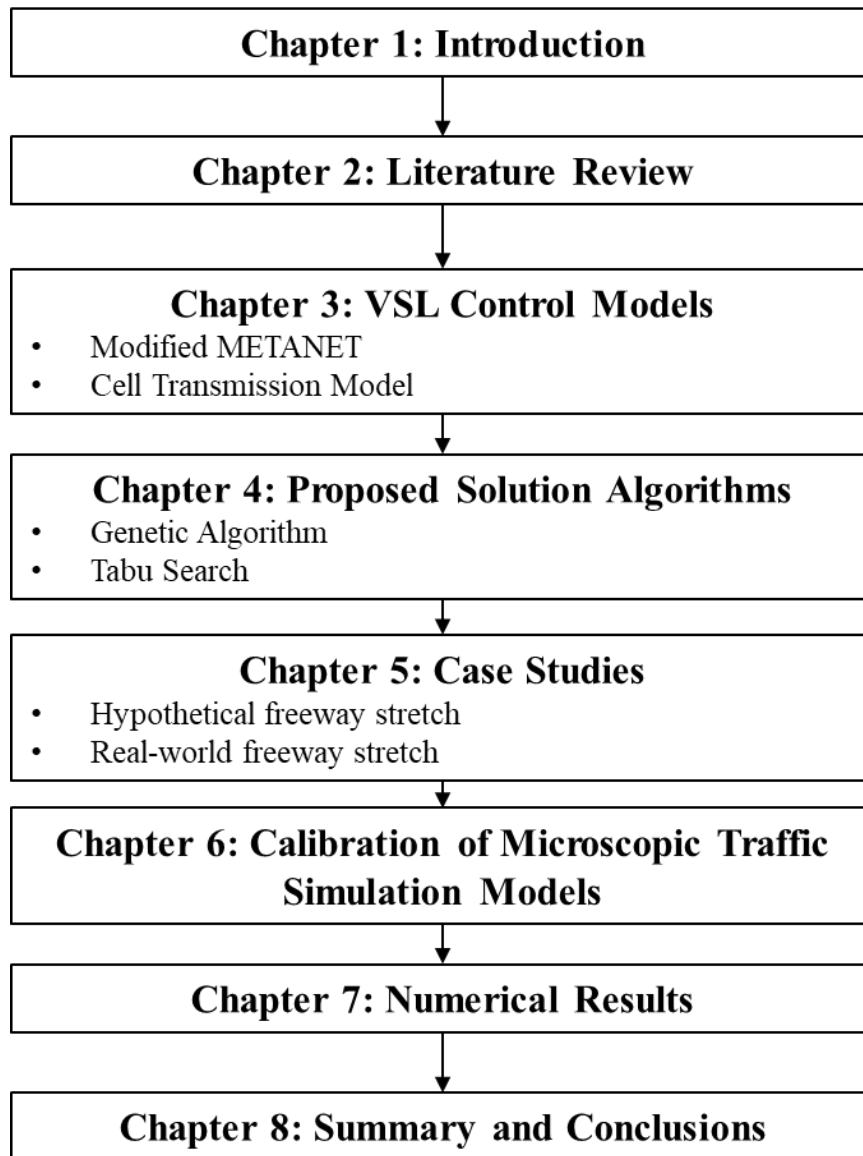


FIGURE 1.1: Research Structure

CHAPTER 2: LITERATURE REVIEW

2.1. Introduction

This chapter provides a comprehensive review of the current state-of-the-art and state-of-the-practice of VSL control. This should give a clear picture of VSL models, algorithms, and their applications around the world. Several studies deserve particular attention which will provide a solid basis for this research.

The following sections are organized as follows. Section 2.2 presents the theoretical background of freeway speed control, including the introduction of fundamental diagram (FD) and impacts of VSL control on traffic states (such as the critical density and freeway capacity). Section 2.3 reviews the VSL control approaches that have been developed by the researchers in detail. Approaches are divided into four common categories: MPC approach, feedback approach, optimal control approach, and shock wave theory. In section 2.4, the practices of the VSL control in the Europe, the United States, and other countries are reviewed. VSL systems that are integrated with connected vehicle (CV), autonomous vehicles (AV), and/or CAV are reviewed in section 2.5. Section 2.6 shows common methods that have been developed and adopted to calibrate the parameters of microscopic traffic flow models. Finally, section 2.7 concludes this chapter with a summary.

2.2. Theoretical Background of Freeway Speed Control

2.2.1. Theoretical Background

To learn the theoretical background of freeway speed control, the FD is briefly introduced first. Typically, the traffic conditions do not change substantially in time and space (i.e., in the freeway corridor) (Papageorgiou et al. 2008; Carlson et al. 2010a), and therefore, the relationship among traffic states (e.g., flow, speed, and density) can be approximately represented by the FD. In Figure 2.1, an example of a flow-density diagram (Figure 2.1(a)) and a speed-flow diagram (Figure 2.1(b)) is shown, respectively. The relationship between flow, speed, and density can be represented in the following equation:

$$q = \rho * v$$

where q is the flow, ρ is the density, and v is the speed on the freeway segment.

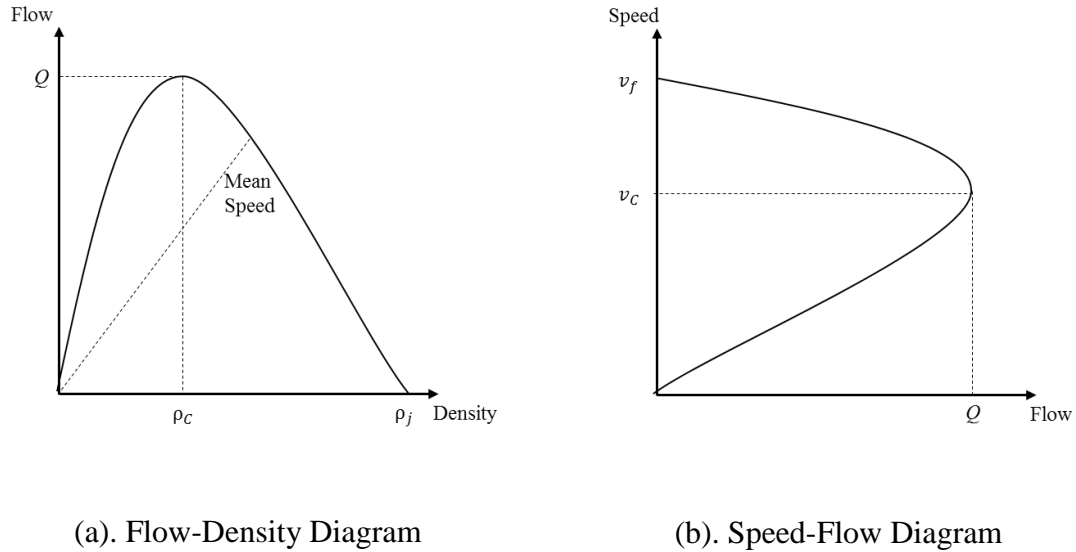


FIGURE 2.1: Fundamental Diagram

Note: Q represents the capacity (passenger cars/hour/lane, i.e., pc/h/lane); ρ_c denotes the critical density (pc/mile/lane); ρ_j is the jam density (pc/mile/lane); v_f means the free flow speed (miles/h); v_c represents the critical speed (miles/h).

In 1993, a simple linear-type flow-density diagram was created by Newell (Newell 1993), which has been applied later as the hypothesis in many studies (Chen et al. 2014; Han et al. 2017; Zhang and Ioannou 2017). The flow-density diagram was divided into uncongested and congested conditions, as shown in Figure 2.2. The calculation would be difficult if the previous parabolic graph was used. Since this linear Simplified Traffic Flow Theory can be displayed mathematically, it is convenient for calculation, and the solution can be derived easily.

2.2.2. Impacts of Speed Limit Control

In VSL systems, the posted speed limits are displayed on the variable message signs (VMS). The appropriate speeds at which drivers should be traveling under current conditions are determined on the basis of traffic conditions, volume detection, and weather information systems (Khondaker and Kattan 2015a).

According to the theoretical assumptions, a lot of research studies have explored the impact of VSL control on the flow-density diagram (Zackor 1991; Hegyi 2004). In Zackor's study (1991), the author found that the VSL control decreases the slope of the flow-density diagram at the critical density point, as shown in Figure 2.2. Zackor (1991) also suggested that there is a cross-point between the speed limit curve and no speed limit curve near the critical density. The capacity with speed limit control is higher than that with no speed limit control at the same critical density point.

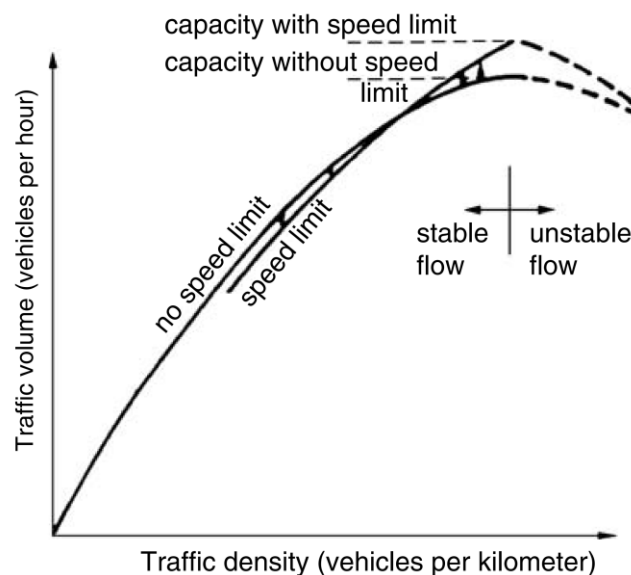


FIGURE 2.2: VSL Control and Flow-Density Diagram (Zackor 1991)

Hegyi et al. (2004) assumed that the VSL control merely replaces the left part of the flow-density curve. A straight line with slope representing the displayed speed limit is shown in Figure 2.3. The curves with the speed limit control and no speed limit meet but they do not actually cross.

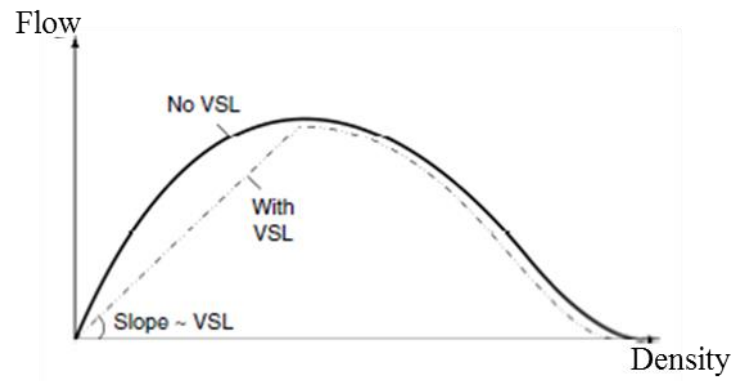
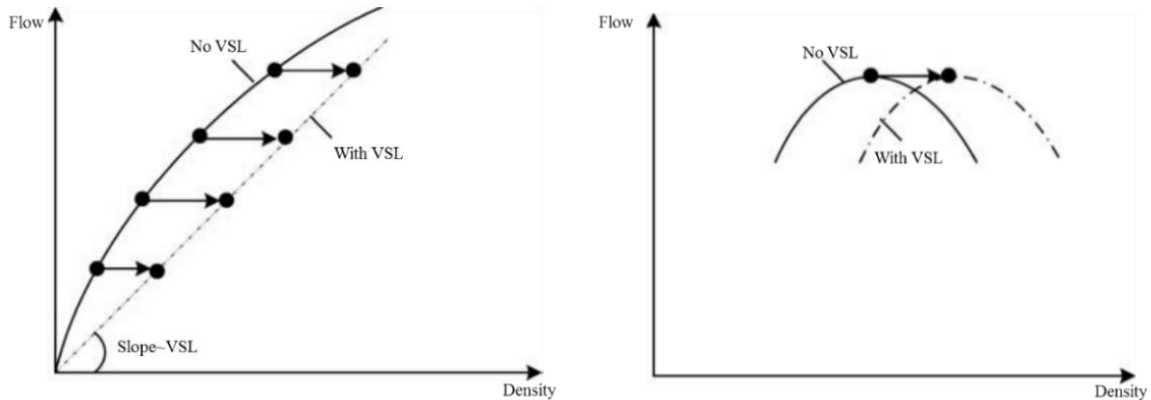


FIGURE 2.3: Hegyi et al.'s Model for VSL Control and Flow-Density Diagram (Hegyi et al. 2004)

Papageorgiou et al. (2008) and Carlson et al. (2010a) explained how VSL control would have impact on the mean speed at the under-critical density in detail in FIGURE 2.4. As can be seen in Figure 2.4(a), the mean speeds at under-critical density points would be reduced due to the application of VSL control. The values of the mean speed depend upon the displayed speed limit values as well as the compliance rate of drivers. If VSL control is used at under-critical traffic conditions, at the same flow, the density would be higher than that with no VSL control. Thus, the operating efficiency would be decreased and travel time would be increased which has also been verified by Cho and Kim (2012). In fact, for very low VSL, there may be no cross point between the curve

with VSL and the curve with no VSL. For the high speed limit value, the cross-point might exist (see Figure 2.4(b)). Papageorgiou et al. (2008) explored where the cross-points are located by using the real world traffic data, and the results showed that the cross-points are located at or beyond the critical density of 15%.



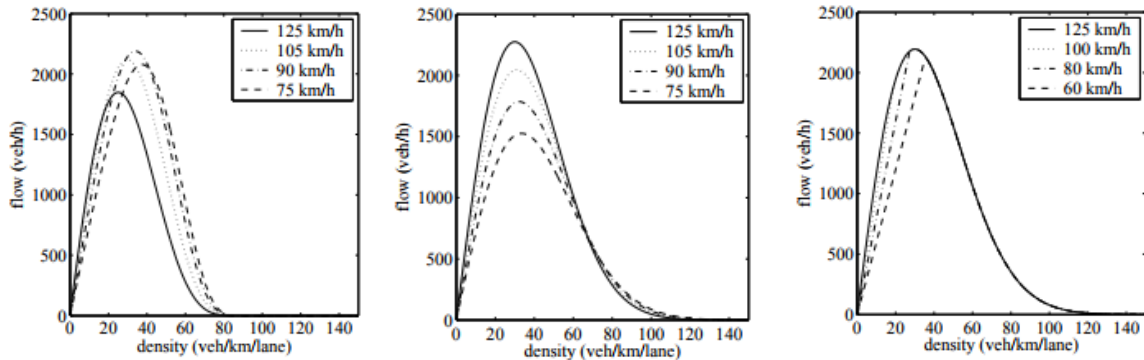
(a). VSL impact on under-critical mean speeds

(b). Cross-point of diagrams with VSL and no VSL

FIGURE 2.4: Expectations of the VSL Impact on Flow-Density Diagram (Papageorgiou et al. 2008)

Later, some researchers studied the impact of speed limit control based on the field observation data. Figure 2.5 presents the flow-density diagram obtained using the field data. Alessandri et al. (1999) found that the speed limit control results in higher freeway capacity and critical density (see Figure 2.5(a)). In the model developed by Lenz et al. (1999), as presented in Figure 2.5(b), the impact of speed limit downscaled the flow-density diagram. In Figure 2.5(c), the FD achieved by Hegyi et al. (2005) was given. The result in Figure 2.5(c) shows that the curves with speed limit and without

speed limit meet, however they do not intersect, which are different from Alessandri et al.'s (1999) and Lenz et al.'s (1999) results.



(a). Alessandri et al. (1999)

(b). Lenz et al. (1999)

(c). Hegyi et al. (2005)

FIGURE 2.5: Flow-Density Diagram under the Impact of VSL Control (Khondaker and Kattan 2015a)

Papageorgiou et al. (2008) explored the impact of VSL on aggregate traffic flow behavior. The authors analyzed the 27 days' field data observed from a European freeway. The flow-density diagram was used. The authors found that VSL control decreases the slope of the flow-density diagram at critical traffic conditions, and the critical densities were shifted to higher values. Higher flows were enabled at the same density values at overcritical traffic states. The authors suggested that the average traffic speeds are slowed down by VSL control, thereby retaining the traffic inflow entering the congestion sections and delaying the activation of downstream bottlenecks.

In a study conducted by Heydecker and Addison (2011), the field data from a VSL-managed freeway were collected and analyzed. The analysis results described that

the VSL control system induces greater freeway density and increases capacity which results in relieved congestion and decreased TTT accordingly.

In conclusion, according to previous studies, the VSL control would induce greater critical density and higher freeway capacity (Alessandri et al. 1999; Papageorgiou et al. 2008; Heydecker and Addison 2011). In addition, due to the implementation of the speed limit control, the inflow volume to the bottlenecks would be retained. Thus, the capacity drop phenomenon at the bottlenecks could be avoided or relieved. As a result, a higher bottleneck discharge volume can be maintained. In this regard, VSL control can help achieve a lot of benefits. Based on the existing studies, the benefits of VSL control are summarized as follows:

(1). Improvements in safety

The reduction in speed variation among vehicles in both the same lanes and adjacent lanes on the same segment can be achieved (Hegyi et al. 2005). The speed differences between the upstream segments and downstream segments are reduced as well (Yang et al. 2017). The reduction in speed variation and differences results in an improvement in safety (Abdel-Aty et al. 2006; Islam et al. 2013; Fang et al. 2014; Li et al. 2014; Khondaker and Kattan 2015b; Li et al. 2016). The reduction in speed differences also synchronizes the behaviors of drivers, and the lane change behavior is also discouraged. As a result, the probability of collisions is decreased due to the VSL control (Islam et al. 2013; Fang et al. 2014; Li et al. 2014).

Other researchers also examined the improvements in safety from other perspectives. For example, in a study conducted by Kononov et al. (2012), the authors explored the relationship among traffic density, speed, and safety and their implications

for setting VSL values on the freeway. The results suggested that, without VSL control, as flow–density increases, the crash rate initially remains constant until a certain critical threshold combination of speed and density is reached. Once the threshold is exceeded, the crash rate increases rapidly. Deployment of the VSL control has the potential to reduce crash rate.

(2). Prevention of traffic breakdown

When traffic is at the congestion state, any disturbance of the flow may generate shockwaves which may result in traffic breakdown. Prevention of traffic breakdown aims to avoid too high densities at the bottleneck through VSL control (Lu and Shladover 2014; Khondaker and Kattan 2015a). For example, Hegyi et al. (2005) used a VSL strategy to suppress shock waves so that higher throughput volume at the bottleneck can be achieved. Kerner (2007) developed a VSL control strategy on the basis of three-phase traffic theory and the results indicated that VSL plays an important role in controlling the state transition and preventing from breakdown phenomena.

(3) Improvement in efficiency

VSL control has been widely applied to improve the operating efficiency which is formulated to minimize the TTT spent on the freeway stretch or maximize the throughput of the bottlenecks. Meanwhile, other efficiency measurements, such as the number of stops, the length of queues, and the total delay, are also significantly reduced (Yang et al. 2017).

Such improvements in efficiency have been verified by Papageorgiou and Kotsialos (2002) who presented the existence of the direct relationship between the TTT and the inflow and outflow of a traffic network. The results indicated that if the inflow

(or demand) of a freeway network can be well limited, it is possible to decrease the TTT considerably. According to Papageorgiou and Kotsialos's (2002) conclusion, VSL control attempts to slow down the traffic and limit the demand at the bottleneck so that the maximum discharge volume at the bottleneck can be metered. In this regard, the TTT can be reduced because of the increased discharge volume with VSL control.

(4). Reduction in emission of greenhouse gas

Typically, highway congestions are associated with increased fuel consumption and emission of GHG. With the VSL control, the stop-and-go conditions and the bottleneck throughput can be significantly improved (Papageorgiou and Kotsialos 2002). Moreover, the vehicles under VSL control do not have to accelerate or decelerate frequently. All these improvements in throughput and mobility result in less emission and fuel consumption (Khondaker and Kattan 2015b; Zhang and Ioannou 2017).

2.3. VSL Control Algorithm

In the past decades, different types of VSL control approaches and algorithms were developed to improve both the safety and efficiency (Lu and Shladover 2014). Since field testing might be costly and produce unexpected and negative results if it is not implemented properly, algorithm-based evaluation with simulation is a good way to examine the effectiveness of VSL controls before actual field testing. Four widely used VSL control approaches, including the MPC, local feedback approach, optimization-based approach, and shock wave theory, are reviewed in the following sections. According to the literature review results in this section, a clear picture of the-state-of-art of VSL control will be provided.

2.3.1. Model Predictive Control (MPC)

2.3.1.1. Fang et al.'s research work

In this study, Fang et al. (2014) adopted the MPC framework for predicting and assessing traffic states on the segments with VSL control. The macroscopic traffic flow model – METANET was used. A precursor-based collision prediction model was employed to assess the level of safety. The optimized speed limits during each control time were determined so that collision probability could be minimized.

2.3.1.2. Ghods et al.'s research work

Ghods et al. (2010) applied the MPC control framework to address the congestion control problem in a freeway network equipped with VSL and RM. Game theory was adopted to optimize the solutions. The METANET traffic flow model was used as the prediction model of the traffic system. The objective function used in the study was to minimize the TTT spent by all the vehicles. The developed control strategies achieved good performance in terms of the solution quality and computational time.

2.3.1.3. Hadiuzzaman and Qiu's research work

Hadiuzzaman and Qiu (2013) applied the CTM to study VSL control on the freeways. This paper proposed a VSL control strategy which considered the FD at recurrent bottlenecks. Two modifications were made to the FD. The first one was the capacity drop at the active bottlenecks and the second one was variable free-flow speeds along the cells with VSL control. Based on the MPC approach, this proposed VSL control model was implemented along a North American urban freeway corridor. Four control scenarios were designed and compared with the uncontrolled scenario. The

simulation results indicated that the improvements in TTT, TTD and traffic flows are around 15.0%, 6.0% and 7.0%, respectively.

2.3.1.4. Hadiuzzaman et al. research work

Hadiuzzaman et al. (2012) developed an analytical model to examine the effectiveness of VSL control. The METANET was used to model the freeway segments with VSL control. The proposed VSL control strategy on the basis of the MPC was implemented on a real freeway corridor. In this study, the objective was to minimize the TTT and maximize the TTD. The results indicated that the VSL control strategy could be implemented to relieve congestion at active bottlenecks.

2.3.1.5. Han et al.'s research work

To resolve freeway jam waves, Han et al. (2017) developed a MPC approach for VSL coordination based on a discrete first-order traffic flow model. The proposed model took the traffic flow feature of jam shock waves into consideration. Minimizing TTT was used as the objective function. The second order MPC approach was used as the benchmark. The result showed that the developed MPC could resolve the freeway jam waves effectively.

2.3.1.6. Hegyi et al.'s research work

In order to suppress shock waves when freeway traffic is dense at a bottleneck, Hegyi et al. (2005) studied the flow-density characteristics under different speed limits and developed a MPC approach to optimally coordinating VSL controls based on the METANET. The objective function was to minimize the TTT while also considering the safety constraints, an example of which was that the speed differences between

consecutive time intervals should be less than 10 km/s. In a following study, Hegyi et al. (2007) applied the proposed VSL control on a 12-km freeway section. The results showed that VSL could be used to effectively suppress shock waves.

2.3.1.7. Islam et al.'s research work

Islam et al. (2013) developed a MPC-based VSL control strategy to evaluate the safety and mobility impacts of the VSL. The second-order traffic flow model – METANET was used to predict the traffic state. The authors performed a sensitivity analysis by varying the VSL updating frequency and speed differences between two successive time steps. The best scenario in term of safety and efficiency was determined. The objective function of this study was to minimize the TTT and maximize the TTD. A precursor-based collision prediction model was developed to quantify the safety. The major findings of this study were summarized as follows: (1) The proposed VSL control strategy improves the safety and mobility compared with the no-control scenario; (2) VSL updating frequency has a significant effect on safety; (3) VSL control with a 5-min speed limit frequency and a 10 km/h maximum speed difference between two successive time steps yield the best control performance.

2.3.1.8. Kattan et al.'s research work

Kattan et al. (2015) developed a candidate VSL system on the basis of space mean speeds (SMSs) collected from the probe vehicles. The MPC-based VSL model was developed to minimize the TTT, which was evaluated on an 8-km freeway stretch in Canada. The performances of the developed VSL system were compared under different scenarios.

2.3.1.9. Lu et al.'s research work

To maximize recurrent bottleneck flow, Lu et al. (2011) proposed a control strategy by combining the VSL control with RM. A first-order traffic flow model was adopted for the design of the control strategy, and RM strategy was developed using the MPC. The objective of the control system was to minimize the TTT and maximize the TTD. The simulation results showed that the developed control strategy improves the bottleneck throughput significantly.

2.3.1.10. Muralidharan and Horowitz's research work

Muralidharan and Horowitz (2015) developed a computationally efficient MPC for freeway congestion control. To simulate traffic state under RM and VSL controls, a modified Link-Node Cell Transmission Model (LN-CTM) was used, which took the capacity drop and ramp weaving effects into account. The objective function was to minimize the TTT and total congestion delay (TCD). A real freeway stretch - I-80E freeway in the Bay area between the Bay Bridge and the Carquinez Bridge was chosen to verify the developed control strategy.

2.3.1.11. Popov et al.'s research work

Adopting a distributed controller design algorithm, Popov et al. (2008) developed a speed limit control approach to resolving freeway shockwaves. Macroscopic traffic flow model - METANET was used to predict the traffic states. The TTT was employed as the objective function. In addition, to guarantee the level of safety, a penalty term was included in the objective function. The designed VSL control system successfully reduced the TTT by approximately 20% compared with no control scenario.

2.3.1.12. Zegeye et al.'s research work

Zegeye et al. (2009) presented a VSL control strategy to improve traffic flow and reduce emissions in a freeway network. The MPC was implemented using the car-following traffic flow model and an emission model which was computed on the basis of average speed. Minimizing the TTT and total emissions (TE) were set as the objective function. The simulation results demonstrated that the MPC based control strategy could obtain improvement in both the mobility and environmental benefits.

A summary is presented in Table 2.1, in which the objective function, traffic prediction model, case study, optimization methodology, control strategy, and comparison performances are summarized and discussed.

TABLE 2.1: Summary of Literature Review on MPC-based VSL Control

Year	Author	Objective Function	Traffic Flow Model	Optimization Methodology	Case Study	Truck Included?!	No. of VSLs	Control Strategy	Scenario	Comparison Performance	Other
2014	Fang et al.	Collision probability	METANET	/	12-km Whitemud Drive freeway corridor	No	2	VSL	No control, VSL control	Crash probability, TTT, TTD	/
2010	Ghods et al.	TTT	METANET	parallel optimization	Hypothetical Freeway Stretch	No	2	VSL and RM	No control, VSL and RM control	Flow, speed, and density profiles	/
2012	Hadiuzzaman and Qiu	TTT, TTD	CTM	/	11-km Whitemud Drive freeway corridor	No	2	VSL	No control, VSL control	Objective function value, TTT, TTD, and flow	/
2013	Hadiuzzaman and Qiu	TTT, TTD	METANET	/	11-km Whitemud Drive freeway corridor	No	1 or 2	VSL	No control, VSL control	Objective function value, TTT, TTD, and flow	/
2017	Han et al.	TTT	Extended CTM	/	Hypothetical Freeway Stretch	No	20	VSL	No control, VSL control	Flow, speed, and density profiles	METANET was used as the benchmark
2005	Hegyi et al.	TTT	METANET	SQP	Hypothetical Freeway Stretch (12-km)	No	12	VSL	No control, VSL control	TTT	/
2007	Hegyi et al.	TTT	METANET	SQP	Hypothetical Freeway Stretch (14-km)	No	20	VSL	No control, VSL control	Flow, speed, and density profiles	/
2013	Islam et al.	TTT, TTD	METANET	/	11-km Whitemud Drive freeway corridor	No	2	VSL	No control, VSL control	Average Crash Probability	Different VSL configuration, such as speed difference between two successive time steps and frequency of speed limit changes
2015	Kattan et al.	TTT	METANET	SQP	8-km stretch of Highway 2, in Calgary, Alberta, Canada	No	/	VSL	No control, VSL control	Delay, speed variance, average speed	Different probe vehicle penetration rates
2011	Lu et al.	TTT, TTD	Developed by the authors	/	I-80W and I-880S and I-580E for afternoon peak traffic	No	/	VSL and RM	No control, VSL only, VSL and RM control	TTT, TTD, and average speed	Driver compliance rate was taken into account
2015	Muralidharan and Horowitz	TTT and TCD	Modified CTM	/	I-80E	No	/	VSL and RM	No control, VSL and RM	Queue length	/

Note: 1. No: "Trucks" was not involved, or may be considered but was not mentioned in the research work.

2.3.2. Local Feedback Approach

VSL control that is developed based on the local feedback approach is another widely used approach. Compared to other approaches, the local feedback approach can not only be solved effectively but also help achieve an acceptable control result. Several representative studies of VSL control on the basis of local feedback are reviewed.

2.3.2.1. Carlson et al.'s research work

Carlson et al. (2011) designed a local feedback-based mainstream traffic flow control (MTFC) VSL controller, taking several practical restrictions and requirements into account, such as discrete VSL, limited VSL time variation, limited VSL space variation, and VSL control period. Such feedback-based MTFC-VSL relied on real-time measurements, which was suitable for field implementations. In this study, the developed VSL was also compared with that on the basis of the optimization algorithm. The comparison results showed that the developed approach approximates the efficiency of the optimal approach.

In 2013, Carlson et al. proposed two feedback VSL controllers (i.e., Lookup controller and proportional-integral (PI) controller) for MTFC. The proposed two controllers were evaluated and compared with the developed controller in 2011 (Carlson et al. 2011) and optimal control approach. A hypothetical freeway corridor was selected as the case study. The comparison results showed that all the feedback controllers exhibited satisfactory control performances which were as good as optimal results.

2.3.2.2. Iordanidou et al.'s research work

Iordanidou et al. (2015) proposed an extended local feedback control strategy for the MTFC through VSL for a freeway network with multiple-bottlenecks. The developed feedback controller was compared with the optimal control. The results indicated that the developed feedback control strategy was robust and could be easily implemented in the field.

2.3.2.3. Jin and Jin's research work

Jin and Jin (2015) formulated VSL control strategies to manage the traffic at a lane-drop bottleneck based on the LWR model and the link queue model. A feedback PI controller was used to form a closed-loop control system, in which the capacity drop at the bottleneck can be formulated and the upstream volume can be metered. The analytical results showed that the developed control system was effective, robust, and stable.

2.3.2.4. Lu et al.'s research work

Based on freeway speed measurement, Lu et al. (2015) developed a simple VSL-VSA (variable speed advisory) control strategy for the bottleneck flow improvement to expand the freeway discharge volume with multiple bottlenecks. A speed-based feedback control was developed instead of the density-based feedback. A real freeway segment was selected as the case study to validate the control strategy. Even with a 10% compliance rate, the control performances, such as TTT, TTD, total number of stops, average speed variation (SV), and total delays (TD), were all improved.

2.3.2.5. Müller et al.'s research work

Müller et al. (2015) adopted local feedback MTFC in a microscopic simulation with VSL control to maximize the discharge throughput at an on-ramp merge bottleneck. Different setups of MTFC-VSL, such as the length of VSL application and acceleration areas and limited variation in time and space, were explored. Simulation results showed that VSL control with shorter acceleration areas could decrease delay effectively.

2.3.2.6. Zhang and Ioannou's research work

Zhang and Ioannou (2017) combined the lane change (LC) recommendation with the VSL control system to improve travel time at the bottlenecks which were caused due to accidents. To reduce the effect of capacity drop at the bottleneck, an upstream lane change solution was developed. Using a feedback control model, the VSL controller was developed based on the CTM. A real freeway segment, i.e., I-710, was used to examine the proposed combined control strategy. The control results showed that travel time, the level of safety, and environmental impact were all improved under different control scenarios in different traffic conditions.

Based on the literature review as presented above, Table 2.2 shows a summary of the VSL studies which were developed on the basis of local feedback approach. In Table 2.2, the case study, the number of VSL signs, scenarios and comparison performances are included.

TABLE 2.2: Summary of Literature Review on VSL Control based on Local Feedback

Year	Author	Traffic Flow Model	Feedback approach	Feedback Based	Case Study	Truck Included? ¹	No. of VSLs	Control Strategy	Scenario	Comparison Performance	Other
2010	Calson et al.	METANET	Cascade feedback controller	Measured density at the bottleneck area, and outflow	Hypothetical freeway stretch	No	2	VSL	No control, Optimal VSL, feedback-based VSL	Flow, speed, and density profiles	/
2013	Calson et al.	METANET	Cascade feedback controller, lookup controller and PI controller	Measured density at the bottleneck area, and outflow	Hypothetical freeway stretch	No	2	VSL	No control, Optimal VSL, feedback-based VSL	Flow, speed, and density profiles	/
2015	Iordanidou et al.	METANET	I-controller and PI-controller	Measured density at the bottleneck area, and outflow	Hypothetical freeway stretch (19.8-km)	No	3	VSL	No control, Optimal VSL, feedback-based VSL	Flow, speed, and density profiles	Multiple bottlenecks
2016	Jin and Jin	LWR	PI feedback controller	Density measurements	Hypothetical freeway stretch	No	1	VSL	No control, VSL control	TTT, queue size, discharging flow rate	/
2015	Lu et al.	/	Measurement-based	Sensor-measured bottleneck speed	I-66 inside the Capital Beltway around Washington, D.C.	No	18	VSL-VSA	No control, VSL-VSA control	TTT, TTD, TD, SV, avg. # of stops	p.m. peak hours; Multiple Bottlenecks; I2V
2015	Müller et al.	METANET	Cascade feedback controller	Measured density at the bottleneck area, and outflow	Hypothetical freeway stretch	No	1	VSL	No control, VSL-VSA control	Flow, speed, and density profiles, TTT	Sensitivity analysis, such as the length of acceleration areas and VSL application areas
2017	Zhang and Ioannou	CTM	Feedback linearization approach	Density measurements	I-710 freeway (10-km)	85% passenger vehicles and 15% trucks	10	VSL and lane change (LC) recommendations	No control, LC only, VSL only, VSL and LC	Fuel consumption, GHG, average time, and safety	/

Note: 1. No: "Trucks" was not involved, or may be considered but was not mentioned in the research work.

2.3.3. Optimization Approach

The VSL control systems developed on the basis of the optimization approach can greatly help achieve promising control performances. Different optimization algorithms, including the SQP algorithm and metaheuristic algorithms, have been explored. This section reviews the optimization approach-based VSL systems.

2.3.3.1. Alessandri et al.'s research work

Alessandri et al. (1999) addressed a VSL control problem by adopting a macroscopic traffic flow model. To relieve the congestion around the bottlenecks, an optimal control problem was formulated. The objective function was to minimize the TTT. The control problem was solved using the Powell's method. Simulation results indicated that the proposed strategy could effectively prevent or reduce congestions.

2.3.3.2. Carlson et al.'s research work

Carlson et al. (2010a) developed a freeway network control framework that integrated VSL with RM to address the congestions at bottlenecks. A second-order traffic flow model – METANET was used to predict the traffic state. The optimal control strategies were formulated as a constrained discrete-time problem. The objective function was to minimize the TTT that was solved by using the advanced motorway optimal control (AMOC) (Kotsialos et al. 2002). By using a hypothetical freeway stretch, the control strategies were examined under different scenarios. The results demonstrated that the proposed control systems could substantially improve the operating efficiency. In the following research work, the proposed control strategies were applied to a large-scale

freeway network (Carlson et al. 2010b). The large-scale case study could be solved efficiently as well.

2.3.3.3. Goatin et al.'s research work

Goatin et al. (2016) introduced a control system integrating VSL with RM which was developed to improve the mobility based on the LWR network model. The overall goal of the optimization in this study was to minimize the TTT and maximize the outflow of the bottleneck. The control problem was solved by the SQP algorithm.

2.3.3.4. Kang et al.'s research work

Kang et al. (2004) presented an optimal VSL control system for freeway work zone operations. The objective function of the VSL control was to maximize the total throughput of the work zone. A set of speed restrictions were given as the model constraints to reflect the needs to improve the level of safety. The simulation results demonstrated that the throughput over the work zone was increased and the average delay over upstream segments of the work zone was reduced.

2.3.3.5. Li et al.'s research work

A VSL control strategy was developed by Li et al. (2014) to reduce the rear-end collision risk at the recurrent bottlenecks. A crash risk prediction model was employed to estimate the risk of rear-end collisions. The CTM was selected to predict the freeway traffic state with VSL control. The GA was adopted to optimize critical control factors, such as the speed change rate, the speed difference between adjacent segments, and the displayed speed limits. Simulation results showed that the rear-end crash potential was reduced by 69.84% under the high demand scenario.

To reduce collision risks and injury severity on large-scale freeway segments, Li et al. (2016) developed an optimal VSL control strategy. The CTM was employed to simulate the traffic state with VSL control, which took the capacity drop phenomenon and stop-and-go condition at the bottlenecks into consideration. The GA was used to optimize the speed limit values. Three scenarios with various VSL signs were developed and compared. The simulation results showed that the collision risks were decreased by 22.62% and the injury severity of crashes was reduced by 14.67%.

2.3.3.6. Soriguera et al.'s research work

Soriguera et al. (2013) developed a VSL control strategy and evaluated the impact of the developed strategy on the freeways in metropolitan areas. The objective function was to reduce the emission and fuel consumption and improve safety. The VSL control strategy was installed on the Barcelona's freeways. The simulation results suggested that an increase in freeway capacity and the easing of congestion was achieved, but the social profitability of VSL on the metropolitan freeway was limited.

2.3.3.7. Yang et al.'s research work

Yang et al. (2015) developed two VSL control strategies to improve the mobility at a recurrently congested freeway bottleneck. In this study, Kalman Filter was adopted to enhance the traffic state prediction on the freeway. The VSL control strategies were to minimize travel time and speed variation (SV), respectively. The results indicated that the travel time and SV were improved due to the VSL control. The comparison measurements, such as the average number of stops and average travel time, showed that the VSL control with the objective to minimize the SV offered more promising benefits for field implementation.

To improve the operating efficiency and level of safety at the work zone areas, Yang et al. (2017) presented a proactive VSL control system. The objective of the VSL control was to minimize the TSV between the upstream segment and the downstream segment. The METANET model was used to predict the traffic states, and the Kalman Filter was adopted to improve the prediction results. The developed VSL system could significantly reduce the speed variation among freeway segments.

In Table 2.3, a summary of the VSL control strategies which were developed by adopting optimization algorithm is presented. The objective function, optimization methodology, case study, and control scenarios are included in Table 2.3.

TABLE 2.3: Summary of Literature Review on VSL Control based on Optimization Algorithm

Year	Author	Objective Function	Traffic Flow Model	Optimization Methodology	Case Study	Truck Included?	No. of VSLs	Control Strategy	Scenario	Comparison Performance	Other
1999	Alessandri et al.	TTT	METANET	Powell's method	Hypothetical Freeway Stretch	NO	/	VSL	With VSL and without VSL	Throughput; mean time; square densities	Extended Kalman-filter
2010a	Carlson et al.	TTT	METANET	AMOC	Hypothetical Freeway Stretch	NO	3	VSL and RM	No-control, VSL, RM, and VSL and RM	Flow, speed, and density profiles	/
2010b	Carlson et al.	TTT	METANET	AMOC	Amsterdam ring-road A10	NO	42	VSL and RM	No-control, VSL, RM, and VSL and RM	Flow, speed, and density profiles	/
2016	Goatin et al.	TTT, throughput	LWR	SQP	9-km freeway stretch	NO	/	VSL and RM	No-control, VSL, and VSL and RM	Queue, average time	/
2004	Kang et al.	Maximize total throughput	/	Linear programming	Hypothetical Freeway Stretch	NO	5	VSL	With VSL and without VSL	Throughput; average delay; average speed	Work-zone
2014	Li et al.	Rear-end crash	CTM	GA	Hypothetical Freeway Stretch	NO	10	VSL	With VSL and without VSL	Reduction of collision potential	Speed change rate and speed difference between adjacent links
2013	Soriguera et al.	Delay, pollutant emissions, fuel consumption, and safety	/	/	A test freeway in Barcelona, Spain	NO	1	VSL	With VSL and without VSL	Delay costs, accident risk penalty, emission and fuel consumption cost	Whole day, stop-and-go periods, free-flow periods
2015	Yang et al.	TTT, speed variation	METANET	/	MD-100 West from MD 713 to Coca-Cola Drive	NO	1	VSL	No-control, VSL, and KF-VSL	Average # of stops; average travel time; speed SD	Kalman-filter
2017	Yang et al.	Speed variation	METANET	/	I-495, Silver Spring, Maryland	NO	4	VSL	With VSL and without VSL	Average delay, number of stops, throughput	Kalman-filter

2.3.4. Shock Wave Theory

2.3.4.1. Hegyi et al.'s research work

To eliminate shock waves on freeways, Hegyi et al. (2008) proposed an approach called SPECIALIST which was developed based on the shock wave theory. Compared with other approaches, the parameters of SPECIALIST could be interpreted easily. A freeway stretch was selected as the case study to demonstrate the algorithm.

In 2009, Hegyi et al. (2009) evaluated the effectiveness of the developed SPECIALIST approach based on the field data. The developed approach was examined by using traffic data collected from the A12 freeway stretch in the Netherlands. About 35% of the shock waves were solved.

Using the detector loops and VSL control, the SPECIALIST could resolve freeway shock waves effectively (Hegyi et al. 2008; Hegyi et al. 2009). To achieve a better control performance, Hegyi et al. (2013) extended the SPECIALIST so that it could be integrated with other technologies, such as in-car detection and actuation and video-based monitoring (VBM) technologies. The Adaptive Smoothing Method (ASM) was employed using various data obtained from detectors and the VBM. The simulation results demonstrated that the integrated SPECIALIST algorithm could considerably reduce the TTT and resolve the freeway shock waves.

2.3.4.2. Chen et al.'s research work

Based on the Kinematic Wave Theory, Chen et al. (2014) developed VSL schemes to increase bottleneck discharge rate at the freeway bottlenecks. Two scenarios

were designed, i.e., steady queue scenario and oscillatory queue scenario. The main control principle of the developed VSL schemes was to resolve the existing queue generated at the bottleneck, and then regulate the upstream inflow to the bottleneck so that the maximum bottleneck discharge volume could be metered and sustained.

2.3.4.3. Chen and Ahn's research work

Chen and Ahn (2015) developed VSL schemes to increase the bottleneck discharge volume at the non-recurrent freeway bottlenecks. The VSL schemes were developed based on the Kinematic Wave Theory. The control principle was similar to Chen et al. (2014). The authors further provided strategies for two scenarios: (1) underutilized capacity at the bottlenecks due to underestimated stable maximum flow; (2) a re-formed queue at the recurrent bottlenecks because of the overestimated maximum discharge rate. The results from the parameter analysis indicated that the proposed VSL control strategy could significantly reduce delay.

2.3.4.4. Han et al.'s research work

To improve bottleneck discharge rates and decrease TTT at the fixed freeway bottlenecks, Han et al. (2017) developed VSL control strategies that were integrated with CV technology on the basis of the Kinematic Wave Theory. Three control strategies were designed: (1) CV only; (2) CV (one lane) and VSL; (3) CV (multiple lanes) and VSL. The analysis results demonstrated that the fast queue clearance at the bottlenecks, smoother transition, and simpler control system could be achieved by the integrated VSL control compared with VSL only.

2.3.4.5. Kerner's research work

Kerner (2007) studied the VSL control on the basis of the three-phase traffic theory. In their study, the target of the VSL control was to improve the bottleneck discharge rates, and thus preventing traffic breakdown. The results showed that in some cases, VSL could significantly suppress moving jams. However, due to the probabilistic characteristics of traffic breakdown at the freeway bottleneck, in some cases, the VSL led to an inducted congested pattern at the bottlenecks. Moreover, designing the VSL control with lane-changing advice (cooperative driving in future) can also have the potential to advise the communicating vehicles upstream of the bottleneck by sending a priority message about possible speed reduction and maintaining minimum space gap, thereby avoiding traffic breakdown.

In terms of the VSL control approaches developed by the different researchers which have been reviewed in the above sections, the following conclusions are summarized:

- (1). Various theories and algorithms have been developed and used to determine the appropriate speed limit values during the control horizon. The MPC approach has been widely used by researchers since it was first developed for VSL control by Hegyi et al. (2005). MPC can predict the evolution of traffic states and calculate the optimal speed limit scheme during the control time period. The advantage of MPC is that different types of control strategies can be integrated into one control system, such as RM (Hegyi et al. 2005) and LC control (recommendation) (Roncoli et al. 2015b). Another important VSL control strategy is SPECIALIST developed by Hegyi et al. (2008) which is an analytical approach for VSL control to resolve the jam waves based

on the shock wave theory. A lot of researchers have developed different types of VSL control framework on the basis of SPECIALIST (Chen et al. 2014; Chen et al. 2015; Han et al. 2017).

(2). The optimization-based VSL control aims to maximize bottleneck throughput or minimize TTT by regulating the vehicles upstream of the bottleneck. Such method has shown promising results in simulation by researchers. Discrete optimization techniques, such as the GA, have been used in existing studies. Such optimization techniques can greatly help search the optimal solution of VSL control which is typically a multi-criterion optimization problem. A discrete speed limit set can also be optimized which can be directly displayed on the VMS.

(3). Different types of traffic flow models were adopted by researchers, such as METANET, CTM, LWR, and other models developed by the researchers (Lu et al. 2011). Among these models, the second-order traffic flow model – METANET (Messmer and Papageorgiou 1990) was used in most of the research studies because the model has been calibrated and validated within a reasonable accuracy (Hegyi et al. 2005; Carlson et al. 2010a; Hadiuzzaman and Qiu 2012; Yang et al. 2017). However, the VSL control model formulated by adopting METANET is a non-linear and non-convex problem (Han et al. 2015), which might result in high computational load especially using the standard SQP algorithm (Hegyi et al. 2005). Moreover, the solution quality might not be good enough. As such, some researchers have been trying to formulate the VSL control as a linear optimization problem (Han et al. 2015; Muralidharana and Horowitz 2015; Roncoli et al. 2015a; Roncoli et al. 2015b). And, the modified CTM model was developed by considering the capacity drop and stop-and-go traffic conditions

at the bottlenecks and ramp weaving effects (Han et al. 2015; Muralidharan and Horowitz 2015; Li et al. 2016).

(4). The fourth finding is that, in most of the existing studies, the authors assumed that the maximum discharge rate at the bottleneck is a constant value. However, the empirical studies suggested that the maximum flow for a freeway stretch section varies (Leclercq et al. 2011). The distribution of the bottleneck maximum discharge rate depends on the vehicle composition and average speed (Shiomi et al. 2011). Only a few researchers have modeled such stochastic maximum bottleneck discharge volume in their research work (Chen et al. 2014; Chen et al. 2015; Han et al. 2017).

(5). Another finding from Table 2.1 – 2.3 is that a few researchers have developed a VSL control strategy in which the mixed traffic flow was taken into consideration. In most studies, except Choi and Oh (2016) and Zhang and Ioannou (2017), the percentage of trucks is not considered or clearly discussed and given. It has been verified that the driver behavior of passenger cars can be affected by the presence of the heavy vehicles (van Lint et al. 2008) because trucks typically occupy more space than passenger cars on freeways. If trucks are not involved in the model, the control results might be significantly different with the presence and increasing percentage of trucks in the real world.

(6). The lane change behaviors should be considered in the model when developing a VSL control strategy. Knoop et al. (2010) studied the relation between the total density and the lane densities under free-flow and congested conditions. The authors discussed the change in lane distribution due to the VSL control and explicitly considered the influence of an on-ramp. At the freeway segments upstream of an on-ramp, the

density at the most right lanes is higher compared to the lane without any ramps. VSL control increased the use of the right lane, and its volume was near capacity. VSL control affected not only the speed of vehicles but also the density distribution in each lane. The merging ratio was influenced by the VSL control. The authors advised that the lane change distribution should be taken into account when implementing a VSL control.

2.4. VSL Practices and Evaluations

VSL control systems have been deployed in the United Kingdom since the 1960s to improve the level of safety (Lu and Shladover 2014). In recent years, due to their benefits, VSL controls have been promoted in European countries, such as Germany (Bertini et al. 2006; Weikl et al. 2013), Netherlands (Hoogendoorn et al. 2013), Sweden (Nissan and Koutsopoulos 2011; Nissan 2013), England (McCabe and Riley 2006), the United States, and South Korea. In this section, the practices of the VSL control systems that have been deployed around the world are reviewed and summarized.

2.4.1. The Practice of VSL Control in European Countries

2.4.1.1. England

One of the well-known applications of VSL controls was on motorway M25 and M4 in England (McCabe and Riley 2006). The objectives of the VSL were to reduce delay, improve safety, and decrease emissions. Various positive outcomes were achieved, such as a reduction in collisions, less lane changing on motorways, decreased travel time, and increased throughput rate. In addition, the overall emission was decreased between 2% and 8%.

2.4.1.2. Germany

VSL control that had been implemented in Germany was designed to improve safety and traffic flow (Bertini et al. 2006). To investigate the effectiveness of the VSL in improving safety and reducing freeway bottleneck congestion in Germany, Bertini et al. (2006) adopted an empirical approach. A feedback to the drivers with VMSs at certain locations along the 18-km freeway stretch was used. The advisory speed limit and warning information were displayed on the VMSs. The data analysis results indicated that a significant improvement in safety was achieved.

Weikl et al. (2013) systematically evaluated a VSL system along a 16.3-km section of Autobahn A9 near Munich in Germany. The authors integrated the loop detector data with freeway data, such as weather, incidents, and downstream congestion information. The practice results showed that the incident rate was decreased with the implementation of the VSL system. However, there was a variation in bottleneck capacity. In some cases, when congestion occurred with VSL control, the capacity drop was slightly larger compared with that without VSL control.

2.4.1.3. Netherlands

A trial with VSL control on freeway A20 (a 4.2-km stretch) near Rotterdam, Netherlands, began on June 2011. The aim of VSL control was to improve the operating efficiency and air quality. Hoogendoorn et al. (2013) assessed the trial by analyzing the collected before-and-after data which included driver behavior change, improvement in safety and mobility, and reduction in emission and noisy. The following improvements were achieved based on the evaluation results: (1) traffic operation on A20 has been significantly improved due to the implementation of the VSL, and the travel time spent

on the freeway stretch was reduced by 20%; (2) a 4% increase in the capacity at the bottlenecks was achieved; (3) a change in driver behavior was caused as a consequence of the VSL control; (4) air quality was slightly improved. For example, the emission of NO_x and particulate matter₁₀ were decreased by 3.7% and 3.6%, respectively; (5) the noise level was improved slightly by 0.2 dB.

2.4.1.4. Sweden

An advisory VSL system was implemented on E4 motorway in Stockholm, Sweden (Nissan and Koutsopoulos 2011; Nissan 2013). Nissan and Koutsopoulos (2011) adopted a statistical method for the evaluation of the impact of the implemented VSL on traffic operations. The before-and-after data were collected and analyzed. However, there was no significant impact on traffic conditions after implementing the advisory VSL system. Thus, Nissan and Koutsopoulos recommended that a mandatory system should be paid more attention (2011). In a following research conducted by Nissan (2013), the author compared the impacts of both the advisory and enforced VSLs by analyzing driver compliance effect on E4 motorway. A microscopic simulation was used. Simulation results indicated the effectiveness of VSL increased as the rates of driver compliance rate increased. The evaluation results also showed that the VSL control had almost no effect on the traffic operation if the driver compliance rate was less than 25%.

2.4.1.5. Spain

In 2009, in the Barcelona metropolitan area, VSL systems were introduced on several congested motorways. Bel and Rosell (2013) assessed the impact of the VSL systems on the emission of NO_x and PM₁₀ using the difference-in-difference method.

Evaluation results showed that the VSL systems reduced NO_x and PM₁₀ by 7.7–17.1% and 14.5–17.3%, respectively. Compared to reducing the maximum speed limit only, VSL control was a more effective environment-friendly strategy.

2.4.2. The Practice of VSL Control in the United States

Several States in the United States have already carried out empirical studies on the practice of VSL control systems, primarily for the improvement in safety and mobility (Lu and Shladover 2014). New Jersey and Michigan are the first two states in the United States that have implemented VSL. Recently, the use of VSL in the United States has increased dramatically (Katz et al. 2017).

2.4.2.1. State of Florida

Abdel-Aty et al. (2006) evaluated the safety improvement of VSL systems using a section of I-4 in Orlando, Florida. The real-time crash likelihood was calculated to reflect the level of safety. The results showed that there is no clear improvement under the low-speed scenarios.

An advisory VSL system was implemented on the 10-mile stretch of I-4 in Orlando by Florida DOT in 2008. The system aimed to enhance speed harmonization. Elefteriadou et al. (2012) evaluated the VSL control system in 2012. However, the evaluation results indicated that the deployed VSL system did not improve the level of safety in terms of the rear-end collisions. The main reason was that drivers did not comply with the displayed speed limits.

2.4.2.2. State of Georgia

To help relieve congestion and improve safety, a VSL system was implemented on I-285 in Georgia by the Georgia DOT (GDOT). The speed limits were reduced in 10-mph increments from 65 mph to a minimum of 35 mph based on real-time freeway situation, such as incidents, congestion, or severe weathers (GDOT 2017). The performance of the VSL system has not been evaluated yet.

2.4.2.3. State of Maryland

Because a total of 39 accidents occurred in 2008 alone, Chang et al. (2011) selected a MD-100 West segment from MD-713 to Coca-Cola Drive to implement VSL control where the speed decreased from 60 mph to 25 mph during peak hours. The VSL control algorithm included reducing approaching vehicles' speed to smooth the transition between the free-flow states and congested states while taking the responses of drivers into account. Two control modules were included: the first module was used to compute the initial speed at each VSL location to minimize the potential queue and the second module was developed to update the displayed speed limit. The testing results showed that the proposed VSL control strategies were effective in the following aspects: shorter travel time and higher average speed and throughput rate compared with no control scenario. Also, the VSL smoothed the transition between the free-flow speed and congested speed (i.e., stop-and-go).

2.4.2.4. State of Minnesota

To decrease the potential occurrence rate of rear-end collisions and resolve the shock waves, an advisory VSL system was deployed for 3 weeks in 2006 at one of the I-

494 work zones in Minneapolis–Saint Paul, Minnesota. A two-stage speed reduction scheme was developed by Kwon et al. (2006) to regulate the traffic flow. Two VMSs were used: one was in the work zone, and the other was at the upstream of the work zone. Field evaluation indicated that a 25% to 35% reduction in speed variation and a 7% increase in total throughput in the morning peak and evening peak, respectively. By comparing the upstream speeds and downstream speeds, during the morning peak, the driver compliance rate had a 20% to 60% correlation level.

In 2010, the Minnesota DOT tested VSL systems on the I-35W freeway stretch in Twin Cities. The control system was designed to resolve the shock waves caused by the recurrent and non-recurrent bottlenecks. The displayed speed limits were determined by the measured upstream speeds, measured speeds near the end of the queue, travel distance, and deceleration rate to minimize the TTT (Kwon et al. 2011). However, the performance of the developed control system has not been evaluated yet.

2.4.2.5. State of Missouri

VSL that has been deployed along Interstate 270 in Missouri State was evaluated by Kianfar et al. (2013). The operational impacts of the VSL were investigated at eight congested bottlenecks. The speed limits were determined on the basis of the traffic sensor data, ranging from 40 – 60 mph, in 5 mph increments. The before-and-after data were collected and compared. The flow-density diagrams were significantly changed at seven out of eight locations. Slight changes in critical density were observed due to the implementation of VSL. Moreover, the changes in maximum flows were inconsistent before and after traffic breakdown. At some locations, the maximum flows increased, and at some other locations, they decreased.

2.4.2.6. State of Nevada

Nevada DOT implemented VSL control along US 395 which parallels I-580 and served as an alternate route when I-580 was closed due to high winds. The regulatory VSL system was about 5 miles. The speed limits were determined on the basis of the wind speeds (Katz et al. 2017).

2.4.3. State of Oregon

The first VSL in Oregon was deployed for a single intersection along Oregon Route 213, west of downtown Portland to regulate traffic and reduce congestion (Katz et al. 2017). The VSL was a regulatory system and still active.

Because of the large crash rates on U.S. 26/Oregon 217 (more than 230 crashes/year, Katz et al. 2017), Oregon DOT chose to implement VSL control along such roadway. The VSL system was an advisory system, which automatically calculated and displayed variable speed limits based on the current traffic and existing weather conditions (Al-Kaisy et al. 2012). The functions of the system included the warning of queues ahead and estimating travel times. The speed limits were determined by in-road, radar-based, and downstream sensors at 1-minute intervals. The displayed speed limit was calculated as the lower of the two values: 85th percentile speed or the speed of downstream plus 5-10 mi/h.

2.4.3.1. State of Tennessee

Tennessee DOT installed a regulatory VSL system along a 9-mile stretch on the I-75 in Chattanooga, Tennessee. Speed limits were calculated based on visibility under fog conditions. This system reliably and instantly provided speed reduction to drivers along I-

75 using environmental sensors which could monitor current weather conditions (Katz et al. 2017).

2.4.3.2. State of Virginia

To relieve congestion and improve safety at work zones, Virginia DOT installed VSLs at a high-volume, congested urban work zone located on I-495 between the Springfield Interchange in Springfield and the Virginia-Maryland state line on the Woodrow Wilson Memorial Bridge (Fudala and Fontaine 2010). The evaluation results indicated that the VSL could create substantial improvements in traffic operations. The authors pointed out that the location of the VSL signs plays an important role in operating performance.

2.4.3.3. State of Washington

DeGaspari et al. (2013) carried out a research to evaluate the impact of the installation of the ATM on travel time reliability. The 5-min interval traffic data collected from the 19 detector locations on I-5 in Washington State were used. The planning time index (PTI) and buffer index (BI) were employed and calculated. Evaluation results demonstrated that a significant improvement in travel time reliability was achieved in most cases. In addition, the authors observed a 5-10% reduction in flow due to drivers' route choice behavior.

State of Wyoming

An advisory and regulatory VSL control system was implemented in 2009 along I-80 by the Wyoming DOT in an effort to improve safety (Sabawat and Young 2013). The displayed speed limits were calculated based on the real-time observed vehicle

speeds and weather conditions. The simulation results evaluated by Sabawat and Young (2013) demonstrated that a significant reduction in speed variation was achieved.

Table 2.4 briefly summarizes the practices of the VSL control in the United States that have been reviewed above. It can be seen from Table 2.4 that the primary functions of the VSL control in the U.S. can be summarized in the following descriptions: congestion (e.g., speed/incident management-related issues), weather (e.g., fogs, wind, and rain), and work zones.

TABLE 2.4: Summary of the Practice of VSL Control in the United States

State	Authors	Year	Objectives	Location	Length of Systems	VSL Type
Florida	Abdel-Aty et al.	2006	Improve safety	I-4	10.5	Regulatory
	Elefteriadou et al.	2012	Improve safety	I-4	10.5	Regulatory
Georgia	Georgia DOT	2017	Relieve congestion and improve safety	I-285	36	Regulatory and Advisory
Maryland	Chang et al.	2011	Reduce congestion, improve safety	MD-100	/	Advisory
Minnesota	Kwon et al.	2006	Work zone	I-494	10	Advisory
	Kianfar et al.	2011	Resolve shock waves	I-35W	18	Advisory
Missouri	Kianfar et al.	2013	Reduce congestion	Interstate 270	/	Advisory
Nevada	Katz et al.	2017	Weather condition, wind speed	US 395	5	Regulatory
	Al-Kaisy et al.	2012	Improve safety	U.S. 26/Oregon 217	7	Advisory
Oregon	Katz et al.	2017	Reduce congestion	Oregon Route 213	Single intersection	Regulatory
Tennessee	Katz et al.	2017	Weather condition, fog	I-75	9	Regulatory
Virginia	Fudala and Fontaine	2010	Work zones	I-495	10	Regulatory
Washington	DeGaspari et al.	2013	Reduce congestion; weather condition	I-5	8	Regulatory
Wyoming	Sawat and Young	2012	Improve safety	I-80	76.5-mi rural stretch	Regulatory and Advisory

2.4.4. The Practice of VSL Control in the Other Countries

2.4.4.1. Seoul, South Korea

To improve the safety and harmonize vehicle speeds on freeways under adverse weather conditions, VSL operation was used as the traffic management tool in Seoul, South Korea (Choi and Oh 2016). A VSL control strategy was developed based on the weather and traffic conditions. The k -nearest neighbors (k -NN) statistics method was adopted to predict weather and traffic conditions. The simulation results indicated that the developed VSL could reduce the total conflicts by 19.10% and 27.27% under moderate and severe foggy weather conditions, respectively.

2.4.4.2. Canada

Allaby et al. (2007) presented an evaluation of a candidate VSL system for an urban freeway in Toronto, ON, Canada. A microscopic simulation model was used to evaluate VSL control's impacts on safety and efficiency. The evaluation results indicated that improvements in safety were achieved during both heavily congested period (peak period) and moderately congested (near-peak period) period. However, the implementation of VSL control increased the travel time under heavily congested, moderately congested, and off-peak congested traffic conditions.

VSL control includes advisory VSL recommendation and mandatory VSL control. According to the above review results of the practices of the VSL control around the world, the objectives of the control are divided into two categories: (1) speed homogenization that focuses on improving the level of safety; and (2) multi-objective that aims to achieve improvement in safety, mobility, and environmental. A brief

summarization of the lessons learned from the practices of VSL control is given as follows:

(1). Based on the evaluation results of some researchers, the performance of VSL control highly depends on the driver compliance rate. As a result, maintaining a high compliance rate is critical to the success of VSL control (Elefteriadou et al. 2012; Nissan 2013; Ma et al. 2016).

(2). The simulation results indicate that VSL controls always result in significant improvements in safety (Bertini et al. 2006; McCabe and Riley 2006; Allaby et al. 2007; Chang et al. 2011; Sabawat and Young 2013; Choi and Oh 2016). However, the impacts on decreasing travel time and/or increasing traffic flow are not always achieved in some research work (Allaby et al. 2007; Weikl et al. 2013). One of the possible reasons is that the implementation of advisory VSL recommendation and mandatory VSL control could result in different driver compliance rate (Lu and Shladover 2014).

In some studies, due to a variety of factors, such as peak hour demand, driver behavior, on-ramp and off-ramp volume, and truck percentage, under particular conditions, VSL control is unable to improve the bottleneck throughput (Katz et al. 2017). In this regard, when developing a VSL control system, all the possible conditions, such as weather, driver behavior, and trucks, should be taken into account.

2.5. Connected Autonomous Vehicles and VSL Control

For improvement of safety, mobility and traffic conditions, and for reduced emission of greenhouse gas, various vehicle automation and communication systems

(VACS) or CV systems have been introduced, which can be exploited for the development of novel control strategies, such as VSL, RM, and route guidance (Fountoulakis et al. 2017). CV technologies enable infrastructure and vehicles to share information about aggregated traffic and individual vehicles in real time. In addition to CV systems, AV systems play an important role in developing highway active traffic management systems, which enable vehicles to be controlled by precise and fast-responding sensors instead of human beings.

CAV technology integrates both CV and AV. In recent years, many researchers have focused on conducting proof-of-concept studies for the VSL control in a CAV environment (Ma et al. 2016; Lu et al. 2015; Grumert et al. 2015; Wang et al. 2016; Talebpour et al. 2013; Yang and Jin 2014). In the following section, the existing CAV studies will be briefly reviewed.

2.5.1. CAV Technologies

CV, AV, and CAV technologies are being developed, tested, and deployed by a variety of companies and public agencies. The introduction of the CAV technologies may result in the improvement in safety and efficiency of the existing transportation system and reduced emissions (TRB 2015). With the development of the CAV technologies, TRB, FHWA, States in the United States (e.g., Texas), and researchers have been conducting studies on institutional and policy, highway design and operations, planning (TRB 2015), traffic operations (McGuckin et al. 2017; Kockelman et al. 2017), and infrastructure needs (Kockelman et al. 2016).

CAV technologies can be exploited for the development of novel traffic estimation and control methodologies. The availability of reliable real-time

measurements or estimates of the traffic state is a prerequisite for successful highway traffic controls. Even though the CAV technologies have not been implemented in the real world, a lot of theoretical research efforts have been carried out. For example, Bekiaris-Liberis et al. (2016) and Fountoulakis et al. (2017) developed macroscopic and microscopic model-based approaches for the estimation of the density, flow, and speed of vehicles in a CAV environment. According to the developed novel traffic state estimation methods on the highways, innovative traffic management and control strategies, such as VSL control, can be developed to mitigate traffic congestion. In the following section, VSL control strategies in a CAV environment will be reviewed, and a summary table will be presented in this section.

2.5.2. CAV and VSL control

With the development of wireless communication and AV technologies, advising or enforcing speed limits for individual vehicles is possible (Shladover et al. 2013). VSL control is one of the CAV applications that uses recommended vehicle motion behavior that is transmitted into vehicles to allow optimization of traffic operations (Ma et al. 2016). Research on CAV remains in an exploratory stage. Studies on VSL in a CV, AV, or CAV are categorized in terms of algorithm development (Ma et al. 2016): (1) sharing information with CV (Han et al. 2017; Lu et al. 2015; Khondaker and Kattan 2015b; Talebpour et al. 2013; Yang and Jin 2014); (2) controlling vehicles in CAV environments (Grumert et al. 2015; Wang et al. 2016).

2.5.2.1. Grumert et al.'s research work

To decrease the occurrences of accidents and increase operating efficiency, Grumert et al. (2015) explored the potential benefits of VSL control that was integrated with CAV (I2V communication) technologies. Traffic efficiency and environmental benefits were discussed. The results of this study demonstrated that a lower acceleration rate and thereby harmonized traffic and reduced GHG were achieved.

2.5.2.2. Khondaker and Kattan's research work

Khondaker and Kattan (2015b) developed a VSL control system for simultaneously improving the mobility, the level of safety, and environmental effects in a CV environment. A multi-objective function was formulated with the aim of minimizing the TTT, Time to Collision (TTC), and reducing environmental impact. Real-time driver compliance rate was also taken into account. The proposed VSL control strategy was solved using the genetic algorithm. Different penetration rates were examined.

2.5.2.3. Roncoli et al.'s research work

Roncoli et al. (2015b) developed an integrated MTFC by considering the VACS. The control system included VSL control, RM, and LC control/recommendation. Based on the first-order multi-lane model for the freeway, a linearly constrained optimal control problem was formulated. A hypothetical freeway stretch was used to illustrate the potential improvements in TTT, average speed, and queue lengths.

2.5.2.4. Stephens et al.'s research work

Stephens et al. (2015) conducted research on Prototype Intelligent Network Flow Optimization (INFLO), Dynamic Speed Harmonization (DSP), and Queue Warning

(QW). The CV technology was adopted when developing the control system. The study explored the CV data that were captured using both cellular communications and DSRC communications. Furthermore, the Small-Scale Demonstration confirmed that the INFLO Prototype System has the latency and processing speed to support INFLO application functionality in an operational traffic environment.

2.5.2.5. Talebpour et al.'s research work

Talebpour et al. (2013) explored the potential benefits of VSL control, such as improvements in resolving shock waves and improving safety. The proposed control strategy was further examined in light of the advancement in CV technology. Based on a cognitive risk-based microscopic simulation model, the control algorithm was developed. In addition, to detect and resolve shock waves, the developed algorithm was combined with a reactive speed limit selection algorithm. The results demonstrated that the implementation of the VSL control resulted in significant improvement in traffic flow.

2.5.2.6. Wang et al.'s research work

Wang et al. (2016) designed and tested a VSL control system that was integrated with in-vehicle controllers via V2I communication to resolve stop-and-go traffic conditions on freeways. Different percentages of AVs were distributed among human-driven vehicles. A hypothetical two-lane freeway stretch was selected as the case study. Simulation results showed that the TTT and average fuel consumption (AFC) were reduced compared with no AV scenario and no control scenario.

2.5.2.7. Yang and Jin's research work

To reduce the emission of GHG, Yang and Jin (2014) developed green driving strategies using inter-vehicle communication (IVC). An advisory speed limit system was designed to smooth the transition of speeds in stop-and-go traffic conditions. Newell's car-following model was adopted to describe the movements of vehicles, and the Comprehensive Modal Emission Model (CMEM) was used to estimate the GHG emissions and fuel consumption. In this research, different penetration rates and communication delays were examined.

Table 2.5 provides a summary of existing VSL control strategies in a CAV environment. The communication method, traffic flow model, methodology, control objective, and case study are included in Table 2.5

TABLE 2.5: Summary Literature Review on VSL and CAV

Study	CV/AV/CAV	Communication	Model	Methodology	Objective	Case	Scenarios	System Performance
Grumert et al. (2015)	CAV	I2V	SUMO, CMEM	Microscopic traffic simulation	Emission	Hypothetical Case	Different update times, penetration rates	CO ₂ , HC, NOx
Han et al. (2017)	CV	V2V	Shock wave theory	Theoretical framework	/	Hypothetical Case	Only CV; One CV lane; Multiple CV lanes	TTT
Khondaker and Kattan (2015b)	CV	V2V	IDM, VT-Micro model, Time to Collision	Optimization-based, GA	Mobility, safety, and emission	Hypothetical Case	Penetration rates	ATT, Collision probability, fuel consumption, delay, no. of stops, SD of speed
Lu et al. (2015)	CV	V2I	/	Speed-based Feedback	Mobility	Freeway stretch between I-66 and VA-267	/	TTT,TTD,TD, speed variation
Roncoli (2015b)	CAV	V2I	CTM	Quadratic programming	TTT and penalty values at the on-ramp	Hypothetical Case	RM, VSL, LC advices	Speed profiles, discharge rate, and queue length
Stephens et al. (2015)	CV	V2I; V2V	/	/	Speed harmonization, queue warning	/	/	Fuel consumption and emission
Wang et al. (2016)	CAV	V2I	SPECIALIST and car-following control algorithm	MPC	Mobility	Hypothetical Case	CFC vehicles	TTT, AFC
Yang and Jin (2014)	CV	V2V	Newell's car-following model, CMEM	Feedback	Emission	Hypothetical Case	Penetration rates; communication delays	Fuel Consumption, GHG

2.6. Calibration of Microscopic Traffic Simulation Models

In this dissertation, a real-world freeway stretch will be selected as the case study. The microscopic simulation will need to be conducted to examine the developed VSL control strategies, including VSL control strategies for mixed traffic flow, VSL with left-lane truck restriction policy, and VSL in a CAV environment. Therefore, the independent parameters, such as headway, acceleration rate, and deceleration rate that are used to describe traffic flow characteristics need to be calibrated first. Even though the microscopic simulation model, such as VISSIM, provides default values for these parameters, simulation under default values often produces unreliable results. Users often have to fine-tune the values so that traffic conditions of real-world case studies can be accurately represented. In short, parameters of microscopic simulation models need to be calibrated and validated. Model calibration plays a crucial role in minimizing the differences between the simulation results and corresponding field measurements, such as traffic volumes, speed, and travel time. In this section, a literature review on the calibration of microscopic simulation models is conducted.

2.6.1.1. Abdalhaq and Baker's research work

Because the calibration is usually formulated as an optimization process which aims to minimize the discrepancy between field and simulated measurements, Abdalhaq and Baker (2014) explored which optimization technique suited more for the calibration problem. The optimization algorithms in this research included the GA, TS, particle swarm optimization (PS), and Simultaneous Perturbation Stochastic Approximation (SPSA). In addition, classical optimization techniques (i.e., Nelder-

Mead and COBYLA) were used as the benchmark. A microscopic traffic simulation model called SUMO was used. The results indicated that the TS and PS performed well for this particular problem and were better than the GA and SPSA.

2.6.1.2. Balakrishna et al.'s research work

Balakrishna et al. (2007) developed a methodology for simultaneously calibrating microscopic simulation model parameters (car-following and lane-changing parameters) by using general traffic measurements, such as Origin-destination (O-D) flows. A large scale network, i.e., the network of Lower Westchester County, New York, was selected for the calibration of the MITSimLab microscopic traffic simulation model. The use of a multiclass O-D matrix to model parkway access restrictions for heavy vehicles was taken into account in this research. The calibration results demonstrated that the developed process was successful in matching prevailing traffic conditions.

2.6.1.3. Cheu et al.'s research work

Cheu et al. (1998) conducted an application of the GA for calibrating the parameters set of FRESIM. The field data were collected on weekdays on a 5.8-km freeway segment at the Ayer Rajar Expressway. The parameter sets during evening peak and midday off-peak periods were calibrated, respectively.

2.6.1.4. Chiappone et al.'s research work

Chiappone et al. (2016) presented a calibration framework which was developed based on the relationship between speed-density. The objective function was to minimize the differences between the real and simulated data sets in the speed-

density diagram. The calibration process was formulated as an optimization problem which was solved by using the GA. The real traffic data collected from the A22 freeway, Italy, were used. The simulation outputs using the Aimsun microscopic simulator were compared with the field measurements. The comparison results indicated that the GA was applicable in the calibration of the microscopic traffic simulation models.

2.6.1.5. Ciuffo et al.'s research work

Ciuffo et al. (2008) presented the results of the application of the OptQuest/Multistart (OQMS) algorithm to calibrate the AIMSUN microscopic model parameters. Freeway E45 Naples–Pompei–Salerno was selected as the case study. The objective function was to minimize the root-mean-square percentage error (RMSPE) between the simulated and collected traffic data, which included both traffic counts and speeds.

2.6.1.6. Hale et al.'s research work

Automated methods of calibration of microscopic traffic simulation models were developed by Hale et al. (2015). To determine which situation can be applied by directed brute force (DBF) searching and SPSA, Hale et al. (2015) assessed the qualities of the two algorithms by using synthetic and real-world case studies. SPSA was found to be the faster method, but DBF was more reliable. For calibrating complex inputs, the DBF was better than SPSA for sensitivity analysis.

2.6.1.7. Hourdakis et al.'s research work

Hourdakis et al. (2003) presented a complete and systematic calibration of the simulation parameters and validation methodology to address the issues related to the calibration of microscopic traffic simulation models. The test site was a 20-km long freeway corridor of TH-169 northbound starting from the interchange with I-494 and ending at I-94. The simulator employed in this study was AIMSUN. The sum of squared errors of the main-line speeds was used as the objective function.

2.6.1.8. Jha et al.'s research work

Through using the MITSIMLab, Jha et al. (2004) presented a framework for the calibration of microscopic traffic simulation models. The entire metropolitan area of Des Moines, Iowa, was selected as the case study, which was a large-scale roadway network. The authors estimated O-D flows of this large-scale network. The results indicated that the developed framework was applicable to large-scale microscopic traffic modeling.

2.6.1.9. Kim et al.'s research work

In some cases, only the distribution of traffic data is available. In order to calibrate microscopic traffic simulation models using such data, Kim et al. (2005) developed a method so that the simulated travel time could represent the field travel time. The Wilcoxon rank-sum test, the Moses test and the Kolmogorov–Smirnov test were adopted. The travel time on a signalized roadway in Houston, Texas was used. The validation results indicated that valid simulation results could be achieved using the developed method.

2.6.1.10. Lee and Ozbay's research work

Lee and Ozbay (2009) proposed a calibration methodology - enhanced simultaneous perturbation stochastic approximation (E-SPSA) which was developed based on the Bayesian sampling approach and the SPSA optimization method. To evaluate the performance of the proposed E-SPSA calibration approach, Mean square variation (MSV) was selected as the objective function. The microscopic simulation tool – PARAMICS was used.

2.6.1.11. Ma and Abdulhai's research work

Ma and Abdulhai (2002) adopted the GA for calibrating microscopic traffic simulation models. A new software – GENOSIM was developed on the basis of the GA. The software was implemented in the Port Area network in downtown Toronto, Canada. The microscopic traffic simulation platform - Paramics was selected in this research. The objective was to minimize the discrepancy between the simulation measurements and field traffic data. Also, four types of objective functions and different GA configurations were examined.

2.6.1.12. Ma et al.'s research work

Ma et al. (2007) compared three different heuristic methods (i.e., SPSA, GA, and Trial-and-Error (IA) Method) for the calibration of microscopic traffic models. The global and local model parameters were selected. Several real roadway networks in northern California were chosen as the case studies and coded in Paramics. The results indicated that the SPSA and IA could reach the same level of accuracy with fewer iterations and computing time than GA.

2.6.1.13. Menneni et al.'s research work

Menneni et al. (2008) developed a microsimulation calibration methodology to match the traffic data from the field and simulation in the speed–flow diagrams. The developed methodology was applied to the US-101 freeway network in San Francisco, California. The GA was employed as the optimization algorithm in this research. The developed methodology was compared with the methods developed in the previous research. The comparison results indicated that the developed methodology performed better.

2.6.1.14. Park and Qi's research work

To achieve high credibility for a traffic simulation model, Park and Qi (2005) developed a procedure for the calibration of microscopic traffic simulation models. VISSIM was used in this study. To determine the calibration performance, the simulated results were compared to multiple days' traffic data obtained at a real world crossing. The GA was adopted. The comparison results indicated that the calibrated results could represent the field conditions

2.6.1.15. Paz et al.'s research work

Paz et al. (2012) developed a calibration methodology for CORSIM models. The SPSA algorithm was used. In this study, the objective function was to minimize the sum of the root mean square (RMS) of overall links between actual speed and simulated speed. The results indicated that the developed calibration methodology is effective in calibrating the parameters of CORSIM models.

2.6.1.16. Paz et al.'s research work

Paz et al. (2015) developed a Memetic Algorithm (MA) for the calibration of the microscopic traffic flow simulation models. The developed MA included a combination of the GA and simulated annealing (SA) algorithms. Two different Corridor Simulation (CORSIM) traffic systems were calibrated. In addition, the comparison between the developed MA and SPSA algorithm was presented. The calibration results were similar between the two algorithms. However, the computing time of the MA-based calibration process was greater than that of the SPSA.

2.6.1.17. Toledo et al.'s research work

Toledo et al. (2004) presented a framework for calibrating microscopic traffic simulation models using aggregate traffic data. The interaction between inputs and parameters of the microscopic traffic simulation models was taken into account. The O-D flows were estimated in this study. The estimation of O-D flows was based on the generalized least square. The case study developed by the Highway Capacity and Quality of Service (HCQS) committee of the Transportation Research Board was selected in this study. The microscopic traffic simulation model – MITSIMLab was used to demonstrate the developed framework.

A summary table is given in Table 2.6, in which the case study, objective function and optimization algorithm(s) used in each study during the calibration process are summarized and presented. According to the summary table, parameters which have been selected to be calibrated and the optimization algorithms that have been adopted by the researchers are discussed.

1. Calibration Parameters

It can be seen in Table 2.6; there is substantial variation in the number of parameters (from 2 to 15) being calibrated among these case studies. However, most parameters seem to be only related to driver behavior. For example, Ciuffo et al (2008) only calibrated driver's reaction times and speed acceptance. In Cheu et al.'s (1998) research, the mainline free-flow speeds upstream and downstream of North Buena Vista Road off-ramp and the free-flow speeds at on-ramps and off-ramps, as well as the parameters that control the movement of vehicles (e.g., minimum car-following distance and sensitivity factor) were calibrated, and a total of 12 parameters were calibrated in Cheu et al.'s research. In Paz et al.'s (2015) study, 11 parameters for freeways and 15 parameters for surface streets were calibrated. Generally speaking, a small number of parameters enable the researchers to pay more attention to each parameter when their values are changed. However, some other parameters may have little impact on the performance individually, but could have a significant impact when combined. As such, the optimal parameter set obtained may only be a local optimal calibration solution. On the other hand, with more parameters, the calibration solution can be closer to an optimal one although the solution space can be significantly larger and the time it takes to find the optimal parameter set can also be much longer.

2. Optimization Algorithms

The studies in Table 2.6 developed various optimization methodologies for calibration. As one can see from Table 2.6, the GA and SPSA were widely used in previous calibration studies. To reduce computational time and also improve the

quality of the solution, other algorithms were also used, such as OQMA, non-linear programming techniques, PS, and IA.

GA has been used as a popular calibration method for micro-simulation models and it has been proven that near-global optima can be obtained. For example, Cheu et al. (1998) used the GA approach to calibrate FRESIM parameters, and the objective was to match FRESIM detector outputs with the Singapore case expressway data. In 2002, Ma and Abdulhai (2002) used the GA based optimization approach to calibrate the PARAMICS model. In this study, simple GA, steady-state GA, and crowding GA were implemented and compared. Park and Qi (2005) proposed a GA based procedure for the calibration of VISSIM simulation models. The calibrated parameters obtained by the procedure can be used to effectively represent the field traffic conditions. Both Menneni et al. (2008) and Chiappone et al. (2016) used GA to minimize the differences between the real data and simulated data in the speed-density graph.

SPSA has gained favor as an efficient method for optimizing computational expenditures in recent years, which does not depend on evaluating feasible solutions at each iteration when the searching direction is updated. For example, Ma et al. (2007) introduced SPSA and calibrated the PARAMICS traffic simulation model, and compared it with GA. Results showed that SPSA could obtain similar accuracy but with less computational time. Research Needs Statement for simulation model calibration was posted by the TRB in 2008, and it was clearly mentioned that SPSA algorithm could be used to solve large noisy problems in a computationally attractive fashion based on recent research (TRB 2003). In 2009, Lee and Ozbay (2009)

selected E-SPSA (i.e., Enhanced SPSA) and successfully demonstrated PARAMICS calibration with it. More recently (i.e., 2014-2015), SPSA was used to calibrate and its calibration results were compared with those using other algorithms. For example, Hale et al. (2015) compared SPSA with the DBF method. The results showed that SPSA was faster than the DBF method which was proposed in the paper, but it also appeared to be less reliable.

In recent years, the calibration results of different techniques or algorithms were also presented. For example, Ma et al. (2007) tested and compared three heuristic optimization methods: the GA, SPSA and IA methods. Abdalhaq and Baker (2014) applied GA, TS, PS and SPSA to calibrate a traffic simulation model called SUMO, while classical optimization techniques, i.e., Nelder-Mead and COBYLA were also used as a baseline comparison. Due to the inherent complexity involved in calibrating microscopic traffic simulation models, the metaheuristic approaches were proposed which can pursue good local (and potentially even global) optimal solution(s).

TABLE 2.6: Summary of Literature on the Calibration of Microscopic Traffic Simulation Models

Authors	Algorithm	Metric	Fitness Function	Performance Measurements ¹	No. of Calibration Parameters ²	Case Study	Software
Abdalhapp and Baker (2014)	GA, TS, PS, and SPSA	Travel Time	$\sum_{i=1}^n \frac{ sim_i - observed_i }{observed_i}$	Average Fitness	4 (deceleration, acceleration, and driver imperfection etc.)	A signalized segment in a vital city center	SUMO
Balakrishna et al. (2007)	SPSA	O-D flows	Minimize the difference between observed and fitted measurements	RMSPE, GEH, RMSN	2 (Car-following and lane-changing coefficients)	Freeway network, Lower Westchester County, New York	MITSimLab
Cheu et al. (1998)	GA	Average speed, Average volume	$\frac{\sum_{t=1}^T x^{field}(t) - x^{FRESIM}(t) }{T}$	Fitness Value and Average Absolute Errors	12 (free-flow speeds, Minimum car-following distances, lag to acc. etc.)	Ayer Rajar Expressway, in Singapore,	FRESIM
Chiappone et al. (2016)	GA	Speed, Density	$\frac{1}{N} \sum_{k=1}^N \left[\frac{1}{2} (D_k - D_k(\beta))^2 + \frac{1}{2} (S_k - S_k(\beta))^2 \right]$	Speed-Density graph	3 (reaction time, min. distance between vehicle, and max. desired speed)	A22, freeway, Italy	AIMSUN
Ciuffo et al. (2008)	OQMS	Traffic Counts, Speeds	$RMSPE(q, v) = \sqrt{\frac{1}{42 * 2 * 2} \sum_{i=1}^{42} \sum_{j=1}^{2} \sum_{d=1}^{2} \left(\frac{q_{fd}^{obs} - q_{fd}^{sim}}{q_{fd}^{obs}} \right)^2 + \frac{1}{42 * 2 * 2} \sum_{i=1}^{42} \sum_{j=1}^{2} \sum_{d=1}^{2} \left(\frac{v_{fd}^{obs} - v_{fd}^{sim}}{v_{fd}^{obs}} \right)^2}$	RMSPE, RMSE, GEH	2 (driver's reaction time and speed acceptance)	E45 Naples-Pompei-Salerno freeway	AIMSUN 5.1.8
Hale et al. (2015)	SPSA and DBF	Speed and Density	Minimize the Difference between Simulated and Field-measured outputs	Objective Function Value	5 (entry headway, and off-ramp reaction distance etc.)	I-95 near Jacksonville, FL	FRESIM
Hourdakakis et al. (2003)	Non-linear programming techniques	Speed	$\sum_{j=1}^m \sum_{i=1}^n (v_{st}^j - v_{dt}^j)^2$	RMSE, Theil's Inequality Coefficient	12 (max. acc. rate, max. speed diff, and avg. speed etc.)	TH-160 from the interchange with I-494 and ending with I-94	AIMSUN
Jha et al. (2004)	Trial and error approach	O-D flows and traffic counts	Minimize the deviations between estimated and observed traffic counts and between the estimated O-D flows and field O-D flows	Traffic counts, travel times	2 (Route choice parameters and driving behavior)	Des Moines area network	MITSimLab

Kim et al. (2005)	GA	Travel Time	$\frac{\sum_{i=1}^n S_i - O_i }{O_i} \cdot n$	Moses', Wilcoxon, KS Test, and MAER	6 (average standstill distance, and lane change distance etc.)	Arterial section of Bellaire Boulevard, Houston, Texas	VISSIM
Lee and Ozbay (2009)	Enhanced SPSA	Flow, Speed	$\sum_{\text{lane time}} \sum_{i=1}^n \left[\frac{ Q_{\text{real}} - Q_{\text{sim}} }{Q_{\text{real}}} + \frac{ S_{\text{real}} - S_{\text{sim}} }{S_{\text{real}}} \right]$	K-S test	2 (mean headway and mean reaction time)	I-880 in Hayward, California	PARAMICS
Ma and Abduhai (2002)	GA	Flow	$\frac{\sum_{i=1}^n Q_{\text{real}} - Q_{\text{sim}} }{\sum_{i=1}^n Q_{\text{real}}}$	GRE	2 (mean headway and mean reaction time)	Port area network, Toronto, Canada	PARAMICS
Ma et al. (2007)	SPSA, GA, and IA	Capacity, Critical Occupancy	$\sum_{i=1}^M [GHE(cap_i) + A \times GHE(occ_i)]$	GEH	10 (MTH, MRT, and AGGR etc.) ³	SR-99, Sacramento, California	PARAMICS
Menneni et al. (2008)	GA	Maximum 5-min flows	Sum of all the speed-flow area in the field data that is not covered by simulated data	Flow-Speed graph	5 (CC1, CC2, CC3, CC4, and CC5)	US-101, San Mateo, California	VISSIM
Park and Qi (2005)	GA	Average Travel Time	$\frac{ TT_{\text{field}} - TT_{\text{sim}} }{TT_{\text{field}}}$	ANOVA test, Scatter plots	6 (look ahead distance, average standstill distance, and gap time etc.)	An intersection at the junction of Route 15 and Route 250, Virginia	VISSIM
Paz et al. (2012)	SPSA	Speed	$\sum_{i=1}^T \sqrt{\sum_{j=1}^T (V_i - V_{\text{simulated-}i})^2}$	GEH	5 (driver behavior, vehicle performance etc.)	A network with 38 links, and a network with 20 links	CORSIM
Paz et al. (2015)	Memetic Algorithm, and SPSA	Vehicle Counts and Speeds	$\frac{1}{\sqrt{N}} \sum_{m=1}^T \left[W^* \sqrt{\sum_{i=1}^N \left(\frac{V_{i,t} - V(\theta)_{i,t}}{V_{i,t}} \right)^2} + (1-W)^* \sqrt{\sum_{i=1}^N \left(\frac{S_{i,t} - S(\theta)_{i,t}}{S_{i,t}} \right)^2} \right]$	GEH	11 for freeway and 15 for surface streets (pedestrian delays, and max. deceleration etc.)	A portion of the Pyramid Highway in Reno, NV and a hypothetical network provided by McTrans	CORSIM
Toledo et al. (2004)	Systemic search approach	O-D flows, travel times	Minimize the difference between observed and simulated O-D flows and travel times	Speeds on freeway sections and arterial sections	2 (Driving behavior, and Route choice parameters)	Three major freeways: I-5, I-405, and Route 133.	MITSimLab

Note: 1. RMSPE: root mean square percent error RMSE: root-mean-square error GEH: Geoffrey E. Havers statistics MAER: mean

absolute error ratio GRE: global relative error RMSN: Normalized root-mean-square error

2. MTH: mean target headway MRT: mean reaction time AGGR: driver aggressiveness.

2.7. Summary

A comprehensive review and synthesis of the current and historical research efforts that are related to VSL control approaches, the practice of VSL control, VSL control in CAV environments, and the calibration of microscopic traffic simulation models, have been discussed and presented in the preceding sections. This is intended to provide a solid reference for and assistance in formulating VSL control strategies and developing effective control strategies for future tasks.

CHAPTER 3: VSL CONTROL MODELS

3.1. Introduction

In order to overcome the shortcomings of previous studies as mentioned in Chapter 2, VSL control models are developed in this chapter based on the METANET model and CTM. Mixed traffic flows are taken into account in the developed models. In addition, another active traffic management strategy, i.e., left-lane truck restriction, is also integrated with the VSL control, and the corresponding model is developed. To formulate a first-order control model which can be solved efficiently, the VSL control based on the CTM is developed and presented. VSL control for mixed traffic flows in a CAV environment is also formulated in this chapter. The objective function (e.g., minimizing the sum of the TTT, TSV, and TSD) and constraints of these VSL controls are described.

In short, this chapter develops several VSL control strategies, including VSL control for mixed traffic flow (both trucks and cars), integrated VSL control and truck restriction policy, and VSL control in a CAV environment. The remainder of this chapter is organized as follows. Section 3.2 briefly describes two traffic flow models (i.e., METANET and CTM). Section 3.3 presents the VSL control models that are developed based on the METANET models. Section 3.4 formulates the VSL control model on the basis of the CTM. Section 3.5 shows the car-following behaviors of CAV. Section 3.6 discusses the methods which can be used to determine the critical volume for multiple bottlenecks. Section 3.7 presents the integrated VSL control system in a CAV

environment. Section 3.8 describes the objective function and constraints of the VSL control models, and a summary in section 3.9 concludes this chapter.

3.2. Traffic Flow Model

In this section, two traffic flow models are used, i.e., the METANET which is a second-order traffic flow model and cell transmission model which is a first-order traffic flow mode. Both models have been used to develop VSL control strategies. The two models are briefly introduced in this section.

3.2.1. METANET Model

In the basic METANET model, for the convenience of description, the selected freeway stretch is divided into N segments, and let the length of segment i be l_i , as shown in Figure 3.1. The discrete time step used in the METANET model is T .

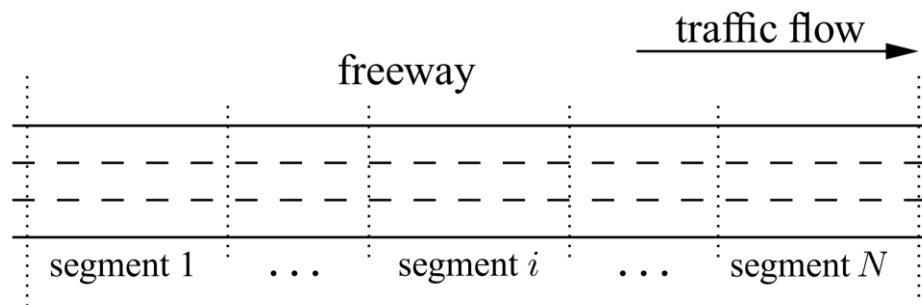


FIGURE 3.1: An Illustration for the METANET Model

Density on segment i during the time interval $k+1$ can be calculated by the following equation:

$$\rho_i(k+1) = \rho_i(k) + \frac{T}{l_i} [q_{i-1}(k) - q_i(k) + r_i(k) - s_i(k)] \quad (1)$$

The average space-mean speed on segment i during time interval $k+1$ can be computed by Eq. (2), which is proposed by Papageorgiou et al. (1989).

$$v_i(k+1) = v_i(k) + \frac{T}{\tau} \{V[\rho_i(k)] - v_i(k)\} + \frac{T}{l_i} [v_{i-1}(k) - v_i(k)] v_i(k) - \frac{\nu T}{\tau l_i} \frac{\rho_{i+1}(k) - \rho_i(k)}{\rho_i(k) + \kappa} \quad (2)$$

where τ , ν , and κ are global parameters that can be calibrated to any case study.

In Eq. (2), $V[\rho_i(k)]$ is the static speed-density relationship corresponding to the fundamental diagram (Carlson et al. 2010). In addition, $V[\rho_i(k)]$ can be calculated by the using following equation:

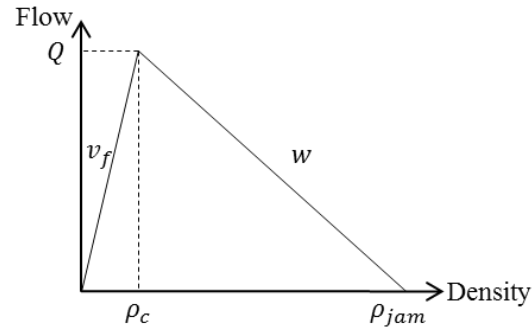
$$V[\rho_i(k)] = v_f \exp \left[-\frac{1}{a} \left(\frac{\rho_i(k)}{\lambda_i \rho_c} \right)^a \right] \quad (3)$$

The relations between flow, density and speed can be expressed as follows:

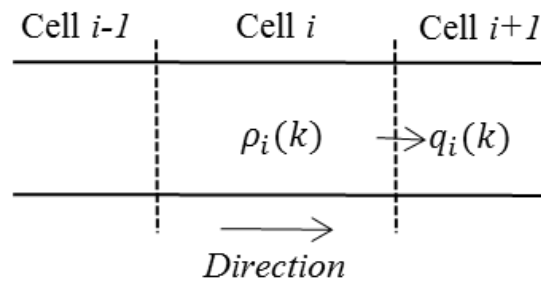
$$q_i(k) = \rho_i(k) v_i(k) \quad (4)$$

3.2.2. Cell Transmission Model (CTM)

The FD is simplified as having a triangular relationship between flow and density, as shown in Figure 3.2. In Figure 3.2(a), v_f is the free flow speed, Q is the freeway capacity, ρ_{jam} denotes the jam density, ρ_c means the critical density, and w represents the shock wave speed.



(a) Fundamental Diagram

(b) Cell i on A Freeway StretchFIGURE 3.2: Fundamental Diagram and Cell i

The demand and supply functions for cell i during time interval k are defined as follows:

Demand function:

$$D(\rho_i(k)) = \min\{Q, v_f \rho_i(k)\} \quad (5)$$

Supply function:

$$S(\rho_i(k)) = \min\{Q, w\{\rho_{jam} - \rho_i(k)\}\} \quad (6)$$

Once the demand and supply functions are determined, the traffic volume which flows out of cell i (see Figure 3.2(b)) is written as (Daganzo 1994):

$$\begin{aligned}
q_i(k) &= \min \{D(\rho_i(k)), S(\rho_{i+1}(k))\} \\
&= \min \left(v_f \rho_i(k), Q, w \{ \rho_{\text{jam}} - \rho_{i+1}(k) \} \right)
\end{aligned} \tag{7}$$

3.3. METANET and VSL Control

3.3.1. VSL Control at a Lane Drop Bottleneck

To formulate the VSL control model in this section, the following notation are introduced.

$i \in \mathbf{N}$ i -th segment on the studied freeway

$k \in \mathbf{K}$ k -th time interval

$q_D(k)$ mainstream demand during time interval k , (pc/h);

θ magnitude of the capacity drop, (%);

Q capacity upstream of the bottleneck, (pc/h/lane);

Q_b maximum discharge flow upstream of the bottleneck, $Q_b = Q(1 - \theta)$,
(pc/h/lane);

ρ_c critical density upstream of the bottleneck, (pc/mile/lane);

C maximum discharge volume at the bottleneck, (pc/h);

λ_i the number of lanes on segment i ;

v_f free flow speed, (miles/h);

N_c the user-specified number of control segments upstream of the bottleneck;

N the total number of studied segments, $N = |\mathbf{N}|$, $N \geq N_c$;

K the total number of time intervals, $K = |\mathbf{K}|$;

- T the discrete time step used in the METANET model;
- T_p prediction time interval;
- T_c VSL control horizon (i.e., the frequency that the variable speed limit is updated);
- l_i the length of segment i , (miles);
- $r_i(k)$ on-ramp volume on segment i during time interval k , (pc/h);
- $s_i(k)$ off-ramp volume on segment i during time interval k , (pc/h);
- w_1, w_2 weights reflecting the relative importance of two components including total travel time and total speed variation respectively, and $w_1 + w_2 = 1$;
- VTT value of travel time, (\$/hour);
- VSV value of speed variation, (\$*hour/miles)).
- $u_i(k)$ speed limit (to be initialized first and then optimized) on segment i during time interval k (miles/h). If no VSL control is deployed on segment i ,
- $$u_i(k) = v_f.$$
- $q_i(k)$ traffic volume entering control segment $i+1$ from segment i during time interval k (veh/h);
- $\rho_i(k)$ mean density on segment i during time interval k (pc/mile);
- $v_i(k)$ mean speed on segment i during time interval k (miles/h).

A regular lane-drop bottleneck might be caused due to incidents, work zone activities, physical lane drop, and/or lane closure, etc. Under such scenario, the total discharging flow rate of the studied freeway stretch will be reduced which can

If VSL control $u_i(k)$ is implemented on segment i during time interval k , according to Carlson et al. (2010a), $V[\rho_i(k)]$ will be modified as follows:

With VSL control:

$$V[\rho_i(k)] = u_i(k) \exp \left[-\frac{1}{a} \left(\frac{\rho_i(k)}{\lambda_i \rho_c} \right)^a \right] \quad (8)$$

In this study, according to Carlson et al. (2010a) and Hadiuzzaman et al.'s (2013) result, $a=2$ will be used.

3.3.2. VSL Control for Mixed Traffic Flows

In a review of the VSL control in the literature, although promising results have been obtained, one critical issue that is related to the VSL operation remain to be addressed, i.e., the mixed traffic flow should be considered. In the real world, various types of vehicles are traveling on the roadway, including cars, vans, and trucks. To represent the behaviors of different types of vehicles, researchers have developed the traffic models (including both the first-order and second-order models) for multi-class vehicles, and some of the developed traffic models were used to design traffic control systems, such as VSL, RM, and RG, to regulate mixed traffic flows. Wong and Wong (2002) modified the LWR model to the multi-class version with different speed distribution. Bagnerini and Rasclé (2003) developed a multiclass traffic flow model which took into account the behaviors of different vehicle types. The first-order FASTLANE model developed by van Lint et al. (2008) was used to model different vehicle classes on the motorways, in which the dynamic passenger car equivalents (pce) are described. Based on the FASTLANE model, Schreiter et al. (2011) proposed a RM

strategy. The results indicated that the multi-class controller achieved better control performances. In terms of extending the second-order macroscopic models, such as METANET, to the multi-class context, several related research has been performed as well. Deo et al. (2009) extended the METANET model for two vehicle classes including cars and trucks. Through taking the interaction between cars and trucks into account, a two-class extension of the METANET was developed by Pasquale et al. (2014). In Liu et al.'s (2014; 2016; 2017) research, a multi-class second-order traffic model was developed in which each vehicle class was subject to its own single-class fundamental diagram. Both the MPC (Liu et al. 2017) and receding horizon parameterized control (RHPC) (Liu et al. 2016) were adopted based on the developed multi-class model. Pasquale et al. (2015; 2017) designed different control schemes (including RM and RG) based on the developed two-class macroscopic models to relieve congestion and reduce emission on the freeways.

To formulate the VSL control model for mixed traffic flows in this section, besides the notations in section 3.3.1, the following notation is introduced.

$j \in J$ j -th vehicle type

ϕ_j the percentage of vehicle type j on the studied freeway segment, (%);

$r_{i,j}(k)$ on-ramp volume of vehicle type j on segment i during time interval k ,
(veh/h);

$s_{i,j}(k)$ off-ramp volume of vehicle type j on segment i during time interval k ,
(veh/h);

$\eta_{i,j}(k)$ dynamic pce value of vehicle type j on segment i during time interval k ;

sd_j gross stopping distance of vehicle type j , (ft);

t_j minimum headway of vehicle type j , (s);

$v_{i,j}(k)$ average speed of vehicle type j on segment i during time interval k ,
(miles/h);

$\rho_{i,j}(k)$ density on segment i of vehicle type j during time interval k , (veh/mile);

$q_{i,j}(k)$ traffic volume of vehicle type j entering segment $i+1$ from segment i
during time interval k , (veh/h);

$E\rho_i(k)$ effective density on segment i during time interval k , (pce/mile);

$Eq_i(k)$ effective flows entering segment $i+1$ from segment i during time interval
 k , (pce/h);

$Ev_i(k)$ effective speed on segment i during time interval k , (miles/h);

$C_{\text{dis}}(k)$ maximum discharge volume at the bottleneck for mixed traffic flow
during time interval k , (pce/h).

3.3.2.1. Dynamic Passenger Car Equivalents (PCE)

In the real world, there are different classes of vehicles on the freeways, e.g., cars and trucks. Such differences in classes of vehicles are called traffic heterogeneity. The accuracy of the freeway traffic operations models can be more or less affected by the traffic heterogeneity. For example, more trucks on the freeways are more likely to induce congestion at a lower traffic demand compare with low truck percentages (van Lint et al. 2008). Generally, the researchers studied the traffic flow models by converting the other classes of vehicles to the PCE. The HCM defined the PCE as “the number of passenger

cars that are displaced by a single heavy vehicle of a particular type under prevailing roadway, traffic and control conditions” (HCM 2000). The PCE value has been studied based on different traffic conditions by the researchers (Chanut and Buisson 2003; van Lint et al. 2008). In free-flow speed conditions, the distance gap between vehicles is much larger than the length of a vehicle. The effect of heavy vehicles can be negligible. Whereas, in congested condition (i.e., the density is greater than the critical density), the effect of heavy vehicles cannot be ignored. In addition, with different speeds, the distance gaps between different vehicles are also different. For example, with higher speed, vehicles need to maintain a larger distance gap to guarantee their safety. With VSL control, since the speed limits change at different time intervals, the PCE value might also change. To accurately model the effective traffic state (e.g., effective flow, density, and speed) with VSL control, a dynamic pce value which involves the physical characteristics of vehicles and the prevailing speeds traveling on the freeways is used. The dynamic PCE value is defined by van Lint et al. (2008). The equation which can be used to calculate dynamic PCE value of vehicle type j during time interval k on segment i is shown as follows:

$$\eta_{i,j}(k) = \eta(sd_j, t_j, v_{i,j}(k)) = \frac{sd_j + t_j v_{i,j}(k)}{sd_{\text{car}} + t_{\text{car}} v_{i,\text{car}}(k)} \quad (9)$$

Eq. (9) is obtained as the gross distance gaps of vehicle type j divided by the gross distance gaps of passenger car, which ensures that the pce value is dynamic and depends upon the characteristics of the vehicles as well as the prevailing speeds. The gross distance gaps of vehicle type j equals the gross stopping distance of vehicle type j sd_j plus the minimum headway of vehicle type j times the prevailing speeds of vehicle type j .

For example, the speed of passenger car on segment i during time interval k is $v_{i,\text{car}}(k)$.

Based on the definition, the gross distance gap of passenger cars on segment i during time interval k can be computed by $sd_{\text{car}} + t_{\text{car}}v_{i,\text{car}}(k)$, as shown in Eq. (9).

Based on Eq. (9), the effective density $E\rho_i(k)$ on segment i during time interval k can be described as follows:

$$E\rho_i(k) = \sum_{j=1}^J \eta_{i,j}(k) \rho_{i,j}(k) \quad (10)$$

3.3.2.2. Bottleneck Discharge Volume

As shown in Figure 3-3, a hypothetical three-lane freeway stretch with a lane-drop bottleneck is used in this study. If only cars are traveling on the freeway stretch, since there are two lanes available for use, the ideal maximum discharge volume at the bottleneck is $C_{\text{ideal}}=2Q$, where Q (pce/h/lane) is the capacity of the freeway segment upstream of the bottleneck. However, due to the capacity drop phenomenon at the bottlenecks which has been verified by many researchers (Hadiuzzaman et al. 2012; Li et al. 2016; Zhang and Ioannou 2017), the capacity upstream of the bottleneck will be decreased to Q_b (pce/h/lane), which can be calculated by $Q_b=Q*(1-\theta)$, in which θ is the magnitude of the capacity drop (measured in percentage). The real maximum bottleneck discharge volume will be $C_{\text{real}}=2Q_b$. However, in cases with different types of vehicles, since heavy vehicles need more space and longer time to change lanes compared to passenger cars. As a result, the bottleneck discharge volume will be negatively affected. In the HCM, how to compute the mixed-vehicle capacity of a freeway segment at the critical point on the freeway stretch with the lowest capacity is given (HCM 2000). In the equation provided by HCM (2000), the mixed-vehicle capacity is computed by PCE

capacity, number of lanes at the critical point, heavy-vehicle adjustment factor, driver population adjustment factor, and peak hour factor (PHF). In this study, the critical point is at the lane-drop bottleneck. The discharge volume at time interval k can be calculated as follows:

$$C_{\text{dis}}(k) = Q_b * \lambda_c * f_{HV}(k) * f_p * PHF \quad (11)$$

where $f_{HV}(k)$ means the dynamic heavy-vehicle adjustment factor at time interval k , f_p represents the driver population adjustment factor, and PHF is the peak-hour factor.

Note that, due to the capacity drop upstream of the bottleneck, Q_b is used in Eq. (11).

Based on HCM (2000), $f_{HV}(k)$ is computed using the following equation:

$$f_{HV}(k) = \frac{1}{1 + \sum_{j=1}^J \phi_j (\eta_{\text{bottleneck},j}(k) - 1)} \quad (12)$$

In Eq. (12), $\eta_{\text{bottleneck},j}(k)$ is the dynamic PCE value of vehicle type j at the bottleneck during time interval k which can be computed using Eq. (10). The dynamic heavy vehicle adjustment factor at time interval k can be calibrated by using Eq. (12). Generally, according to Eq. (11) and Eq. (12), in cases where different types of vehicles are involved, the maximum discharge volume $C_{\text{dis}}(k)$ at each time interval k is less than that with passenger cars only, i.e., $C_{\text{dis}}(k) \leq C$.

3.3.2.3. VSL Control Model

As shown in Figure 3.3, the studied freeway is divided into N segments, and the length of each segment is l_i . The number of segments with VSL control is N_c . The second order macroscopic traffic flow model METANET is used to predict the traffic states of

each class of vehicle on the selected freeway segment. Since there are J types of vehicles on the studied freeway segment, an extended METANET is developed and briefly introduced as follows.

According to the previously defined variables, the density of vehicle type j on segment i during time interval $k+1$ can be calculated by the following equations:

$$\rho_{i,j}(k+1) = \rho_{i,j}(k) + \frac{T}{l_i} (q_{i-1,j}(k) - q_{i,j}(k) + r_{i,j}(k) - s_{i,j}(k)) \quad (13)$$

It should be noted that, as shown in Figure 3.3, segment $i-1$ is upstream of segment i . The average space-mean speed of vehicle type j on segment i during time interval $k+1$ can be estimated by Eq. (14), in which the density is the effective density $E\rho_i(k)$ on segment i .

$$\begin{aligned} v_{i,j}(k+1) = & v_{i,j}(k) + \frac{T}{\tau} \{V[E\rho_i(k)] - v_{i,j}(k)\} \\ & + \frac{T}{l_i} [v_{i-1,j}(k) - v_{i,j}(k)] v_{i,j}(k) - \frac{vT}{\tau L_i} \frac{E\rho_{i+1}(k) - E\rho_i(k)}{E\rho_i(k) + \kappa} \end{aligned} \quad (14)$$

where τ , v , and κ are the global parameters of METANET which can be calibrated to any case study. $V[E\rho_i(k)]$ can be computed by using the following equation:

$$V[E\rho_i(k)] = v_{f,j} \exp \left[-\frac{1}{a} \left(\frac{E\rho_i(k)}{\lambda_i \rho_c} \right)^a \right] \quad (15)$$

With VSL control $u_i(k)$ on segment i during time interval k , $V[E\rho_i(k)]$ is modified as follows (Carlson et al. 2010a):

$$V[E\rho_i(k)] = u_i(k) \exp\left[-\frac{1}{a}\left(\frac{E\rho_i(k)}{\lambda_i\rho_c}\right)^a\right] \quad (16)$$

In this study, the parameter a in Eq. (15) and Eq. (16) set as 2. The relationship between flow, speed and density of vehicle type j during time interval k can be expressed by the following equation:

$$q_{i,j}(k) = \rho_{i,j}(k)v_{i,j}(k) \quad (17)$$

Based on Eq. (9) and Eq. (17), the effective flow on segment i during time interval k can be calculated by the following equations (van Lint et al. 2008):

$$Eq_i(k) = \sum_{j=1}^J \eta_{i,j}(k) q_{i,j}(k) \quad (18)$$

Based on Eq. (10) and Eq. (18), the effective speed on segment i during time interval k can be computed by

$$Ev_i(k) = \frac{Eq_i(k)}{E\rho_i(k)} \quad (19)$$

3.3.3. VSL Control and Lane Truck Restriction

Among these ATM strategies, ML is a type of freeway lane which is operated with management schemes to guide traffic flow and/or optimize throughput. Types of ML include truck lane restrictions, toll managed lanes, bus lanes, and dynamic lanes (Mirshahi et al. 2007). With yearly increases in truck percentage on the highways, more and more U.S. highways use truck lane restrictions to reduce the impact of trucks on cars, on which trucks are not allowed to drive in certain lanes. Truck lane restrictions have been adopted in some states (e.g., Florida, California, Louisiana, and Maryland) in the U.S. (Radhakrishnan and Wilmot 2009; Wolshon et al. 2009). Researchers have proved

that such restrictions policy can increase sight distance in lanes without trucks as well as permitting the orderly movements of trucks (Radhakrishnan and Wilmot 2009; Wolshon et al. 2009; Cate and Urbanik 2004). As a result, the operational safety and efficiency on highways can be improved (Wolshon et al. 2009; Cate and Urbanik 2004). In this section, a VSL control strategy for mixed traffic flows is developed. The left lane truck restriction policy (TRP) is implemented to decrease the impact of trucks on cars.

To formulate the VSL control model in this section, besides the notations in the previous sections, the following notation is introduced.

- λ_i^{TR} The number of TR lanes on segment i ;
- λ_i^{NTR} The number of NTR lanes on segment i ;
- t_{LC} The time that a driver takes to decide and execute a lane change, (s);
- $v_i^{\text{TR}}(k)$ Average speed in the TR lanes on segment i during time interval k ,
(mi/h);
- $\rho_i^{\text{TR}}(k)$ Density in the TR lanes on segment i during time interval k ,
(pce/mi/lane);
- $q_i^{\text{TR}}(k)$ Traffic volume in the TR lanes on segment i during time interval k ,
(pce/h/lane);
- $\eta_{i,j}^{\text{NTR}}(k)$ Dynamic pce value of vehicle type j on segment i during time interval k
in the NTR lanes;
- $v_{i,j}^{\text{NTR}}(k)$ Average speed of vehicle type j on segment i during time interval k in the
NTR lanes, (mi/h);

$\rho_{i,j}^{\text{NTR}}(k)$ Density on segment i of vehicle type j during time interval k in the NTR lanes, (veh/mi/lane);

$q_{i,j}^{\text{NTR}}(k)$ Traffic volume of vehicle type j on segment i during time interval k in the NTR lanes, (veh/h/lane);

$E v_i^{\text{NTR}}(k)$ Equilibrium speed on segment i during time interval k in the NTR lanes, (mi/h).

$E \rho_i^{\text{NTR}}(k)$ Equilibrium density on segment i during time interval k in the NTR lanes, (pce/mi/lane);

$E q_i^{\text{NTR}}(k)$ Equilibrium traffic volume on segment i during time interval k in the NTR lanes, (pce/h/lane);

$\pi_i^{\text{NTR} \rightarrow \text{TR}}(k)$ The fraction of choice-makers per unit time who wish to change from a NTR lane to a TR lane;

$\pi_i^{\text{TR} \rightarrow \text{NTR}}(k)$ The fraction of choice-makers per unit time who wish to change from a TR lane to a NTR lane;

$LC_i^{\text{NTR} \rightarrow \text{TR}}(k)$ A desired lane change volume from NTR lanes to TR lanes, (pce/h);

$LC_i^{\text{TR} \rightarrow \text{NTR}}(k)$ A desired lane change volume from TR lanes to NTR lanes, (pce/h);

$\Phi_i^{\text{NTR} \rightarrow \text{TR}}(k)$ Traffic volume with lane change from NTR lanes to TR lanes on segment i during time interval k , (pce/h);

$\Phi_i^{\text{TR} \rightarrow \text{NTR}}(k)$ Traffic volume with lane change from TR lanes to NTR lanes on segment i during time interval k , (pce/h).

A hypothetical freeway stretch with a lane-drop bottleneck is developed and used for model presentation, as shown in Figure 3.4. In Figure 3.4, a four-lane freeway corridor with a lane drop is shown, and different types of vehicles are traveling on this freeway corridor. Let the capacity of the freeway segment upstream of the bottleneck be Q (pce/h/lane). Different types of vehicles are involved, including cars and trucks. Trucks need more space and longer time to change lanes, which might decrease the operational efficiency. Lane changes performed by different types of vehicles at the bottleneck will result in the capacity drop (Hadiuzzaman et al. 2013). The real bottleneck capacity will be $3Q_b$. Such lane drop bottleneck might lead to prolonged travel time and huge speed variation among vehicles traveling between the upstream sections and the bottleneck (Yang et al. 2017).

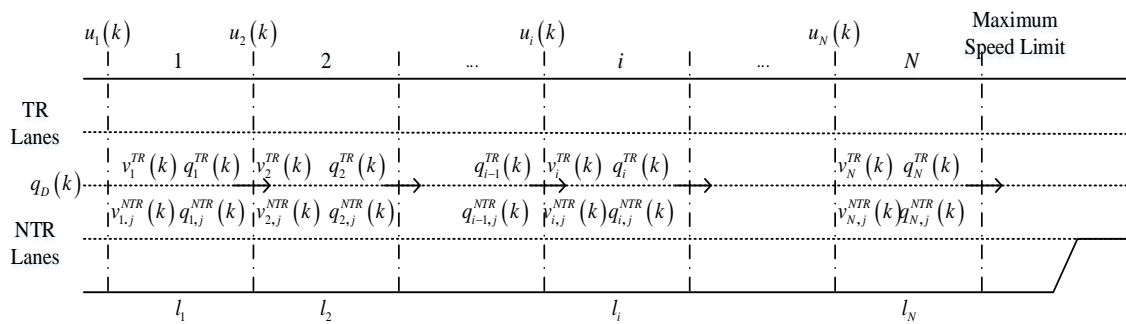


FIGURE 3.4: Illustration of the VSL Control and Truck Lane Restrictions

A VSL control under the left-lane TRP is implemented to regulate the vehicles so that the bottleneck capacity can be metered. The selected freeway stretch is divided into

N segments. Trucks are not allowed to travel in the left λ_j^{TR} lanes. It can be seen from Figure 3.4 and Figure 3.5, due to the TRP, each roadway segment is divided into two parts: TR lanes and NTR lanes. In the TR lanes, only cars are allowed to travel. In the NTR lanes, there are different classes of vehicles which are called traffic heterogeneity. When considering the traffic heterogeneity in a traffic flow model, the other classes of vehicles are always converted to the pce (van Lint et al. 2008; Deo et al. 2009)

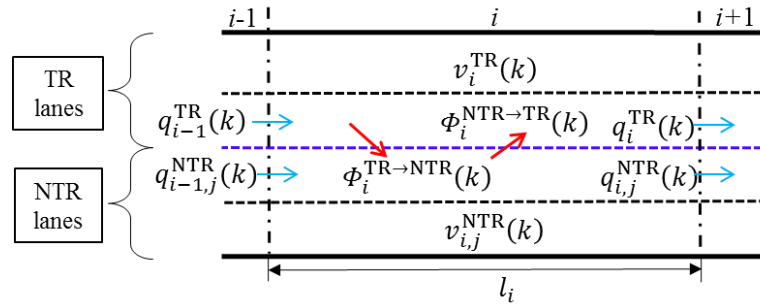


FIGURE 3.5: Illustration of VSL Control and Truck Lane Restriction on Segment i

Cars can change their lanes between the TR and NTR lanes based on the traffic conditions. Such lane change behavior of cars cannot be ignored and needs to be accounted for in the control model. In this study, the macroscopic traffic flow model METANET is used to predict the traffic state in both the TR and NTR lanes. In the following parts, how to compute the dynamic pce in the NTR lanes, lane change volume between NTR lanes and TR lanes, and the modified METANET model are presented.

3.3.3.1. Lane-changing Volume

As a matter of fact, the lane-changing behavior depends on numerous factors (e.g., human driver behavior, the number of lanes, environmental conditions, traffic

conditions, and traffic signs) which is hard to model accurately. To estimate the lane-changing volume, it has always been assumed that the drivers might consider a lane change when one of the adjacent lanes offers a higher speed or a lower density for the basic lane-changing flow model (Roncoli et al. 2015; Laval and Daganzo 2006). In Roncoli et al. (2015), the authors modeled the lane-changing volume based on the traffic densities in each lane. In this study, based on the speed differences and demand and supply function on a freeway corridor, a method to compute the lane-changing volume was developed by Laval and Daganzo (2006). Due to the TRP, only cars can change between the TR and NTR lanes, and thus, trucks will not be included in the model. The method to estimate the lane-changing volume is introduced as follows. It should be noted that, for modeling purpose, a triangular fundamental diagram is assumed and used (Laval and Daganzo 2006).

The demand function of on segment i in the TR lanes and NTR lanes during time interval k can be computed by

$$D_i^{\text{TR}}(k) = \min\{Q, v_{f,\text{car}} \rho_i^{\text{TR}}(k)\} \quad (20)$$

$$D_i^{\text{NTR}}(k) = \min\{Q, v_{f,\text{car}} \rho_{i,\text{car}}^{\text{NTR}}(k)\} \quad (21)$$

The supply function on segment i in the TR lanes and NTR lanes during time interval k are

$$S_i^{\text{TR}}(k) = \min\{Q, w(\rho_j - \rho_i^{\text{TR}}(k))\} \quad (22)$$

$$S_i^{\text{NTR}}(k) = \min\{Q, w(\rho_j - E\rho_i^{\text{NTR}}(k))\} \quad (23)$$

In Eq. (23), in the NTR lanes, the equilibrium density $E\rho_i^{\text{NTR}}(k)$ is used which is computed by

$$E\rho_i^{\text{NTR}}(k) = \sum_{j=1}^J \rho_{i,j}^{\text{NTR}}(k) \eta_{i,j}^{\text{NTR}}(k) \quad (24)$$

The traffic composition of car on segment i is

$$P_{i,\text{car}}^{\text{NTR}}(k) = \frac{\eta_{i,\text{car}}^{\text{NTR}}(k) * v_{i,\text{car}}^{\text{NTR}}(k) * \rho_{i,\text{car}}^{\text{NTR}}(k)}{\sum_{j=1}^J \eta_{i,j}^{\text{NTR}}(k) * v_{i,j}^{\text{NTR}}(k) * \rho_{i,j}^{\text{NTR}}(k)} \quad (25)$$

By using Eq. (23) and Eq. (25), the supply function of cars in the NTR lanes on segment i during time interval k is (van Lint et al. 2008)

$$S_{i,\text{car}}^{\text{NTR}}(k) = S_i^{\text{NTR}}(k) * P_{i,\text{car}}^{\text{NTR}}(k) \quad (26)$$

According to (Laval and Daganzo 2006), the fraction of choice-maker per unit time wishing to change from NTR lane to TR lanes or from TR lanes to NTR lanes on segment i during time interval k is

$$\pi_i^{\text{NTR} \rightarrow \text{TR}}(k) = \frac{\max\{0, v_i^{\text{TR}}(k) - v_{i,\text{car}}^{\text{NTR}}(k)\}}{v_{f,\text{car}} t_{\text{LC}}} \quad (27)$$

$$\pi_i^{\text{TR} \rightarrow \text{NTR}}(k) = \frac{\max\{0, v_{i,\text{car}}^{\text{NTR}}(k) - v_i^{\text{TR}}(k)\}}{v_{f,\text{car}} t_{\text{LC}}} \quad (28)$$

With VSL control, Eq. (27) and Eq. (28) are respectively modified as follows:

$$\pi_i^{\text{NTR} \rightarrow \text{TR}}(k) = \frac{\max\{0, v_i^{\text{TR}}(k) - v_{i,\text{car}}^{\text{NTR}}(k)\}}{u_i(k) t_{\text{LC}}} \quad (29)$$

$$\pi_i^{\text{TR} \rightarrow \text{NTR}}(k) = \frac{\max\{0, v_{i,\text{car}}^{\text{NTR}}(k) - v_i^{\text{TR}}(k)\}}{u_i(k) t_{\text{LC}}} \quad (30)$$

A desired lane change volume from NTR lanes to TR lanes or from NTR lanes to TR lanes on segment i during time interval k can be estimated by

$$LC_i^{\text{NTR} \rightarrow \text{TR}} = T \pi_i^{\text{NTR} \rightarrow \text{TR}}(k) D_i^{\text{NTR}}(k) \quad (31)$$

$$LC_i^{\text{TR} \rightarrow \text{NTR}} = T \pi_i^{\text{TR} \rightarrow \text{NTR}}(k) D_i^{\text{TR}}(k) \quad (32)$$

As shown in Figure 3.5, in the TR lanes, during time interval k , the total desired volume entering segment i equals the volume $q_{i-1}^{\text{TR}}(k)$ flows out of segment $i-1$ plus the lane change volume $LC_i^{\text{NTR} \rightarrow \text{TR}}(k)$ from the NTR lanes, i.e. $q_{i-1}^{\text{TR}}(k) + LC_i^{\text{NTR} \rightarrow \text{TR}}(k)$. If $q_{i-1}^{\text{TR}}(k) + LC_i^{\text{NTR} \rightarrow \text{TR}}(k)$ is less than the available capacity on segment i , i.e., supply function $S_i^{\text{TR}}(k)$, all the demands can be satisfied. All the vehicles, including traveling from segment $i-1$ and lane changing from the NTR lanes, are able to advance to the target segment, i.e., segment i ; otherwise, the lane change volume should be computed based on the available capacity. Noted that, this study assumes that the volume from segment $i-1$ is satisfied first. Based on the assumption, the traffic volume with lane change from the NTR lane to the TR lanes on segment i during time interval k can be calculated as follows:

$$\Phi_i^{\text{NTR} \rightarrow \text{TR}}(k) = \min \left\{ 1, \frac{S_i^{\text{TR}}}{q_{i-1}^{\text{TR}}(k) + LC_i^{\text{NTR} \rightarrow \text{TR}}(k)} \right\} LC_i^{\text{NTR} \rightarrow \text{TR}}(k) \quad (33)$$

The traffic volume with lane change from the TR lanes to the NTR lanes on segment i during time interval k can be computed based on the same principle.

$$\Phi_i^{\text{TR} \rightarrow \text{NTR}}(k) = \min \left\{ 1, \frac{S_{i,\text{car}}^{\text{NTR}}}{q_{i-1}^{\text{NTR}}(k) + LC_i^{\text{TR} \rightarrow \text{NTR}}(k)} \right\} LC_i^{\text{TR} \rightarrow \text{NTR}}(k) \quad (34)$$

The lane change volume difference in the TR and NTR lanes on segment i during time interval k can be computed by

$$\Delta\Phi_i^{\text{TR}}(k) = \Phi_i^{\text{NTR} \rightarrow \text{TR}}(k) - \Phi_i^{\text{TR} \rightarrow \text{NTR}}(k) \quad (35)$$

$$\Delta\Phi_i^{\text{NTR}}(k) = \Phi_i^{\text{TR} \rightarrow \text{NTR}}(k) - \Phi_i^{\text{NTR} \rightarrow \text{TR}}(k) \quad (36)$$

3.3.3.2. Extended METANET Model

The studies (Knoop et al. 2010; Soriguera et al. 2017; Duret et al. 2012) modeled the lane distribution showing that the lane distribution could be affected by some characteristics of freeway layout (e.g., the number of lanes) and the control strategies (e.g., VSL and TRP). For instance, a speed limit of 60 km/h significantly increased the utilization of the shoulder lane (Knoop et al. 2010). In the absence of control, there is a higher incentive for vehicles with higher traveling speed to travel in the center or median lanes (Duret et al. 2012). VSL control and TRP profoundly impacted the lane distribution and reduced the speed difference between the shoulder lane and passing lane (Duret et al. 2012). As a result, according to the previous findings, the different flow distribution in each lane might lead to different traffic flow parameters (e.g., free flow speed) in each lane (Roncoli et al. 2015). In addition, due to the TRP, the traffic characteristics in the TR and NTR lanes are different as well. To accurately account for these characteristics (such as the difference in flow and speeds), the traffic state under VSL and TRP in the TR and NTR lanes are respectively considered. In this study, the second order macroscopic traffic flow model METANET is used.

For the convenience of both computation and description of the basic METANET model, the selected freeway is divided into N segments, as presented in Figure 3.4. Let the length of segment i be l_i and the discrete time step used in the METANET model be T . Note that segment $i-1$ is upstream of segment i .

3.3.3.3. TR lanes

The density on segment i in the TR lanes during time interval $k+1$ can be calculated by the following equations, in which the lane change volume difference in the TR lanes $\Delta\Phi_i^{\text{TR}}(k)$ is included:

$$\rho_i^{\text{TR}}(k+1) = \rho_i^{\text{TR}}(k) + \frac{T}{l_i} (q_{i-1}^{\text{TR}}(k) - q_i^{\text{TR}}(k) + \Delta\Phi_i^{\text{TR}}(k)) \quad (37)$$

The average space-mean speed on segment i in the TR lanes during time interval $k+1$ is

$$\begin{aligned} v_i^{\text{TR}}(k+1) &= v_i^{\text{TR}}(k) + \frac{T}{\tau_{\text{TR}}} (V[\rho_i^{\text{TR}}(k)] - v_i^{\text{TR}}(k)) \\ &+ \frac{T}{l_i} (v_{i-1}^{\text{TR}}(k) - v_i^{\text{TR}}(k)) v_i^{\text{TR}}(k) \\ &- \frac{v_{\text{TR}} T \rho_{i+1}^{\text{TR}}(k) - \rho_i^{\text{TR}}(k)}{\tau_{\text{TR}} l_i \rho_i^{\text{TR}}(k) + \kappa_{\text{TR}}} - \frac{\delta_{\text{TR}} T \Delta\Phi_i^{\text{TR}}(k) v_i^{\text{TR}}(k)}{l_i \rho_i^{\text{TR}}(k) + \kappa_{\text{TR}}} \end{aligned} \quad (38)$$

where τ_{TR} , v_{TR} , κ_{TR} , and δ_{TR} are the global parameter in the TR lanes which can be estimated to any case study. It should be noted that, since the traffic conditions in the TR lanes might be different from that in the NTR lanes, the global parameters of TR lanes are accounted in Eq. (38). In order to account for the speed drop caused by the lane-changing phenomena, the term $-\frac{\delta_{\text{TR}} T \Delta\Phi_i^{\text{TR}}(k) v_i^{\text{TR}}(k)}{l_i \rho_i^{\text{TR}}(k) + \kappa_{\text{TR}}}$ is included in Eq. (38), which is

based on (Bekiaris-Liberis et al. 2016). $V[\rho_i^{\text{TR}}(k)]$ is calculated by the following equation:

$$V[\rho_i^{\text{TR}}(k)] = v_{f,\text{car}} \exp \left[-\frac{1}{a} \left(\frac{\rho_i^{\text{TR}}(k)}{\rho_c} \right)^a \right] \quad (39)$$

With VSL control $u_i(k)$ on segment i during time interval k , $V[\rho_i^{\text{TR}}(k)]$ is modified as follows (Hegyi et al. 2005):

$$V[\rho_i^{\text{TR}}(k)] = \min \left(u_i(k) \exp \left[-\frac{1}{a} \left(\frac{\rho_i^{\text{TR}}(k)}{\rho_c} \right)^a \right], (1 + \alpha) u_i(k) \right) \quad (40)$$

where $(1 + \alpha)$ is the non-compliance factor. According to Hadiuzzaman et al. (2013), a is set as 2.

The outflow of each segment in the TR lanes equals the density times the mean speed:

$$q_i^{\text{TR}}(k) = \rho_i^{\text{TR}}(k) v_i^{\text{TR}}(k) \quad (41)$$

3.3.3.4. NTR Lanes

In the NTR lanes on segment i during time interval $k+1$, the speed, density, and flow can be estimated based on the same principle. The density on segment i of vehicle type j in the NTR lanes during time interval $k+1$ can be calculated by (Deo et al. 2009)

$$\begin{aligned} \rho_{i,j}^{\text{NTR}}(k+1) = & \rho_{i,j}^{\text{NTR}}(k) + \frac{T}{l_i} (q_{i-1}^{\text{NTR}}(k) - q_i^{\text{NTR}}(k)) \\ & + r_{i,j}(k) - s_{i,j}(k) + \Delta\Phi_{i,j}^{\text{NTR}}(k) \end{aligned} \quad (42)$$

In Eq. (42), it should be noted that there are no trucks changing from the TR lanes to the NTR lanes, and thus $\Delta\Phi_{i,\text{truck}}^{\text{NTR}}(k) = 0$. Since there are vehicles traveling from the on-ramps and leaving the main lane at the off-ramps, the on-ramp volume $r_{i,j}(k)$ and off-ramp volume $s_{i,j}(k)$ are included in Eq. (42).

The average space-mean speed of vehicle type j on segment i during time interval $k+1$ can be calculated by

$$\begin{aligned}
v_{i,j}^{\text{NTR}}(k+1) = & v_{i,j}^{\text{NTR}}(k) + \frac{T}{\tau_{\text{NTR}}} \left(V_j \left[E\rho_i^{\text{NTR}}(k) \right] - v_{i,j}^{\text{NTR}}(k) \right) \\
& + \frac{T}{l_i} \left(v_{i-1,j}^{\text{NTR}}(k) - v_{i,j}^{\text{NTR}}(k) \right) v_{i,j}^{\text{NTR}}(k) \\
& - \frac{v_{\text{NTR}} T}{\tau_{\text{NTR}} l_i} \frac{E\rho_{i+1}^{\text{NTR}}(k) - E\rho_i^{\text{NTR}}(k)}{E\rho_i^{\text{NTR}}(k) + \kappa_{\text{NTR}}} \\
& - \frac{\delta_{\text{NTR}} T}{l_i} \frac{v_{i,j}^{\text{NTR}}(k) \left(\Delta\Phi_{i,j}^{\text{NTR}}(k) + r_{i,j}(k) \right)}{E\rho_i^{\text{TR}}(k) + \kappa_{\text{NTR}}}
\end{aligned} \tag{43}$$

where τ_{NTR} , v_{NTR} , κ_{NTR} , and δ_{NTR} are the global parameter in the NTR lanes.

The term $-\frac{\delta_{\text{NTR}} T}{l_i} \frac{v_{i,j}^{\text{NTR}}(k) \left(\Delta\Phi_{i,j}^{\text{NTR}}(k) + r_{i,j}(k) \right)}{E\rho_i^{\text{TR}}(k) + \kappa_{\text{NTR}}}$ is added to estimate the speed reduction

due to the lane-changing and on-ramp (Hegyí et al. 2005). In Eq. (43), the density is the equilibrium density in the NTR lanes $E\rho_i^{\text{NTR}}(k)$ on segment i . Without VSL control,

$V_j \left[E\rho_i^{\text{NTR}}(k) \right]$ is calculated

$$V_j \left[E\rho_i^{\text{NTR}}(k) \right] = v_{f,j} \exp \left[-\frac{1}{a} \left(\frac{E\rho_i^{\text{NTR}}(k)}{\rho_c} \right)^a \right] \tag{44}$$

If $E\rho_i^{\text{NTR}}(k) \leq \rho_c$, the traffic condition in the NTR lanes is free-flow speed

condition, and $V_j \left[E\rho_i^{\text{NTR}}(k) \right]$ is

$$V_j \left[E\rho_i^{\text{NTR}}(k) \right] = \min \left(v_{f,j} \exp \left[-\frac{1}{a} \left(\frac{E\rho_i^{\text{NTR}}(k)}{\rho_c} \right)^a \right], (1+\alpha)u_i(k) \right) \tag{45}$$

If $E\rho_i^{\text{NTR}}(k) > \rho_c$, under congested traffic condition, according to Liu et al. (2014;

2017) and Deo et al. (2009), the following relationship can be achieved:

$$V_1[E\rho_i^{\text{NTR}}(k)] = V_2[E\rho_i^{\text{NTR}}(k)] = \dots = V_j[E\rho_i^{\text{NTR}}(k)] \quad (46)$$

$$V_j[E\rho_i^{\text{NTR}}(k)] = \min \left(\begin{array}{l} \sum_{j=1}^J P_{i,j}^{\text{NTR}}(k) v_{f,j} \exp \left[-\frac{1}{a} \left(\frac{E\rho_i^{\text{NTR}}(k)}{\rho_c} \right)^a \right], \\ (1 + \alpha) u_i(k) \end{array} \right) \quad (47)$$

where $P_{i,j}^{\text{NTR}}(k)$ is the traffic composition of vehicle type j on segment i , and

$$P_{i,j}^{\text{NTR}}(k) = \frac{\eta_{i,j}^{\text{NTR}}(k) * v_{i,j}^{\text{NTR}}(k) * \rho_{i,j}^{\text{NTR}}(k)}{\sum_{j=1}^J \eta_{i,j}^{\text{NTR}}(k) * v_{i,j}^{\text{NTR}}(k) * \rho_{i,j}^{\text{NTR}}(k)}$$

A simple queue equation for estimating the queue lengths at the on-ramp which is located on segment i is used (Pasquale et al. 2014).

$$w_{i,j}(k+1) = w_{i,j}(k) + T(d_{i,j}(k) - r_{i,j}(k)) \quad (48)$$

The on-ramp volume $r_{i,j}(k)$ of vehicle type j during time interval k can be estimated by

$$r_{i,j}(k) = \min \left\{ d_{i,j}(k) + \frac{w_{i,j}(k)}{T}, r_{i,j}^{\max}, r_{i,j}^{\max} \frac{\rho_j - E\rho_i(k)}{\rho_j - \rho_c} \right\} \quad (49)$$

where $r_{i,j}^{\max}$ is the on-ramp capacity for class j .

The outflow of vehicle type j on each segment in the NTR lanes is

$$q_{i,j}^{\text{NTR}}(k) = \rho_{i,j}^{\text{NTR}}(k) v_{i,j}^{\text{NTR}}(k) \quad (50)$$

The equilibrium volume flowing out of the segment i in the NTR lanes is

$$Eq_i^{\text{NTR}}(k) = \sum_{j=1}^J \eta_{i,j}^{\text{NTR}}(k) q_{i,j}^{\text{NTR}}(k) \quad (51)$$

The equilibrium space-mean speed on segment i in the NTR lanes is estimated by

$$Ev_i^{\text{NTR}}(k) = Eq_i^{\text{NTR}}(k) / E\rho_i^{\text{NTR}}(k) \quad (52)$$

According to Bekiaris-Liberis et al. (2016), the boundary conditions in this study are determined, i.e., the virtual downstream density at the end of the link and the virtual upstream speed at the beginning of the link.

The virtual upstream speed at the beginning of the link in the TR and NTR lanes are respectively assumed by

$$v_0^{\text{TR}}(k) = v_1^{\text{TR}}(k) \quad (53)$$

$$v_{0,j}^{\text{NTR}}(k) = v_{1,j}^{\text{NTR}}(k) \quad (54)$$

The virtual downstream density at the end of the link in the TR and NTR lanes are assumed as follows:

$$\rho_{N+1}^{\text{TR}}(k) = \rho_N^{\text{TR}}(k) \quad (55)$$

$$E\rho_{N+1}^{\text{TR}}(k) = E\rho_N^{\text{TR}}(k) \quad (56)$$

3.4. CTM and VSL Control

The CTM has been adopted in many studies to develop a first-order VSL control strategy (Hadiuzzaman and Qiu 2013; Li et al. 2016; Han et al. 2017). However, in such research efforts, the control model failed to involve heavy vehicles. It has been verified that the driver behavior of passenger cars can be largely affected by the presence of heavy vehicles (van Lint et al. 2008). Moreover, the traffic flow model involving mixed traffic flows could result in more accurate and also better outcomes compared to that without considering mixed traffic flows. For example, Deo et al. (2009) and Liu et al. (2014, 2016) extended the METANET model in which the heavy vehicles were taken

into consideration. A smaller TTT could be achieved by using the extended METANET model. Thus, in this study, an extended CTM involving heavy vehicles is developed.

There are numerous on- and off-ramps or lane drops on a freeway stretch, particularly in the metropolitan area. During the high demand period, more than one bottleneck might be activated because of the ramp weaving effects, lane drops, accidents, and/or work zones. Meanwhile, several shock waves can be created, and vehicles are forced to slow down upstream of these bottlenecks. Drivers have to frequently accelerate and decelerate which may result in huge variations in traveling speeds. The overall operational efficiency and safety can be considerably deteriorated. If a VSL control is only implemented to relieve congestion and eliminate the shock wave at one bottleneck, even though the efficiency in the control area is improved, it may not help improve the overall efficiency. For example, if the maximum discharge volume of a downstream bottleneck is less than the controlled outflow from the upstream bottleneck, the congestion at the downstream bottleneck will still be formed. In this regard, a systematic VSL control framework for a freeway corridor with multiple bottlenecks needs to be developed. For simplicity purpose, the following assumptions are made:

(1) Under free flow traffic conditions, the average speeds of trucks are less than cars'; while in congested traffic conditions, the trucks' speeds equal to cars' speeds;

(2) Traffic flow parameters, such as the free flow speed, capacity, critical density, shock wave speed, and jam density, might be different at different bottlenecks, but it is assumed that the values of such parameters on the cells upstream of the nearest bottleneck are the same.

To formulate the VSL control model in this section, besides the notations in the previous sections, the following notation is introduced.

$m \in \mathbf{M}$ m -th bottleneck.

Q_m capacity upstream of the m -th bottleneck, (pce/h/lane);

$Q_{m,b}$ maximum discharge flow upstream the m -th bottleneck, $Q_{m,b} = Q_m(1 - \theta_m)$ (pce/h/lane);

θ_m magnitude of the m -th capacity drop, (%);

$\rho_{m,jam}$ jam density upstream of the m -th bottleneck, (pce/mi/lane);

$\rho_{m,c}$ critical density upstream of the m -th bottleneck, (pce/mi/lane);

w_m backward shock wave speed of the m -th bottleneck, (mph);

$v_{j,m,f}$ free flow speed of vehicle type j upstream of the m -th bottleneck, (mph);

$\rho_{j,m,jam}$ jam density of vehicle type j upstream of the m -th bottleneck, (veh/mi/lane);

$\rho_{j,m,c}$ critical density of vehicle type j upstream of the m -th bottleneck, (veh/mi/lane);

$D_{i,j}(k)$ demand function for vehicle type j on cell i during time interval k , (pce/h/lane);

$S_i(k)$ supply function on cell i during time interval k , (pce/h/lane);

$P_{i,j}(k)$ traffic composition of vehicle type j on cell i during time interval k .

Figure 3.6 presents a freeway stretch on which there are M bottlenecks. The freeway stretch is divided into N cells. The m -th bottleneck which is caused due to the high traffic demands from the on-ramp (see Figure 3.6) is selected as an example to illustrate the CTM-based VSL control model in this study. The capacity upstream of the

m -th bottleneck is Q_m . Because of the capacity drop, the maximum discharge rate of m -th bottleneck is $Q_{m,b}$.

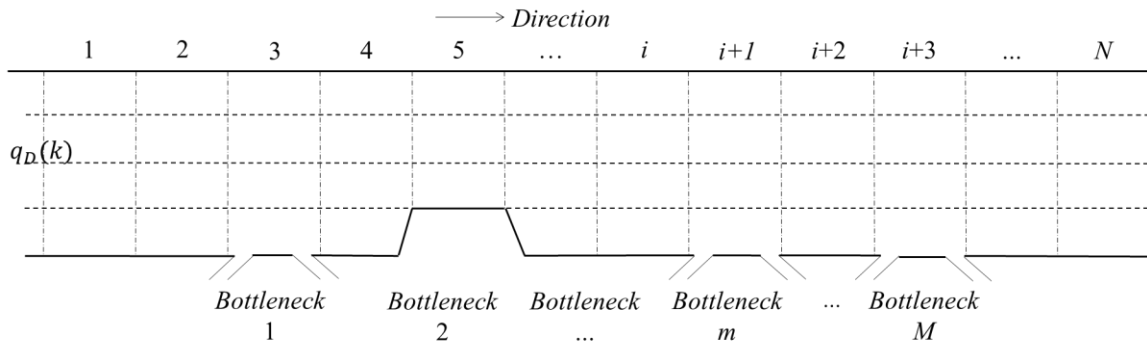
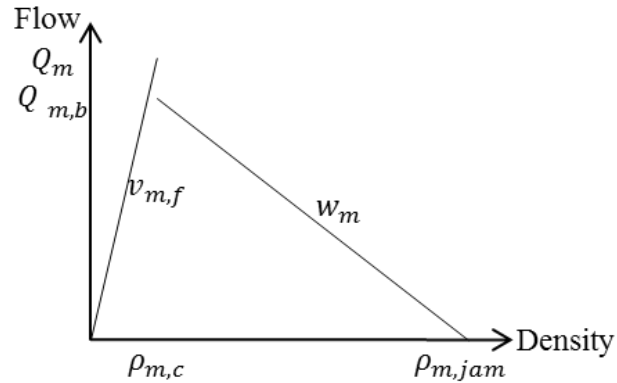
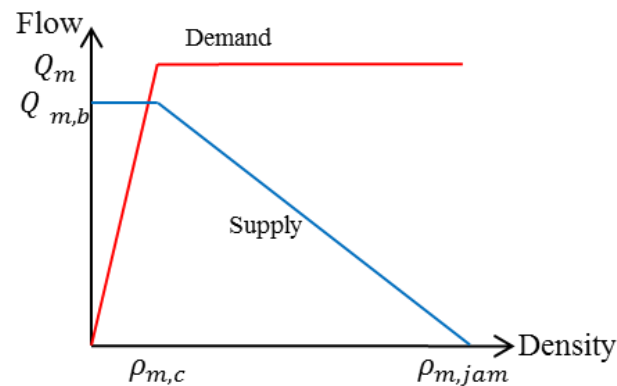


FIGURE 3.6: An Illustration of A Freeway Stretch with Multiple Bottlenecks

Some researchers have tried to incorporate the capacity drop into the classical CTM by changing the demand and supply functions (Lebacque 2003; Han et al. 2017) or using a discontinuous FD (Hadiuzzaman and Qiu 2013; Li et al. 2016). In this study, to model the capacity drop phenomenon at the bottlenecks, a discontinuous FD, as shown in Figure 3.7(a), is used. Figure 3.7(b) presents the assumed demand and supply line of the modified CTM.

(a) FD with A Capacity Drop at the m -th Bottleneck

(b) Demand and Supply Lines

FIGURE 3.7: FD and the Demand and Supply Lines

Since the traffic parameters of each vehicle type are different, in order to model mixed traffic flows, a combined FD needs to be developed. Assuming that there are two types of vehicles, a combination of the FD (with capacity drops) of the two vehicles classes is developed on the basis of Liu et al. (2014), as shown in Figure 3.8. In Figure 3.8, $\rho_{j,c}$, $v_{j,f}$, $\rho_{j,jam}$, Q_j , $Q_{j,b}$, and w_j ($j=1,2$) are the critical density (veh/mile/lane), free flow speed (mph), jam density (veh/mile/lane), capacity (veh/h/lane), capacity drop (veh/h/lane), and shock wave speed of vehicle type j , respectively. Note that the free flow

speed of vehicle type 1 is greater than vehicle type 2, i.e. $v_{1,f} > v_{2,f}$. As shown in Figure 3.8, the density $\rho_{2,c}^*$ linking the two FDs can be computed as follows (Liu et al. 2014; Liu et al. 2017).

$$\rho_{2,c}^* = \frac{w_1 \rho_{1,jam}}{w_1 - v_{2,f}} \tag{57}$$

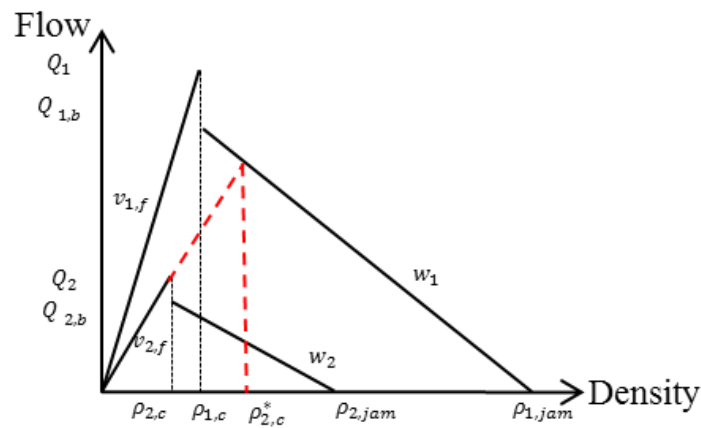


FIGURE 3.8: FD with Capacity Drops at the m -th Bottleneck for Two Vehicle Classes

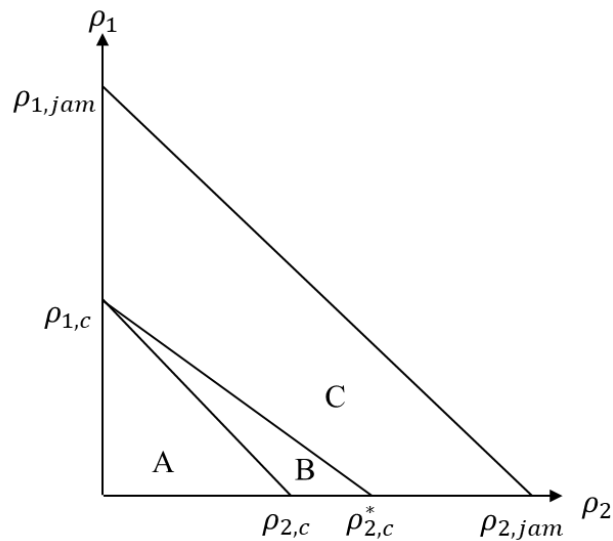


FIGURE 3.9: Traffic Regimes for Two Vehicle Classes

According to the density ρ_j ($j=1, 2$), three traffic conditions can be distinguished (see Figure 3.9) (Liu et al. 2014):

(1). Condition A: If $\frac{\rho_1}{\rho_{1,c}} + \frac{\rho_2}{\rho_{2,c}} \leq 1$, both the two vehicle types are in free-flow

conditions;

(2). Condition B: If $\frac{\rho_1}{\rho_{1,c}} + \frac{\rho_2}{\rho_{2,c}} > 1$ and $\frac{\rho_1}{\rho_{2,c}^*} + \frac{\rho_2}{\rho_{2,c}} \leq 1$, vehicle type 1 is in congested

traffic condition, and vehicle type 2 is in free-flow conditions;

(3). Condition C: If $\frac{\rho_1}{\rho_{2,c}^*} + \frac{\rho_2}{\rho_{2,c}} > 1$ and $\frac{\rho_1}{\rho_{1,jam}} + \frac{\rho_2}{\rho_{2,jam}} \leq 1$, both the two vehicles

types are in congested traffic conditions.

In the following parts of this section, the extended CTM for mixed traffic flows is developed based on the previous assumptions and discussions. According to Eq. (9), the equilibrium density on cell i during time interval k is calculated as follows:

$$E\rho_i(k) = \sum_{j=1}^J \eta_{i,j}(k) \rho_{i,j}(k) \quad (58)$$

Based on the FD in Figure 3.7(a) and demand and supply lines in Figure 3.7(b), the demand function for vehicle type j on cell i during time interval k with VSL control is given

Demand function:

$$D_{i,j}(k) = \begin{cases} u_i(k) \rho_{i,j}(k) \eta_{i,j}(k) & \text{if } \rho_{i,j}(k) \leq \rho_{j,m,c} \\ Q_m & \text{if } \rho_{i,j}(k) > \rho_{j,m,c} \end{cases} \quad (59)$$

The supply function on cell i during time interval k with VSL control is defined as:

Supply function:

$$S_i(k) = \begin{cases} Q_{m,b} & \text{if } E\rho_{i,j}(k) \leq \rho_{m,c} \\ w_m(\rho_{m,\text{jam}} - E\rho_i(k)) & \text{if } E\rho_{i,j}(k) > \rho_{m,c} \end{cases} \quad (60)$$

The density of vehicle type j on cell i during time interval $k+1$ can be calculated by the following equation (Deo et al. 2009):

$$\rho_{i,j}(k+1) = \rho_{i,j}(k) + \frac{T}{l_i} (q_{i-1,j}(k) - q_{i,j}(k) + r_{i,j}(k) - s_{i,j}(k)) \quad (61)$$

In Eq. (61), in order to estimate $q_{i,j}(k)$, it is assumed that traffic demand of vehicle type j traveling from cell i to cell $i+1$ is proportional to the traffic composition of cell i (van Lint et al. 2008). The traffic composition of cell i is

$$P_{i,j}(k) = \frac{\eta_{i,j}(k) * v_{i,j}(k) * \rho_{i,j}(k)}{\sum_{j=1}^J \eta_{i,j}(k) * v_{i,j}(k) * \rho_{i,j}(k)} \quad (62)$$

For the first cell, the percentage of vehicle type j equals to the traffic composition of the demand input. By using Eq. (60), (61) and (62), the volumes of vehicle type j entering cell $i+1$ from cell i during time interval k is

$$q_{i,j}(k) = \frac{1}{\eta_{i,j}(k)} \min(D_i(k), P_{i,j}(k) S_{i+1}(k)) \quad (63)$$

The equilibrium volume $Eq_i(k)$ that flows out of cell i during time interval k is described as follows:

$$Eq_i(k) = \sum_{j=1}^J \eta_{i,j}(k) q_{i,j}(k) \quad (64)$$

The average space mean speed of vehicle type j on cell i during time interval k is determined according to the following traffic conditions. Note that it is assumed that the free flow speed of vehicle type j is greater than that of vehicle type $j+1$ (In other words, they are sorted in descending order).

(1). If $\sum_{j=1}^J \frac{\rho_{i,j}(k)}{\rho_{j,m,c}} \leq 1$, all the vehicle types are in free flow conditions. The average

speed of vehicle type j on cell i during time interval k is $v_{i,j}(k) = \min(v_{j,m,f}, u_i(k))$.

(2). If $\sum_{j=1}^J \frac{\rho_{i,j}(k)}{\rho_{j,m,c}} > 1$ and $\sum_{j=1}^{j'} \frac{\rho_{i,j}(k)}{\rho_{j'+1,m,c}^*} + \sum_{j=j'+1}^J \frac{\rho_{i,j}(k)}{\rho_{j,m,c}} \leq 1$, vehicle type $1 \dots j'$ are in

congested traffic conditions, and vehicle type $j'+1 \dots J$ are in free flow traffic

conditions. According to Eq. (57), $\rho_{j'+1,m,c}^*$ is defined by $\rho_{j'+1,m,c}^* = \frac{w_m \rho_{j',m,jam}}{w_m - v_{j'+1,m,f}}$.

The average speeds of vehicle class $1 \dots j'$ on cell i during time interval k are

$v_{i,j}(k) = \frac{w_m (\rho_{m,jam} - E\rho_i(k))}{E\rho_i(k)}$. The average speeds of vehicle type $j'+1 \dots J$ on cell i

during time interval k are estimated by $v_{i,j}(k) = \min(v_{j,m,f}, u_i(k))$.

(3). If $\sum_{j=1}^{j-1} \frac{\rho_{i,j}(k)}{\rho_{j,m,c}^*} + \frac{\rho_{i,j}(k)}{\rho_{j,m,c}} > 1$ and $\sum_{j=1}^J \frac{\rho_{i,j}(k)}{\rho_{j,m,jam}} \leq 1$, all the vehicle types are in

congested traffic conditions, where $\rho_{j,m,jam} = \frac{\rho_{m,jam}}{\eta_{j,jam}}$, $\eta_{j,jam} = \frac{sd_j}{sd_{car}}$.

The average speed of vehicle type j on cell i during time interval k is estimated by

$$v_{i,j}(k) = \frac{w_m(\rho_{m,\text{jam}} - E\rho_i(k))}{E\rho_i(k)}.$$

3.5. Connected and Autonomous Vehicles

Typically, the methods developed and used to model CAVs can be mainly classified into two categories: modeling based on the modified traffic flow models (Treiber et al. 2000; Shladover et al. 2012; Khondaker and Kattan 2015b; Li et al. 2017) and modeling on the basis of the experimental data (Milanés et al. 2014; Milanés and Shladover 2014). Even though the model based on the real experimental data is more reliable, due to the high cost, current general unavailability and safety consideration, a modified traffic flow model is commonly employed by researchers.

3.5.1. Intelligent Driver Model

According to some existing studies (Khondaker and Kattan 2015b; Li et al. 2017), the intelligent driver model (IDM) developed by Treiber et al. (2000) is adopted to model the car-following characteristics of CAVs. Compared with other models, only a few parameters of the IDM need to be calibrated. In addition, the IDM can be used to describe both the free flow and congested conditions.

In the IDM, the acceleration $a(k)$ during time interval k can be computed by Eq. (65) and Eq. (66):

$$a(k) = a \left[1 - \left(\frac{v(k)}{v_0} \right)^4 - \left(\frac{s^*(k)}{s(k)} \right)^2 \right] \quad (65)$$

$$s^*(k) = \max\left(0, s_0 + v^* HW + \frac{v(k)\Delta v(k)}{2\sqrt{ab}}\right) \quad (66)$$

where $v(k)$ represents the current vehicle's speed, v_0 is the desired speed, $s(k)$ denotes the gap distance between two vehicles in the same lane, s_0 means the minimum gap distance at standstill, HW is headway, $\Delta v(k)$ is the speed difference between the leading vehicle and current vehicle, a is maximum acceleration, and b is the desired deceleration. It should be pointed out that the desired speed v_0 equals to the VSL value $u_i(k)$ on cell i where the vehicle is traveling during a control time interval k (Khondaker and Kattan 2015b).

Through modifying the parameters of the IDM, such as the acceleration and deceleration rate and headway time, the AVs can be simulated (Kesting et al. 2008). By incorporating the V2V wireless communication technology, such as dedicated short-range communications (DSRC), into AVs, the CAVs can be modeled. The communicated data within the communication range, such as speed, acceleration rate, and gap distance of the immediate predecessor, can be obtained through the V2V (Shladover et al. 2015; Wang et al. 2016). Note that in this study, except for passenger cars, the other types of vehicles (e.g., trucks) are human-driven vehicles. An AV is formulated by adopting the IDM with its headway being smaller than the human-driven vehicle's. If an AV is following another AV, it uses the CAV car-following model, with the smallest headway. If an AV is following a human-driven vehicle, the headway that this AV takes will be less than that a human-driven vehicle will otherwise take (Shladover et al. 2012).

3.5.2. Connected Autonomous Vehicles Platooning

Among different types of CAV technologies, vehicle platooning has been drawing increasing attention due to its promising potential in improving operational efficiency and safety. Typically, two common control policies are being used in vehicle longitudinal (or platooning) control - the constant spacing (CS) and constant time-gap (CT) policy, and with the CT policy has been being favored in mixed traffics (Chen et al. 2017). In 2014, Milanés and Shladover tested the CACC system on the basis of the CT policy for passenger cars (Milanés and Shladover 2014). Currently, researchers have explored the benefits and characteristics of vehicle platooning (Rahman and Abdel-Aty 2017; Deng 2016; Jai and Ngoduy 2016; Bang and Ahn 2017; Treiber et al. 2000). For example, Rahman and Abdel-Aty (2017) evaluated the safety benefits of CV's platooning. Deng (2016) analyzed the impact of heavy-duty vehicle platooning on average speeds, traffic flow rate, fuel efficiency, and average number of lane changes. Chen et al. (2017) examined the stability of truck platooning on uphill grades.

In the following section, vehicle's car following behavior, such as vehicles in the platoon and leading autonomous vehicle, is given.

3.5.2.1. Vehicle in the Platoon

According to Milanés and Shladover (2014), vehicle's car following behavior under the field-tested CACC of passenger cars can be approximated by the following model, in which cars in a platoon follow the CT:

$$e_p = x_{p-1} - x_p - HWv_p \quad (67)$$

$$v_p = v_{p-\text{prev}} + k_p e_p + k_d \dot{e}_p \quad (68)$$

where e_p is the gap error of the p -th consecutive vehicle, x_{p-1} is the current position of the preceding vehicle, x_p and v_p are the current position and speed of the subject vehicle respectively, HW is the current time-gap setting, and v_{p-prev} is the speed of the subject vehicle in the previous iteration, k_p and k_d capture the controller feedback gains to minimize the gap error, which are set to be $k_p = 0.45$ and $k_d = 0.25$ on the basis of field testing (Milanés and Shladover 2014).

When the speed of a CACC vehicle is determined, the position of the subject vehicle is

$$x_p = x_{p-prev} + v_p \Delta t \quad (69)$$

where x_{p-prev} is the position of the subject vehicle in the previous iteration, and Δt is the time step in the microscopic simulation that is set to be 0.1s.

3.5.2.2. Leading Autonomous Vehicle

The leading vehicle of each platoon is controlled by the ACC model in Milanés and Shladover (2014). The acceleration of the leading vehicle is modeled based on the distance and speed errors.

$$a_p = k_1 (x_{p-1} - x_p - HW v_p) + k_2 (v_{p-1} - v_p) \quad (70)$$

where a_p represents the acceleration of the p -th vehicle; k_1 and k_2 denote the ACC model coefficients. The values of $k_1 = 0.23 \text{ s}^{-2}$ and $k_2 = 0.07 \text{ s}^{-2}$ are used on the basis of the field experimental data (Milanés and Shladover 2014).

Based on the estimated acceleration rate of the leading vehicle, its speed and position are updated using the following equations:

$$v_p = v_{p\text{-prev}} + a_p \Delta t \quad (71)$$

$$x_p = x_{p\text{-prev}} + v_p \Delta t + \frac{a_p \Delta t^2}{2} \quad (72)$$

3.5.3. Platoon Control

According to the platoon formation strategy in Rahman and Abdel-Aty (2017), the platoon control framework used in this study is shown in Figure 3.10.

The framework depicted in Figure 3.10 contains two parts – maintaining a platoon and forming a platoon. If a CAV is already in a platoon, and such vehicle will not change its lane. Based on the leading vehicle's traveling information collected via V2V, the vehicle's speed will be computed by using Eq. (67) and Eq. (68).

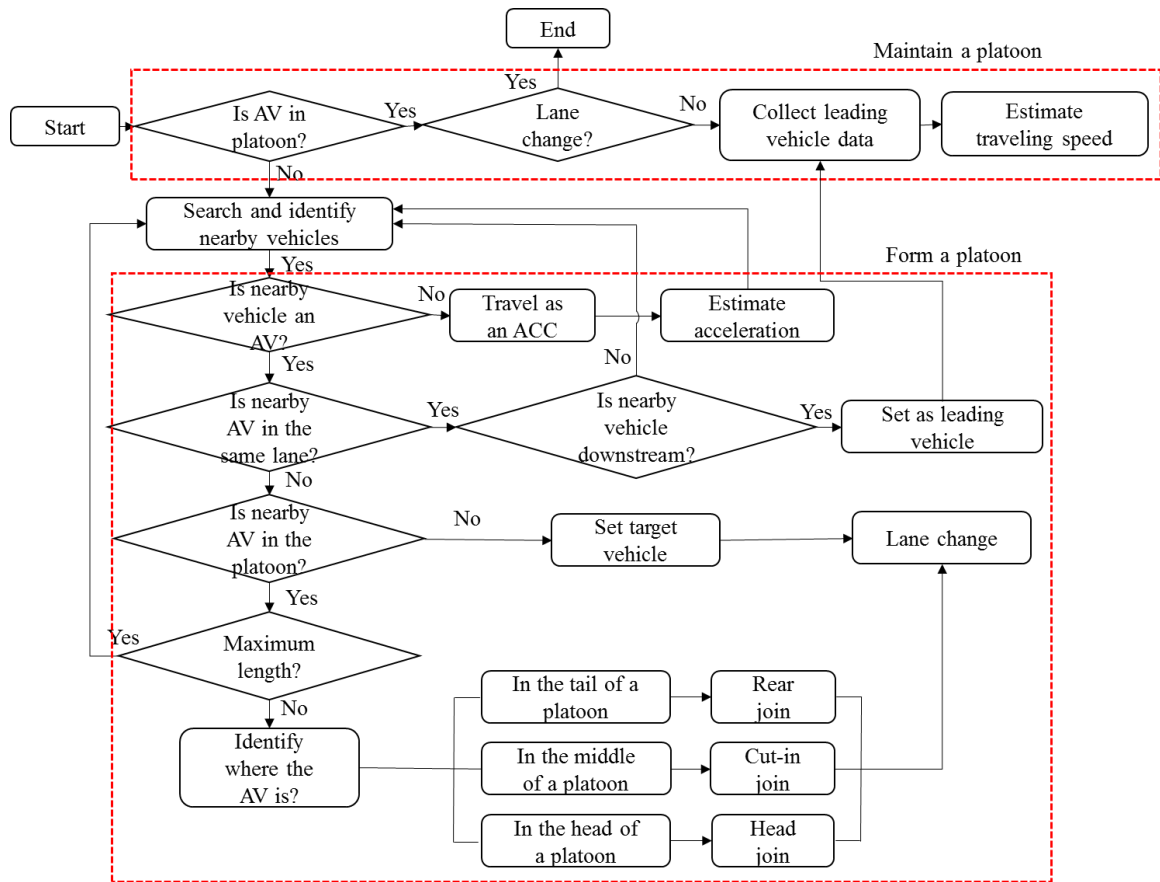


FIGURE 3.10: Control Framework for CAVs to Form and Maintain Platoons

For the vehicles that are not in a platoon, to join a platoon, the CAV searches and identifies the vehicles in the adjacent left and right two lanes. The following situations are discussed:

(1). If all the adjacent vehicles are not CAVs, the current CAV will travel as a regular AV, whose headway will be less than human-driven vehicles. The acceleration rate of the vehicle is estimated by Eq. (70).

(2). If the current vehicle and its front vehicle are traveling in the same lane, and the front vehicle is a CAV, the current vehicle sets the front vehicle as the target vehicle. The current vehicle will follow the target vehicle with a smaller headway. If a CAV

traveling in front of the current vehicle is not in the same lane as the current vehicle, the front CAV is set as the target vehicle by the current vehicle. The current vehicle changes (if possible) to the target lane where the target CAV is traveling and follows the target vehicle.

(3). If a CAV platoon is traveling in the adjacent lane (either left lane or right lane) of the current vehicle, to join the platoon, based on the position of the current vehicle, three joining schemes are implemented - rear join, cut-in join, and front join (Rahman and Abdel-Aty 2017). The three joining schemes are depicted in Figure 3.11. After identifying a proper target vehicle, according to the current speed, accelerated rate, and position, the lane changing maneuver will be performed to join a platoon. In order to form a platoon, some CAVs need to change lane after they enter the freeway segment. The lane change behavior of CAVs is manipulated using the lane changing model of VISSIM (Rahman and Abdel-Aty 2017).

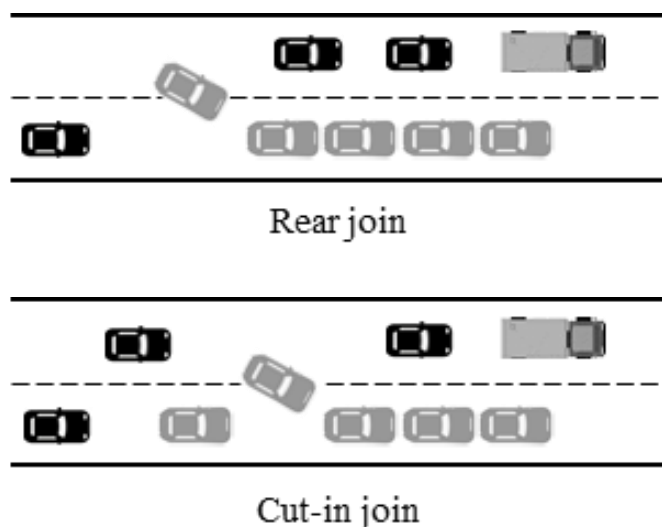


FIGURE 3.11: Illustration of a CAV That Joins to Form a Platoon on the Freeway

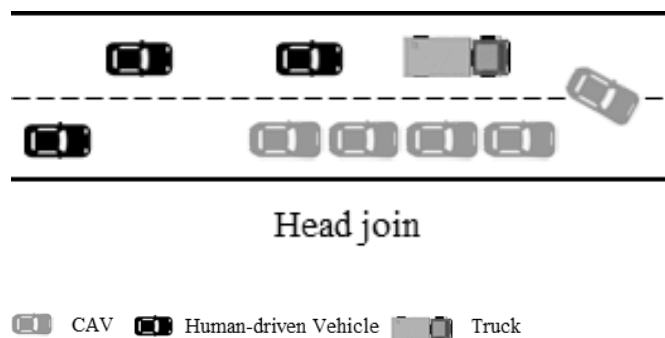


FIGURE 3.11, continued

For the vehicles in a platoon, the smallest headway is employed, i.e.,

$HW_{\text{platoon}} = 0.6s$, which is smaller than the headway of the leading vehicle of the platoon,

i.e., $HW_{AV} = 1.1s$, as shown in Figure 3.12.

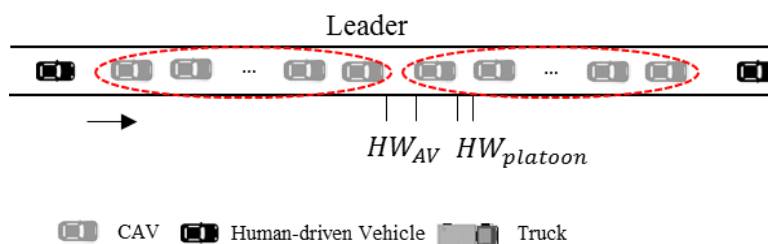


FIGURE 3.12: Illustration of the Headways of CAVs

It should be noted that the car-following model used was developed based on four cars and examined under the scenario of ten cars (Milanés and Shladover 2014). In addition, a larger number of vehicles in a platoon increases the distance between the first and last following vehicle, which might result in a larger response delay (Shladover et al. 2012). Thus, in this study, the maximum number of passenger cars in a platoon is limited to ten vehicles, and the minimum number of vehicles to maintain a platoon is set as 4. If

the length of platoon is 10, the platoon is not allowed to join. The lane changing behavior of the human-driven vehicles is suggested by VISSIM. The platoon control of CAVs is implemented as Dynamic Link Library (DLL), which is written in C++.

3.6. VSL Control for Multiple Bottlenecks

To the best of current knowledge, it is well noted that only a few researchers have developed VSL control strategies for multiple bottlenecks (Iordanidou et al. 2015; Lu et al. 2015). For example, Iordanidou et al. (2015) proposed the MTFC for multiple bottlenecks based on the local feedback theory. The most critical bottleneck was identified and employed to determine the overall MTFC action. Lu et al. (2015) also adopted the local feedback theory to relieve the congestion for a freeway corridor with multiple bottlenecks. The measured speeds at the bottlenecks were used to determine the speed limit values. Since the maximum discharge rate at each bottleneck might be different, whether or not the downstream bottleneck is able to receive the upstream volume that it is optimized by the VSL control, can greatly determine the overall control performance. According to the discussions in Lu et al.'s (2015) research, the following five situations are discussed:

(1). If the upstream bottleneck's maximum discharge volume Q_u equals downstream bottleneck's bottleneck capacity Q_d , i.e., $Q_u = Q_d$, as pointed by Lu et al. (2015), this is an ideal case for operation. Through a VSL control system, the congestion at each bottleneck can be effectively relieved.

(2). If $Q_u > Q_d$, and the cells between the upstream and downstream bottlenecks are filled up at a certain period, as shown in Figure 3.13(a). The critical volume of the

upstream and downstream bottlenecks is $Q_{\text{critical}} = \min(Q_u, Q_d) = Q_d$. In this case, a constraint should be added to guarantee that the controlled volume $Q_{VSL,u}(k)$ flowing out of the upstream bottleneck is less than or equal to the critical volume, i.e.,

$Q_{VSL,u}(k) = \min(q_u, Q_{\text{critical}})$, where q_u is the volume that flows out of the upstream

bottleneck. Under this situation, a VSL control system is deployed in this study, as shown in Figure 3.13(a).

(3). If $Q_u > Q_d$, but the cells between the two bottlenecks are not filled up even after a long period of time (see Figure 3.13(b)). In such situation, no extra constraints are needed to be added to the traffic volume flowing out of the upstream bottleneck. In this study, two VSL control systems are implemented at each bottleneck, respectively (see Figure 3.13(b))

(4). If $Q_u < Q_d$, but the cells between the upstream and downstream bottlenecks are filled up at a certain period. Figure 3.13(c) depicts an example to illustrate this situation. When the traffic demand $r_u(k)$ at the on-ramp located upstream of the downstream bottleneck is greater than $Q_d - Q_u$, a queue spillover might be formed to the upstream bottleneck. The queue further blocks the on-ramp vehicles. In this case, a constraint is added to control the volume flowing out of the upstream bottleneck, i.e.,

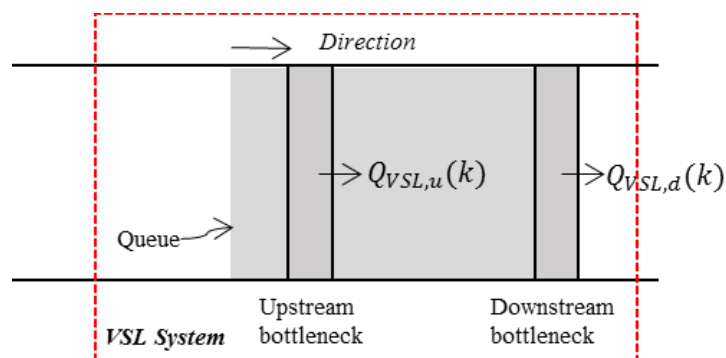
$Q_{VSL,u}(k) = \min(q_u, Q_d - r_u(k))$. Note that, such situation can also be addressed by using

ramp metering, and the demand from the on-ramp after control should satisfy

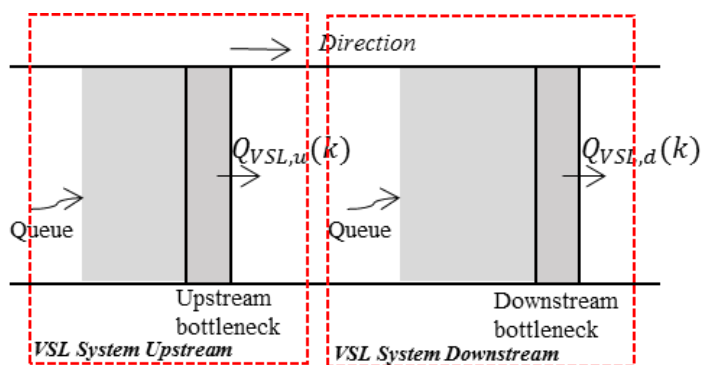
$\min(r_u(k), Q_d - Q_u)$. However, the ramp metering is beyond discussion in this study. In

this situation, a VSL system that simultaneously controls the upstream and downstream bottlenecks is deployed, as shown in Figure 3.13(c).

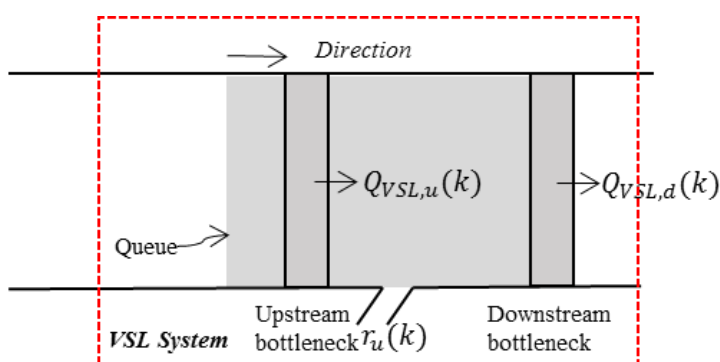
(5). If $Q_u < Q_d$, and the cells between the two bottlenecks are not filled up. Such situation is similar to situation 3.



(a) Situation 2: $Q_u > Q_d$



(b) Situation 3: $Q_u > Q_d$



(c) Situation 4: $Q_u < Q_d$

FIGURE 3.13: An Illustration of Multiple Bottlenecks under Different Conditions

When solving real-world case studies, the above five situations should be well checked to determine the critical volume. Some particular scenarios might exist. In Figure 3.13(c), for example, if $Q_u = Q_d$ and on-ramp demand $r_u(k)$ is greater than zero, the critical volume will be $Q_d - r_u(k)$ under this scenario.

3.7. Integrated Control System

To develop an integrated control system, the V2V, V2I and I2V communication are incorporated into the VSL control. At a time interval k , the VSL controller predicts traffic state on cell i during $k+1$ time period using the traffic data collected through loop detectors during time interval k . The optimized speed limits set can be obtained by using the developed optimization algorithm.

In the integrated control system, the detailed traffic data of the AVs can be collected through the V2I communication. The speed limits which are displayed on the VMS will be determined on the basis of the optimized and collected average speeds of AVs (Khondaker and Kattan 2015b; Hale et al. 2016). In this study, the method developed by Khondaker and Kattan (2015b) is employed. The displayed speed limit on cell i during time interval k is computed using Eq. (73) and (74).

$$u_i^{\text{dis}}(k) = (1 + \alpha_i(k)) * u_i(k) \quad (73)$$

$$\alpha_i(k) = \frac{v_{i,AV}(k-1) - u_i(k-1)}{u_i(k-1)} \quad (74)$$

where $v_{i,AV}(k-1)$ is the collected average speeds of AVs on cell i during time interval $k-1$; $u_i^{\text{dis}}(k)$ is the displayed speed limit on cell i during time interval k ; $u_i(k)$ is

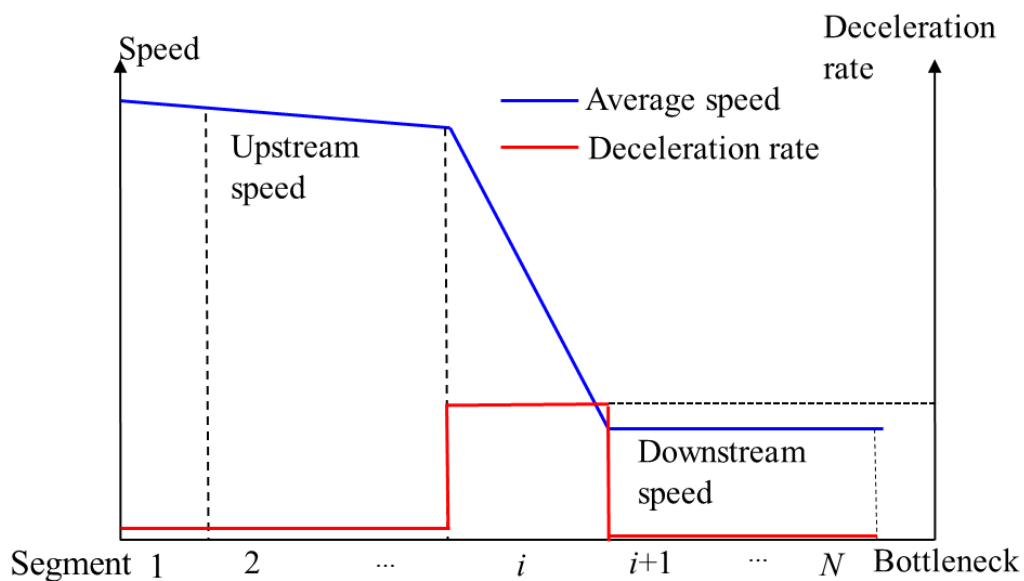
the optimized speed limit on cell i during time interval k ; $\alpha_i(k)$ is the relative difference between the traveling speed and displayed speed limit.

The speed limit information is sent to all the AVs directly through the I2V communication. The transmission distance is determined by the range of wireless communication media (Shladover et al. 2015). It is assumed that the transmission between the control signals and AV is via DSRC, and its communication range is about 656ft (i.e., about 200m) (Wang et al. 2016). The AVs receive the speed limits information, and these vehicles will pass the VSL signs at a speed in line with the displayed speed limit. Note that, the communication delay is not considered in this study. The human-driven vehicles (e.g., cars and trucks) read the speed limit information when they pass the VSL signs. Human-driven vehicles respond differently to the posted speed limit. Some drives may follow the speed limit, while others may not. However, all CAVs will follow the optimized speed limit homogeneously. As all the vehicles on the freeway are traveling under the updated speed limits, the aggregate traffic state of a cell changes accordingly. The updated traffic state data will then be collected and sent to the VSL controller for the next control horizon.

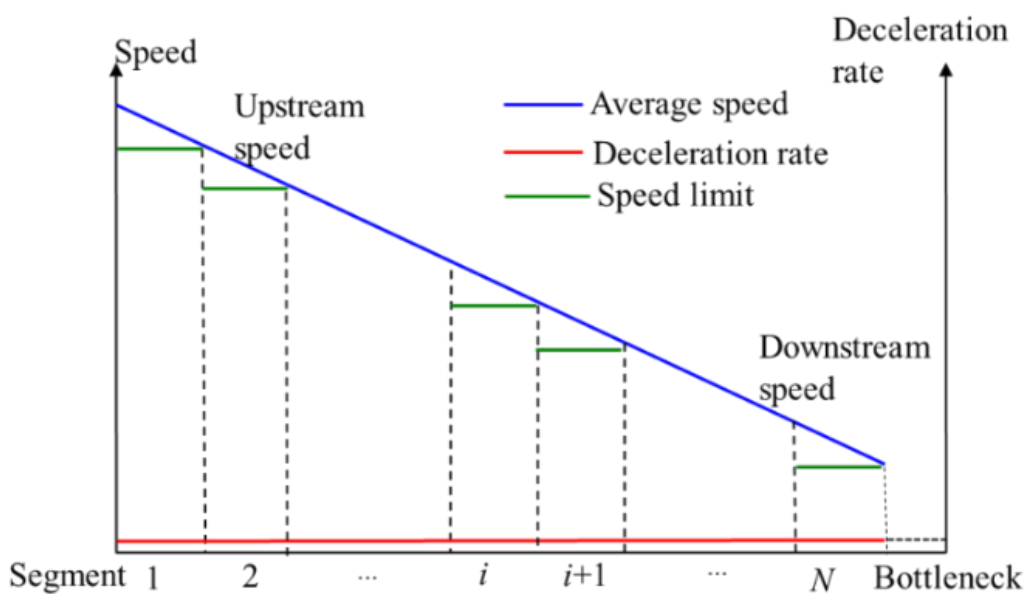
3.8. Objective Function and Constraints

To improve the operational efficiency and the level of safety for the vehicles traveling upstream of and at the bottlenecks, different types of objective functions have been developed when formulating the VSL control models. The objective function used includes minimizing TTT, TSV, TTD, or minimizing TTC. Among these objective functions, minimizing TTT has been widely used to improve the operational efficiency at

the recurrent and non-recurrent bottlenecks, and therefore, the TTT will be included as part of the objective function in this study. In addition, minimizing TSV is also accounted for in the objective function to smooth the speed transition. Queue forms and accumulates fast at the bottleneck when traffic demand is greater than the bottleneck capacity. The discharge volume at the lane drop bottleneck will be greatly reduced. In Figure 3.14, the traveling speeds and deceleration rate are presented. Generally, the speeds in the vicinity of the bottleneck are much less than the upstream speeds, and the vehicles traveling from the upstream might have to decelerate quickly in a very short time at some point (e.g., on segment i) before arriving the bottleneck. Such phenomenon can result in a very high deceleration rate on segment i . In summary, the speed variations between the upstream segments and downstream segments around the bottleneck are huge, which can significantly increase the possibility of rear-end collisions. In this regard, smoothing the speed transition from upstream to downstream and decreasing the deceleration rate should be explicitly accounted for in the VSL control model. According to Yang et al. (2017), Figure 3.14(b) presents an ideal condition of the VSL control. With VSL control, vehicles in both the TR and NTR lanes traveling from the upstream can gradually slow down. A constant and low deceleration rate can be maintained before they arrive at the bottleneck due to the VSL control. As such, the speed variations will be significantly reduced and the level of safety can be greatly improved. In addition, to minimize the difference between the posted speed limits on each controlled segments and the speeds of cars and trucks, minimizing the TSD will also be included as part of the objective function in this study.



(a) Speed and Deceleration Rate without VSL



(b) Speed and Deceleration Rate with VSL

FIGURE 3.14: Speed and Deceleration Rate with and without VSL Control

3.8.1. VSL Control for Relieving Congestion at A Lane Drop Bottleneck

As discussed, the objective of the proposed VSL control is to minimize the travel time and the total speed variation for the studied freeway stretch. However, it is well noticed that the unit of total travel time (i.e., hours) and that of the total speed variation (i.e., miles/hour) are different. The two terms cannot be directly measured on the same scale. Such two terms need to be converted to monetary values by introducing two parameters, i.e., VTT (value of travel time) and VSV (value of speed variation). The objective function is presented as follows:

min

$$\begin{aligned}
 J = & w_1 VTT \sum_{k=1}^{T_p} \sum_{i=1}^N (T \rho_i(k) l_i) \\
 & + w_2 VSV \sum_{k=1}^{T_p} \sum_{i=1}^N \left| u_i(k) - \left(\frac{N-i}{N} v_0(k) + \frac{i}{N} v_N(k) \right) \right|
 \end{aligned} \tag{75}$$

The first term of the objective function is the total value of travel time which is computed by multiplying *VTT* by the total travel time incurred by all vehicles within the studied freeway segments (including controlled segments and non-controlled segments).

The total travel time is computed by $\sum_{k=1}^{T_p} \sum_{i=1}^N (T \rho_i(k) l_i)$ which can be used to reflect the control efficiency.

The second part represents the total value of speed variation which is computed by the total speed variation times the *VSV*. Note that the total speed variation itself is measured by the difference between the speed limits (including VSL on the controlled freeway segments and uncontrolled speed limits upstream of the controlled segments) and real speeds on all controlled and uncontrolled freeway segments. The main purpose

of taking the total speed variation into account is to harmonize the upstream speeds and speeds at the bottleneck.

The uncontrolled segments are included in the objective function because such segments upstream of the controlled ones also contain many vehicles which might be more or less affected due to the VSL control. Note that in Eq. (75), if no VSL is implemented on segment i , then $u_i(k) = v_f$. In addition, $v_0(k)$ and $v_N(k)$ are the speeds detected from the most upstream and downstream detectors during time interval k , respectively.

Furthermore, w_1 and w_2 are introduced to reflect the trade-offs between the total value of travel time and total value of speed variation. It should be pointed out that the two weights may be dependent upon the researchers' experience and/or engineering judgment. Different settings for these two weights might result in a different optimal set of VSLs using the developed solution methodology. However, a reasonable optimal set of VSLs can always be obtained, once a specific weight set is assigned for the total value of travel time and total value of speed variation.

In order to guarantee the drivers' safety, the following constraints are also introduced:

C1: To guarantee drivers' safety and the operating efficiency on the subject freeway segments, all $u_i(k)$ should be less than a maximum value but greater than a minimum value ($v_{\min} \leq u_i(k) \leq v_f$). Hence, $u_i(k)$ is a discrete value which belongs to a set $V = \{15, 20, 25, 30, 35, 40, 45, 50, 55, 60, 65, 70 \text{ miles/h}\}$.

C2: To ensure the safety of operation of VSL control, the change in speeds between two consecutive time steps and two consecutive controlled segments should be limited by a pre-specified value (i.e., 10 miles/h):

(a): speed difference between two consecutive time steps on the same segment i

$$|u_i(k+1) - u_i(k)| \leq 10 \quad (76)$$

(b): speed difference between two consecutive control segments during the same time interval k

$$|u_i(k) - u_{i-1}(k)| \leq 10 \quad (77)$$

C3: With the VSL control, the bottleneck discharge volume should be improved in that the discharge volume flowing out of the last controlled segment (i.e., segment N in FIGURE 3.1.) should be less or equal to the maximum discharge volume at the bottleneck:

$$q_N(k) \leq C \quad (78)$$

3.8.2. VSL Control for Mixed Traffic Flows

The objective of this section is to minimize the TTT, TSV between the speed limit and the most upstream and most downstream speeds, and the TSD between the speed limit and effective speeds on the controlled segments. The objective function and constraints are given as follows:

min

$$\begin{aligned}
J = & w_1 T \sum_{k=1}^{T_p} \sum_{i=1}^N \sum_{j=1}^J (\eta_{i,j}(k) \rho_{i,j}(k) L_i) \\
& + w_2 \sum_{k=1}^{T_p} \sum_{i=1}^N \left| u_i(k) - \left(\frac{N-i}{N} \sum_{j=1}^J \phi_j v_{0,j}(k) + \frac{i}{N} \sum_{j=1}^J \phi_j v_{N,j}(k) \right) \right| \\
& + w_3 \sum_{k=1}^{T_p} \sum_{i=N-N_c+1}^N |u_i(k) - Ev_i(k)|
\end{aligned} \tag{79}$$

Subject to

$$v_{\min} \leq u_i(k) \leq v_{\max} \tag{80}$$

$$|u_i(k+1) - u_i(k)| \leq 10 \tag{81}$$

$$|u_i(k) - u_{i-1}(k)| \leq 10 \tag{82}$$

$$Eq_N(k) = \sum_{j=1}^J \eta_{N,j}(k) q_{N,j}(k) \leq C_{dis}(k) \tag{83}$$

$$\begin{aligned}
u_i(k) \text{ is a discrete value } V = \{15, 20, 25, 30, 35, 40, 45, 50, 55, 60, 65, \\
70 \text{ miles/h}\}
\end{aligned} \tag{84}$$

The first term of the objective function is the TTT spent by all the vehicles within the N studied freeway segments, which is used to ensure the efficiency of the VSL control. The second part is the TSV between speed limits on segment i and real speeds of vehicle type j detected from the most upstream and most downstream detectors. It should be noted that, for the second part of Eq. (79), if there is no VSL on segment i , $u_i(k)$ equals the maximum speed limit, i.e., 70 miles/h. $v_{0,j}(k)$ and $v_{N,j}(k)$ in Eq. (77) are the speeds of vehicle type j detected from the most upstream and downstream detectors during time interval k , respectively. The third part is the TSD between the speed limit

displayed on the controlled segment i and the effective speed on the controlled segment i . The second and the third part can be used to ensure the safe operations of VSL control. The uncontrolled segments are included in the objective function because the vehicles on such segments upstream of the controlled segments might be affected due to the VSL. w_1 , w_2 , and w_3 are introduced to reflect the trade-offs between the TTT, TSV, and TSD, making the VSL control problem a multi-objective optimization problem. Different settings for w_1 , w_2 , and w_3 might result in a different optimal speed limit set at each time interval. Once a specific weight set is given by the researchers for the TTT, TSV, and TSD, an optimal speed limit set during each control time interval on the studied freeway segment can be obtained and identified.

Constraint (80) is used to guarantee the drivers' safety as well as the operating efficiency. All $u_i(k)$ should be less than a predefined maximum value v_{\max} but greater than a predefined minimum value v_{\min} , i.e. $v_{\min} \leq u_i(k) \leq v_{\max}$.

Constraint (81) and (82) ensure the safe operation of the VSL control. The change in speeds between two consecutive time steps on the same segment and two consecutive controlled segments at the same time interval should be limited by a pre-specified value (i.e. 10 miles/h).

Constraint (83) is used to improve the bottleneck discharge volume, i.e. through the VSL control, the volume of effective flow that flows out of the last controlled segment at every time interval k should be less or equal to the maximum discharge volume of the bottleneck at time interval k , i.e. $C_{dis}(k)$.

Only discrete speed limit can be displayed on the VMS, and the last constraint gives all the possible speed limit values of $u_i(k)$, $V = \{15, 20, 25, 30, 35, 40, 45, 50, 55, 60, 65, 70 \text{ miles/h}\}$

3.8.3. VSL Control and Lane Truck Restriction Policy

As discussed, the objective of the combined VSL control is to minimize the TTT, TSD, and TSV which can be estimated by the following equations.

$$TTT = T \sum_{k=1}^{T_p} \sum_{i=1}^N \left(\lambda_i^{\text{TR}} l_i \rho_i^{\text{TR}}(k) + \sum_{j=1}^J \lambda_i^{\text{NTR}} l_i \rho_{i,j}^{\text{NTR}}(k) + w_{i,j}(k+1) \right) \quad (85)$$

$$TSD = \sum_{k=1}^{T_p} \sum_{i=N-N_c+1}^N \left| u_i(k) - \left(\frac{\lambda_i^{\text{TR}}}{\lambda_i} v_i^{\text{TR}}(k) + \frac{\lambda_i^{\text{NTR}}}{\lambda_i} E v_i^{\text{NTR}}(k) \right) \right| \quad (86)$$

$$TSV = \sum_{k=1}^{T_p} \sum_{i=1}^N \left| u_i(k) - \left(\frac{N-i}{N} \left(\frac{\lambda_i^{\text{TR}}}{\lambda_i} v_1^{\text{TR}}(k) + \frac{\lambda_i^{\text{NTR}}}{\lambda_i} E v_1^{\text{NTR}}(k) \right) + \frac{i}{N} \left(\frac{\lambda_i^{\text{TR}}}{\lambda_i} v_N^{\text{TR}}(k) + \frac{\lambda_i^{\text{NTR}}}{\lambda_i} E v_N^{\text{NTR}}(k) \right) \right| \right| \quad (87)$$

Eq. (85) is the TTT spent by all the vehicles in the TR and NTR lanes on all the segments. The TTT is used to ensure the efficiency of the VSL control.

Eq. (86) is the TSD between the speed limits and the sum of weighted speeds in the TR lanes and effective speeds in the NTR lanes on the controlled segment i .

Eq. (87) is the TSV between speed limits on segment i and speeds on the most upstream and most downstream segments in the TR lanes and NTR lanes, respectively. For Eq. (86) and Eq. (87), if there is no VSL on segment i , $u_i(k)$ equals the maximum speed limit, i.e., 70 mi/h. $v_1^{\text{TR}}(k)$ and $v_N^{\text{TR}}(k)$ in (87) are the speeds on the first and most

downstream segments during time interval k in the TR lanes. $E_{v_1}^{\text{NTR}}(k)$ and $E_{v_N}^{\text{NTR}}(k)$ in (87) are the equilibrium speeds on the first and last segments during time interval k in the NTR lanes, respectively.

According to Eq. (85) – Eq. (87), the following objective function is used

min

$$J = - \left(w_1 \frac{TTT_{\text{NO}} - TTT_{\text{VSL}}}{TTT_{\text{NO}}} + w_2 \frac{TSD_{\text{NO}} - TSD_{\text{VSL}}}{TSD_{\text{NO}}} + w_3 \frac{TSV_{\text{NO}} - TSV_{\text{VSL}}}{TSV_{\text{NO}}} \right) \quad (88)$$

Subject to

$$v_{\min} \leq u_i(k) \leq v_{\max} \quad (89)$$

$$|u_i(k+1) - u_i(k)| \leq 10 \quad (90)$$

$$|u_i(k) - u_{i-1}(k)| \leq 10 \quad (91)$$

$$q_N(k) = \lambda_N^{\text{TR}} q_N^{\text{TR}}(k) + \lambda_N^{\text{NTR}} E q_N^{\text{NTR}}(k) \leq \lambda_{\text{bottleneck}} Q_b \quad (92)$$

$$u_i(k) \text{ is a discrete value, } u_i(k) \in V,$$

$$V = \{15, 20, 25, 30, 35, 40, 45, 50, 55, 60, 65, 70 \text{ miles/h}\}$$

In Eq. (88), TTT_{NO} , TSD_{NO} , and TSV_{NO} are the TTT, TSD, and TSV without VSL control, respectively. The uncontrolled segments (i.e., from segment 1 to segment $N - N_c$ in this study) are also included. w_1 , w_2 , and w_3 are introduced to reflect the trade-off between the TTT, TSD, and TSV.

3.8.4. VSL Control in a CAV Environment

In order to efficiently improve the mobility and suppress shock waves for the freeway with multiple bottlenecks, more than one VSL control system might need to be

implemented. For convenience of illustration, the notations related to the VSL control systems are given as follows: Let the total number of VSL control systems implemented on the selected freeway stretch be S . In the s -th VSL control system, the number of cells is N_s , and $\sum_{s=1}^S N_s = N$. Suppose that cell i is in the s -th VSL control system,

$$vsl_{s-1} < i \leq vsl_s, \text{ and } vsl_s = N_1 + N_2 + \dots + N_s.$$

As the main indicator for evaluating the operational efficiency, minimizing TTT spent by all types of vehicles in a highway network has been widely adopted when developing a VSL control strategy, which is also included as a part of the objective function in this study to ensure the overall efficiency. Furthermore, to smooth the speed transmission from the most upstream to the most downstream cell and decrease the deceleration rate in a VSL control system (Yang et al. 2017), minimizing TSV is also explicitly accounted for in this study. The objective function and constraints are given as follows.

min

$$\begin{aligned} J = & w_1 T \sum_{k=1}^{T_p} \sum_{i=1}^N \sum_{j=1}^J \rho_{i,j}(k) l_i \\ & + w_2 \sum_{j=1}^J \sum_{k=1}^{T_p} \sum_{s=1}^S \sum_{i=vsl_{s-1}+1}^{vsl_s} \left[u_i(k) - \left(\frac{vsl_s - i}{N_s} v_{vsl_{s-1},j}(k) + \frac{i - vsl_{s-1}}{N_s} v_{vsl_s,j}(k) \right) \right] \\ & + \sum_{s=1}^{S-1} \left(u_{vsl_s}(k) - u_{vsl_{s+1}}(k) \right)^2 \end{aligned} \quad (93)$$

Subject to

$$v_{\min} \leq u_i(k) \leq v_{\max} \quad (94)$$

$$|u_i(k+1) - u_i(k)| \leq 10 \quad (95)$$

$$|u_i(k) - u_{i-1}(k)| \leq 10, vsl_{s-1} < i \text{ and } i-1 \leq vsl_s \quad (96)$$

$$u_i(k) \in V, V = \{15, 20, 25, 30, 35, 40, 45, 50, 55, 60, 65, 70 \text{ mph}\}$$

The first term of the objective function is the TTT spent by all types of vehicles on the studied freeway corridor. The second term is the speed variation between speed limits on cell i and the traveling speeds of vehicle type j on the most upstream and most downstream cells of the s -th control system. The third term is a penalty function used to ensure that the speed differences between two consecutive cells that are not in a same VSL control system will not be too large so that the safe operation of the overall VSL control can be guaranteed. Note that, in Eq. (95), if no VSL is implemented on cell i , then $u_i(k) = v_{j,m,f}$. In the objective function, w_1 and w_2 are introduced to reflect the trade-offs between the TTT and TSV.

3.9. Summary

This chapter describes the VSL control model used in this study. Based on the METANET and CTM, the VSL control models for mixed traffic flows are developed. In addition, the car-following models (including the IDM and PATH model) of the CAV is presented in this chapter as well. Different objective functions are formulated for different VSL control strategies to improve the operational efficiency and safety.

CHAPTER 4: PROPOSED SOLUTION ALGORITHMS

4.1. Introduction

Typically, the VSL control is formulated as a discrete-time constrained non-linear optimal control problem. The formulated optimal control problems relying on the macroscopic second-order (e.g., METANET) and first-order mode (e.g., CTM) are often nonlinear and nonconvex, which are hard to solve (Pasquale et al. 2016). In order to efficiently solve these problems, some solution algorithms (including feasible direction algorithm (FDA) and SQP algorithm) have been adopted. One of the approaches is the AMOC which was developed based on the FDA (Carlson et al. 2010a, 2010b; Roncoli et al. 2015; Pasquale et al. 2015; Kotsialos et al. 2002, 2004). Such approach can be used to solve the control problem efficiently even for complicated ones. For example, the AMOC was employed in Carlson et al. (2010b), in which a large-scale motorway network was used and tested. Pasquale et al. (2015) adopted the AMOC to solve a complicated problem. Two types of vehicles were considered, and the objective was to reduce freeway emissions and congestion. In addition, Hegyi et al. (2005) proved that the SQP could help achieve good quality solutions for such problems as well. However, both the FDA and SQP belong to the gradient-based algorithms. Even though the gradient-based algorithms are efficient for solving nonlinear optimization, such algorithms might be time-consuming or sometimes cannot even obtain feasible solutions if the objective function is not differentiable or is actually discontinuous (Pasquale et al. 2016). Thus, the derivative-free optimization algorithms (e.g., GA and TS), which have been adopted in many

transportation research fields, such as transit network optimization (Fan and Machemehl 2006; Fan and Machemehl 2008), decision on congestion pricing (Fan and Gurmu 2014), and calibration of microscopic traffic simulation models (Yu and Fan 2017), can also be used to solve such control problems. Some researchers have already developed, tested and compared the derivative-free algorithms with the FDA. For instance, Pasquale et al. (2016) compared the solution quality of SA and global optimization (GO) algorithm with the FDA. The comparison results demonstrated that the gradient-free algorithms provided good quality but less efficient solutions, and the FDA computed efficient solutions but with long implementation time.

In this chapter, because of the discrete speed limit values during every control time period, discrete optimization algorithms are adopted to solve the VSL control models that have been developed in chapter 3. Since the SQP has been used and verified by Hegyi et al. (2005) which could help achieve acceptable solutions, the SQP is chosen as the benchmark to examine the solution quality of the proposed discrete optimization algorithms used in this research. Two heuristic algorithms, i.e., TS algorithm and GA, are used and presented in this chapter.

This rest of this chapter is organized as follows. Section 4.2 presents the SQP-based solution framework for the VSL control. Section 4.3 describes how tabu search algorithm is adopted to solve the VSL control. Section 4.4 shows the genetic algorithm based solution framework for the VSL control. Finally, in section 4.5, a summary concludes this chapter.

4.2. Sequential Quadratic Programming (SQP)

SQP is one of the most successful numerical solution methods for the constrained nonlinear optimization problems. The method generates steps by solving quadratic sub-problems. SQP is appropriate for solving small and large problems and is well-suited to solving problems with significant nonlinearities.

The SQP aims to solve the nonlinear programming problem

$$\min J(u)$$

subject to

$$\phi(u) = 0$$

$$\psi(u) \leq 0$$

where u is the vector of optimization variables, $J(u)$ means the objective function, $\phi(u)$ denotes the vector of nonlinear equality constraints, and $\psi(u)$ represents the vector of nonlinear inequality constraints.

The SQP algorithm can be viewed as a generalization of Newton's method for unconstrained optimization in that it finds a step away from the current point by minimizing a quadratic model of the problem. Several software packages including MATLAB are based on this algorithm. The SQP algorithm replaces the objective function with the quadratic approximation $\nabla f(x_k)^T d + \frac{1}{2} d^T \nabla_{xx}^2 L(x_k, \lambda_k) d$ and replaces the constrained functions by linear approximations. The detailed information of about the SQP algorithm can be referred to Fletcher (2007). The flow chart of the SQP is shown in Figure 4.1. It should be noted that the solutions achieved by the SQP might not be

discrete values for the VSL control problems. Therefore, such speed limit solutions are rounded to nearest five so that the solutions/values achieved can be displayed on the variable message signs in the real world.

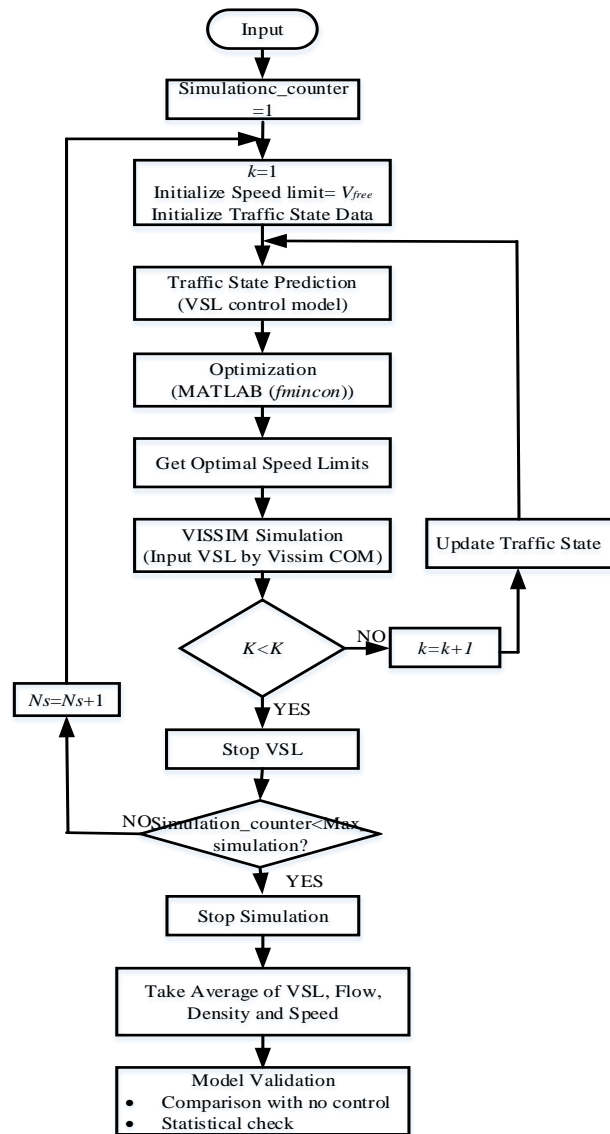


FIGURE 4.1: SQP Based Solution Framework for the VSL Control

4.3. Tabu Search Algorithm

The introduction and formulation of the tabu search method draw mainly on the theoretical work from Glover (Glover 1986; Glover 1990). Tabu search explores the new solutions by moving from one solution to another with the best objective function in its neighborhood at each iteration. The process should continue until the stopping criterion has been satisfied. Moreover, Tabu search memorizes a list of tabu candidate solutions. These candidate solutions will not be repeated in the subsequent iterations and the list will be updated at each iteration. The new candidate solution is accepted if it has not previously been memorized as tabu or even if it is an undesirable candidate solution.

Let the set $S(x)$ define a “neighborhood function” which consists of the moves from the current solution to a next trial solution. Let T denote a subset of S which contains elements that are called “tabu moves”. “OPTIMUM” denotes the objective function evaluator. On the basis of the work by Glover (1989), a procedure of TS can be described as follows:

Step 1. Select an initial $x \in X$ and let $x^* := x$.

Set the iteration counter $k = 0$

Begin with $T = \emptyset$.

Step 2. If $S(x) - T$ is empty, go to step 4.

Otherwise, set $k := k + 1$

Select $s_k \in S(x) - T$ such that $s_k(x) = \text{OPTIMUM}(s(x) : s \in S(x) - T)$.

Step 3. Let $x := s_k(x)$.

If $c(x) < c(x^*)$, where x^* denotes the best solution currently found, let $x^* := x$.

Step 4. If the number of iterations k has reached the maximum number of iterations or since x^* was last improved, or if $S(x) - T = \emptyset$ upon reaching this step directly from Step 2, stop.

Otherwise, update T and return to Step 2.

The advantage of TS is in its incorporation of adaptive memory and responsive exploration. It explores local minima and at the same time it has a strategy to explore new areas of solution space.

Tabu search is employed as the candidate solution technique to solve the VSL control problems because it has been proven to have the capability of providing a robust search as well as a near optimal solution in a reasonable time in other transportation fields (Fan and Machemehl 2008). A systematic description for the tabu search-based implementation model for the VSL control strategy is presented in the following sections.

4.3.1. Solution Representation

At any time interval k , the total number of freeway segments is N , and the number of segments with VSL is N_c . A candidate set of VSL controls during time interval k on the controlled segments can be represented by $U(k) = [u_{N-N_c+1}(k) \dots u_i(k) \dots u_N(k)]$, where $u_i(k)$ denotes the value of speed limit on the i -th freeway segment with VSL control during time interval k .

4.3.2. Initial Solution

When the time interval k equals 1, the initial solution for the tabu search algorithm is set as the free flow speed $U_{\text{initial}}(1) = \underbrace{[v_f, v_f, \dots, v_f]}_{N_c}$. Based on this initial solution, the optimal VSL solution set $U_{\text{optimal}}(1)$ will be obtained during the first time interval. At the second time interval, this optimal VSL solution set $U_{\text{optimal}}(1)$ will be used and set as another initial solution $U_{\text{initial}}(2)$, which will be used again to obtain the optimal VSL solution set $U_{\text{optimal}}(2)$, and so on. In short, $U_{\text{optimal}}(k)$, the optimal VSL solution set during each following time interval k , is always obtained based on the $U_{\text{initial}}(k)$ that is equal to $U_{\text{optimal}}(k-1)$, the optimal VSL solution set during previous time interval $k-1$.

4.3.3. Neighborhood Structure

It should be noted that how the neighborhood is defined might affect the solution of VSL control, and that only discrete speed limit values can be displayed (e.g., 65 miles/h, 50 miles/h, or 45 miles/h). As such, the move distance for the tabu search is set as 5 miles/h or -5 miles/h. The neighborhood of a feasible speed limit set for the VSL control is obtained by adding the move distance (i.e., 5 miles/h or -5 miles/h) to any of the speed limits in the VSL solution set. Meanwhile, the new solutions in the neighborhood which are obtained by making such moves must satisfy all the constraints as specified in Eq. (76) and (77). For example, at time interval $k-1$, the optimal speed limit set is (60, 55, ..., 35, 25). By adding the move distance, the neighborhood of a

feasible speed limit set for the VSL control at time interval k is obtained with respect to constraints, i.e., **C1** and **C2**. An example of the new first five feasible solutions in the neighborhood at time interval k is

$$\begin{bmatrix} 60, 50, \dots, 30, 20 \\ 60, 60, \dots, 25, 20 \\ 70, 60, \dots, 40, 35 \\ 65, 55, \dots, 35, 25 \\ 55, 50, \dots, 45, 35 \end{bmatrix} .$$

4.3.4. Moves and Tabu Status

At the beginning of the tabu search, i.e., iteration=1, no move is tabu. When iteration is greater than 1, the best non-tabu move will be executed, or a tabu move that generates a better solution will also be implemented. Once a move is performed, the reverse move will be declared tabu.

Figure 4.2 depicts a flow chart that provides the tabu search-based solution framework for the VSL control strategy. The VSL control system consists of four main steps: data collection, traffic state prediction (by using METANET), optimizing variable speed limits (tabu search algorithm), and implementing the optimal speed limits (Yang et al. 2017). The real-time traffic state (e.g., flow, speed and density), will be collected by running simulations using VISSIM. Based on the current traffic state, the METANET model is used to predict the traffic state with respect to the speed limit scheme set (either initialized or optimized in the neighborhood). At the same time, the objective function will be calculated. The local optima will be updated at each iteration. The tabu search algorithm will not stop until the stopping criterion is satisfied. The optimal speed limit scheme will be saved. A MATLAB application program is developed to feed the optimal

speed limit values to VISSIM through the component object model (COM) interface. Furthermore, the VSL control strategy should be developed using several simulation runs in order to best simulate and represent different traffic conditions in the real world. The maximum number of simulation runs (i.e., Max_Simulation in Figure 4.2) equals to 10. After running all the simulations, the average speed limits and traffic state data will be calculated. In addition, MATLAB is chosen as the implementation language in this study.

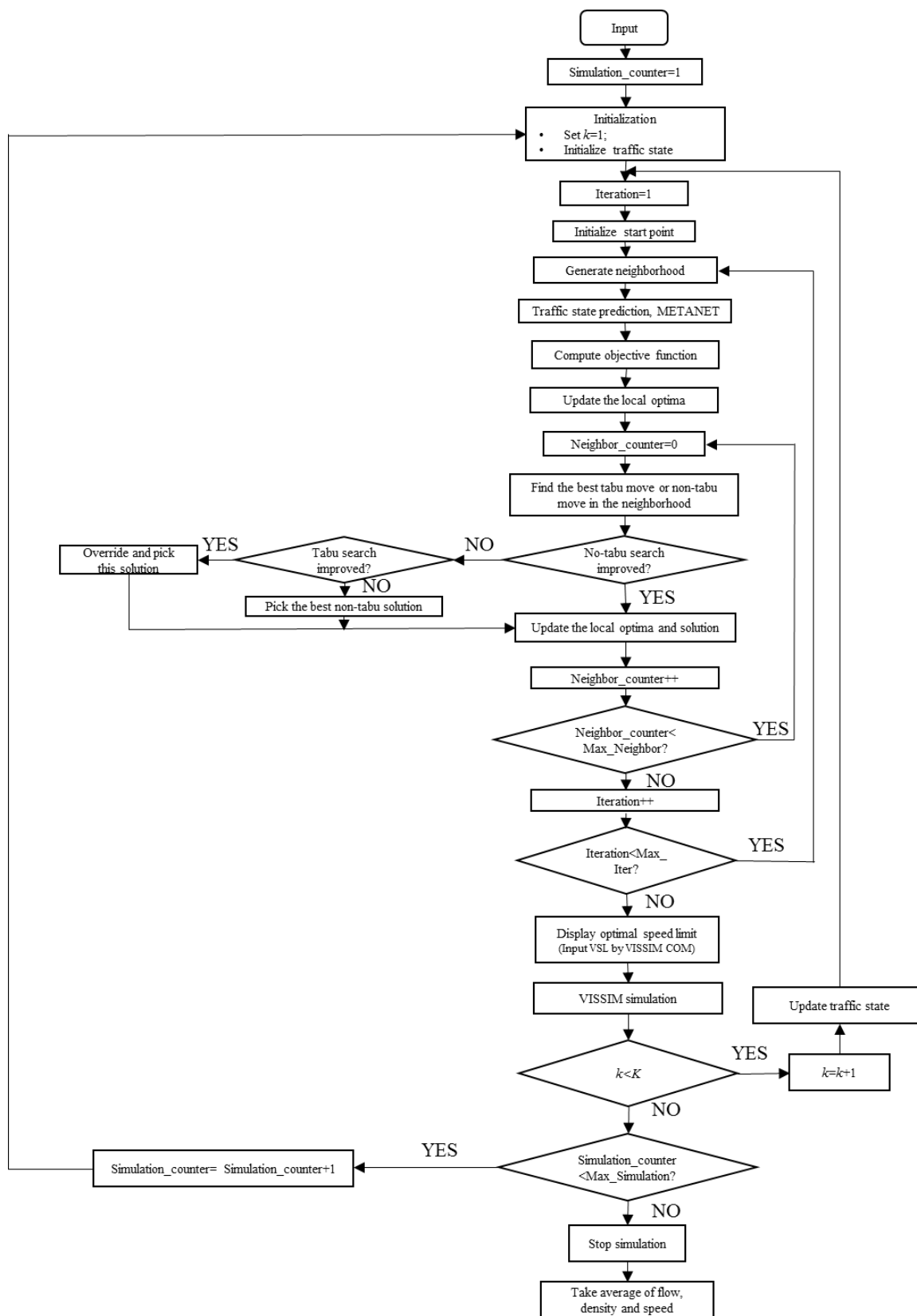


FIGURE 4.2: A Tabu Search Based Solution Framework for the VSL Control

4.4. Genetic Algorithm

GA is a well-known metaheuristic search algorithm for solving constrained or unconstrained optimization problems, which is developed based on biological evolution. GA can help to obtain a near-optimal solution in a reasonable amount of time in the transportation fields, such as network design problems (Fan and Machemehl 2006; Fan and Gurmu 2014) and microscopic traffic simulation model calibration problems (Cheu et al. 1998). The population in GA is evolved by selection, crossover, and mutation. Generally speaking, the GA starts from a random population set, and the objective function value of each individual in the population is evaluated. Not only does GA help to get the optimal speed limit set during the control time period, but it also provides the optimal solutions in terms of discrete speed limit values. As a result, GA is used to optimize the objective function of the VSL control in this study.

The developed VSL control strategy is formulated as a constrained discrete time dynamic optimal control problem which will be optimized by the GA. A systematic description for the GA-based VSL control strategy is shown as follows: At any time interval k , the total number of freeway segment is N , and N_c freeway segments are controlled with VSL. Note that several uncontrolled segments (the number of uncontrolled segments is $N-N_c$) are also included in the VSL model, which are located upstream of the controlled segments. The candidate speed limit set on the controlled segments at time interval k can be represented by $U(k) = (u_{N-N_c+1}(k), \dots, u_i(k), \dots, u_N(k))$, where $u_i(k)$ is the speed limit value on the i -th segment with VSL at time interval k . Suppose that at time interval $k-1$, the optimal VSL solution set is $U_{\text{optimal}}(k-1)$. The new

population of GA (i.e. candidate set of VSL controls on the controlled segments) at time interval k is generated on the basis of $U_{\text{optimal}}(k-1)$ with respect to constraint. To optimize the objective function, the decision variables should be encoded into a binary string meeting the desirable required precision. In this study, the speed limit set $V = \{15, 20, \dots, 65, 70\}$ is converted to a new data set $V_{\text{new}} = \{3, 4, \dots, 13, 14\}$ by dividing it by 5. The required precision is one place after the decimal point. Based on the new data set V_{new} , the minimum required number of bits m_i for representing a speed limit variable in GA is 7 which can be calculated by equation $2^{m_i-1} - 1 < (14-3) * 10 < 2^{m_i} - 1$ (Fan and Gurmu 2014). After the objective function is optimized, the optimal speed limit set $U_{\text{optimal}}(k)$ at time interval k which is used for VISSIM simulation can be achieved as the optimized solution set (obtained based on V_{new} , and non-integer solutions are rounded to integer solutions) times 5. For example, at time interval $k-1$, the optimal speed limit set is (60, 55, ..., 35, 25), an example of the new first five population of GA at time interval k is shown in Figure 4.3. A chromosome of the speed limit set at time interval k on all controlled segments should be formed which represents a possible optimal solution when adopting the GA. The number of segments with VSL control is N_c , and therefore, N_c decision variables are involved in the GA procedure at each time interval k . FIGURE 4.3 shows the chromosome structure for the speed limit set on the controlled freeway segment at time interval k for the first five populations.

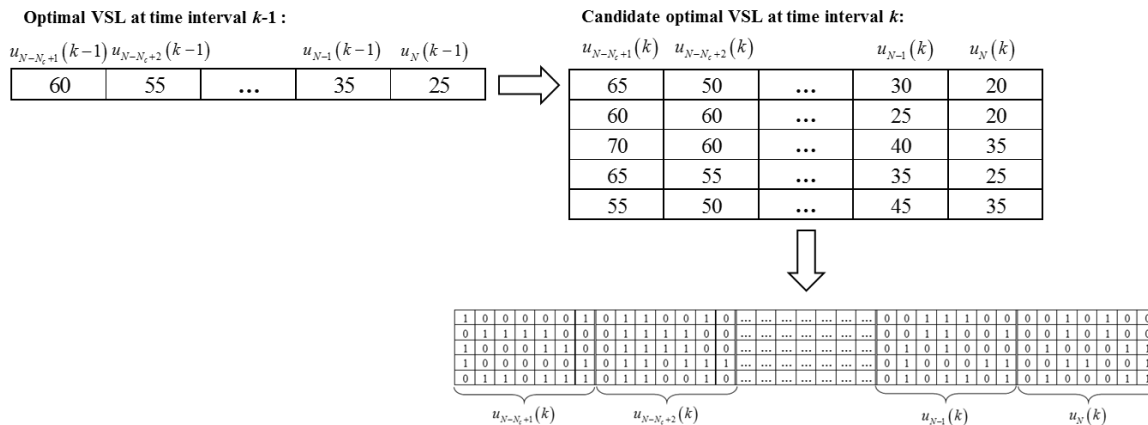


FIGURE 4.3: Illustration of GA Procedure and the Proposed Chromosome Structure at Time Interval k

Typically, VSL control system includes four steps: data collection, traffic state prediction, optimizing variable speed limit, and implementing the optimal speed limits (Yang et al. 2017). Figure 4.4 presents the GA based optimization process for the developed VSL control strategy. The four steps are stated as follows.

- Data collection: Using the detectors installed on the freeway in VISSIM, the average traffic data on each cell (such as flow, speed, and density at the current time interval) are collected.
- Traffic state prediction: The modified METANET or CTM is used to estimate the traffic state on the selected freeway cells during the next control horizon by using the collected traffic data of each vehicle type.
- Optimization process: According to the predicted traffic data (with respect to different speed limit sets), the objective function value will be computed. A set of speed limits are initialized randomly. The objective function value of each individual in the population is evaluated. Based on the objective function values, a new population is

selected with respect to the probability distribution. By using the mutation and crossover operators, the new population can be generated. Once one of the stopping criteria is met, the current best solution is saved and used as the optimal solution. Note that two stopping criteria are used for GA: the maximum number of generations (i.e., 1000) and the average relative change (between the best objective function value at the current iteration and that has been achieved up to the current iteration) is less than or equal to 10^{-6} . The best speed limit set at the current generation is selected for parenthood to conduct crossover and mutation. The GA module is developed by using MATLAB.

- VISSIM simulation: The desired speed distribution in VISSIM is used to reflect the VSL. The displayed speed limit set will be sent to VISSIM and used for simulation by MATLAB. The updated simulation results will be collected and saved. The VISSIM simulation is run with different random seeds to represent different traffic conditions.

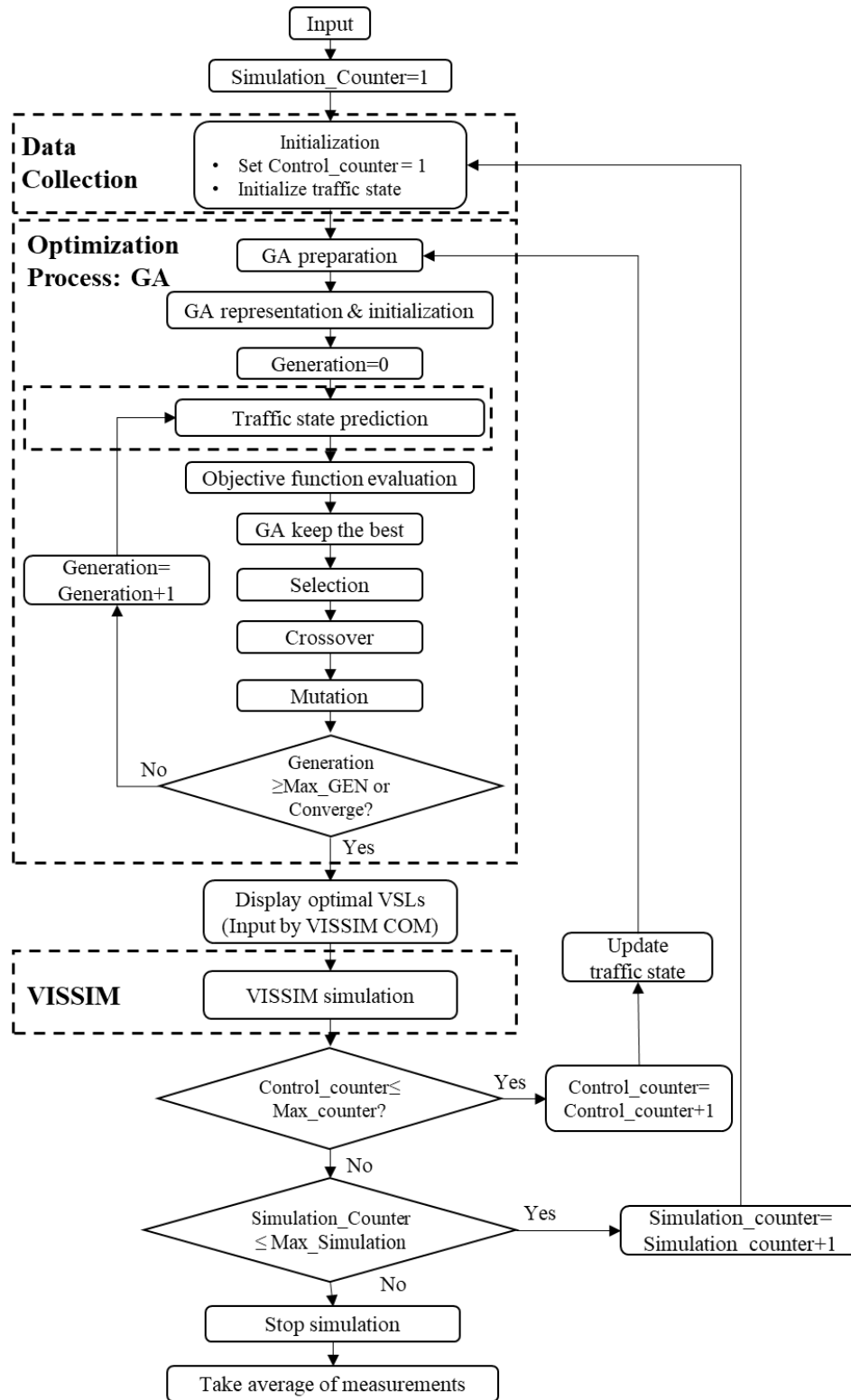


FIGURE 4.4: A Genetic Algorithm Based Solution Framework for the VSL Control

4.5. Summary

This chapter focuses on the introduction of proposed solution algorithms for VSL control strategies. The methodology includes the SQP, TS, and GA. The SQP is selected as the benchmark to examine the solution quality of the TS and GA. Detailed information about the TS and GA are described. The solution frameworks for the VSL control of the three algorithms are presented.

CHAPTER 5: CASE STUDIES

5.1. Introduction

This chapter presents case studies that are designed and used in this dissertation. The case studies include two hypothetical freeway corridors and one real-world freeway stretch. The chapter is organized as follows. Section 5.2 describes hypothetical freeway corridors, including the number of lanes, freeway mainline demand, on-ramp demand, and truck percentage involved. Section 5.3 shows the detailed information about the real-world case study collected from PeMS. Finally, in section 5.4, a summary concludes this chapter.

5.2. Hypothetical Freeway Segment

5.2.1. Case Study for VSL Control at a lane drop bottleneck

A hypothetical three-lane (i.e., $\lambda = 3$) freeway of 6.5 miles, as presented in Figure 5.1, is designed and used. The freeway is divided into seven segments (L_1 - L_7). The last segment L_7 contains an acceleration area, where vehicles can accelerate to merge with the main traffic on the freeway. One on-ramp and one off-ramp is on segment 4 (L_4), respectively. The demand profiles are shown in Figure 5.2. The first figure in Figure 5.2 shows the demand profiles for mainstream input $q_D(k)$, and the second is the demand profiles for the on-ramp segment. The simulation time is 2.5 hours, which includes a 0.5-

hour warm-up time. The percentage of the mainstream flow that leaves the freeway at the off-ramp is set to be 2%.

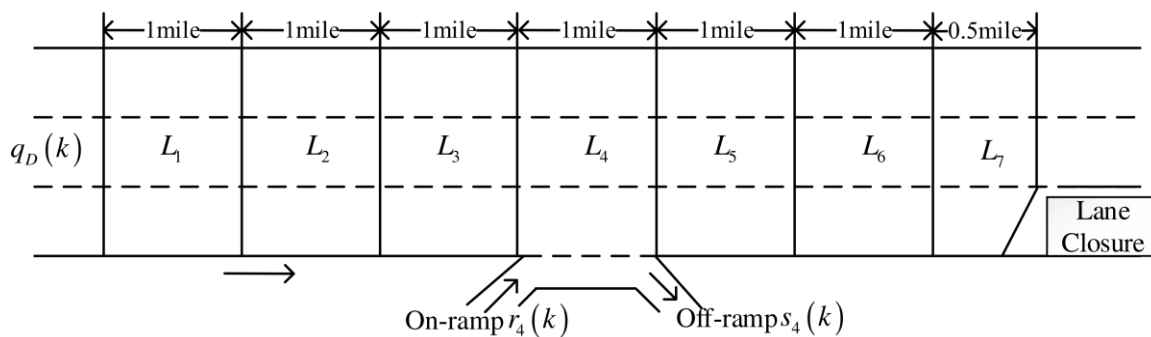


FIGURE 5.1: Hypothetical Freeway Stretch with One On-Ramp and Off-Ramp

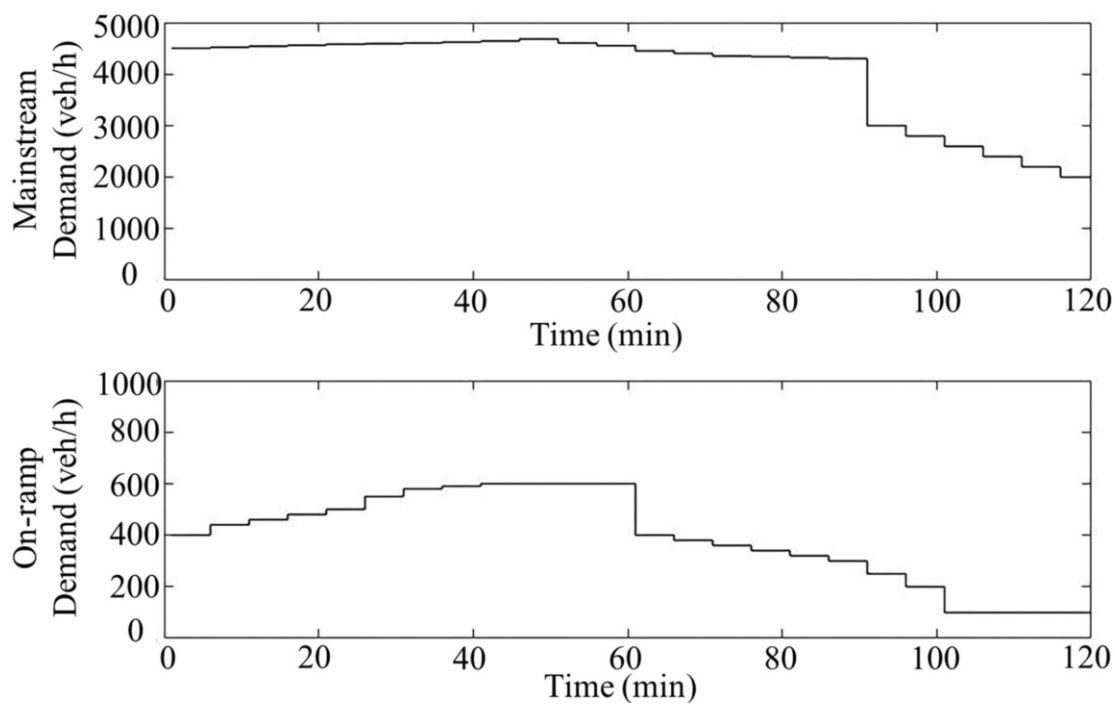


FIGURE 5.2: Demand Profiles

5.2.2. Case Study for VSL Control and Mixed Traffic Flows

Figure 5.3 presents a hypothetical freeway stretch with three lanes (i.e., $\lambda_i=3$), one on-ramp, and one off-ramp. One out of three through lanes is closed. During peak hours, severe congestion may be caused due to the lane drop. The entire freeway stretch is divided into seven segments, as shown in Figure 5.4, from L_1 to L_7 . An acceleration area is contained in the last segment (i.e., L_7), where the vehicles that flow out of the control area can accelerate and merge to the main lane. The total number of studied segments in this study is six (from L_1 to L_6), i.e., $N=6$. The length of each of the six studied freeway segments is 1 mile. Five VSLs are implemented for the variable speed limit control on the freeway segment from L_2 to L_6 (i.e., $N_c=5$). The first segment is uncontrolled. Since vehicles on the first segment might be affected due to the VSL control on L_2 to L_6 , this uncontrolled segment is still included in the study. The position of detectors and VSL signs are also illustrated in Figure 5.3.

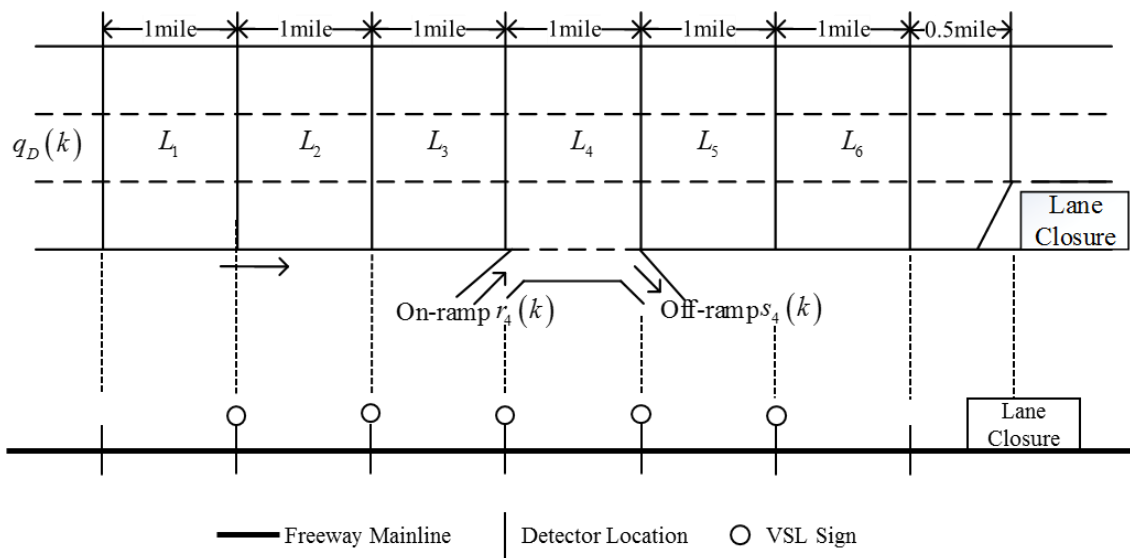


FIGURE 5.3: Case Study and VSL Signs

The demand profiles for the mainstream input is depicted in the first figure in Figure 5.2. Two types of vehicles (i.e., $J=2$) travel on the selected freeway segments, 90% of which are passenger cars (i.e., $\phi_{\text{car}}=90\%$) and 10% are trucks (i.e., $\phi_{\text{truck}}=10\%$). The demand profiles for the on-ramp with 100% passenger cars is given in Figure 5.2. The percentage of the mainstream flow that leaves the freeway at the off-ramp is set to be 2%. No trucks leave the freeway at the off-ramp.

5.2.3. Case Study for VSL Control and Truck Lane Restriction Policy

A hypothetical freeway stretch is depicted in Figure 5.4. The entire freeway is divided into seven segments. According to Carlson et al. (2011), the last segment (i.e., L_7 in Figure 5.4) is the acceleration segment, where vehicles flowing out of the control area can accelerate and merge to the main lane. The freeway stretch has four lanes ($\lambda_i=4$, $i=1, 2, 3, 4, 5, 6$), one on-ramp, and one off-ramp. A lane is closed halfway of the 7th segment, as shown in Figure 5.4. Such a lane drop can lead to severe congestion during peak hours. The number of studied segments is 6 ($N=6$), i.e., L_1 to L_6 . The length of the six studied segments is 1 mile (i.e., $l_i=1$ mile). The number of segments with VSL control is 5 ($N_c=5$), i.e., L_2 to L_6 . There is no VSL control on segment L_1 , but the vehicles and their associated travel time on the first segment are explicitly accounted for in the control model. The truck lane restriction policy is implemented on the freeway corridor.

The demand profiles for the mainstream input are given in Figure 5.5. There are two ($J=2$) types of vehicles traveling on the freeway stretch. The percentage of cars is 90% (i.e. $\phi_{\text{car}}=90\%$) and the percentage of trucks is 10% (i.e. $\phi_{\text{truck}}=10\%$). The demand profiles for the on-ramp with 90% cars and 10% trucks are shown in Figure 5.5. The

percentage of the mainstream traffic that leaves the freeway for both cars and trucks at the off-ramp is set to be 2%. In addition, a limit of 50 cars and 5 trucks is imposed for the on-ramp (Pasquale et al. 2015).

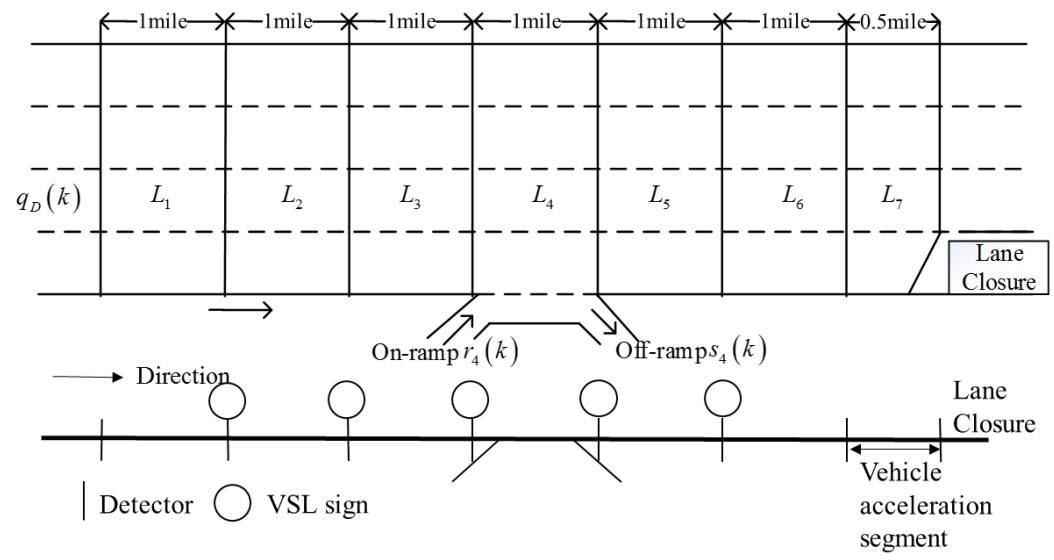


FIGURE 5.4: A Hypothetical Freeway Stretch with One On-Ramp and Off-Ramp

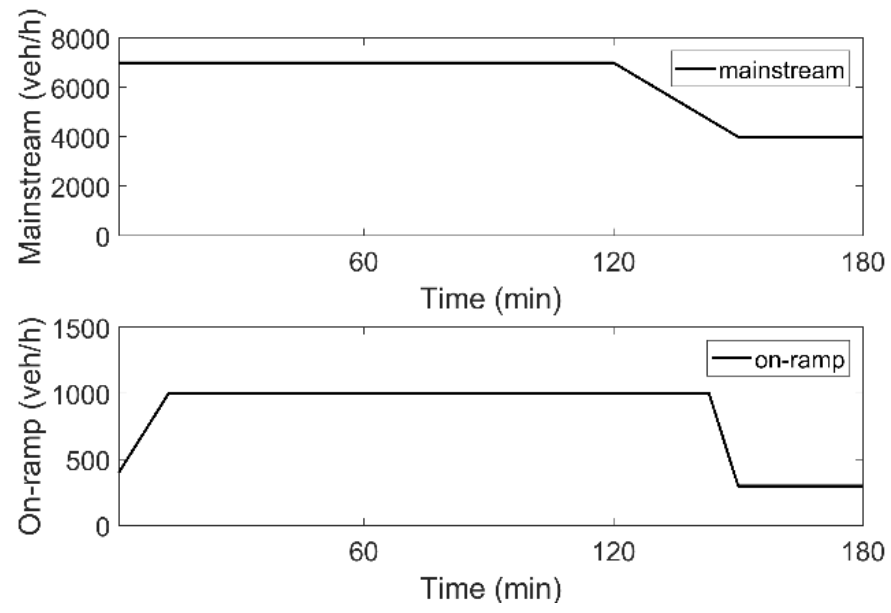
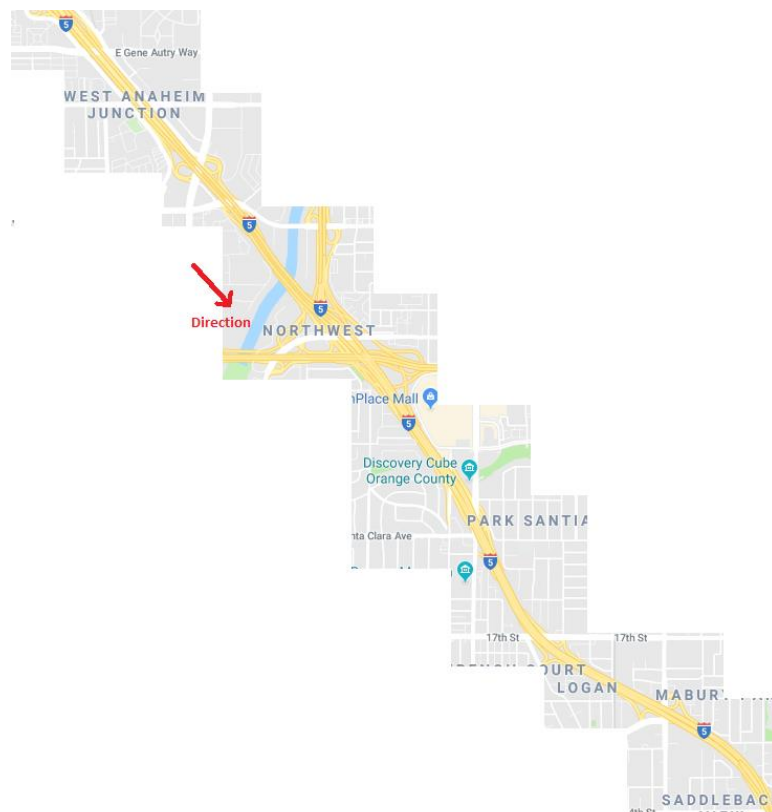


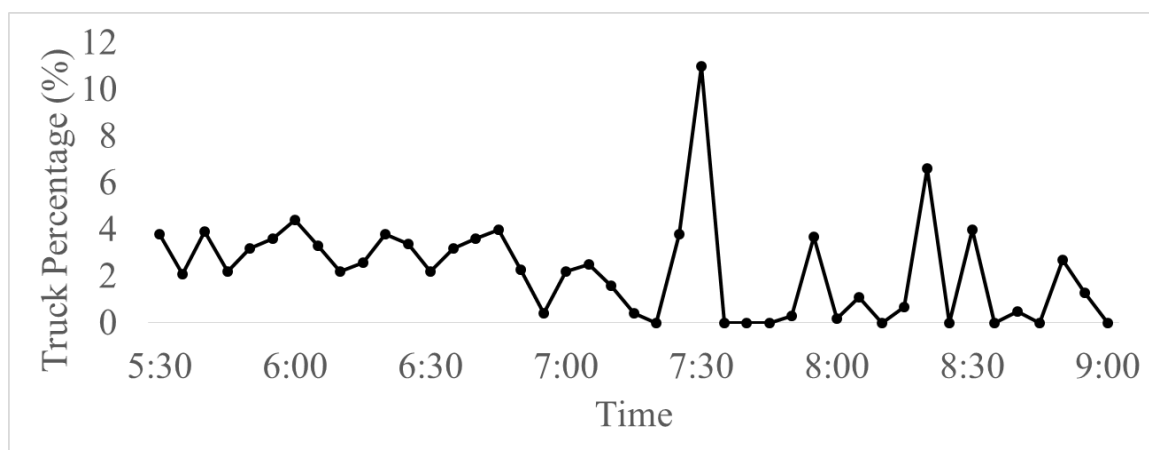
FIGURE 5.5: Demand Profiles

5.3. Real World Freeway Segment

A real-world freeway corridor is selected, which is located in the Interstate 5 (I-5) in Los Angeles, California, as shown in Figure 5.6(a). The studying period is from 5:30 am to 9:00 am on weekdays. The first 30 minutes is used as the warm-up time in VISSIM. The field data is aggregated into 5-min counts. The length of the selected freeway corridor is about 5 miles. There are 9 on-ramps and 7 off-ramps along the case study. Such freeway is a mixed-flow stretch. The number of cars and trucks were recorded in the PeMS database (<http://pems.dot.ca.gov/>), and the percentage of trucks and passenger cars varies by time of day. The presence of trucks is represented by a percentage of the total number of vehicles every 5 minutes and is entered into VISSIM as the demand input. The truck percentage during the study period is presented in Figure 5.6(b).



(a) Map of the Case Study



(b) Truck Percentage vs. Study Period

FIGURE 5.6: (a) Map of the Case Study; and (b) Truck Percentage vs. Study Period

5.4. Summary

This chapter focuses on describing the case studies (including the hypothetical and real-world freeway corridors) developed and used in this dissertation. The detailed information (e.g., truck percentage, mainline demand profiles, the implementation of variable message signs, and on-ramp and off-ramp demand) of about these case studies is presented.

CHAPTER 6: CALIBRATION OF MICROSCOPIC TRAFFIC SIMULATION MODELS USING METAHEURISTIC ALGORITHMS

6.1. Introduction

Due to the cost effectiveness, risk-free, and high-speed benefits (Ciuffo et al. 2008), microscopic traffic simulation has been widely used in transportation planning, design, and analysis. In recent years, the microscopic approach has also been given more importance in traffic operations and safety studies. Many microscopic simulation models (such as VISSIM, CORSIM, and SUMO) have been widely used. In these simulation models, there are independent parameters that are used to describe traffic flow characteristics (e.g., driver behavior and traffic control operations). Even though these microscopic simulation models provide default values for these parameters, simulation under default values often produces unreliable results. Users often have to fine-tune the values so that traffic conditions of real case studies can be accurately represented. Therefore, the parameters of microscopic simulation models need to be calibrated and validated. Model calibration plays a crucial role in minimizing the differences between the simulation results and corresponding field measurements, such as traffic volumes, speed, and travel time.

To obtain a close match between the observed and simulated traffic measurements, one has to perform a proper calibration of microscopic traffic simulation model parameters. Because there are a large number of unknown parameters involved, the calibration process can be a time-consuming and complex task. As a result, such a

calibration process has been formulated as an optimization model in which a huge search space exists due to a wide range of each relevant model parameters. The optimal set of parameters is solved and obtained so that the objective function can be minimized (Ciuffo et al. 2008; Ma et al. 2007; Kim et al. 2005; Ma and Abdulhai 2002; Park and Qi 2005; Lee and Ozbay 2009; Hourdakis et al. 2003; Chiappone et al. 2016; Menneni et al. 2008; Abdalhap and Baker 2014; Paz et al. 2015; Hale et al. 2015). However, such optimization process typically does not have gradient information to assist the search for an optimum solution (Ma et al. 2007; Hourdakis et al. 2003). Researchers cannot directly apply mathematical programming methods, and therefore metaheuristic methods (such as the GA, SPSA, or IA), are used to search for optimal parameter values.

Among these algorithms, GA has been widely used due to its easy implementation and good performance in calibration and optimization (Ma et al. 2007; Kim et al. 2005; Ma and Abdulhai 2002; Park and Qi 2005; Chiappone et al. 2016; Menneni et al. 2008; Abdalhap and Baker 2014; Paz et al. 2015; Fan and Gurmu 2014; Fan and Machemehl 2006; Fan and Machemehl 2004). However, other algorithms, such as TS method, may also provide an effective solution to the calibration problem. TS has been widely applied in many fields since it was first proposed by Glover in 1977 (Glover 1986). It has been successfully used to obtain optimal or sub-optimal solutions to problems, such as the traveling sales person, timetabling and layout optimization, and transit route network optimization (Fan and Machemehl 2008).

To the best of current knowledge, the authors of this study have noticed that the TS has rarely been used for the calibration of microscopic simulation model parameters. Furthermore, all these research efforts have used one algorithm to calibrate the

microscopic simulation models. However, it is believed that the warm start method (using the solutions obtained from one algorithm as a starting point for another algorithm) will have superior performance compared to using a single algorithm alone (Fan et al. 2008). As such, this study attempts to use TS to calibrate the parameters of the microscopic traffic simulation model (i.e., VISSIM) with a real-world freeway case. At the same time, GA works as a baseline comparison because GA can obtain an acceptable calibration result which has been proven by many researchers (Ma et al. 2007; Ma and Abdulhai 2002). Perhaps the most significant contribution of this chapter is to introduce the warm start concepts and use the warm start methods for the first time for calibration. In particular, GA, TS, and a combination of the GA and TS (including both warmed GA and warmed TS methods) are implemented to calibrate the microscopic traffic simulation models. Particular attention is given to the algorithm comparisons and warm start component. To implement this process, the existing GA tool in MATLAB is used, and new TS tools algorithms are developed and implemented in MATLAB for calibration. The optimization techniques are used and attached to VISSIM 7.0 via COM interface so that the data can transfer between MATLAB and VISSIM. The calibration results of GA, TS, warmed GA, and warmed TS methods are then evaluated, compared and discussed.

The rest of this chapter is organized as follows: Section 6.2 discusses the calibration methods in which the objective function is given first and the GA and TS methods are then introduced. The VISSIM calibration parameters are also described. Section 6.3 provides a case study to illustrate the calibration framework, and the simulation and calibration results are also discussed in detail. Finally, a summary concludes this chapter in section 6.6.

6.2. Calibration Methods

6.2.1. Objective Function

Calibration of a microscopic traffic simulation model is the process aimed at defining or fine-tuning the values of the parameters of the model so that the discrepancy between observed and simulated traffic measurement is minimum. In this regard, the general optimization framework is formulated as follows.

$$\min f(M^{\text{obs}}, M^{\text{sim}})$$

Subject to the constraints:

$$l_{\theta_i} \leq \theta_i \leq u_{\theta_i}, i=1 \dots n$$

where

θ_i = the vectors of continuous variable (i.e. model parameters to be calibrated).

$f(\cdot)$ = Objective function (or fitness function).

$M^{\text{obs}}, M^{\text{sim}}$ = Observed and simulated traffic measurements.

$l_{\theta_i}, u_{\theta_i}$ = The respective lower and upper bounds of model parameter θ_i .

n = number of variables.

In this study, the objective function, Mean Absolute Normalized Error (MANE) (Ciuffo and Punzo 2009; Hollander and Liu 2008), is provided by Eq. (1). The calibration problem using the flow and speed data as performance measures is formulated as follows:

$$\text{Minimize } MANE(q, v) = \frac{1}{N} \sum_{j=1}^N \left(\frac{|q_{\text{obs},j} - q_{\text{sim},j}|}{q_{\text{obs},j}} + \frac{|v_{\text{obs},j} - v_{\text{sim},j}|}{v_{\text{obs},j}} \right)$$

Where

$q_{\text{obs},j}, v_{\text{obs},j}$ = actual flow and speed for a given time period j .

$q_{\text{sim},j}, v_{\text{sim},j}$ = simulated flow and speed for a given time period j .

N = total number of observations.

To solve the optimization problem based on the objective function as presented above, different solution methods are developed in this study. The GA and TS algorithm method are briefly described, followed by the discussion of the VISSIM calibration parameters.

6.2.2. Genetic Algorithm

The GA is inspired by the concept of biological evolution. Its population is evolved by selection, crossover and mutation. Selection is applied so that better solutions have higher probabilities of being used in producing new populations (solutions). Crossover and mutation are applied to generate new solutions. The GA starts from a random population set and evaluates candidate solutions at every generation. The GA has been shown to obtain near-global optima when calibrating parameters in the microscopic traffic simulation models. Figure 6.1 shows the GA calibration process.

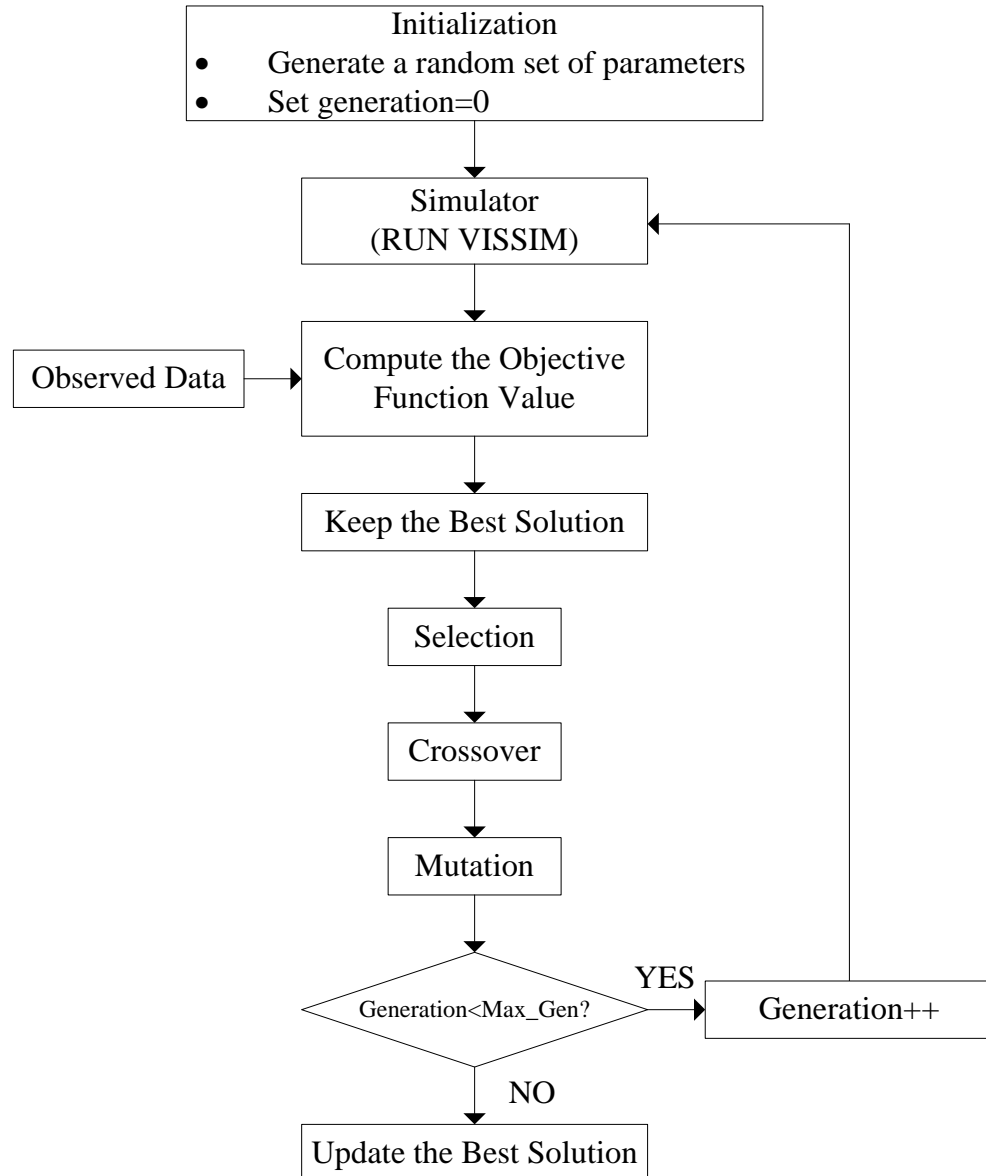


FIGURE 6.1: GA Calibration Process

6.2.3. Tabu Search

TS was originally used to solve discrete optimization problems. However, in this study, the parameters are all continuous. According to the algorithm in Glover (1990), an implementation of continuous domain problems is proposed. For each continuous

parameter, there are two moves: move and anti-move. Move is adding a small amount (called move distance), while anti-move is subtracting a small amount (anti-move distance).

Move distance and anti-move distance of the i -th parameter are defined as:

$$\text{Move Distance: } D_{m,i} = a_{m,i} * (u_i - l_i), \quad 0 < a_{m,i} < 1, \quad i=1 \dots n.$$

$$\text{Anti-Move Distance: } D_{anti-m,i} = b_{anti-m,i} * (u_i - l_i), \quad -1 < b_{anti-m,i} < 0, \quad i=1 \dots n.$$

Where

$a_{m,i}$, $b_{anti-m,i}$ = move distance weight and anti-move distance weight of the i -th parameter.

l_i , u_i = the lower and upper bounds of the i -th parameter.

n = the number of parameters.

After a move and anti-move, the neighborhood will be generated whose size will be twice the number of initial solutions. Figure 6.2 presents the flow chart of TS.

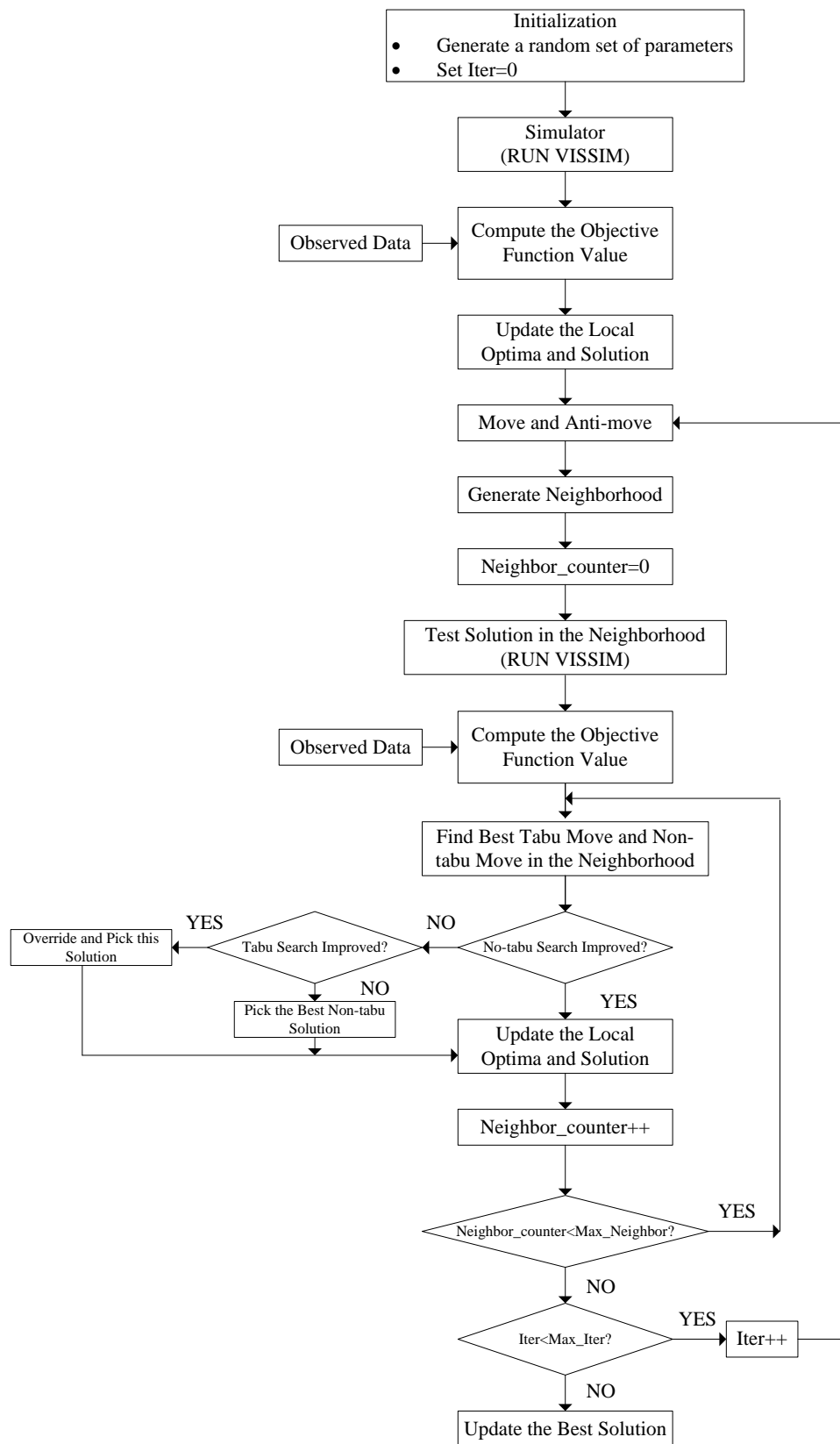


FIGURE 6.2: TS Calibration Process

6.2.4. VISSIM Calibration Parameters

VISSIM attempts to capture the physical and the human components of traffic, which is developed according to the Wideman model (Yu and Fan 2017). The Wideman model was based on a psychophysical car following model. The basic concept of the car-following model is that drivers of faster-moving vehicles are sensitive to the changes in distance and speed of slower moving vehicles in front of them (Brackstone and Liu 2008).

A variety of user-controlled parameters are included by VISSIM, which are often difficult to collect on the field and have to be calibrated. Driver behavior parameters and vehicle performance parameters are the two general calibration parameters in VISSIM. Driver behavior parameters, which include car-following and lane-change parameters, have been considered in many studies. In this study, car-following parameters which can significantly affect the simulation flows are selected and used as the candidate calibration variables in this chapter. Based on Lownes and Machemehl (2006), CC0-CC5 and CC7 are selected. Detail information about the sensitivity results can be found in Lownes and Machemehl (2006). The selected car-following parameters and their VISSIM code, their corresponding descriptions in VISSIM, feasible ranges, and units are shown in Table 6.1.

TABLE 6.1: Car-following Parameters in VISSIM

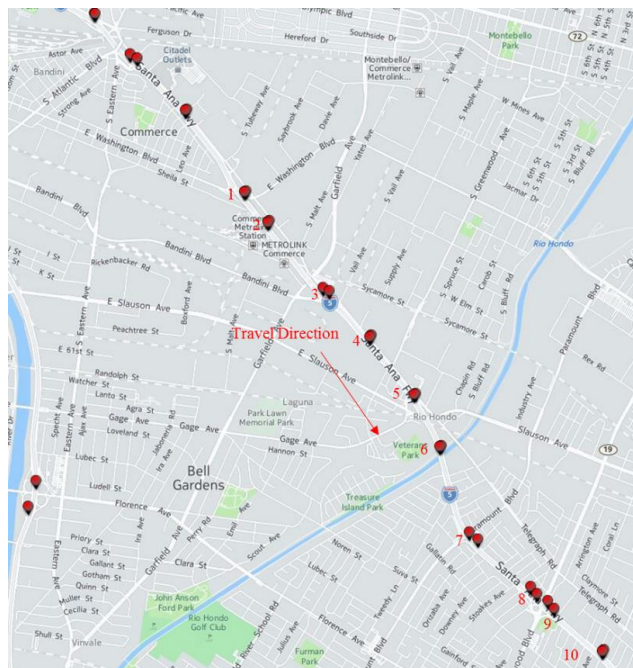
VISSIM Code	Description	Feasible Range (Min.~ Max.)	Unit
CC0	Standstill distance: Desired distance between lead and following vehicle at v = 0 mph	2~10	ft
CC1	Headway Time: Desired time in seconds between lead and following vehicle	0.5~1.5	sec
CC2	Following Variation: Additional distance over safety distance that a vehicle requires	5~20	ft
CC3	Threshold for Entering 'Following' State: Time in seconds before a vehicle starts to decelerate to reach safety distance (negative)	-15 ~ -4	sec
CC4	Negative 'Following' Threshold: Specifies variation in speed between lead and following vehicle	-2 ~ -0.1	ft/s
CC5	Positive 'Following Threshold': Specifies variation in speed between lead and following vehicle	0.1 ~ 2	ft/s
CC7	Oscillation Acceleration: Acceleration during the oscillation process	0.5~1.5	ft/s ²

6.3. Numerical Results

6.3.1. Freeway Segment

Data was obtained from a portion of the I-5 freeway in the city of Los Angeles, California, as shown in Figure 6.3(a). It should be noted that this freeway segment is used to show as an example to illustrate and test the calibration methods developed in this chapter which is different from the case study shown in Figure 5.6. The study period spans 1 hour of the a.m. peak, from 7:30 to 8:30 a.m. on October 19, 2016, and the field

traffic data (i.e., flow and speed) is aggregated into 5-min counts. This freeway stretch is a four-lane with 5 on-ramps and 6 off-ramps. The length of the selected freeway segment is about 5 miles. There are 10 detectors on the selected freeway, and the positions and the number of the detectors are shown in Figure 6.3(a). The freeway segment is created in the VISSIM model based on the data from the PeMS, the position of off-ramps and on-ramps is presented in Figure 6.3(b). The selected I-5 freeway is a mixed-flow stretch. The number of cars and trucks are recorded in the PeMS database, and the mix of trucks and cars varies by time of day. It has been verified that the car drivers' behavior can be affected by heavy vehicles, such as trucks (Dowling et al. 2004). Therefore, the presence of trucks is represented by a percentage of the total number of vehicles every 5 minutes which is entered into the VISSIM. Figure 6.4 presents the truck percentage of demand input during the study period.



(a) Map of the Case Study from the PeMS



(b) VISSIM Model

FIGURE 6.3: I-5 (a) Map of the Case Study from the PeMS, (b) VISSIM Model

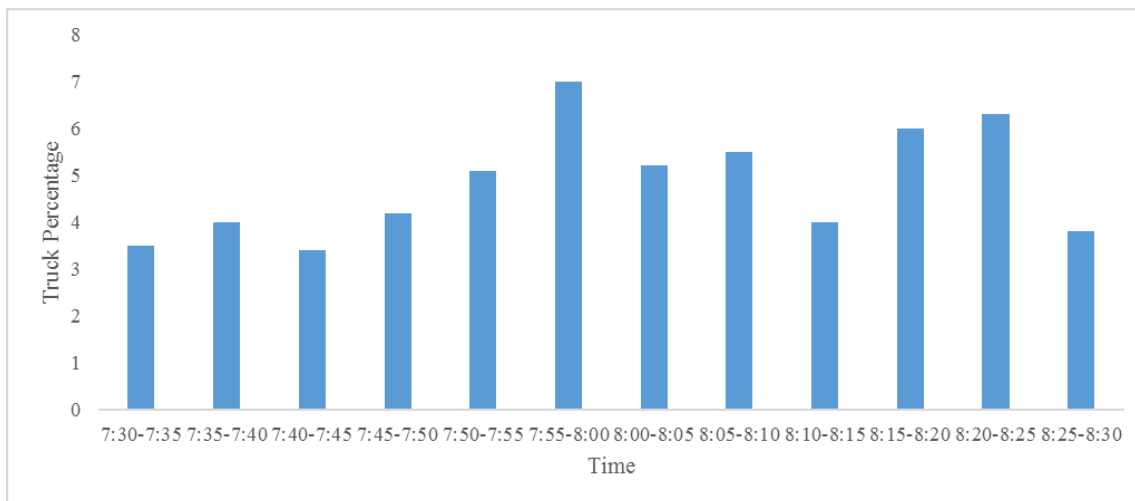
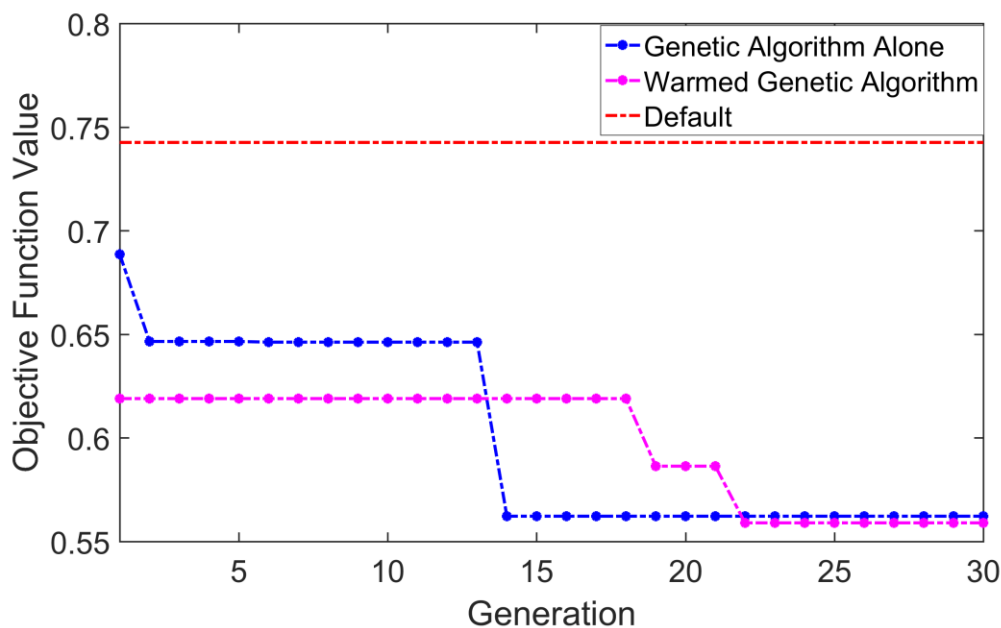


FIGURE 6.4: Truck Percentage vs. Time throughout the Study Period

6.3.2. Calibration Results

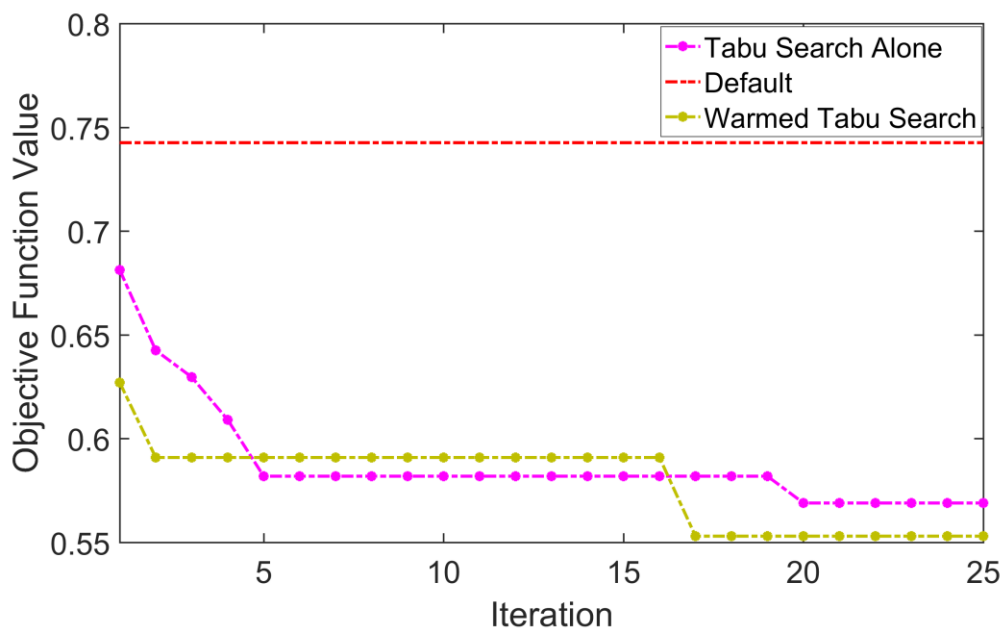
The GA and TS methods are integrated with the VISSIM model to calibrate the selected parameters. For GA-based calibration, a population of chromosomes are generated in the population. Each chromosome represents a feasible solution and will be passed onto the VISSIM for simulation by MATLAB. Based on the simulated flow and speed data, the objective function value is calculated by using Eq. (1). If the objective function value does not meet the stopping criterion, the GA will generate a new population after the implementation of selection, crossover, and mutation. Until meeting the stopping criterion or reaching the maximum number of generations, this process will not be stopped. In this case, there are 30 generations and the population size is set to be 10. Meanwhile, the crossover rate is set as 0.8 and mutation rate is 0.2.

TS starts with a random set of solutions. In every iteration, the neighborhood of a solution will be searched by the Tabu technique. The best solution will be chosen as the next candidate point. In this study, the move distance of TS is set as $0.05 * (u_i - l_i)$ ($i=1, \dots, 7$), and the anti-move distance is determined to be $-0.04 * (u_i - l_i)$ ($i=1, \dots, 7$) (Yu and Fan 2017). The total number of iterations used for the TS method is 25. Furthermore, there are 7 parameters which need to be calibrated. As discussed before when introducing TS, after the move and anti-move, the neighborhood solutions will be generated whose size will be twice the number of initial solutions. In every iteration, there are 14 solutions in the neighborhood and one has to run these 14 solutions and compare them with those contained in the tabu list.



(a) GA Objective Function Value vs. Generation

FIGURE 6.5: Values of Objective Function during the Optimization Period



(b) TS Objective Function value vs. Iteration

FIGURE 6.5, continued

Figure 6.5(a) and Figure 6.5 (b) present the GA and TS objective function values during the optimization period respectively. The correspondent objective function value calculated using default parameters is also shown. The y-axis represents the minimum objective function value up to every iteration (or generation) and the x-axis denotes the number of iterations (or generations). As expected, the objective function value using any metaheuristic methods is better than that using the default parameters. In Figure 6.5, one can also clearly see that the warmed GA improves the GA (alone) results, but the improvement is not that significantly. However, the warmed TS is observed to be significantly better than the TS alone.

Figure 6.6 presents the comparison of the flow profiles both for field measurements from the I-5 freeway and simulation results with the default and optimized

parameters. The optimized parameters of the GA, warmed GA, TS, and warmed TS methods are run 30 times, and the average flow is recorded. A better matching to the field flow is clearly exhibited by using the optimized parameters (of both the GA and TS methods) compared with the simulation results by using the default parameters. Also, the TS results appear to be similar to the GA-based flow profiles. The warmed GA and warmed TS are observed to be better than the GA alone and TS alone (e.g., flow profiles at Detector 10).

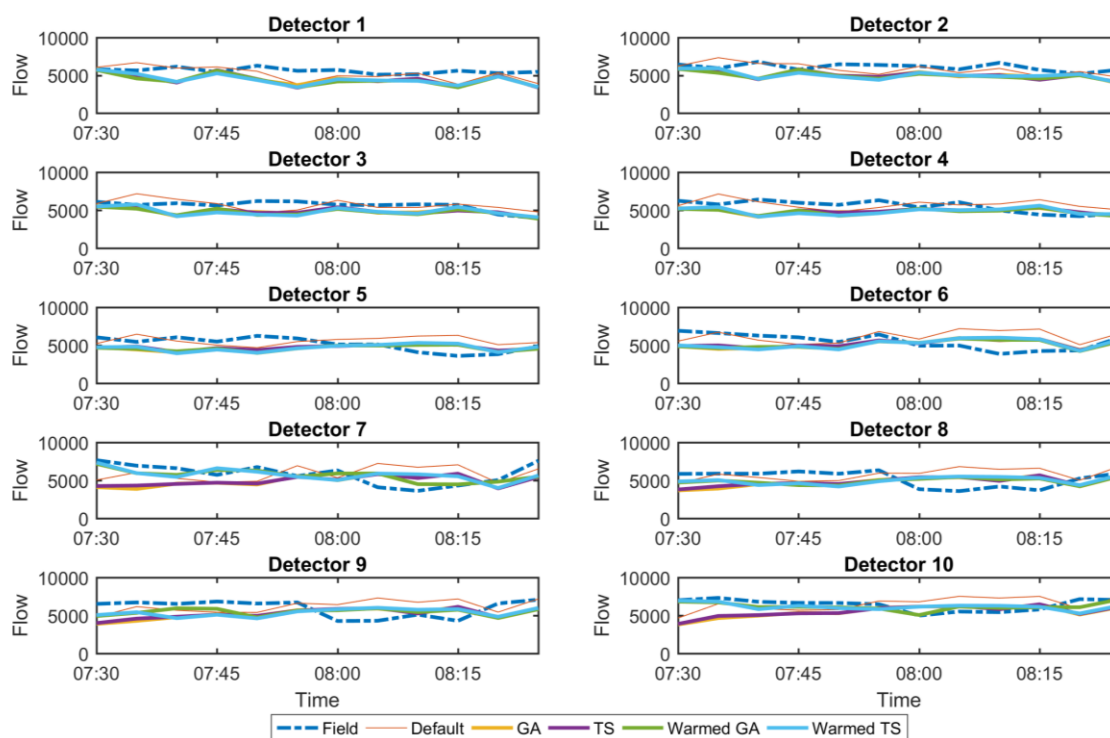


FIGURE 6.6: Flow Profiles for Field Measurement and Simulation Outputs Comparison between GA and TS

6.3.3. Comparison between GA and TS Methods

To illustrate the advantage of the proposed TS, a comparison with the GA is provided. The Geoffrey E. Havers (GEH) statistic index is calculated in this study. GEH index can work as a criterion for acceptance, or otherwise rejection, of the model. If the GEH value is less than 5 in the 85% of simulated values, an acceptable goodness of fit is considered (Ciuffio 2008; Hourdakis et al. 2003).

More specially, the performances of all algorithms (both GA and TS alone, and warmed GA and TS) for the calibration of microscopic simulation model parameters are shown in Table 6.2. The objective function values, GEH flow and speed indexes, and the running times are included in Table 6.2. The objective function values of the GA and TS methods are smaller than that obtained by using the default parameters, and they are almost identical, which means that TS can obtain a similar calibration result to GA. Both the warmed GA and TS improve the performance (i.e., objective function value) of GA and TS alone, respectively. All the GEH-flow indexes of GA, warmed GA, TS and warmed TS are less than 5 for 100%, and GEH-speed statistic values of GA, warmed GA, TS and warmed TS are lower than 5 for 95.8%, 96.5%, 96.8% and 96.2% respectively. For TS based calibration, the deviation of the simulated values with respect to the measurement is smaller than 5 in 96.2% (speed) or 100% (flow), which clearly indicated that the TS model performs very well (and even slightly outperforms the GA method). In terms of computing efficiency, the computation time for the (warmed) TS is longer than (warmed) GA using the same computer configuration, in part due to the fact that TS conducts more VISSIM runs than GA in this case. Based on this study, warmed TS

(which uses the solution from the GA as a warm start), is recommended for the calibration of microscopic traffic simulation models.

TABLE 6.2: Comparison between GA and TS Methods

Algorithm	Objective Function	GEH: Flow	GEH: Speed	Running Time (h)
Default	0.743	/	/	/
GA Alone	0.562	<5 for 100% case	<5 for 95.8% case	8.4
Warmed GA	0.559	<5 for 100% case	<5 for 96.5% case	8.4
TS Alone	0.568	<5 for 100% case	<5 for 96.2% case	10.8
Warmed TS	0.553	<5 for 100% case	<5 for 96.8% case	10.8

6.4. Summary

Due to the complexity of the calibration of microsimulation models, more reliable and efficient metaheuristic optimization methods should be developed and compared. In this study, another metaheuristic optimization method (i.e., Tabu Search) is developed and applied to calibrate microscopic traffic simulation model parameters. The warm start concept is also introduced and applied. The MATLAB and VISSIM microsimulation software are used as the basis of the study. The calibration methods are implemented and tested in a case study by using traffic data collected from the I-5 freeway segment in Los Angeles, California. The flow and speed data are used to build the objective function in order to minimize the discrepancy between the observed and simulated traffic

measurements. The field traffic measurements are compared with the corresponding results obtained by using software VISSIM. The calibration is formulated as an optimization problem in which the objective function value is to be minimized. The parameters that were reported to significantly affect the simulation outputs are selected and calibrated. Using the best optimized parameters by using the GA, TS, warmed GA, and warmed TS, all the simulated results (i.e., flow profiles) can fit to the field measurements. According to the GEH statistic index, TS can be a very good method which performs very well to calibrate microscopic traffic simulation model parameters. All metaheuristic algorithms are also compared in terms of the calibration quality. The results show that warmed TS outperforms other tested algorithms and therefore is recommended for calibrating microscopic traffic simulation models.

CHAPTER 7: NUMERICAL RESULTS

7.1. Introduction

As described in Chapter 3, the objective functions of the VSL control are formulated to improve the bottleneck efficiency and the level of safety. Solution methodologies and case studies are presented in previous chapters. This chapter focuses on the numerical results of the proposed developed VSL control systems (including mixed traffic flows and VSL control in a CAV environment). Numerical results of different VSL control strategies are presented and analyzed in detail.

The remainder of this chapter is organized as follows. Section 7.2 describes the numerical results of VSL control at a lane drop bottleneck. Section 7.3 presents the simulation results of VSL control for mixed traffic flows. Section 7.4 discusses the comprehensive numerical results of control strategy which combines the VSL and left-lane truck restriction policy for mixed traffic flows. Sections 7.5 and 7.6 investigate the VSL control in a CAV environment, with and without platooning, respectively. Finally, a summary concludes this chapter in Section 7.7.

7.2. VSL Control at a Lane Drop Bottleneck

7.2.1. Calculation of the Traffic Model Parameters

A VSSIM model is used to simulate the traffic traveling on the freeway segments as shown in Figure 5.1. Based on the 1-min traffic data which is generated by VISSIM, the traffic model parameters can be calculated. The calculation method in Dervisnglu et

al.'s (2009) research is used. In Dervisnglu et al.'s (2009) paper, how to estimate the free-flow speed, capacity and critical density, and magnitude of the capacity drop were presented. The method is briefly introduced as follows:

Free flow speed v_f : the free-flow speed is estimated by performing a least-square fit on the flow-density FD where the simulation speed is greater than 60 miles/h;

Capacity Q and critical density ρ_c : the maximum value of flow on a freeway segment is assigned as the capacity of the segment. The critical density of a segment is defined as the maximum value of flow divided by free-flow speed.

Magnitude of the capacity drop θ : A constrained least-squares regression is performed to fit the congested flow and density where the value of density is greater than the critical density. The point where the regression line crosses x-axis is assigned as the jam density. When the density of the quantile regression for the congested traffic data equals critical density, the corresponding flow is assigned as the Q_b . The magnitude of the capacity drop can then be calculated.

Finally, the following parameters are used in this study: $Q=2220$ veh/h/lane, $Q_b=2100$ veh/h/lane, $v_f=67.2$ miles/h, $\rho_c=33.03$ veh/mile/lane, $\theta=5.4\%$. In this case, since two lanes are available at the bottleneck area, the maximum discharge volume of bottleneck is $C=2Q_b=4200$ veh/h. In addition, the total number of time intervals in this case is $K=120$ (i.e., 120 1-minute time intervals within 2 hours).

7.2.2. Calibrating Parameters of the METANET

An objective function is chosen to minimize the speed and flow errors so that the optimal global parameters $X = [\tau, \nu, \kappa]$ in the METANET model can be calibrated. The objective function is

$$\min f = \sum_{i=1}^N \sum_{k=1}^K \left(\left(\frac{v_{i,\text{measured}}(k) - v_{i,\text{predicted}}(k)}{(v_{i,\text{measured}}(k) + v_{i,\text{predicted}}(k))/2} \right)^2 + \left(\frac{q_{i,\text{measured}}(k) - q_{i,\text{predicted}}(k)}{(q_{i,\text{measured}}(k) + q_{i,\text{predicted}}(k))/2} \right)^2 \right)$$

Where:

$v_{i,\text{measured}}(k)$ = measured speed on segment i during time interval k by VISSIM;

$v_{i,\text{predicted}}(k)$ = predicted speed on segment i during time interval k by METANET;

$q_{i,\text{measured}}(k)$ = measured flow on segment i during time interval k by VISSIM;

$q_{i,\text{predicted}}(k)$ = predicted flow on segment i during time interval k by METANET.

This optimization model is solved by using the SQP algorithm in MATLAB, i.e., a method called *fmincon*. The SQP algorithm starts with a user-defined start point, and searches the optimal point in the solution space until the improvement in the objective function stops. The lower bound and upper bound of these three global parameters are $X_{\min} = [0.05, 10, 10]$ and $X_{\max} = [0.2, 60, 60]$ respectively. Note that the required precision is two places after the decimal point. The objective function is a non-linear non-convex problem, and therefore only local optima can be found. Different starting points are tested to find a good local optimal solution. Finally, the obtained optimal global parameters

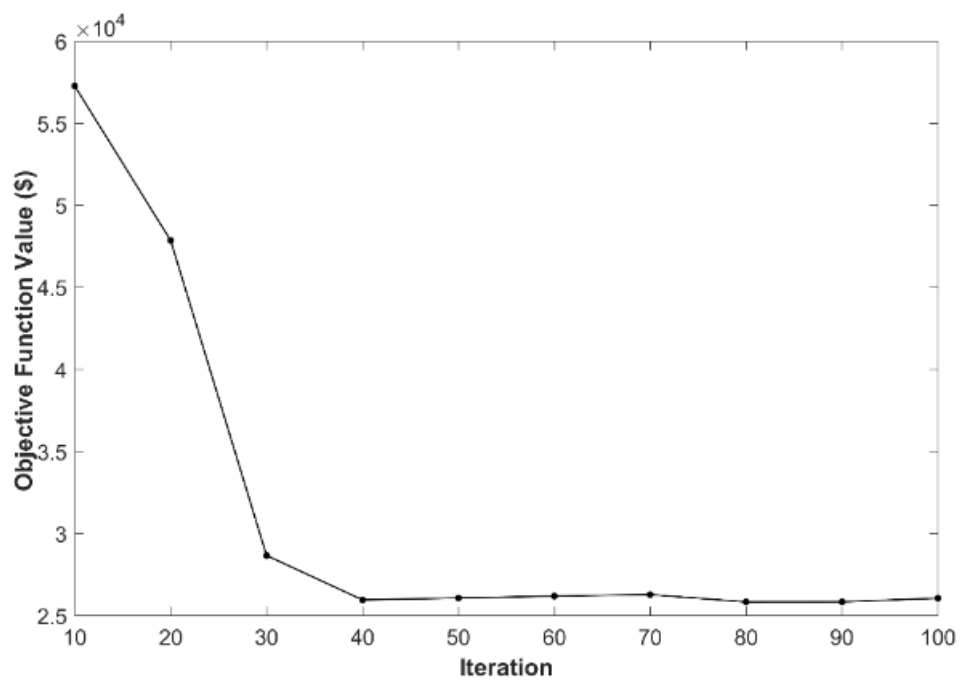
values are $X_{\text{optimal}} = [0.1, 50.44, 59.99]$, and the corresponding optimal objective function value is 25.55.

7.2.3. Sensitivity Analyses

The proposed VSL control strategy that is solved by tabu search algorithm is implemented on the freeway segment as shown in Figure 5.1. Based on the measurement of the current traffic states, which is obtained by running simulations using VISSIM, the future traffic states are predicted. Using the proposed VSL control strategy and tabu search algorithm, the VSL solution set that minimizes the objective function over a given future time horizon (i.e. $T_p=5\text{min}$) is saved and displayed on the VMS in VISSIM. Furthermore, the speed limits will change every minute (i.e., $T_c=1\text{min}$). The discrete time step used in the METANET model is $T=10\text{s}$. The number of control segments used is 5 (L2-L6 in Figure 5.1, $N_c=5$), and the quantity of studied segments is 6 (i.e., L_1-L_6 in Figure 5.1, $N=6$). It should be pointed out that driver compliance rate is an important component of the VSL control. VSL control with different driver compliance rates has been studied in many research efforts. For example, in Lu et al.'s (2010) study, simulation results indicated that the total travel time achieved in the case of 30% driver compliance rate was almost identical to that in the 100% driver compliance rate case. In Yang et al.'s (2017) research, the result showed that the decrease in the compliance rate can reduce the operational efficiency of the VSL control. In this study, the driver compliance rate is set as 100%.

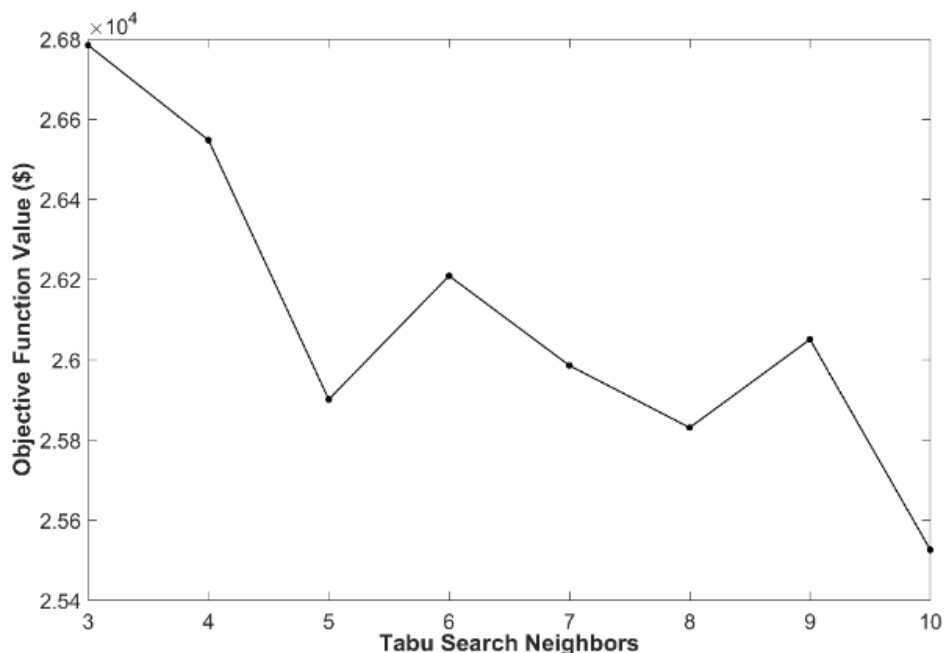
The chosen parameters, such as the number of iterations and search neighbors, might greatly affect the performance of the proposed tabu search. The objective function

in this study involves two components, i.e., total value of travel time and total value of speed variation. Note that VTT refers to the value of travel time which has been suggested by the U.S. DOT (USDOT 2016). Based on the USDOT’s research, VTT is set as 20 \$/hour in this study. However, VSV is very hard to determine and cannot be directly obtained from any of the existing studies. As such, the VSV is assumed to be 15 \$*hour/miles. It is believed that improving travel time and reducing speed variation are equally important for the VSL control. Therefore, the related sensitivity analyses are conducted based on weights of 0.5 and 0.5 for the total value of travel time and total value of speed variation. Figure 7.1 presents the sensitivity analyses of the number of iterations and the number of search neighbors.



(a) Iteration

FIGURE 7.1: Sensitivity Analyses for the Tabu Algorithm



(b) Tabu Search Neighbors

FIGURE 7.1, continued

The effect of the number of iterations is examined by varying the value from 10 to 100 and the result is given in Figure 7.1(a). As can be seen, as the number of iterations increases, the value of the objective function tends to decrease. The least objective function value achieved with the 90 iterations. Therefore, an iteration of 90 is recommended.

The effect of search neighbors is investigated by choosing this number ranging from 3 to 10. The result is provided in Figure 7.1(b). In Figure 7.1(b), the least objective function value occurs with 10 neighbors, which indicates that 10 might be the optimal neighbor. As a result, 10 is recommended.

In addition, different weight sets might affect the solution quality of the VSL control. A numerical result is presented in Figure 7.2 to show the effects on solution

quality of the VSL control by varying the weight (i.e., w_1) of total travel time from 0.1 to 0.9. Note that, $w_1+w_2=1$. As can be seen, when $w_1=0.9$, the objective function is the least, which clearly suggest that the total value of speed variation dominates the value of total travel time in the objective function. For illustration convenience, $w_1=0.9$ and $w_2=0.1$ are chosen for further analyses.

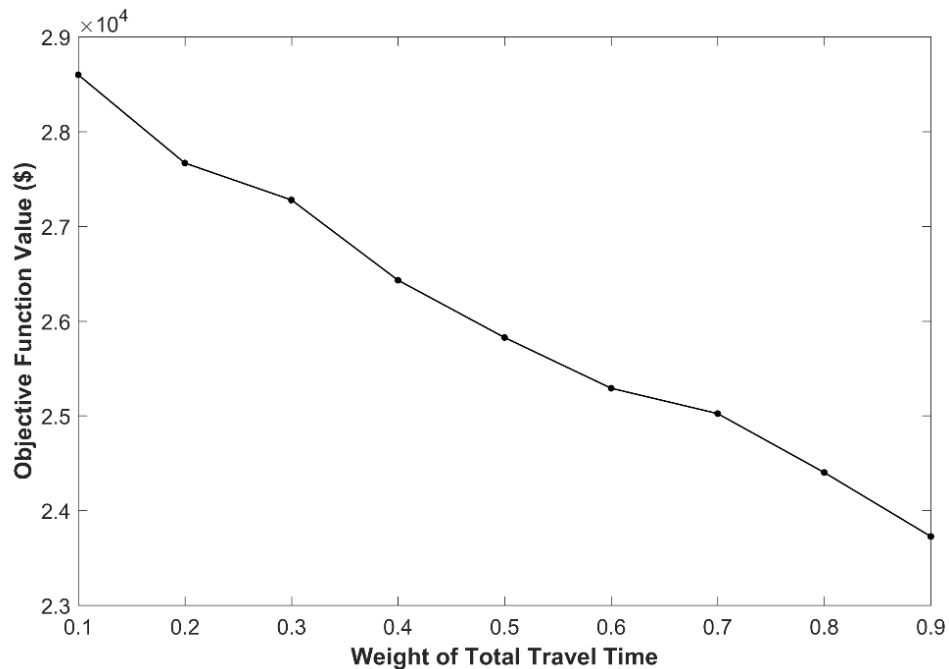


FIGURE 7.2: Sensitivity Analyses for the Weight of Total Travel Time

7.2.4. Control Results

As mentioned, the control performance based on the proposed tabu algorithm might greatly depend upon the chosen value of parameters inherent in the algorithm. By assigning a weight set to total value of travel time and total value of speed variation, the sensitivity analyses are conducted. The parameters that result in the least value are

selected, either by optimization or for convince. Such parameters are then used at different chosen weight set levels to see how objective function value varies.

In this section, the chosen optimal parameters and weight set are used and applied to the VSL control on the selected freeway, and the control results are given.

Furthermore, the performances of tabu algorithm are also compared to the SQP algorithm as a benchmark to examine the solution quality. A MATLAB based method called *fmincon*, which is developed based on the SQP algorithm, is used to solve the VSL control problem. It should be noted that, the optimal solution which is solved by SQP might not be an integer. Such continuous values are rounded to the nearest 5 miles/hour (e.g., 53.4miles/hour will be rounded to 55 miles/hour, and 51.2 miles/hour will be rounded to 50 miles/hour). The rounded integer values are displayed on the VMS in VISSIM, and the corresponding traffic states are saved. Three scenarios are included in this section: without VSL control, VSL control solved by the tabu search algorithm, and VSL control solved by the SQP.

Table 7.1 presents numerical results for the comparisons using the hypothetical freeway in Figure 5.1. Without VSL control, the total travel time is about 1295.17 hours, and the total speed variation is about 12146.66 miles/h. With VSL control, both the total travel time and the total speed variation have been improved, especially the total speed variation. The improvement percentages of total speed variation in the solution which was given by tabu search algorithm and SQP are 84.06% and 83.13% respectively. The improvement percentages of total travel time for tabu search and SQP are 10.69% and 6.85% respectively, which are presented in Table 7.1.

As can be seen from Table 7.1, the total travel time and total speed variation optimized by the SQP algorithm are 1206.47 hours and 2048.92 miles/h, respectively, which are both greater than those optimized by the tabu search. In addition, the improvement percentages of SQP are less than tabu search for both total travel time and total speed variation. As a result, the solution quality of tabu search algorithm outperforms SQP algorithm. In the following section, the VSL control results which were given by the tabu search algorithm (including traffic state profiles, optimal speed limit schemes, and speed profiles at a chosen time interval) are presented.

TABLE 7.1: Summary of Simulated Scenarios ($N_c=5$)

Scenarios	Total Travel Time (h)	Total Speed Variation (mi/h)	Objective Function Value (\$)	Improvement (%)	
				Total Travel Time	Total Speed Variation
Without Control	1295.17	12146.66	41533.05	/	/
Tabu Search Control Results	1156.76	1936.39	23726.26	10.69%	84.06%
SQP Control Results	1206.47	2048.92	24789.84	6.85%	83.13%

When no VSL control is implemented, the resulting average flow, speed and density profiles in the segment immediately upstream of the bottleneck (i.e., L_0) are shown in Figure 7.3. The flow reaches the bottleneck capacity at around $t=15$ min. However, after $t=15$ min, a visible decrease can be observed in traffic flows and meanwhile the speed drops to 15 miles/h. At the same time, the density increases from 50

veh/mile to about 270 veh/mile in a short time period. One can see that such trend continues for a long time, and even towards the end of the simulation, the speed and density have not recovered. The related average flow, speed, and density profiles with VSL control are also shown in Figure 7.3. One can clearly see that, compared to the no VSL control scenario, flow, speed and density are all improved. The VSL control maintains a steady condition in which the average discharge flow is close to the maximum bottleneck throughput volume (i.e., $C=4200$ veh/h). Due to the VSL control, the speed and density can recover to a normal level when the demand is less than the bottleneck capacity at the end of the simulation. Figure 5.6 shows the optimal speed limit scheme for the VSL control on each controlled segments during the entire simulation period.

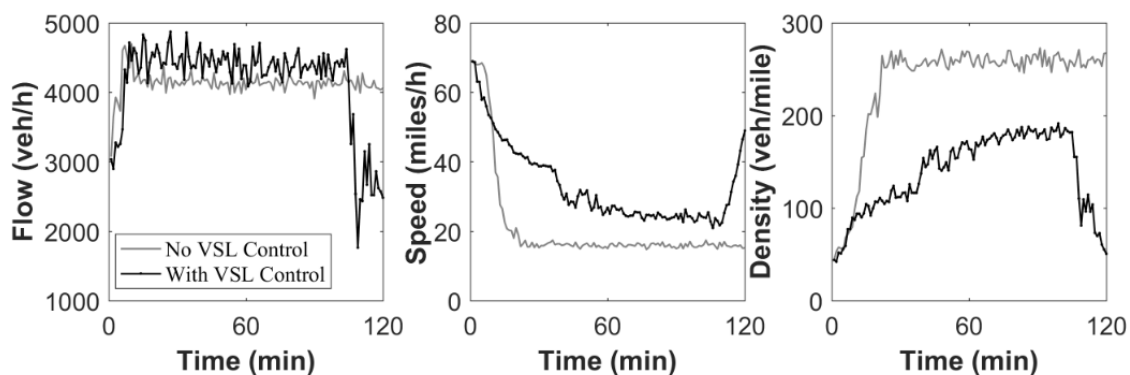


FIGURE 7.3: Flow, Density, and Speed Profiles

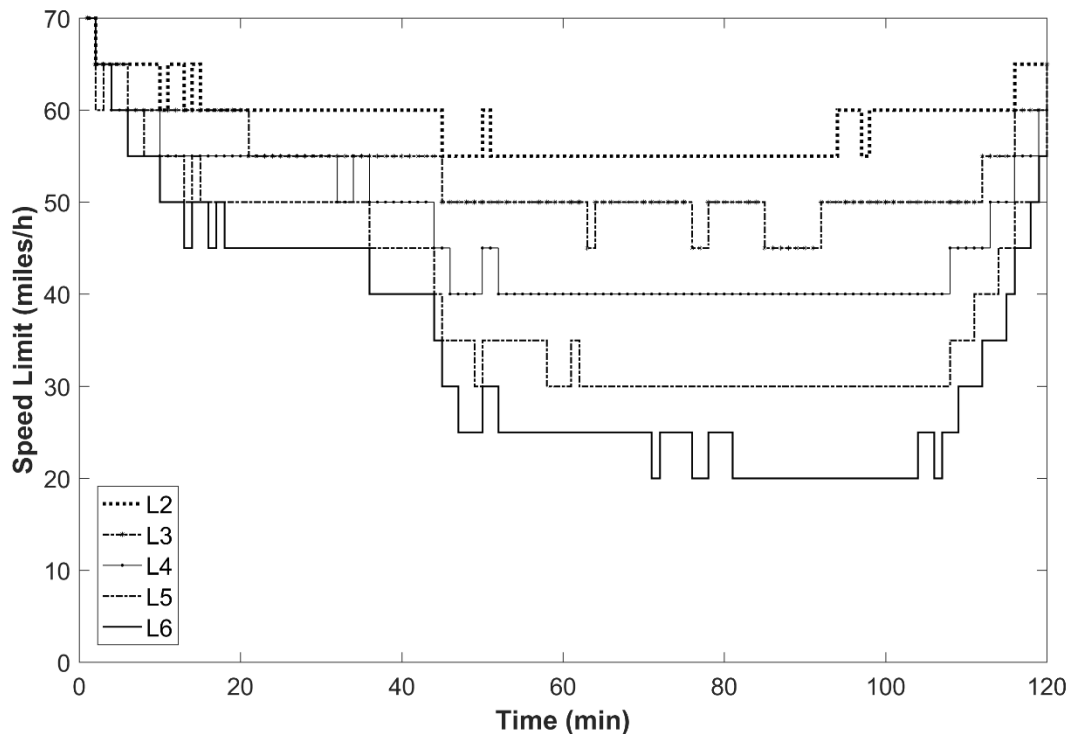


FIGURE 7.4: Optimal VSL Values for VSL Control during Each Time Interval

To clearly illustrate that the VSL control can decrease the total speed variation, the speed profiles on all six (L_1 - L_6 in Figure 5.1) freeway segments without control and with control during the chosen time period are presented. In Figure 7.5, the speed profiles at $k=68$ min are given. As can be seen from the figure, without VSL control, when vehicles drive from segment L_3 to segment L_4 , the drivers have to reduce their speed abruptly from about 68 miles/hour to about 20 miles/hour. This high speed variation might increase the possibility of accidents. Since minimizing the total value of speed variation is one of the objectives of VSL control in this study, the vehicles driving from the upstream should gradually slow down. As shown in Figure 7.5, due to the VSL control, the drivers can slow down on each segment. With respect to the constraint, the speed difference between the consecutive controlled segments at the same time interval is

less than 10 miles/h. Compared to the no VSL control scenario, the speed has been greatly harmonized and the level of safety on the freeway can be significantly improved.

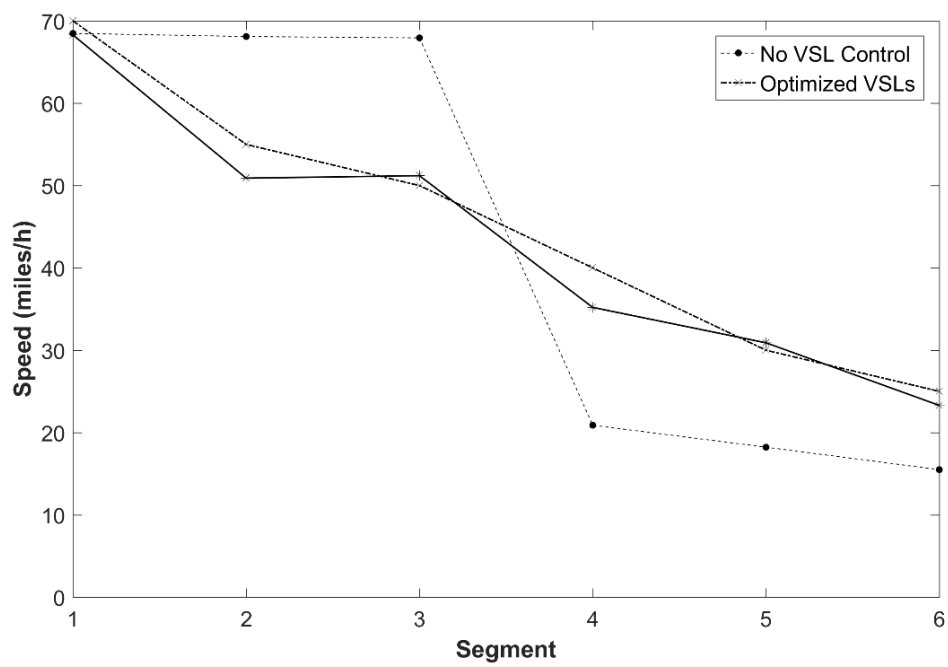
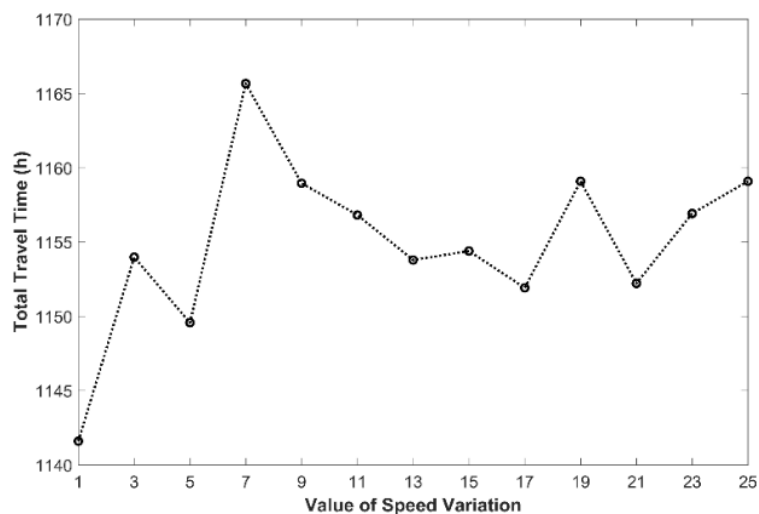


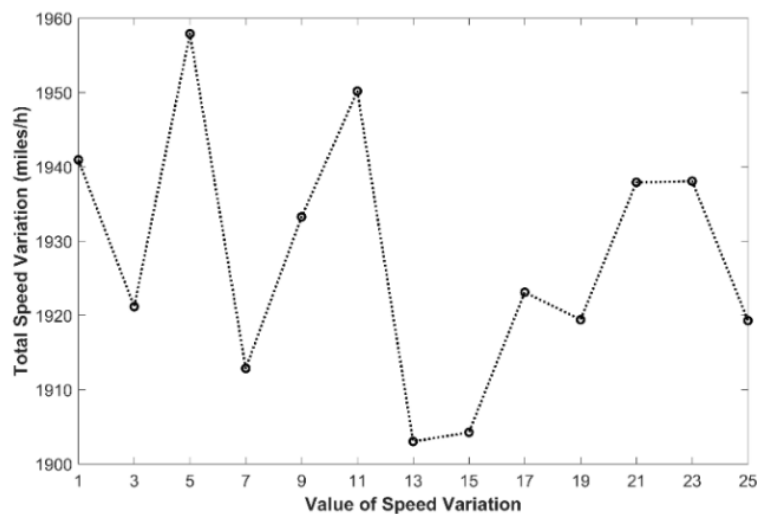
FIGURE 7.5: Speed Profiles on Each Segment at $k=68\text{min}$

As mentioned in the “Sensitivity Analyses” section, *VTT* has been studied and a rule-of-thumb value has been suggested by the USDOT in the U.S., while *VSV* needs to be assumed. In this section, all the control results are obtained based on the assumption that *VSV* is set as 15 \$*hour/miles, which may not be the exact value of *VSV*. Along that line, a sensitivity analysis of *VSV* is conducted by varying it from 1 to 25. Note that the value of *VTT* is still set as 20 \$/hour. The performances of the VSL control including total travel time, total speed variation, and objective function value are presented in Figure 7.6(a) through Figure 7.6(c), respectively. It can be seen from Figure 7.6(a) that the total travel time has an increasing trend as the value of *VSV* increases. However, in

Figure 7.6(b), no clear relationship between total speed variation and the value of *VSV* can be observed. Moreover, as can be clearly seen from Figure 7.6(c), as the value of *VSV* increases, the objective function value increases.



(a) Total Travel Time vs. *VSV*



(b) Total Speed Variation vs. *VSV*

FIGURE 7.6: VSL Control Performances vs. *VSV*

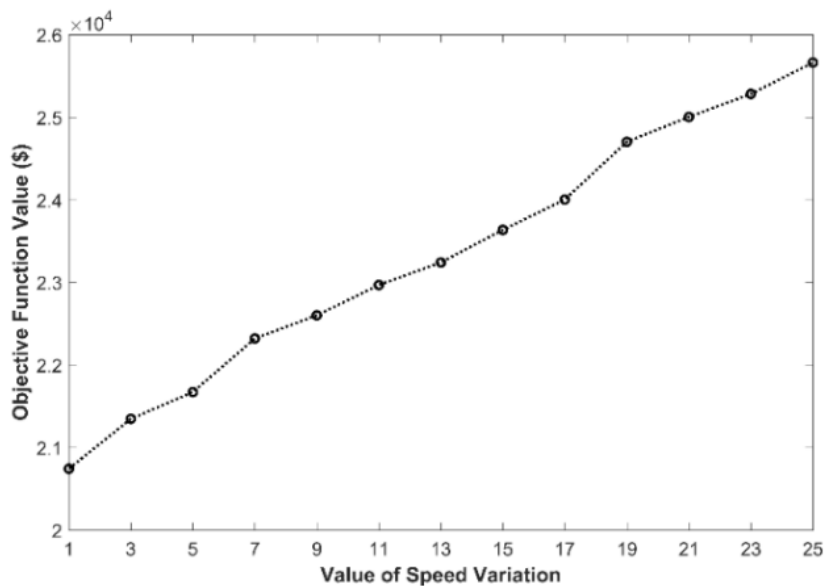
(c) Objective Function Value vs. *VSV*

FIGURE 7.6, continued

7.2.5. Effects of the Number of VSL Control Segments

Up to this point, no researchers have studied the relationships between the number of VSL control segments and the objective function. In reality, determining the appropriate required number of VSLs for operations is highly desirable. As one can see, VSL control systems are very extensive due to the wide variety of parameters and procedures involved (e.g., the length of control segment, the length of control horizon, or the chosen weight set level for each component of the objective function). However, it is expected that in most cases, the relationships between the number of VSL control segments and the objective function should be similar, and a common conclusion can still be obtained.

How the number of VSL control segments might affect the total value of travel time and total value of speed variation is first studied in this section. In Table 7.2, the control results of the total value of travel time only (i.e., the weight of total speed variation is 0) and total value of speed variation only (i.e., the weight of total travel time is 0) with different number of VSL control segments are shown. It should be noted again that, in this section, the values of VTT and VSV are set as 20 \$/hour and 15 \$*hour/miles, respectively. Table 7.2 shows the total travel time and total speed variation obtained from the simulation. The number of control segments ranges from 1 to 5. As can be seen, the relationship between the number of VSL control segments and total travel time and total speed variation can be presented as follows. Generally speaking, as the number of control segments increases, the total travel time increases. With more VSLs, the speed limit on the controlled segments might be less than the free flow speed. As a result, the density on such segments will also be greater. The total travel time is calculated based on the density on the studied freeway, so the total travel time will be greater than that under the free flow speed scenario. In Table 7.2., one can see that no matter how many VSLs are used, the total travel time is less than that under the scenario without control (which is 1295.17 veh-h as shown in Table 7.1). Because, as shown in Figure 7.3, VSL control can improve the bottleneck discharge volume. Furthermore, as the number of VSLs increases, the total speed variation decreases. With more control segments, the speed can gradually decrease all the way from the most upstream to the most downstream segments. As such, the total speed variation decreases. In addition, the VSL control strategy that minimizes total value of travel time only can also improve the total speed variation compared to that under the no-control scenario (which is 12146.66

miles/h as shown in Table 7.1). However, compared to others, the improvement percentage is not significant with one or two VSL control segments on the studied freeway segments. It can also be seen from Table 7.2 that VSL control strategy that minimizes the total value of speed variation only also results in an improvement of total travel time, compared to the scenario without VSL control.

TABLE 7.2: Total Value of Travel Time Only and Total Value of Speed Variation Only

Total Value of Travel Time only ($w_1=1, w_2=0$)					
Number of Control Segments	Control Segments	Total Travel Time (h)	Total Speed Variation (mi/h)	Improvement (%)	
				Total Travel Time	Total Speed Variation
$N_c=1$	L_6	915.45	10861.6	29.32%	10.58%
$N_c=2$	L_5, L_6	916.55	9553.28	29.23%	21.35%
$N_c=3$	L_4-L_6	918.38	6117.44	29.09%	49.64%
$N_c=4$	L_3-L_6	925.72	4770.9	28.53%	60.72%
$N_c=5$	L_2-L_6	991.45	3991.52	23.45%	67.14%

Total Value of Speed Variation only ($w_1=0, w_2=1$)					
Number of Control Segments	Control Segments	Total Travel Time (h)	Total Speed Variation (mi/h)	Improvement (%)	
				Total Travel Time	Total Speed Variation
$N_c=1$	L_6	927.67	9966.61	28.37%	17.95%
$N_c=2$	L_5, L_6	932.48	7322.81	28.00%	39.71%
$N_c=3$	L_4-L_6	983.69	4623.1	24.05%	61.94%
$N_c=4$	L_3-L_6	1057.65	2272.63	18.34%	81.29%
$N_c=5$	L_2-L_6	1187.76	1763.95	8.29%	85.48%

Figure 7.7 presents the combined objective function value with different number of VSL control segments. The effect of the weight of total value of travel time is examined by varying w_1 from 0.1 to 0.9. It can be seen from the Figure 7.7, with the same weight set, the objective function values with more VSL control segments are less than the values with less control segments. When the number of control segments is the same, as the weight of total value of travel time w_1 increases, the objective function value decreases. When the weight set is chosen as $w_1=0.9$ and $w_2=0.1$, the least objective function value occurs with 4 VSL points (i.e., $N_c=4$). Also, according to the result in Table 7.2 and Figure 7.7, if the VSL control strategy aims to harmonize the travel speeds within the control segments, more control segments should be implemented.

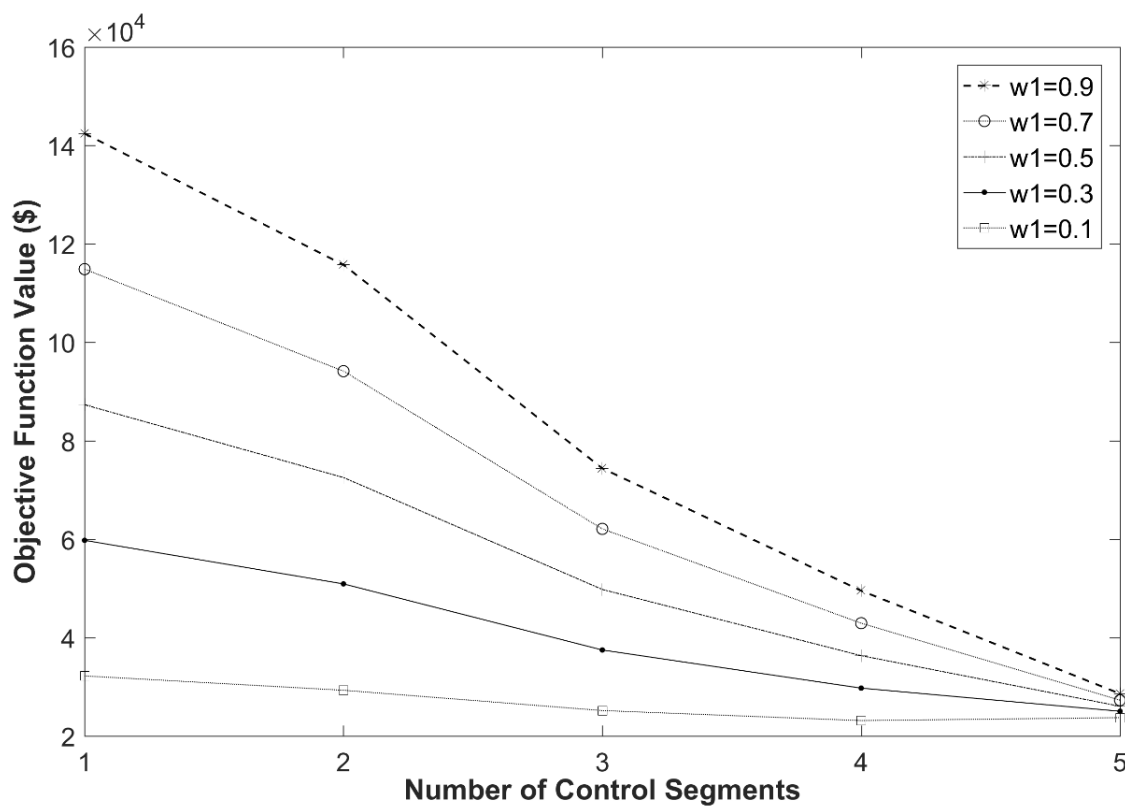


FIGURE 7.7: Objective Function and the Number of VSL Control Segments

7.3. VSL Control for Mixed Traffic Flows

7.3.1. Calibration of Global Parameters of METANET

In this section, the global parameter of the modified METANET is calibrated. The global parameter set is set as $X = [\tau, \nu, \kappa]$. The discrete time step used in the METANET model is $T=10$ s. An objective function is selected to minimize the total error between the measured and predicted speeds and flow of vehicle type j

min

$$f = \sum_{i=1}^N \sum_{k=1}^K \sum_{j=1}^J \left(\left(\frac{v_{i,j,\text{measured}}(k) - v_{i,j,\text{predicted}}(k)}{(v_{i,j,\text{measured}}(k) + v_{i,j,\text{predicted}}(k))/2} \right)^2 + \left(\frac{q_{i,j,\text{measured}}(k) - q_{i,j,\text{predicted}}(k)}{(q_{i,j,\text{measured}}(k) + q_{i,j,\text{predicted}}(k))/2} \right)^2 \right)$$

Subject to

$$X_{\min} \leq X \leq X_{\max}$$

$$X_{\min} = [0.05, 10, 10]$$

$$X_{\max} = [0.2, 60, 60]$$

Where:

$v_{i,j,\text{measured}}(k)$ = measured speed of vehicle type j on segment i during time interval

k by VISSIM;

$v_{i,j,\text{predicted}}(k)$ = predicted speed of vehicle type j on segment i during time interval

k by METANET;

$q_{i,j,\text{measured}}(k)$ = measured flow of vehicle type j on segment i during time interval k

by VISSIM;

$q_{i,j,\text{predicted}}(k)$ = predicted flow of vehicle type j on segment i during time interval k by METANET.

The objective function is also solved by the SQP algorithm. It should be pointed out that the required precision is two places after the decimal point. Different start points are tested to find a good local optimal solution. Finally, the optimal solution set used in this section is $X_{\text{optimal}} = [0.1, 10.00, 59.95]$, and the corresponding objective function value is 459.34.

7.3.2. Control Results

The proposed GA procedure is implemented to help optimize the VSL control problem by using the MATLAB software package. It should be noted that the case study which is presented in Figure 5.2 is used in this section. The total simulation time is 2.5 hours, which includes a 0.5 hour warm-up period. The traffic data which is generated by VISSIM is collected every 1-min, and therefore the total number of time interval $K=120$ in this study. Moreover, the average minimum headway uses the default value in VISSIM (i.e., $CC1=0.9s$), which is the same for cars and trucks, i.e. $t_{\text{car}} = t_{\text{truck}} = 0.9s$. In addition, the gross stopping distance sd_j of vehicle type j equals the length of vehicle type j plus the distance gap (i.e. the standstill distance in VISSIM and the value is $CC0=4.92$ ft) (van Lint et al. 2008). The length of passenger cars is set to be 15.62 ft and the length of trucks is set to be 33.51 ft (the length of HGV in VISSIM) which are from the VISSIM. Finally, the gross stopping distance of passenger cars $sd_{\text{car}} = CC0 + 15.62 = 20.54$ ft and the gross stopping distance of trucks $sd_{\text{truck}} = CC0 + 33.51 = 38.43$ ft.

The speed limit set of the VSL control changes every minute (i.e., $T_c=1$ min), and the prediction time horizon is set as 5min (i.e., $T_p=5$ min). Different weight sets might affect the solution quality of VSL control. In this study, it is assumed more importance is paid to the TTT, and as such, the weight of the TTT is set as 0.6. A sensitivity analysis of the weight of TSV is conducted by setting the weight of TTT as 0.6 and varying the weight of TSV. All of the GA parameters, such as population sizes, the number of generations, mutation rate, and crossover rate, use the default settings in *MATLAB* software package for GA. The numerical result is presented in Figure 7.8. Note that $w_1 + w_2 + w_3 = 1$. Also, for illustration convenience, $w_1=0.6$, $w_2=0.2$, and $w_3=0.2$ are selected for further analyses.

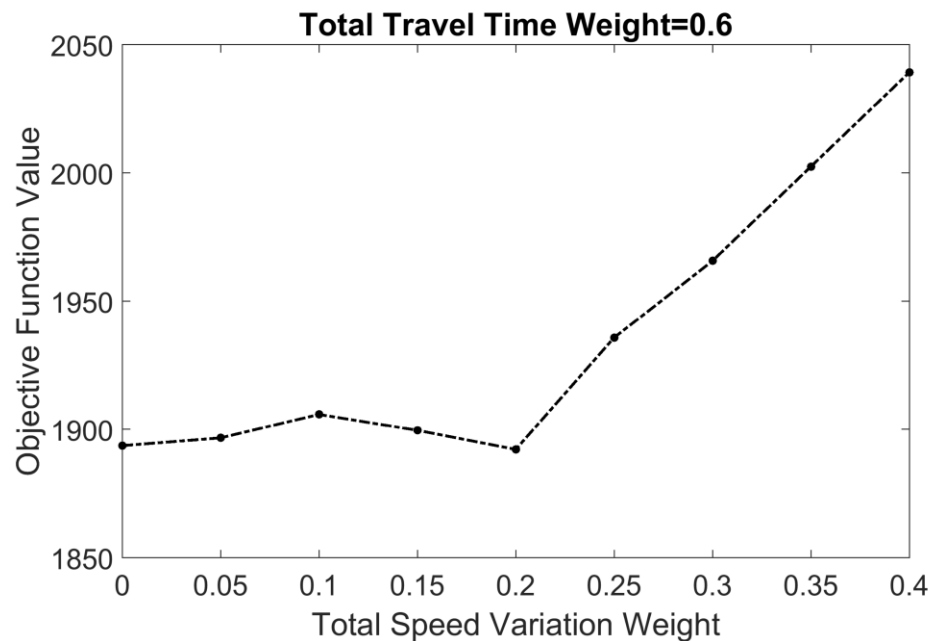


FIGURE 7.8: Sensitivity Analysis for the Weight of Total Speed Variation

The weight set (0.6, 0.2, 0.2) is used and applied to the VSL control on the selected freeway segments, as shown in Figure 7.8. The driver compliance rate is set as 100%. Three scenarios are included in this section: without VSL control, the VSL control optimized by GA, and the VSL control solved by the SQP. The continuous optimal speed limits optimized by the SQP are rounded to the nearest 5 miles/h. Both the optimized speed limit set solved by GA and rounded integer values are displayed on the VMS in VISSIM. The corresponding simulation flow, speed, and density are saved, including the effective traffic data of both passenger cars and trucks. The simulation is run with ten different random seeds for 2.5 hours with a 0.5 hour being the warm-up period. The average TTT, TSV, and TSD are calculated so that the simulation results with VSL control and without VSL control can be compared.

Table 7.3 shows a summary of simulated results. The numerical results in Table 7.3 are used for the comparisons. Without VSL control, the TTT is about 1876.83pce-h, the TSV is about 16783.67miles/h, and the TSD is about 10831.1miles/h. With VSL control, the TTT, TSV, and TSD are all improved. The improvement percentages of TTT in the solution which were optimized by GA and SQP are 15.51% and 14.56% respectively, indicating that the operational efficiency has been improved with VSL control. Both the TSV and TSD have been greatly improved by the VSL control, which indicates the VSL control can significantly homogenize travel speeds of vehicles at the bottleneck area. Such speed homogenizations can improve the safety and reduce the possibility of collisions/accidents, which have been proven by many researchers (Hegyí et al. 2005; Fang et al. 2014; Li et al. 2016). It can also be seen from Table 7.3, the TTT, TSV, and TSD optimized by the SQP are all greater than those optimized by the GA. In

addition, the corresponding improvement percentages of SQP are less than the GA for all the TTT, TSV, and TSD. As a result, the solution quality of GA outperforms the SQP, which is similar to Yeniay's result (2005). In a study conducted by Yeniay (2005), SQP and GA were compared. 15 representative constrained nonlinear programming problems were selected. The results indicated that in most cases, the SQP could not give better solutions than those found by using GA.

TABLE 7.3: Summary of Simulated Results

Scenario	TTT (pce-h)	TSV (miles/h)	TSD (miles/h)	Improvement (%)		
				TTT	TSV	TSD
Without Control	1876.83	16783.67	10831.1	/	/	/
GA results	1585.67	2719.71	1984.26	15.51	83.79	81.68
SQP results	1603.58	2742.87	2048.59	14.56	83.66	81.09

In addition, Figure 7.9 presents the objective function values of the SQP and GA vs. iterations when the control time period is set as 5 min, 20 min, 40 min, 60 min, 80 min, and 100 min, respectively, in which the speed limit sets optimized by the GA and SQP for the five segments are also included. One can also see from Figure 7.9 that for these six control time intervals, in most cases, GA achieves a better objective function value than the SQP except when $t=80$ min. And, the number of iterations (or generations) of GA is greater than SQP's. The selection of the initial point of SQP is important. With a good initial point, the solution quality of the SQP might be better than GA. For some

problems, the SQP might get trapped with local optimum solutions rather far from the true optimal solutions (e.g., $t=5$ and 100 min in Figure 7.9). To compare the efficiency of SQP and GA, the computing times of the two algorithms are collected. The computing time of SQP is about 90.23 min. GA's computing time is about 128.63 min, which is longer than SQP. The computing time indicates that SQP is more efficient than GA. However, in terms of the solution quality, GA outperforms SQP and therefore, is recommended for use to solve the VSL control problem. The control results which are optimized by the GA are given in the following section.

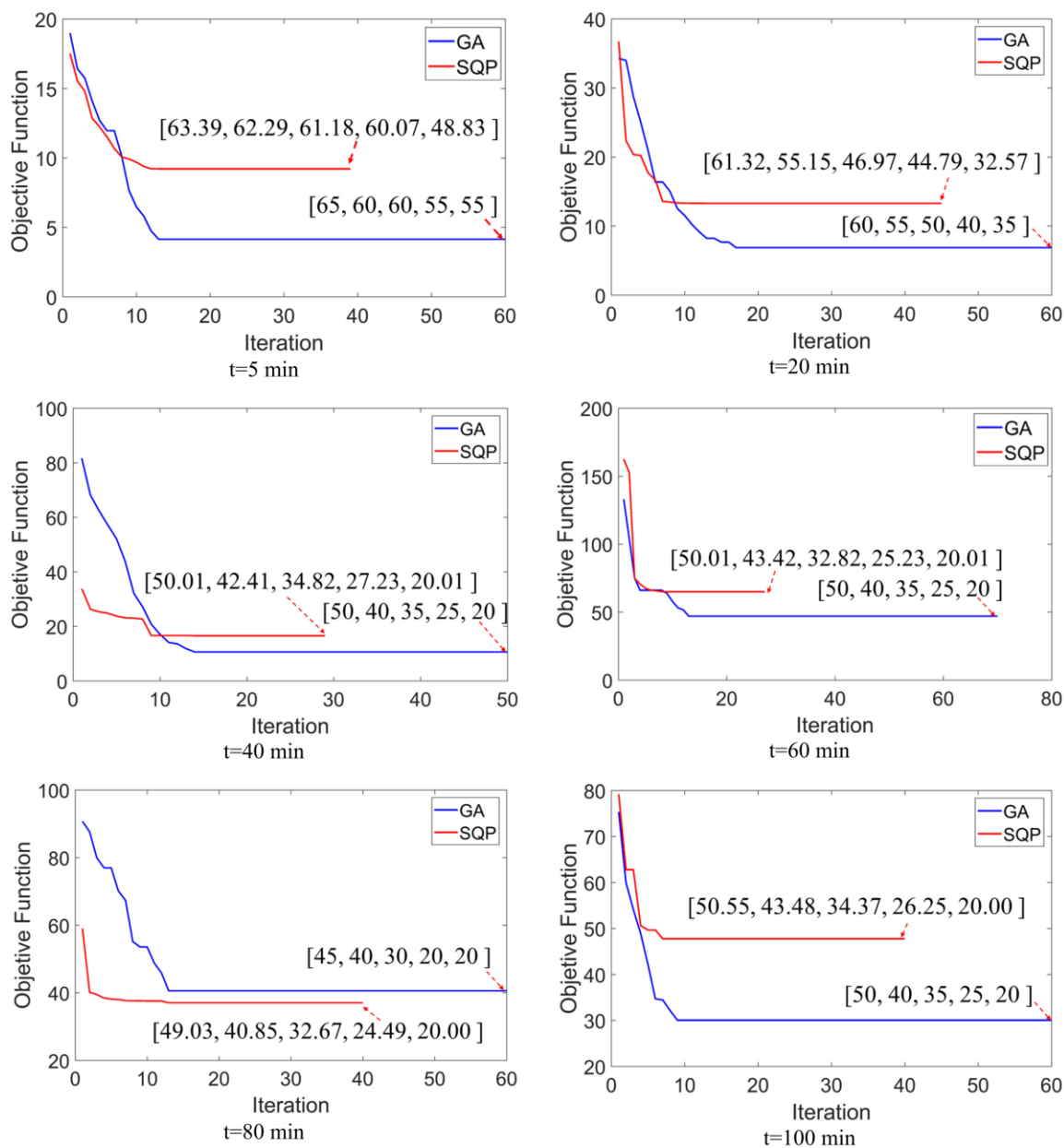
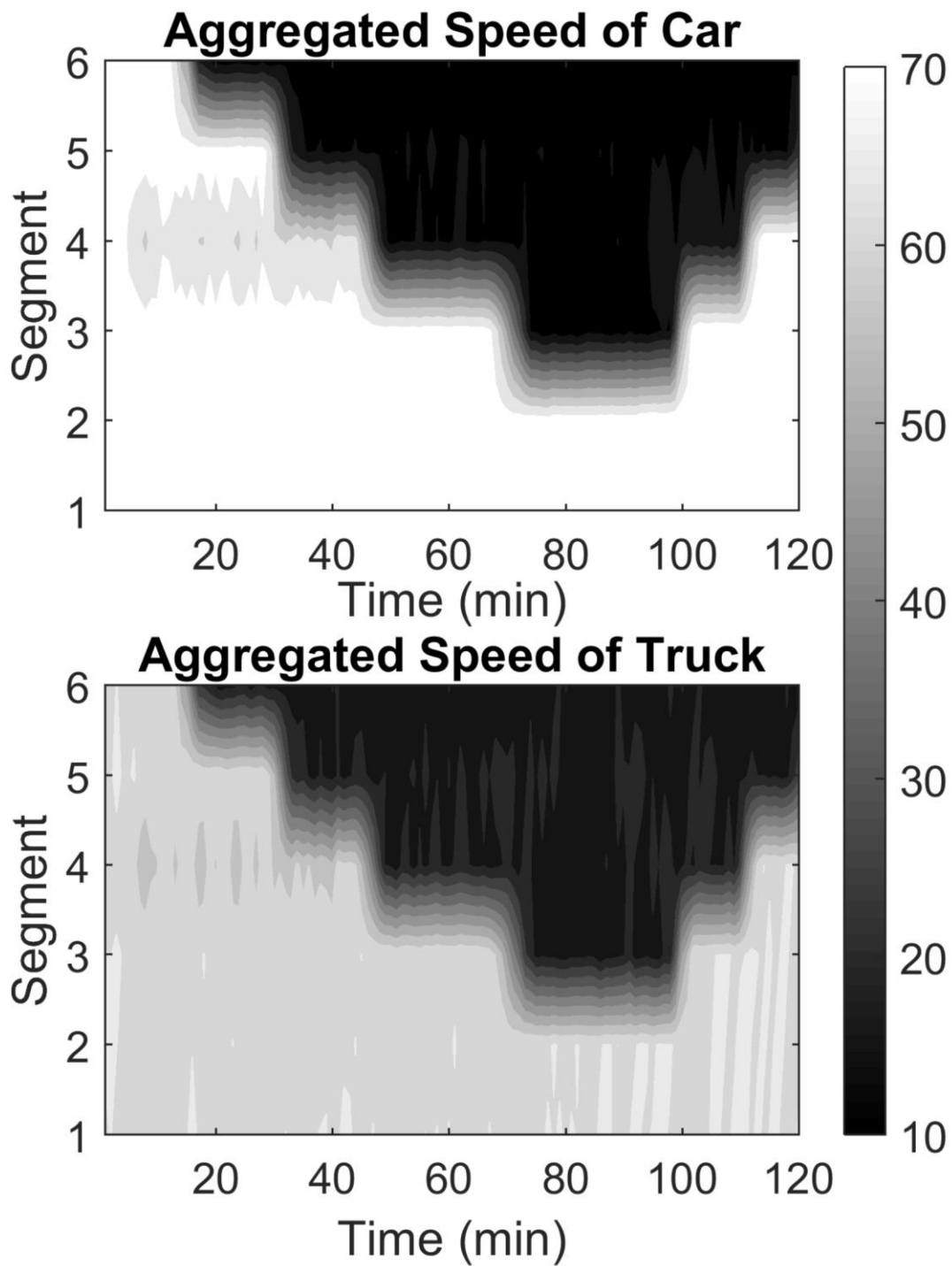


FIGURE 7.9: Objective Function Values of the SQP and GA vs. Iterations

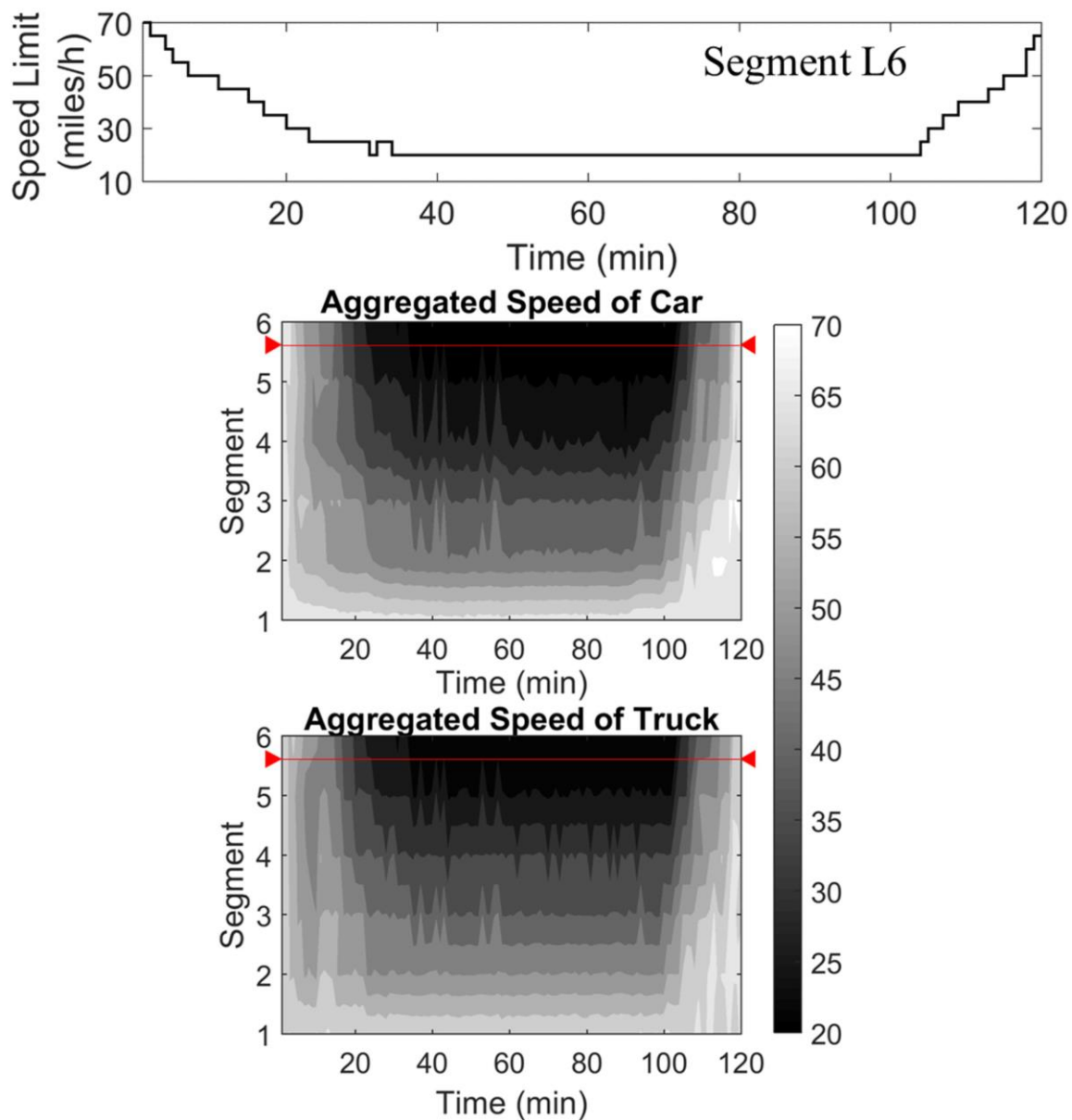
Traffic demands on the selected freeway stretch are large, resulting in prolonged total travel time, huge speed variation, and significant speed difference. Figure 7.10(a) presents the speed contour of car and truck observed on each freeway segment without VSL control. The x-axis is the simulation time, and the y-axis is the segment. The color

scale represents the observed average speeds during the entire simulation period. The bottleneck activates due to the lane closure when traffic demand is greater than the bottleneck capacity. The queue which forms at the bottleneck increases in length and propagates toward the upstream segments. It can be seen from Figure 7.10(a), the speed variation between the upstream segments and bottleneck are large for both cars and trucks. The speed profiles in Figure 7.10(a) illustrate that lower speeds (less than 20 miles/h) on the last freeway segment (i.e., *L6*) for both cars and trucks remain even at the end of the simulation without VSL control.



(a) Speed Contour on Each Segment without VSL Control

FIGURE 7.10: Speed Contours on Each Segment without and with VSL Control



(b) Speed Contours on Each Segment with VSL Control

FIGURE 7.10, continued

The speed contours on each segment with VSL control are illustrated in Figure 7.10(b). The optimal speed limit (solved by the GA) is also included in Figure 7.10(b) as an example to present the speed profiles with VSL control on segment *L6*. It can be seen in Figure 7.10(b), the gradual change of color is presented, which indicates that a smooth

transition between speeds on each segment for both cars and trucks can be achieved due to the VSL control. In Figure 7.10(b), the resulting speed profiles for both cars and trucks on segment L_6 are consistent with the optimal speed limit on this segment during all time intervals. With VSL control, the speeds of cars and trucks on controlled segment begin to increase as the simulation runs, as depicted in Figure 7.10(b). In addition, Figure 7.11 shows the optimal speed limit scheme for the VSL control on each controlled segments during the entire simulation period.

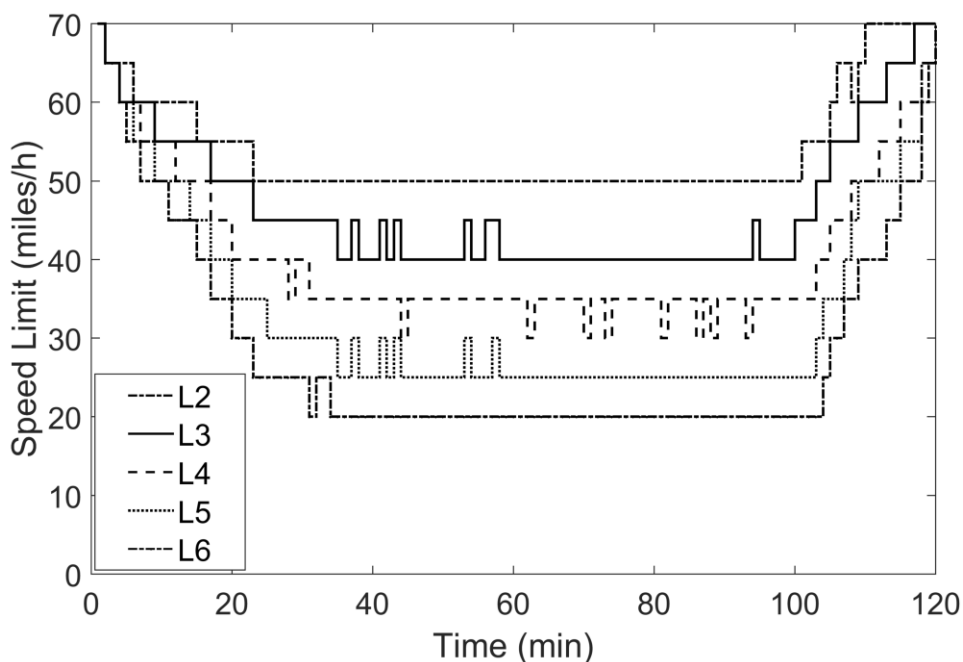
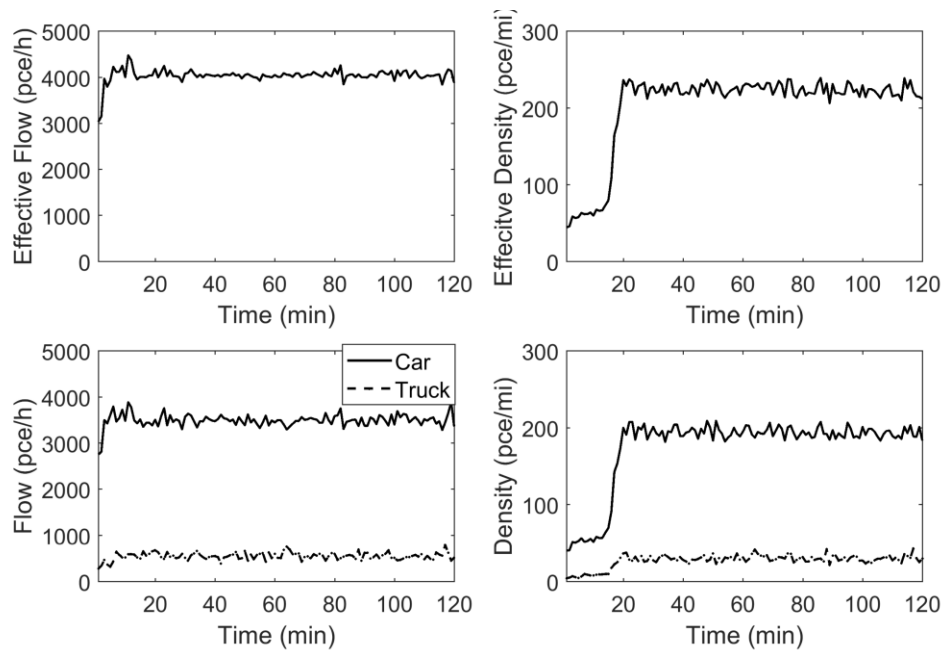


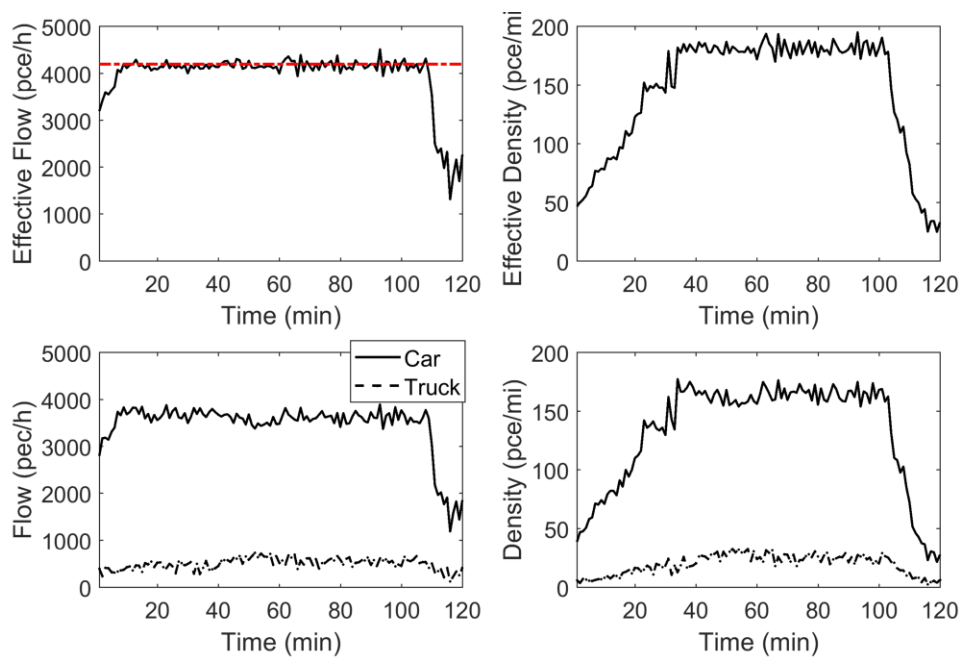
FIGURE 7.11: Optimal Speed Limit Scheme for the VSL Control on Each Segment

Figure 7.12(a) and Figure 7.12(b) show the traffic flow and density profiles during the whole simulation period on the last controlled segment (i.e. L_6 , as shown in Figure 5.2) without control and with the VSL control solved by the GA. Figure 7.12(a) presents that, when the demand is greater than the maximum discharge volume of the

bottleneck, a drop in flow and an increase in density are observed on the freeway segment. As can be seen in Figure 7.12(a), due to the congestion, the effective flow is about 4000 pce/h. Figure 7.12(b) shows the results with VSL control. Before the traffic breakdown occurs, the VSL control is activated. Due to the VSL control, the number of vehicles entering the bottleneck is metered. As presented in Figure 7.12(b), the effective flow with VSL control maintains a steady condition and a relative high average discharge volume (less than 4200 pce/h) is obtained compared to the effective flow without VSL control. In addition, compared to the results without VSL control, the effective density is also improved. For example, the density profiles in Figure 7.12(a) illustrate that high density (more than 220 pce/mile) remain even at the end of the simulation without VSL control. However, with VSL control, the effective density begins to decrease as the simulation runs, as depicted in Figure 7.12(b).



(a) Flow and Density without VSL Control



(b) Flow and Density with VSL Control

FIGURE 7.12: Flow and Density without and with VSL Control

The driver compliance rate is a key factor which might affect the control performance of the VSL control. The relation between driver compliance rate and VSL control has been studied by the researchers. In Lu et al.'s (2010) study, the TTT with 30% and 100% compliance rates were compared, and the resulting TTTs were almost identical. Yang et al. (2017) showed that different driver compliance rates can result in different control performances. As the driver compliance rate decreases, the improvement percentage of VSL also decreases. In this study, a sensitivity analysis of driver compliance rate is conducted by varying the value from 50% to 100%, and the result is shown in Figure 7.13. In terms of TTT, TSV, and TSD, the VSL controls with different driver compliance rates outperform the scenario without control (as shown in Table 7.3). The VSL control with 100% driver compliance rate produces the best performance. It can be seen from Figure 7.13, as the driver compliance rate increases, the objective function value and its three components decrease which is line with the existing studies (Yang et al. 2017).

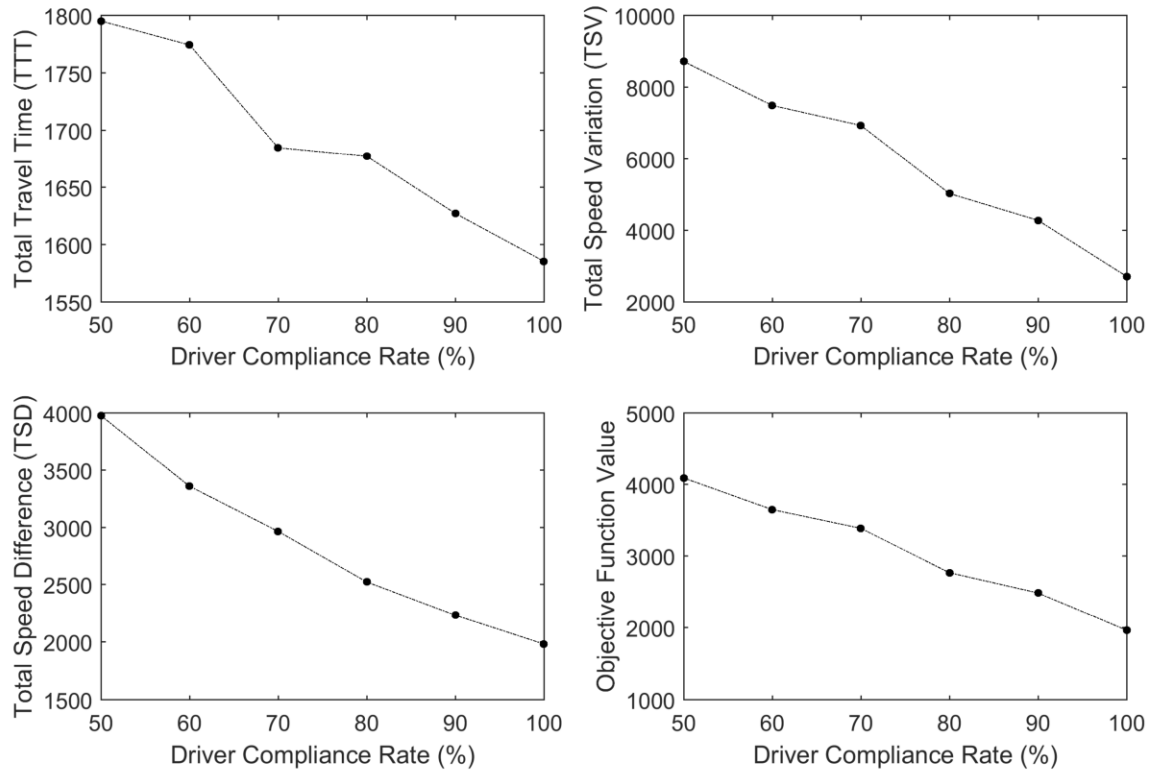


FIGURE 7.13: Driver Compliance Rates and Control Performances

7.3.3. Truck Percentage and VSL Control

In the previous sections, the truck percentage is set to be 10% during the entire simulation period. However, in reality, the truck percentage might be different during different time intervals. Moreover, high truck percentage might greatly affect the VSL control results. Thus, the relationship between truck percentage and the control results is explored in this section. A multi-objective is formulated for the VSL control, which contains TTT, TSV, and TSD. Such three components with different truck percentages are also presented.

The effect of truck percentage is investigated by varying it from 1% to 20%, and the values of each performance measure of the VSL control with each truck percentage including the TTT, TSV, TSD, and objective function value are shown in Figure 7.14(a) through Figure 7.14(d) respectively. Note that, the driver compliance rate in this section is 100%. The relationship between truck percentage and VSL control can be presented as follows. Generally speaking, as the truck percentage increases, the average gap distance between vehicles will be larger and the total number of vehicles per mile on the studied freeway segments will be less. Since the total demand is the same, it needs more time to discharge all the vehicles. As a result, the TTT increases with the increasing percentage of trucks, which is clearly shown in Figure 7.14(a). Moreover, increasing the truck percentages indicates more trucks travel on the freeway. The speeds of passenger cars can be more negatively affected due to the increasing number of trucks, which result in an increase in the speed difference/variation on the studied freeway. As such, both the TSV (Figure 7.14(b)) and TSD (Figure 7.14(c)) increase as the truck percentage increases. In addition, as shown in Figure 7.14(d), as the percentage of truck increases, the objective value also increases. The sensitivity analyses indicate that the increase of truck percentage reduces the overall operational efficiency and safety of the proposed VSL control system.

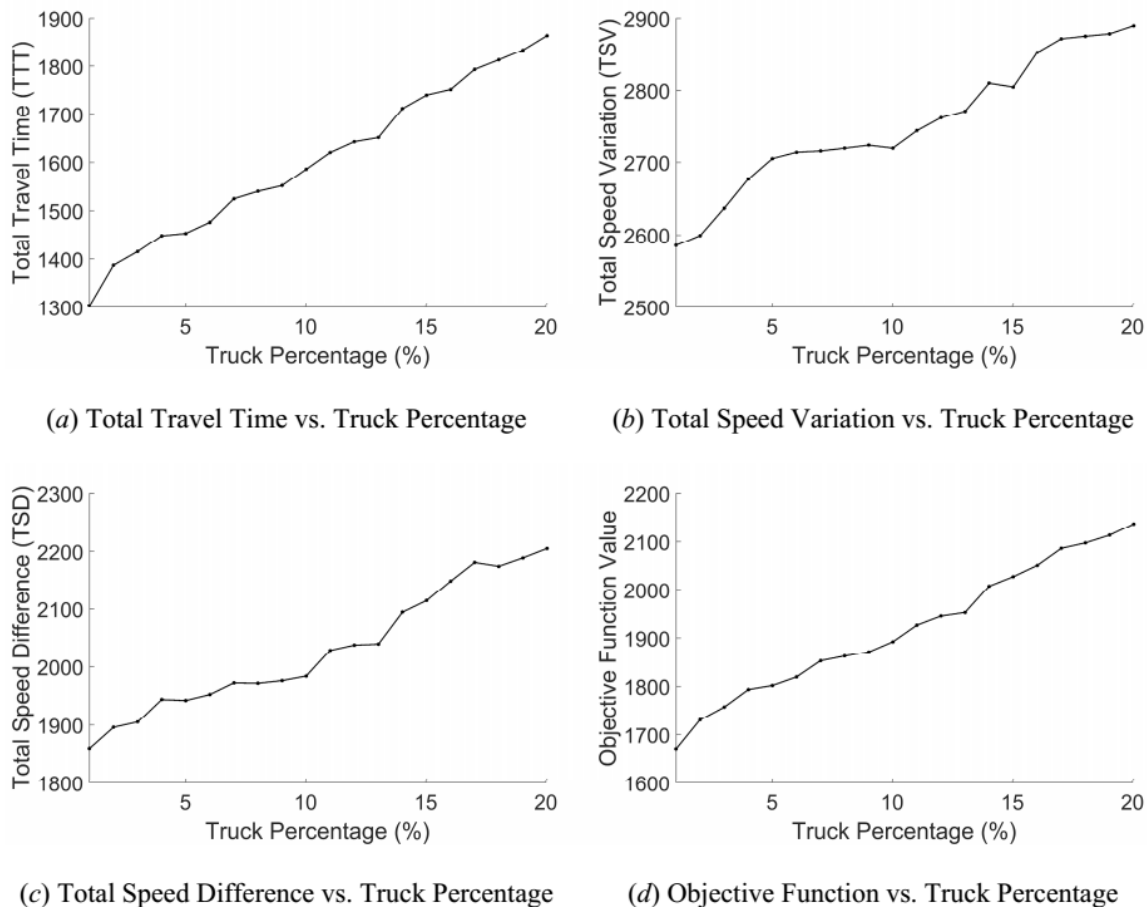


FIGURE 7.14: Truck Percentage vs. Objective Function and Its Components

7.4. Combined VSL Control and Truck Lane Restriction

VISSIM is used to simulate the vehicles traveling on the freeway stretch, as shown in Figure 5.3. Trucks are represented by the HGV (heavy goods vehicles) in VISSIM 7.0. According to Lavel and Daganzo (2004), the lane change time t_{LC} is set as 3.0s. The whole simulation period is 3.5 hours, and a 0.5-hour warm-up period is included. The traffic data generated by the VISSIM is collected every 1 min. As a result, the total number of time interval $K=180$. As mention, the dynamic pce value in the NTR

lanes needs to be computed. The vehicle's physical characteristics and driver behavior parameters (such as average minimum headway, the length of vehicles, and the standstill distance of vehicles) are needed. The default minimum headway in VISSIM is used ($CC1=0.9s$). Such value is the same for both the cars and trucks in the NTR lanes, i.e., $t_{car} = t_{truck} = 0.9s$. The safety distance sd_j of vehicle type j equals the length of vehicle type j plus the distance gap (i.e., $CC0$, the standstill distance in VISSIM which is set as $CC0=4.92$ ft). The length of a passenger car is set to be 15.62 ft, and the length of a truck is set to be 33.51 ft (the length of HGV in VISSIM), both of which are adopted from the VISSIM. Finally, the safety distance of passenger cars $sd_{car} = CC0 + 15.62 = 20.54$ ft and the safety distance of trucks $sd_{truck} = CC0 + 33.51 = 38.43$ ft.

7.4.1. Computing the Global Parameters of the Extended METANET Model

The extended METANET model is used. It should be pointed out that, the computation process is performed without VSL control, and trucks are not allowed to travel in the left two lanes. Eight global parameters included in the extended METANET model, i.e. $\tau_{TR}, \nu_{TR}, \kappa_{TR}, \delta_{TR}, \tau_{NTR}, \nu_{NTR}, \kappa_{NTR}$, and δ_{NTR} , need to be computed to minimize the total error between the measured speeds and flows in VISSIM and predicted speeds and flows. The global parameter set is set as

$\mathbf{X} = [\tau_{TR}, \nu_{TR}, \kappa_{TR}, \delta_{TR}, \tau_{NTR}, \nu_{NTR}, \kappa_{NTR}, \delta_{NTR}]$. The discrete time step used in the

METANET model is $T=10s$.

The total error in the TR lanes is

$$Dif_{TR} = \sum_{i=1}^N \sum_{k=1}^K \left(\frac{v_{i,sim}^{TR}(k) - v_{i,pre}^{TR}(k)}{(v_{i,sim}^{TR}(k) + v_{i,pre}^{TR}(k))/2} \right)^2 + \left(\frac{q_{i,sim}^{TR}(k) - q_{i,pre}^{TR}(k)}{(q_{i,sim}^{TR}(k) + q_{i,pre}^{TR}(k))/2} \right)^2$$

where

$v_{i,sim}^{TR}(k)$ and $q_{i,sim}^{TR}$ are the simulation speed and flow in the TR lanes on segment i

during time interval k by VISSIM respectively;

$v_{i,pre}^{TR}(k)$ and $q_{i,pre}^{TR}(k)$ are the predicted speed and flow in the TR lanes on

segment i during time interval k respectively.

The total error in the NTR lanes is

$$Dif_{NTR} = \sum_{i=1}^N \sum_{k=1}^K \sum_{j=1}^J \left(\left(\frac{v_{i,j,sim}^{NTR}(k) - v_{i,j,pre}^{NTR}(k)}{(v_{i,j,sim}^{NTR}(k) + v_{i,j,pre}^{NTR}(k))/2} \right)^2 + \left(\frac{q_{i,j,sim}^{NTR}(k) - q_{i,j,pre}^{NTR}(k)}{(q_{i,j,sim}^{NTR}(k) + q_{i,j,pre}^{NTR}(k))/2} \right)^2 \right)$$

where

$v_{i,j,sim}^{NTR}(k)$ and $q_{i,j,sim}^{NTR}(k)$ are the simulation speed and flow of vehicle type j in the

NTR lanes on segment i during time interval k by VISSIM respectively;

$v_{i,j,pre}^{NTR}(k)$ and $q_{i,j,pre}^{NTR}(k)$ are the predicted speed and flow of vehicle type j in the

NTR lanes on segment i during time interval k respectively.

The objective function is

$$\min f = Dif_{TR} + Dif_{NTR}$$

Subject to

$$\mathbf{X}_{\min} \leq \mathbf{X} \leq \mathbf{X}_{\max}$$

$$\mathbf{X}_{\min} = [0.05, 10, 10, 0.1, 0.05, 10, 10, 0.1]$$

$$\mathbf{X}_{\max} = [0.2, 100, 100, 10, 0.2, 100, 100, 10]$$

The objective function is solved by the multi-start SQP in MATLAB R2017a. Note that the required precision is two places after the decimal point. Finally, the optimal solution set used in this study is $\mathbf{X}_{\text{optimal}} = [0.09, 99.99, 57.07, 9.86, 0.08, 96.06, 99.99, 0.11]$, and the corresponding objective function value is 136.28.

7.4.2. Validation the Extended METANET Model

In order to test and demonstrate the validity of the modified METANET model, the global parameters resulting from the computing process are used. For the sake of brevity, segment *L4* (see Figure 5.3) is selected as an example to compare the simulated and predicted speed and flow data in the TR and NTR lanes respectively. As shown in Figure 7.15, the modified METANET can be used to predict the traffic state of cars and trucks in the TR and NTR lanes.

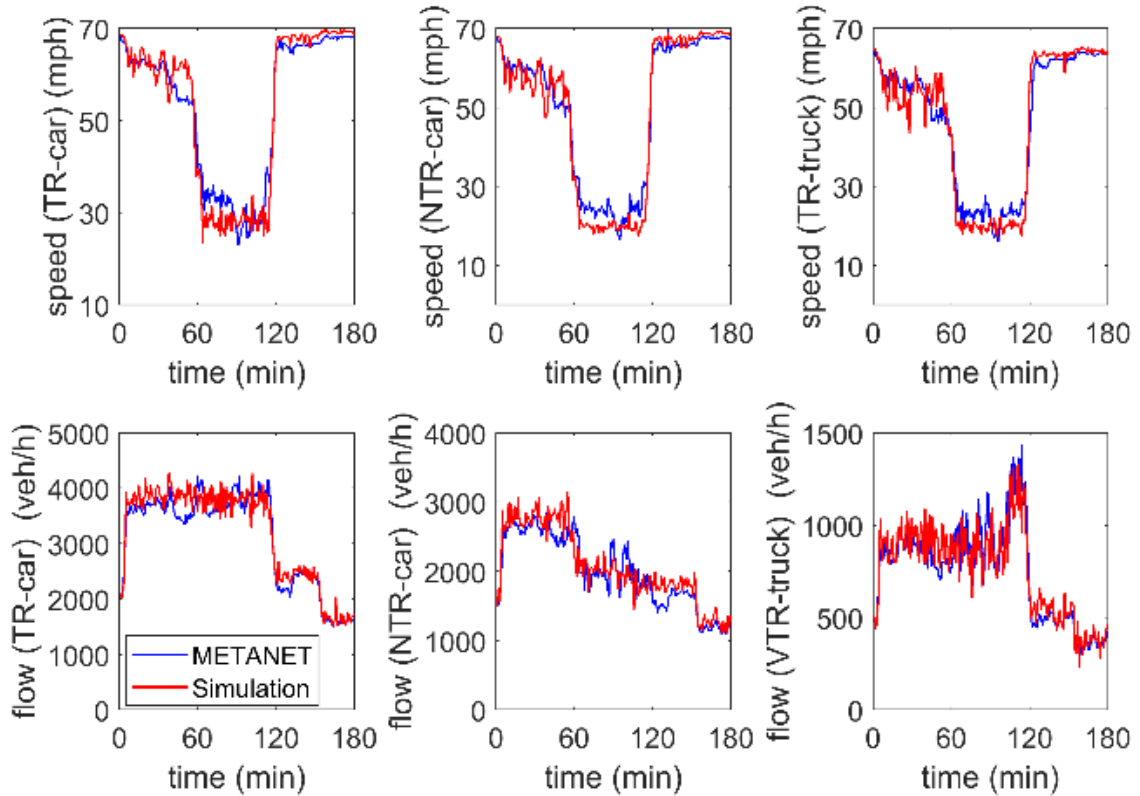


FIGURE 7.15: Comparison between the Simulation Data and Prediction Results in the TR and NTR Lanes on Segment $L4$

7.4.3. Control Results

By using the MATLAB software package, the GA and SA are implemented to optimize the VSL control. The speed limit value on each controlled segment changes every minute (i.e., $T_c=1$ min). The METANET predicted time horizon for the VSL control is set as 5 minutes (i.e., $T_p=5$ min). In addition, the weight set $w_1=0.6$, $w_2=0.1$, and $w_3=0.3$ is used and applied to the VSL control in this section. The driver compliance rate is set as 100% (i.e., $\alpha = 0$). Nine different scenarios are designed and examined. The scenarios and their descriptions are given in Table 7.4. Under scenario 2, 4, 6, and 8,

trucks are not permitted to drive in the leftmost lane, and $\lambda_i^{\text{TR}} = 1$ and $\lambda_i^{\text{NTR}} = 3$, $i=1, \dots, N$. Under scenario 3, 5, 7, and 9, trucks are not allowed to drive in the left two-lane, and $\lambda_i^{\text{TR}} = 2$ and $\lambda_i^{\text{NTR}} = 2$, $i=1, \dots, N$. The corresponding flow, speed, and density are saved, along with all the traffic data of individual vehicles in the TR and NTR lanes. The average TTT, TSD, TSV, and average delay is computed to compare the results among these nine scenarios.

The developed non-linear VSL control are optimized by one of the most widely used derivative-free optimization algorithms, i.e., GA. In addition, the control results are compared with another gradient-free algorithm, i.e., SA.

In Table 7.4, the numerical results of all the nine scenarios are given. Without any control (scenario 1), the TTT and average delay are about 3414.4 veh-h ($TTT_{\text{NO}}=3414.4$) and 519.67 s respectively, the TSD and TSV are about 18289.63 mil/h ($TSD_{\text{NO}}=18289.63$) and 23254.96 mi/h ($TSV_{\text{NO}}=23254.96$), respectively. Under scenario 2 and scenario 3, the left-lane TRP is implemented but without VSL control. It can be seen from Table I, the TTT, TSV, TSD, and average delay under scenario 2 are all slightly improved. For example, compared with scenario 1, the improvement percentage of TTT, TSD, TSV, and average delay under scenario 2 is 0.58%, 1.23%, 1.26%, 2.4%, respectively. Because with the TRP, the negative impact of trucks can be eliminated in the TR lanes. The TTT reduction is in line with the conclusion in the previous studies (Koehne et al. 1993). Also, when the truck percentage is 10%, the left two-lane TRP outperforms the left one-lane TRP.

Under scenario 4 and scenario 5, the VSL control is implemented. According to Liu et al. (2014) and Deo et al. (2009), for comparison purpose, the single-class

METANET model is employed under the two scenarios. The control performances are compared with the results obtained using the extended METANET model in this study. As can be seen in Table I, both the VSL controls optimized by the GA and SA significantly reduce the measurements, especially for the TSD and TSV. Under scenario 4, the improvement percentages of TTT and average delay are about 19.37% and 21.38% compared to scenario 1, which demonstrate that the VSL control improves the operational efficiency. In addition, the improvement percentages of TSD and TSV under scenario 4 are 66.75% and 64.74% compared with those with no control. Such great improvement percentages demonstrate that VSL control significantly homogenizes travel speeds of vehicles and smooth the transition of speeds.

Under scenario 6 to scenario 9, the modified METANET model is adopted. In Table 7.4, under scenario 6 and 7, the modified METANET leads to a better performance than the single class METANET model. For example, under scenario 7, the TTT and average delay are 2712.71 veh-h and 390.56s respectively, which is slightly smaller than that under scenario 5 (i.e., 2758.35 veh-h and 409.06 s).

In addition, one can clearly see in Table 7.4, VSL control with left two-lane truck restriction outperforms VSL control under left one-lane truck restriction when the truck percentage is 10%. For example, the improvement percentage of TTT, TSD, TSV and average delay under scenario 8 is 25.03%, 71.09%, 70.88%, and 28.46%, respectively, which are greater than those under scenario 6.

In Table 7.4, the VSL control optimized by GA and SA provides similar performances. It has been verified that SA provided good quality for the non-linear

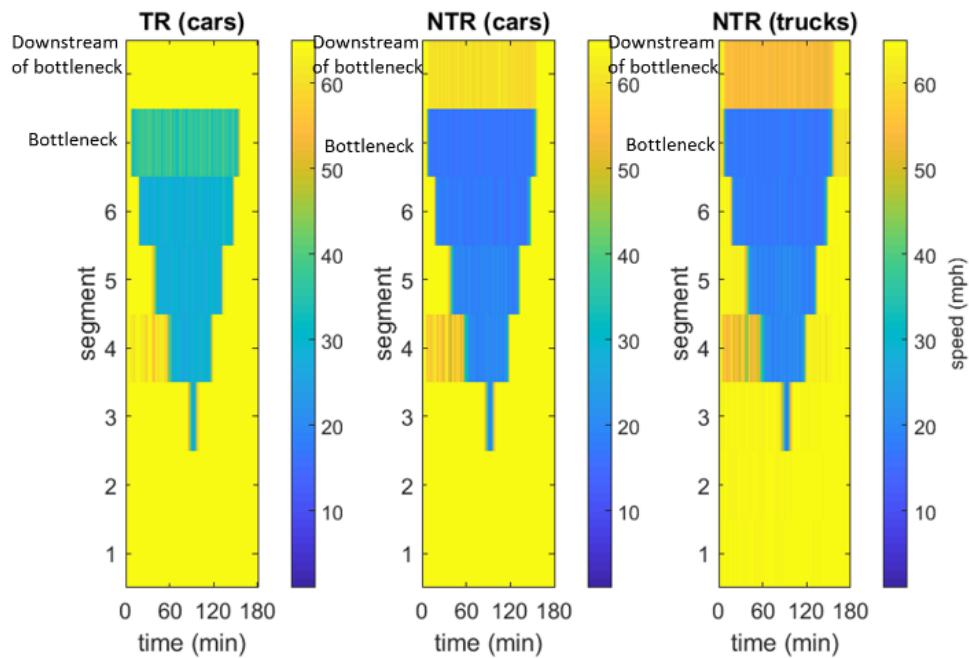
freeway traffic control problems (Pasquale et al. 2016). Thus, the developed GA-based VSL control in this study can be used to solve such problems as well.

In order to clearly illustrate that the developed control strategies relieve the freeway congestion and smooth the speed transition between the upstream and downstream segments, the traffic state profiles under three selected scenarios (i.e., scenario 3, scenario 8, and scenario 9) in Table 7.4 are presented.

Figure 7.16 presents the speed profiles under scenario 3. In Figure 7.16(a), the x-axis is the simulation time, and the y-axis is the segment. The color scale represents the average simulation speeds during the entire simulation period. The lane-drop bottleneck activates when traffic demand is greater than the bottleneck capacity. The queue which forms at the bottleneck increases in length and propagates toward the upstream segments. It can be seen from Figure 7.16(a), the speed variation between the upstream segments and bottleneck are large in both TR and NTR lanes. The vehicles traveling from the upstream have to decelerate abruptly at a segment which might increase the occurrence of rear-end collisions. The speed profiles in Figure 7.16(a) illustrate that lower speeds (less than 20 miles/h) at the bottleneck for both cars and trucks in the NTR lanes. In addition, both the average speeds of cars and trucks in the NTR lanes are less than that in the TR lanes which can be seen from Figure 7.16(a).

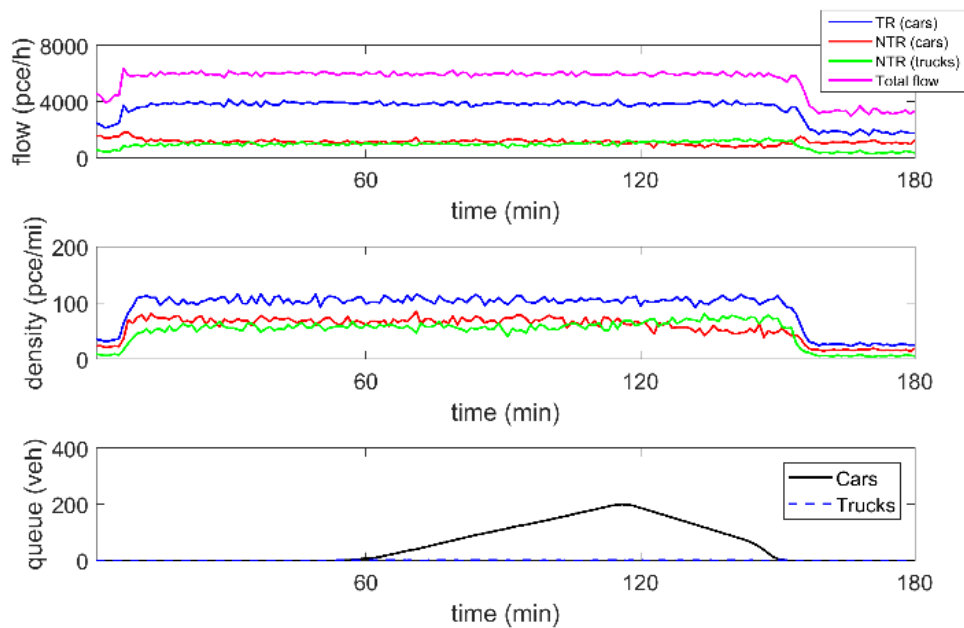
In Figure 7.16(b), the flow and density profiles in the TR and NTR lanes at the bottleneck and the queue profiles at the on-ramp are presented. Scenario 3 is characterized by high congestion in the bottleneck area, under which the density is much higher than the critical density during most of the simulation period. Due to the congestion, the volume flowing out of the bottleneck which is about 6000 pce/h is less than the bottleneck capacity (i.e., 6300 pce/h). Because of the high congestion caused at

the lane-drop bottlenecks, the high density on the segment 4 blocks the vehicles from the on-ramp and a long queue is formed.



(a) Speed Profiles on Each Segment in the TR and NTR Lanes

FIGURE 7.16: Scenario 3



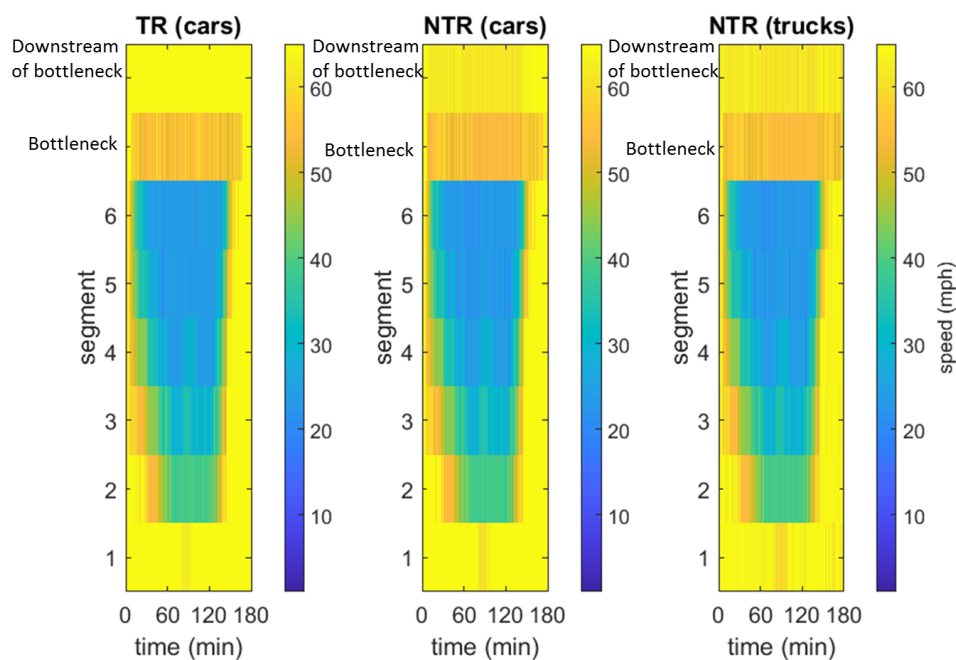
(b) Flow and Density Profiles at the Bottleneck and Queue Length at the On-Ramp

FIGURE 7.16, continued

The speed contours on each segment with VSL control solved by GA are illustrated in Figure 7.17(a). In Figure 7.17(a), the gradual change of color is presented, which indicates that a smooth transition between speeds in the TR and NTR lanes on each segment for both cars and trucks can be achieved due to the VSL control. With VSL control, the speed difference between TR and NTR lanes is also reduced. The flow and density profiles at the bottleneck under scenario 8 are depicted in Figure 7.17(b). As expected, by imposing the VSL control, the flow at the bottleneck is approximately equal to the bottleneck capacity and the density in both TR and NTR lanes are reduced as well. Moreover, the length of the queue at the on-ramp is also reduced.

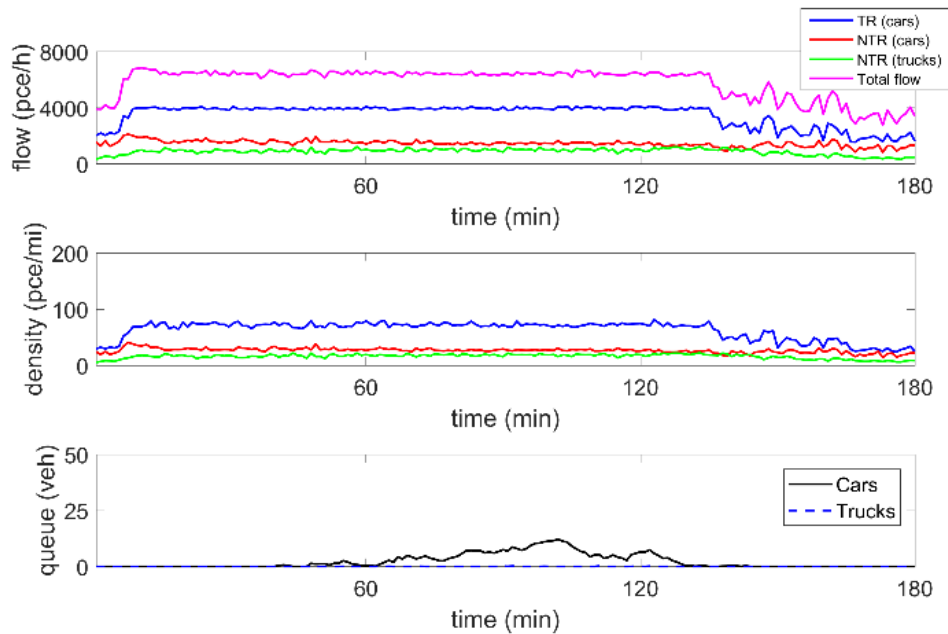
Figure 7.18 presents the control results under scenario 9, under which the VSL control is optimized by using SA. The speed limit values on each segment during the

whole simulation period is given in Figure 7.19. The performances of the SA is similar to GA. However, the speed profiles and the speed limit on each segment are different from scenario 8. Two reasons can explain this. The first one is that local optimal speed limits can be achieved by using the two derivative-free algorithms, and the second reason is that the random seed of VISSIM is different which means that the traffic conditions might be different, and therefore, the simulation performances are different either.



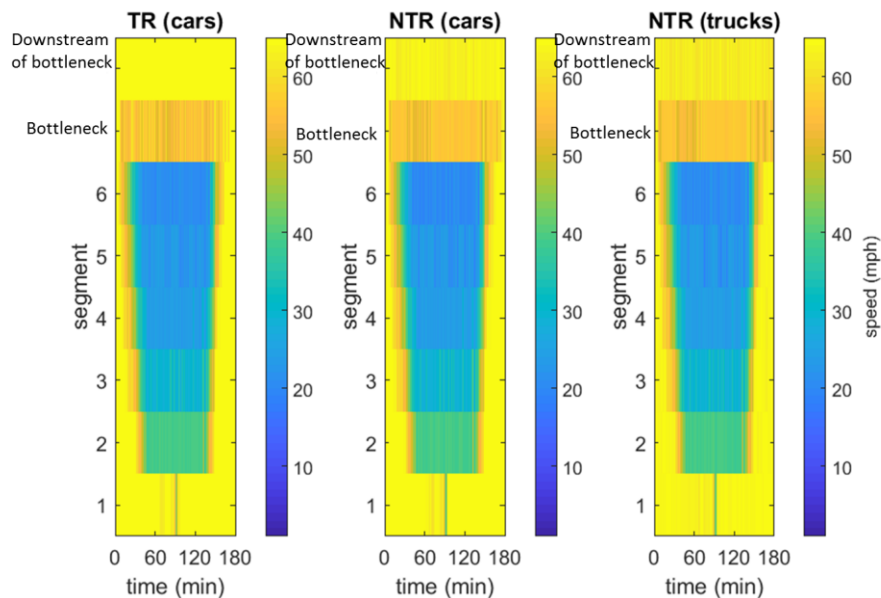
(a) Speed Profiles on Each Segment in the TR and NTR Lanes

FIGURE 7.17: Scenario 8



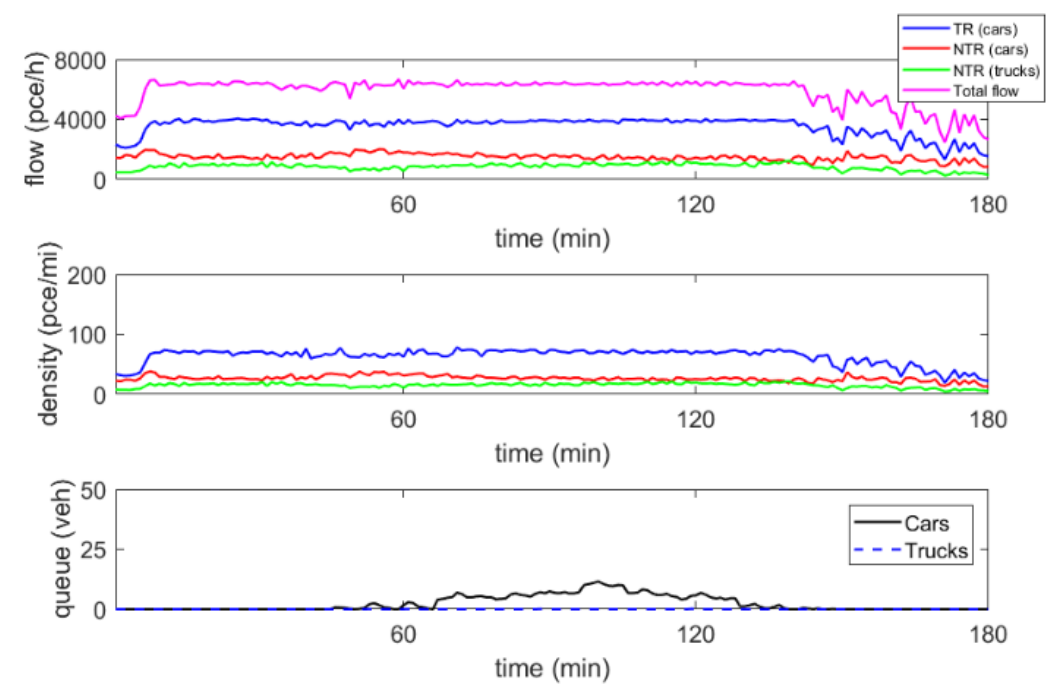
(b) Flow and Density Profiles at the Bottleneck and Queue Length at the On-Ramp

FIGURE 7.17, continued



(a) Speed Profiles on Each Segment in the TR and NTR Lanes

FIGURE 7.18: Scenario 9



(b) Flow and Density Profiles at the Bottleneck and Queue Length at the On-Ramp

FIGURE 7.18, continued

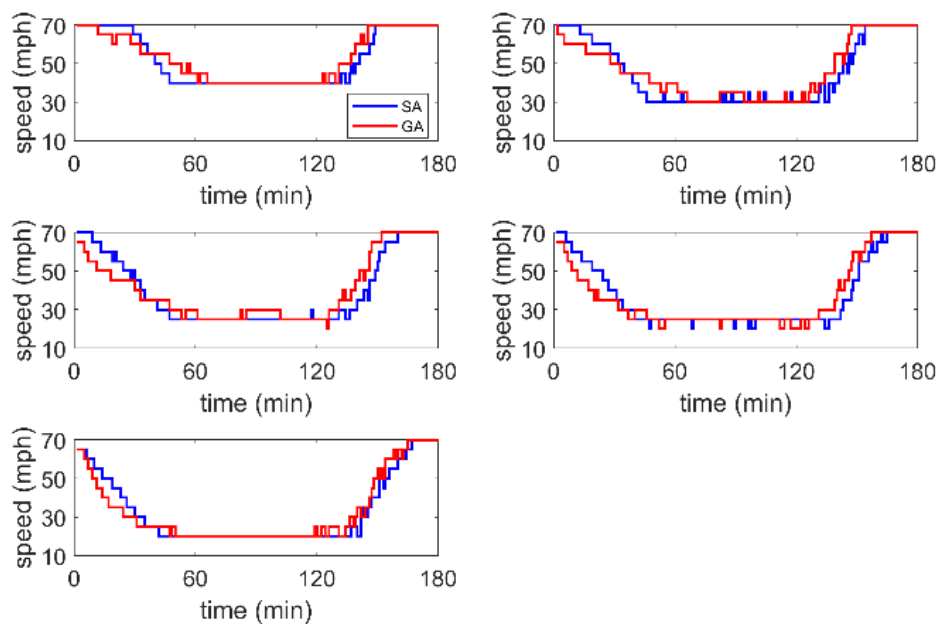


FIGURE 7.19: VSL Profiles Optimized by the SA and GA

As one can see the speed profiles without (see Figure 7.16(a)) and with VSL control (see Figure 7.17(a) and Figure 7.18(a)), the speed differences between the TR lanes and NTR lanes are considerably reduced, which indicates VSL control is effective in achieving speed harmonization between the TR and NTR lanes. Such finding is similar to the finding in Duret et al. (2012). Through comparing the flow profiles at the bottleneck under scenario 3, 8, and 9, it is found that the car volume in the NTR is increased with VSL control. In light of the existing studies, the researchers found that the lane TRP (Duret et al. 2012) and VSL control greatly impact the lane flow distribution and increase the utilization of the shoulder lane (Knoop et al. 2010; Soriguera et al. 2017; Duret et al. 2012). Without VSL control, cars tend to avoid the right lanes (i.e., NTR lanes in this study) and the right lanes are not utilized at capacity (Knoop et al. 2010). With VSL control, the speed difference between the TR lanes and NTR lanes is reduced which results in the utilization of the NTR lanes (Knoop et al. 2010; Duret et al. 2012). As a result, with VSL control, the car volume in the NTR lanes is greater than that under scenario 3, and VSL increases the usage of the NTR lanes.

7.4.4. Sensitivity Analysis

In the previous section, the truck percentage is set as 10% during the entire simulation period. All three scenarios with VSL control can significantly improve the operational efficiency and the level of safety on the selected freeway segments. When the truck percentage is 10%, VSL control with left two-lane truck restriction outperforms the control with left one-lane truck restriction. However, in reality, the truck percentage varies during different time intervals. With different truck percentages on the freeways, the density (pce/mi/lane), speed differential, and lane-changing frequency can be affected

(Radhakrishnan and Wilmot 2009; Koehne et al. 1993). Also, without VSL control, Yang and Regan (2007) examined the effects of the one leftmost lane restricted from trucks and the two leftmost lanes restricted from trucks on traffic congestion and travel time variance. The simulation demonstrated that the two leftmost lanes restricted from trucks achieved more positive effects than the one leftmost lane restricted from trucks. VSL control might also be greatly affected by the high truck percentage. And, the performances of the two control strategies with a high truck percentage (VSL control with left one-lane truck restriction and VSL control with left two-lane truck restriction) might be different from these with a low truck percentage. Thus, in this section, the relationship between the two control strategies and truck percentages are explored. The performance of the two VSL controls (including TTT, TSV, and TSD) corresponding to different truck percentages, is also shown and compared.

The effect of truck percentage is investigated by varying it from 5% to 30%. It is assumed that, with different truck percentage, the traffic flow parameters, such as critical density, are the same. The measurements of the two VSL control strategies are shown in Figure 20(a) through Figure 20(c) respectively. The driver compliance rate is still set as 100%. VSL control results with different truck percentages can be presented as follows. In Figure 20(a), the TTTs of the two control strategies increase with the increasing percentages of the trucks. The possible reason is that as the truck percentage increases, the average gap distance between two vehicles will be larger. The cars that travel in the NTR lanes and travel from the on-ramp to the mainstream can also be more negatively affected by the increasing trucks. As such, both TSD (Figure 20(b)) and TSV (Figure 20(c)) increase as the truck percentage increases. The results shown in Figure 20(a)

through Figure 20(c) indicate that the overall operational efficiency and safety are reduced due to the increase in the truck percentage.

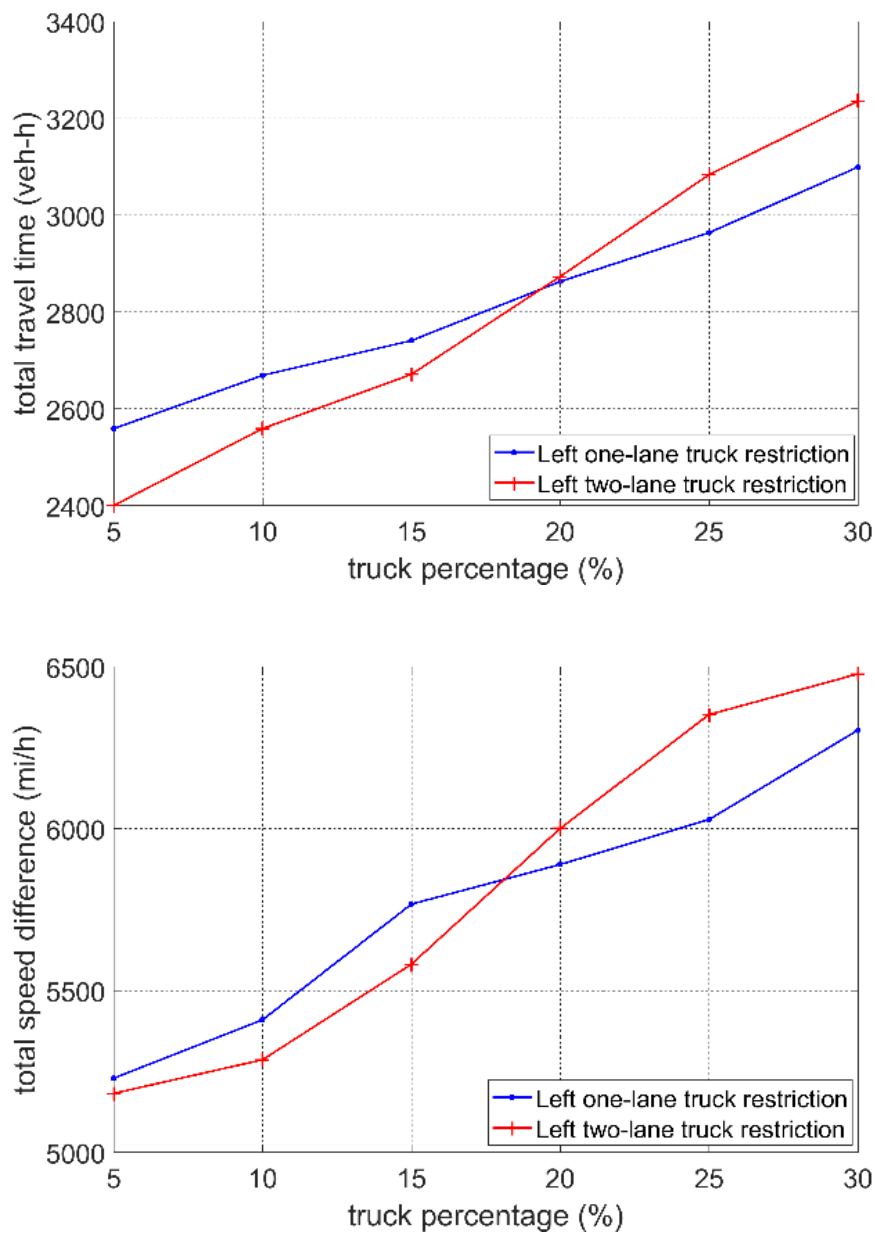


FIGURE 7.20: (a) TTT vs. Truck Percentage. (b) TSD vs. Truck Percentage. (c) TSV vs. Truck Percentage

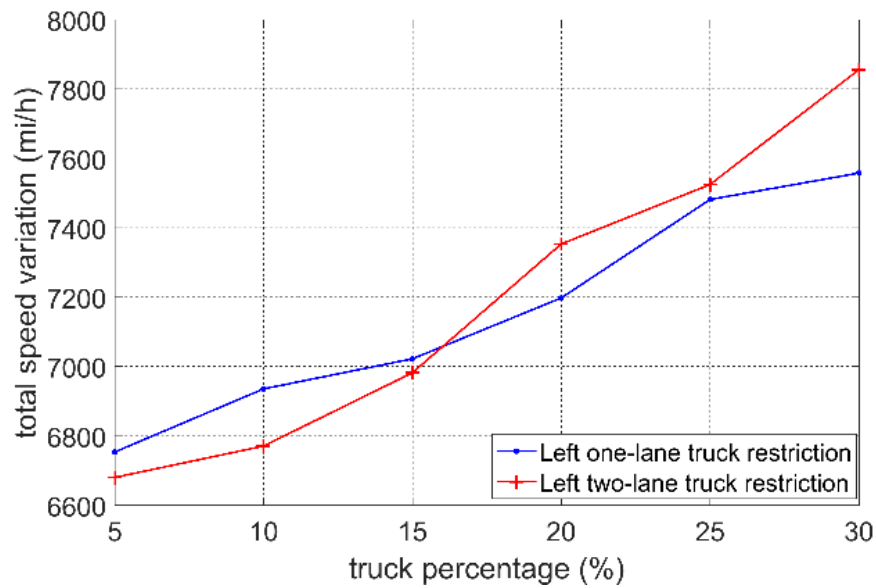


FIGURE 7.20, continued

In Figure 20(a), when the truck percentage is low, the TTT of VSL control with left two-lane truck restriction is less. With the increasing percentages of trucks, the left two-lane truck restriction policy can still better reduce the negative impact of trucks. However, if the truck percentage is too large (such as $>20\%$), for the VSL control with left two-lane truck restriction, since so many trucks are traveling in the right two lanes, the cars traveling from the on-ramp might be blocked and the vehicles which try to leave the mainline through the off-ramp might be delayed. As such, the VSL control strategy with left one-lane truck restriction policy is better for a large truck percentage. Similar results for the TSD and TSV can also be observed from Figure 7.20(b) through Figure 7.20(c).

For the selected four-lane freeway stretch in this study, the comparison results between the two proposed VSL control strategies illustrate that the VSL control with left two-lane truck restriction is recommended with a low truck percentage. When the truck

percentage is high, VSL control under left-one lane truck restriction should be considered. However, it should be well noted that, besides VSL control and TRP, to better reduce the negative impact of a high percentage of trucks on the freeway operation and safety, a driving ban/restriction for trucks needs to be considered as well, especially during peak hour period.

7.5. VSL Control in a CAV Environment

7.5.1. Bottleneck Identification

By using the filed data collected from the PeMS database, a preliminary analysis is performed to identify the positions of bottlenecks. It should be pointed out that bottleneck identification is a complicated process (Fan and Gong 2017; Gong and Fan 2017; Gong and Fan 2018), and this study simply identifies them based on the speed profiles. The huge traffic demands on the I-5 typically result in considerable delays. Figure 7.21 depicts speed contours on a typical weekday. The x-axis is the order of loop detectors (see Figure 7.22 and Figure 7.23 for corresponding positions), and the y-axis is the time interval (from 6 a.m. to 9 a.m.). The color scale represents the collected average speeds during the study period. As can be seen, the speeds are greatly affected in the on- and off-ramps, and lane drops areas. Five bottlenecks can be seen in Figure 7.22, i.e., at detectors 1, 5, 7, 9, and 14 (see Figure 7.23). The speeds at these detectors are dropped to a low value, particularly at the 7th and 9th detectors. It is well noted that the average speeds at the fourth detector are very low and as such, another bottleneck may exist at the fourth detector. However, since the distance between detectors 4 and 5 is only about 0.3 mile which is extremely close, the real presence of the bottleneck at the fourth detector

may be due to the impact of bottleneck at the fifth detector propagating all the way to the upstream, which is also clearly suggested by conducting a careful examination of the speed data. Therefore, the bottlenecks at detectors 4 and 5 are combined into one bottleneck group which is located at detector 5 in this study (Fan and Gong 2017). The developed VSL control framework is intended to relieve the congestion at these bottlenecks. When modeling the freeway corridor in VISSIM, on the basis of the positions of the loop detectors in the real-world, the freeway stretch is re-divided into 14 cells so that the CTM can be easily implemented. The detailed information about the length of each cell is given in Figure 7.23. In addition, according to the positions of bottlenecks and the discussion in the section ‘VSL Control Framework’, three VSL control systems are deployed in this study, i.e., $S=3$. The positions of VSL signs and the control range of the VSL systems are depicted in Figure 7.23 as well. The number of the cells in each VSL control system are 2 ($N_1=2$, $vs_l1=2$), 8 ($N_2=8$, $vs_l2= N_1+N_2=10$), and 4 ($N_3=4$, $vs_l3= N_1+N_2+N_3=14$), respectively.

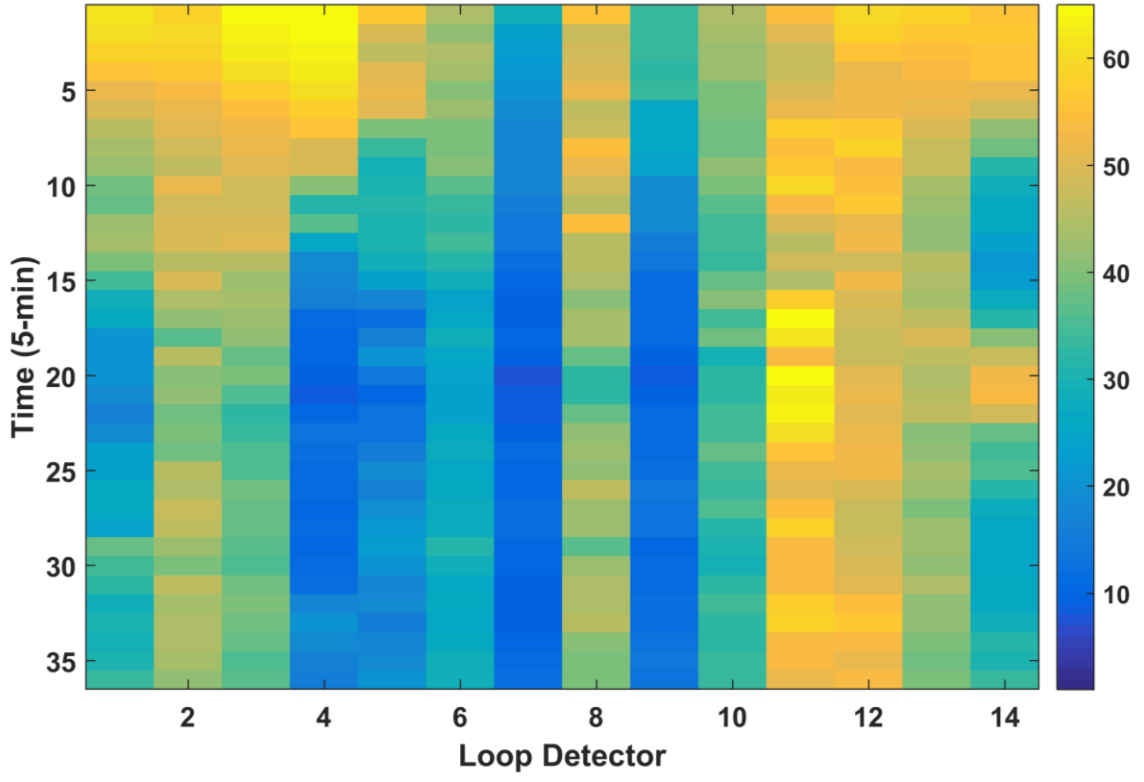


FIGURE 7.21: Speed Profiles at Each Loop Detector

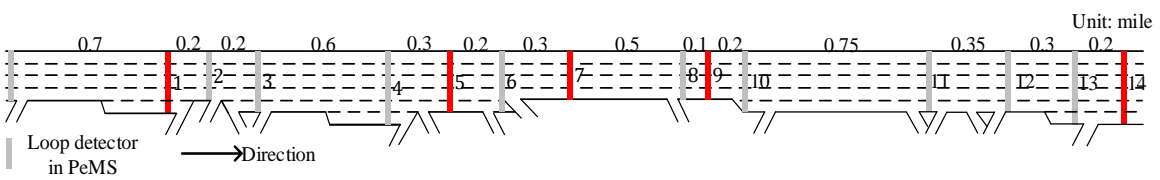


FIGURE 7.22: Information about the Freeway Stretch

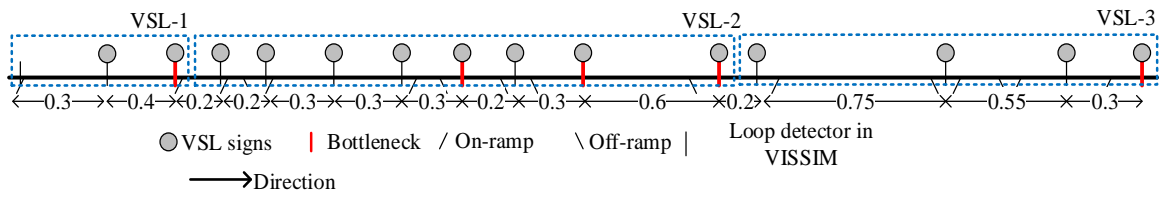


FIGURE 7.23: Deployment of VSL Signs

7.5.2. Calibration Parameters of CTM

Three types of vehicles (i.e., human-driven cars, trucks, and autonomous cars) are included in this study, i.e., $J=3$. Note that the PeMS database does not provide truck percentage at the on-ramps. When simulating in VISSM, the truck percentages at the on-ramps are set to be 0%. The vehicle type HGV (heavy goods vehicles) in VISSIM is used to simulate trucks in the real world.

The traffic parameters (e.g., capacity, jam density, and shock wave speed) at the five bottlenecks need to be computed first using the collected traffic data. The computation method developed by Dervisoglu et al. (2008) is adopted in this study. The computation results are given in Table 7.5. As can be seen in Table 7.5, the range of magnitude of capacity drop is between 4.41% and 15.28%, which is closer to the existing research works (Dervisoglu et al. 2008; Hadiuzzaman et al. 2012). Note that, the free flow speeds of trucks at these five bottlenecks cannot be computed based on the collected traffic data. In Table 7.5, the hypothetical freeway flow speeds of trucks at the five bottlenecks are given, and the corresponding critical densities are computed.

TABLE 7.5: Computation Results of the CTM at Each Bottleneck

Parameters	Bottleneck 1	Bottleneck 2	Bottleneck 3	Bottleneck 4	Bottleneck 5
Capacity (pce/h/lane)	2232	1749	1797	1733	1702
Drop Capacity (pce/h/lane)	2023	1517	1669	1528	1630
Magnitude of Capacity Drop (%)	10.35	15.28	7.66	13.45	4.41
Shock Wave Speed (mph)	10.99	7.26	8.67	8.62	9.24
Critical Density (pce/mile/lane)	34.34	26.33	27.33	26.6	25.66
Jam density (pce/mile/lane)	214.39	235.3	219.86	203.81	202.08
Car					
Free Flow Speed (mph)	64.99	66.42	65.74	65.16	66.32
Critical Density (veh/mile/lane)	34.34	26.33	27.33	26.6	25.66
Truck					
Free Flow Speed (mph)	59.99	61.42	60.74	60.16	61.32
Critical Density (veh/mile/lane)	20.52	15.12	15.45	15.20	14.45

To obtain a close match between the collected and simulated traffic data, the driver behavior parameters of VISSIM, such as standstill distance (CC0) and headway time (CC1), are calibrated. A calibration process was performed by Yu and Fan (2017) in which the differences between the field and simulation speeds and flows at each detector were minimized. For human-driven vehicles (e.g., cars and trucks), parameters of the IDM (e.g., average headway and standstill distance) are based on the calibration results. Parameters that are used to model the car-following characteristics of the AVs and CAVs are selected on the basis of existing studies. Table 7.6 presents relevant parameter values used in this study.

TABLE 7.6: The IDM's Parameter Value

Vehicle Types	HW_j	a	b	s_0
Human-driven vehicle	1.6 s	3.28 ft/s ²	-6.56 ft/s ²	4.13 ft
AV	1.1 s	3.28 ft/s ²	-6.56 ft/s ²	0
CAV	0.6 s	3.28 ft/s ²	-6.56 ft/s ²	0
References	Treiber et al. 2000; Shladover et al. 2012; Milanés and Shladover 2014; Khondaker and Kattan 2015b; Grumert et al. 2015; Li et al. 2017			

To compute the dynamic pce during each control time interval, for human-driven vehicles, the calibration results of the average headway and standstill distance (see Table 7.6) are used, which is the same for both the human-driven cars and trucks. In addition, the gross stopping distance sd_j of vehicle type j equals the length of vehicle type j plus the distance gap (i.e. the standstill distance s_0 in the IDM model) (van Lint et al. 2008).

According to the data provided by the VISSIM, the length human-driven cars, autonomous cars, and trucks are set to be 15.62ft, 15,12ft, and 33.15 ft, respectively. The

gross stopping distance of cars, AVs, and trucks can be computed by

$sd_{\text{car}}=s_{0,\text{car}}+15.62=19.75\text{ft}$, $sd_{\text{AV}}=15.12\text{ft}$ and $sd_{\text{truck}}=s_{0,\text{truck}}+33.15=37.28\text{ft}$, respectively.

7.5.3. Simulation Results

A 3.5-hour simulation with a 30-minute (from 5:30 am – 6:00 am) warm up period is conducted. Using the proposed integrated VSL control framework, the speed limit set that minimizes the objective function over a given prediction horizon (i.e., $T_p=5$ min) is recorded and sent to VISSIM for simulation through MATLAB. The speed limit changes every minute (i.e., $T_c=1\text{min}$), and the total number of time interval in this study is $K=180$ (i.e., 180 1-minute time intervals within 3 hours). The discrete time step used in the control model is $T=10\text{s}$. The proposed GA procedure is implemented by using the MATLAB software package. All the GA parameters, such as population size, the number of generations, mutation rate, and crossover rate, use the default settings in MATLAB. $w_1=0.9$ and $w_2=0.1$ are selected for the simulation (Yu and Fan 2018a; Yu and Fan 2018b). Various scenarios are designed in this study, which are presented in detail in Table 7.7. The first scenario under which all human-driven vehicles including cars and trucks without any VSL control is simulated and used as the reference. Based on scenario 1, the performances of different control strategies (including VSL control, V2X, and/or I2V etc.) are simulated and compared.

The computation time for the proposed VSL control system ranges from 3.6s to 8.1s during each control time horizon. The program is written in MATLAB and evaluated on a computer with i7-4790 @ 3.6 GHz and 16 GB memory. As hardware improves, it is believed that the proposed VSL control strategies will be more computationally efficient and it can potentially be used for real-time applications.

TABLE 7.7: Simulation Scenarios and Descriptions

Scenarios	Description
Scenario 1	With 100% human-driven vehicles and without VSL control
Scenario 2	With 10% CAVs and without VSL control
Scenario 3	With 100% human-driven vehicles, VSL control, and the CTM without considering mixed traffic flows
Scenario 4	With 100% human-driven vehicles, VSL control, and the extended CTM
Scenario 5	With 10% CAVs and VSL control, and the extended CTM
Scenario 6	With 10% CAVs and VSL control, V2I, and the extended CTM
Scenario 7	With 10% CAVs, I2V, V2I, VSL control, and the extended CTM

Table 7.8 shows the simulation results under the seven designed scenarios, in which the TTT, average delays, average number of stops, and emission are computed. Under scenario 1, the TTT is 8140.51 veh-h. The great values of the average delay and number of stops indicate that the congestion on the freeway stretch results in the so-called stop-and-go traffic conditions and huge delays. Under scenario 2, the penetration rate of CAV is 10%. Even though without VSL control, the three efficiency related measurements are slightly improved, and the improvement percentages are 1.87%, 3.75%, and 8.59%, respectively.

The comparisons between scenarios 3 and 4 aim to examine whether the extended CTM outperforms the CTM without considering mixed traffic flows. The selected measurements indicate that better performance, including both efficiency (e.g., smaller TTT and average delays and number of stops) and emission (e.g., smaller emissions of CO₂, NO_x, and particulate), is achieved under scenario 4. For example, the improvement percentage of TTT is 34.43% under scenario 4 which is greater than that under scenario

3. The reason is that when using the CTM without considering heavy vehicles, the controlled equilibrium discharge volume during some periods at the bottlenecks might be overestimated which might affect the bottleneck operational efficiency. As a result, the extended CTM will be adopted in the other scenarios.

The developed VSL control framework in this study is implemented under scenario 4. As can be seen in Table 7.8, the simulation results are considerably better compared to those under scenario 1. The improvement percentages of the TTT, average delays, and average number of stops are 34.43%, 60.4%, and 61.91%, respectively. The reduction in TTT, average delays, and average number of stops demonstrate that the efficiency is significantly improved and stop-and-go traffic conditions are greatly relieved as well. In addition, when integrating VSL control with CAVs including V2V, V2I, and I2V, one can see that the selected measurements outperform those with the VSL control only. For example, the percentage decrease in the average delays under scenario 5 is 65.11%, which is greater than the percentage decrease under scenario 4. Under scenario 6, the displayed speed limit set is adjusted by using the traffic data of AVs collected through the V2I communication, which leads to a better performance than scenario 4 and scenario 5. While under scenario 7 in which the I2V communication is incorporated, the simulation performances are the best compared to all other six scenarios. The simulation results under scenario 5, 6, and 7 indicate the advanced characteristics of the V2X and I2V in improving the operating efficiency.

In addition, the emission presented in Table 7.8 demonstrates the effectiveness of the proposed integrated control strategies in reducing the greenhouse gas emissions and adverse impact on environment. Due to the VSL control systems, vehicles' waiting time

in the queues is significantly reduced. Also, the smoothed transition in speeds reduces the frequency of acceleration and deceleration occurred upstream of the bottlenecks. As a result, the tailpipe emission rate is reduced (Zhang and Ioannou 2017). For example, the emission of CO₂ is decreased by 6.97%, 7.69%, 7.73%, and 7.8% under scenarios 4-7, respectively. The proposed VSL controllers reduce NO_x emission rate by about 8.69% - 9.09%. The emission rate of particulate is also decreased by 5.38% - 5.9%, respectively. In terms of the reduction in emissions, the control systems integrated with V2X and V2I also outperform the VSL control only.

TABLE 7.8: Performance Comparison under Different Scenarios

Scenario	TTT (veh-h)	Average delays (s)	Average number of stops	Emission (g)			Improvement (%)					
				CO ₂	NO _x	Particulate	TTT	Delays	Number of stops	CO ₂	NO _x	Particulate
Scenario 1	8140.51	400.76	67.58	650.33	1734.2	1951	-	-	-	-	-	-
Scenario 2	7988.12	385.75	61.77	641.59	1730.57	1950.45	1.87	3.75	8.59	1.34	0.21	0.03
Scenario 3	5469.65	170.59	26.99	608.91	1585.7	1851.3	32.81	57.43	60.06	6.37	8.56	5.11
Scenario 4	5337.68	158.71	25.74	605	1583.5	1846.12	34.43	60.4	61.91	6.97	8.69	5.38
Scenario 5	5328.65	139.81	25.33	600.32	1578.54	1838.54	34.54	65.11	62.52	7.69	8.98	5.76
Scenario 6	5229.3	128.85	23.38	600.05	1577.99	1836.52	35.76	67.85	65.40	7.73	9.01	5.87
Scenario 7	5211.97	128.74	23.05	599.63	1576.54	1835.98	35.97	67.88	65.89	7.8	9.09	5.9

In order to illustrate the speed harmonization impact of VSL control for freeways with multiple bottlenecks, Figure 7.24 presents the speed contours on each cell during the whole study period under scenario 4. The speed limit during $t=140$ min and speed limit contour on cell 10 are presented in Figure 7.24. It can be seen from Figure 7.24 that, compared to uncontrolled scenario (see Figure 7.21), the speed differences among the adjacent cells are noticeably reduced. With VSL control, vehicles traveling from the upstream can gradually slow down and keep a constant deceleration rate before they arrive at the bottleneck. The simulation speeds at the most congested bottlenecks begin to recover at the end of the simulation. The gradual change of color indicates that a smoother transition of speeds on each cell has been achieved.

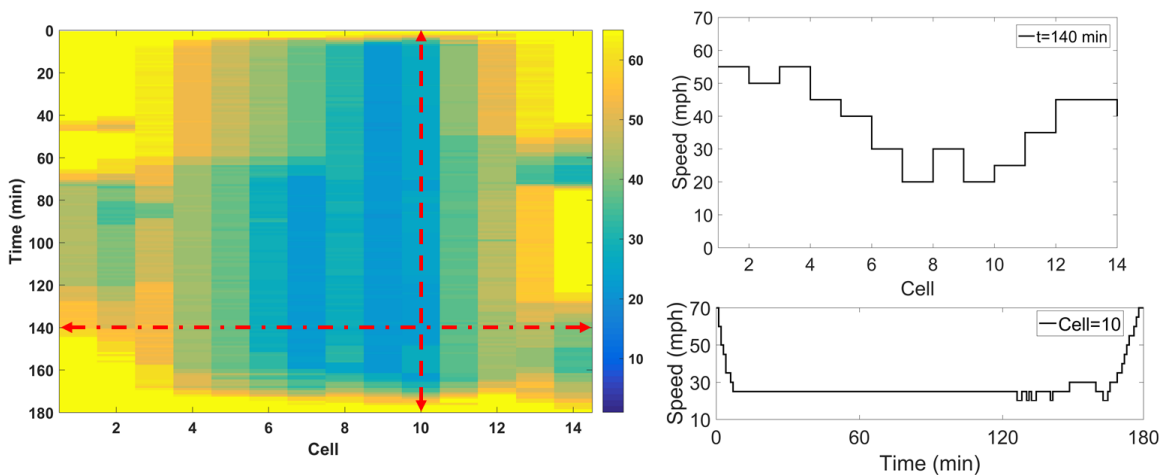
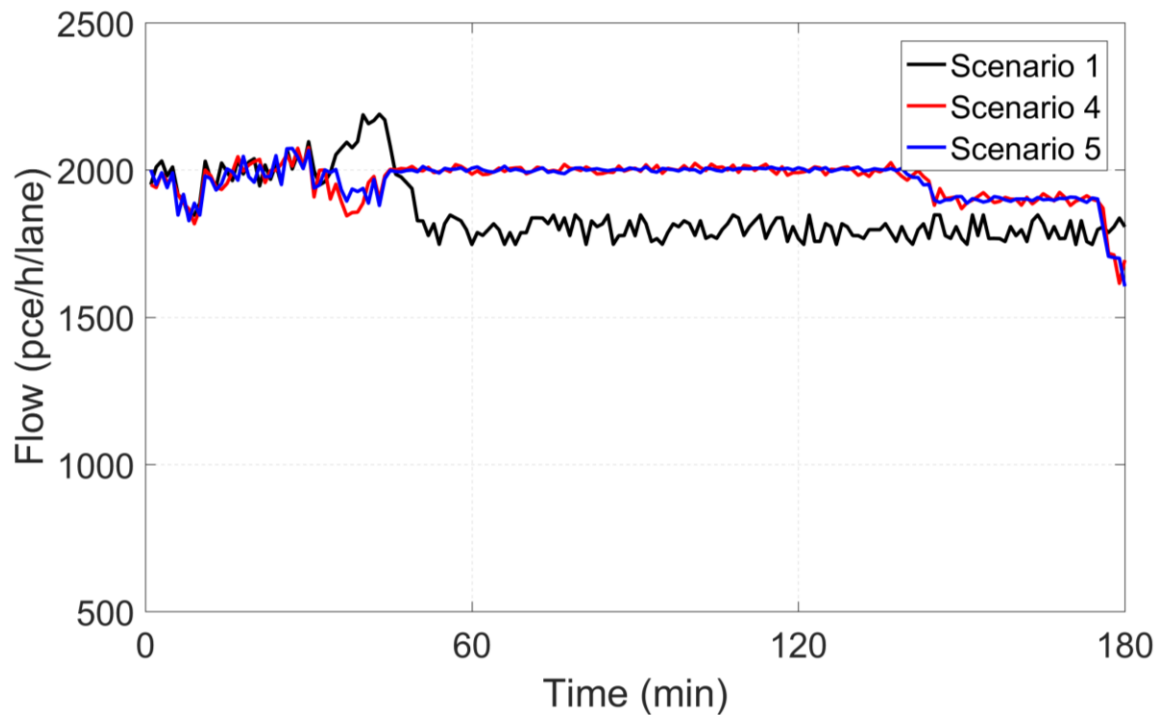


FIGURE 7.24: Contour of Speed Limit under Scenario 4

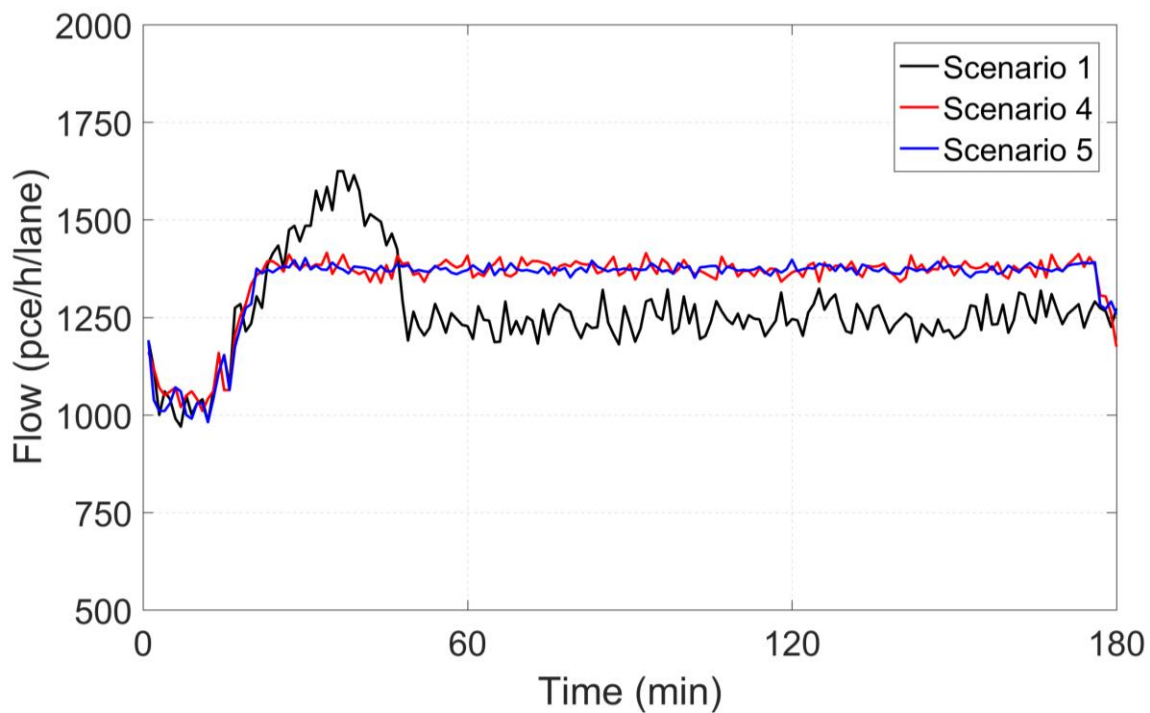
The equilibrium flow (pce/h/lane) profiles during the entire simulation period at these five bottlenecks under scenario 1, scenario 4, and scenario 5 are depicted in Figure 7.25(a) through Figure 7.25(e). When traffic demand is not very high in which the

demand is less than the bottleneck capacity, the VSL control is always not activated. For example, at the bottleneck 2, during the beginning period of the simulation, the flow profiles with VSL control are similar to those without VSL control. However, when traffic demands are greater than the bottleneck capacity, under the scenario without any control, a drop in flow at all the bottlenecks can be observed. The drop percentages are large particularly at bottlenecks 3 and 4. For example, due to the congestion, the equilibrium flow at the first bottleneck drops from 2100 pce/h/lane to about 1800 pce/h/lane (see Figure 7.25(a)). Under the scenarios with VSL control (i.e., scenarios 4 and 5), before the traffic breakdown occurs, the VSL control is activated. Because of the VSL control, the number of vehicles traveling to the bottlenecks can be well metered so that it equals the maximum discharge volume or critical volume of the bottlenecks. The equilibrium flow with VSL control can remain steady and a relative high discharge value can be achieved as well compared to that without VSL control at each bottleneck.

In addition, it should be pointed out that, the outflow of bottleneck 3 with VSL control is less than its maximum discharge volume (see Table 7.5 and Figure 7.25(c)). The reason is that the discharge volume of bottleneck 3 is determined based on the capacity of bottleneck 4 and off-ramp (located between bottlenecks 3 and 4) volume. As can be seen in Table 7.5, the maximum discharge rate of bottleneck 4 is less than that of bottleneck 3. According to previous discussions, the bottleneck capacity of bottleneck 4 is the critical volume of bottlenecks 3 and 4. In order to simultaneously relieve the congestion at bottleneck 4, an extra constraint (the critical bottleneck volume plus the off-ramp volume) is added to bottleneck 3 when implementing the VSL control. The similar control principle is also employed at bottleneck 2 (see Figure 7.25(b)).

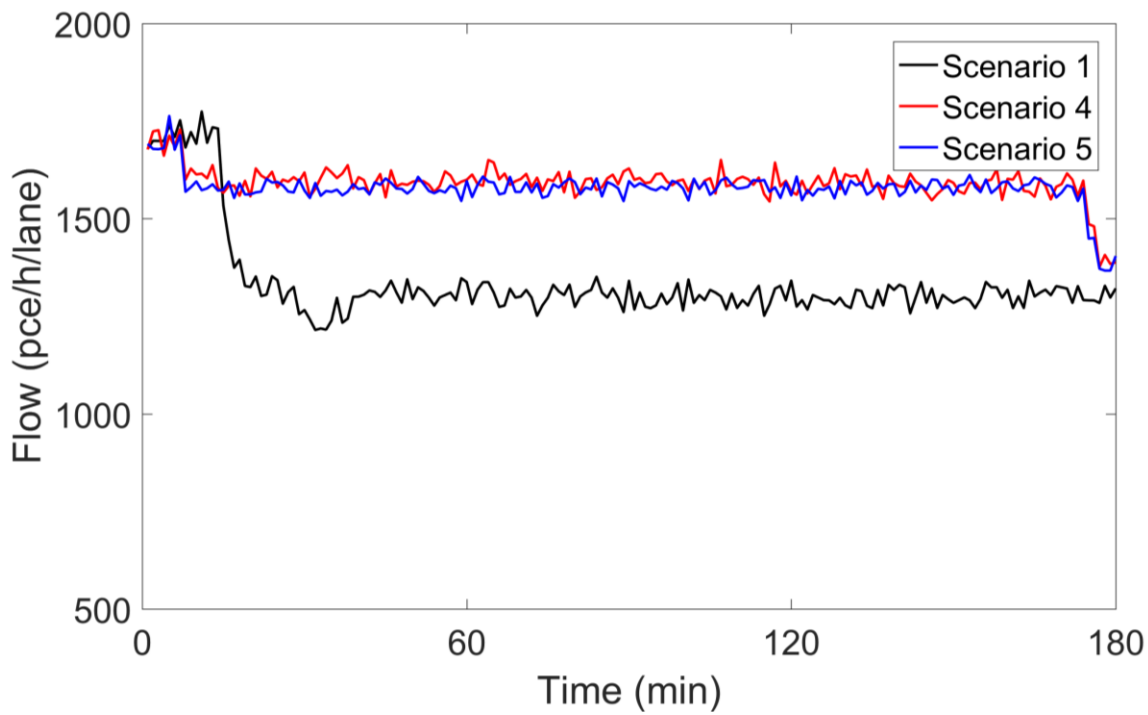


(a) Bottleneck 1

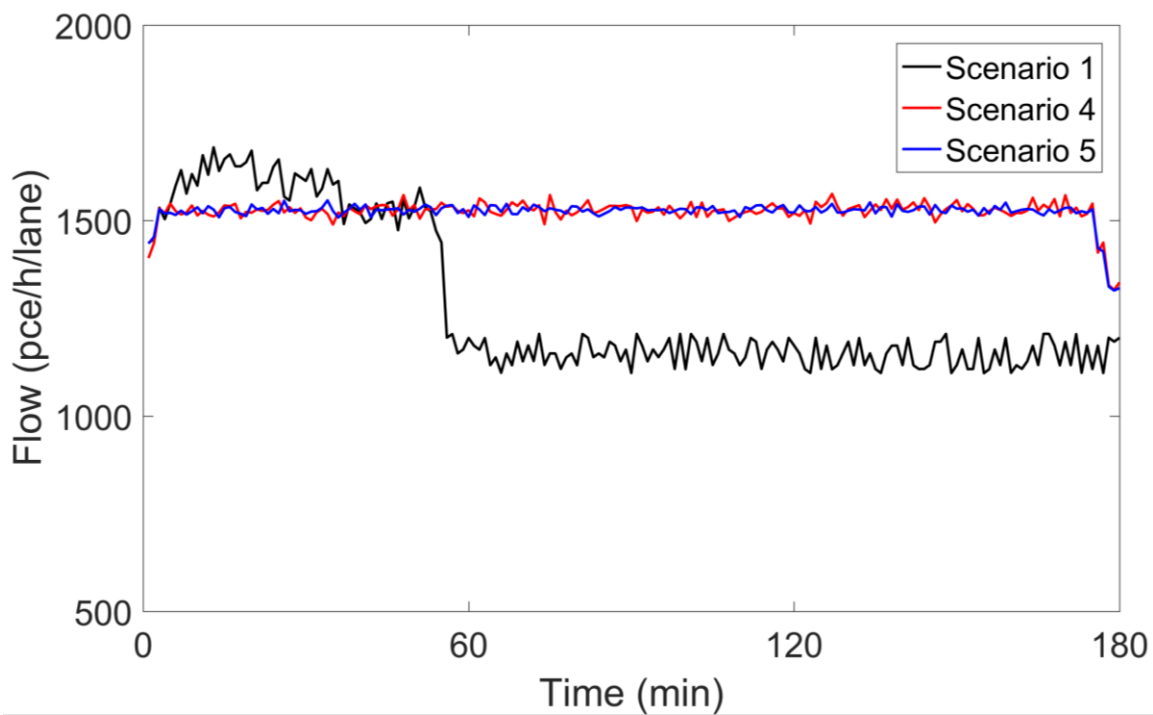


(b) Bottleneck 2

FIGURE 7.25: Flow Profiles at Each Bottleneck

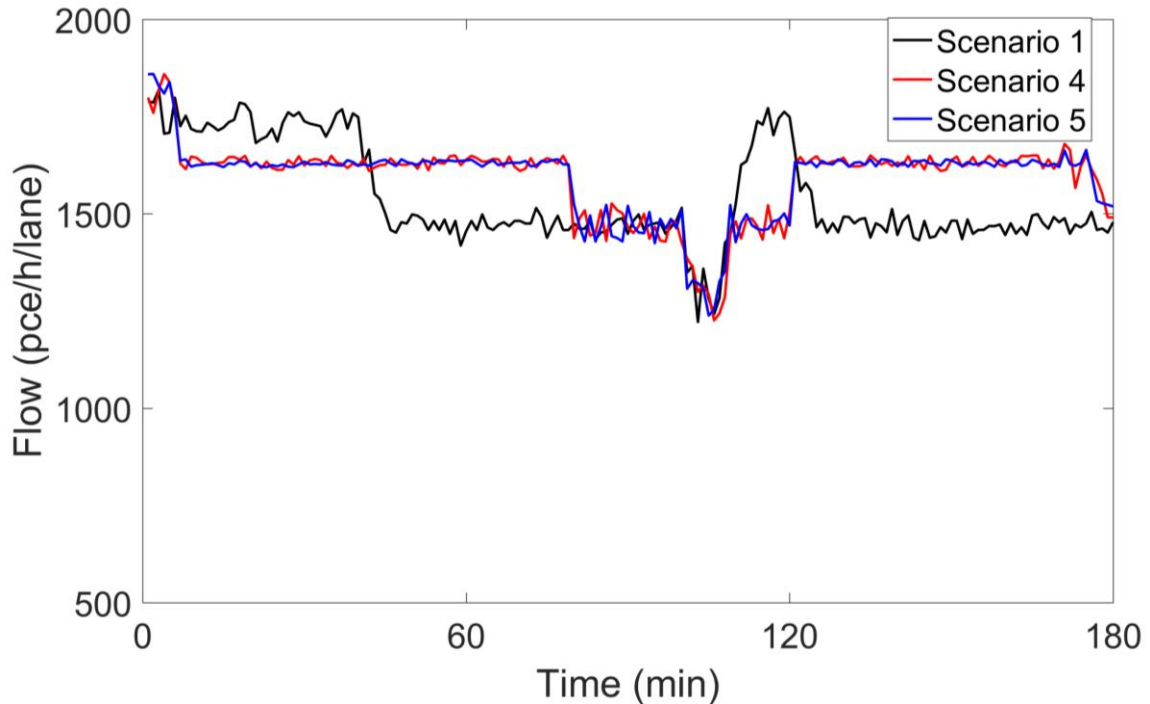


(c) Bottleneck 3



(d) Bottleneck 4

FIGURE 7.25, continued



(e) Bottleneck 5

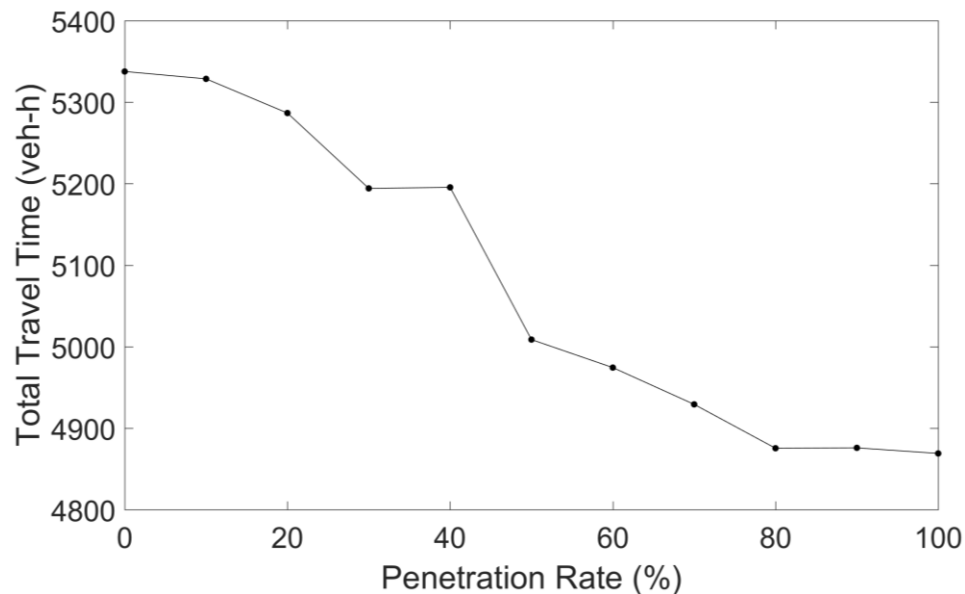
FIGURE 7.25, continued

7.5.4. Sensitivity Analyses

In the previous section, the penetration rate of the CAV is set to be 10%, and the communication range of I2V is 656 ft (about 200 m). It has been verified that as the penetration rate of CAVs increases, the capacity of freeway will also increase (Shladover et al. 2012). The increases in capacity might result in better control performances. In addition, the communication range of I2V technology might also affect the operational efficiency and the emissions of CO₂, NO_x, and Particulate (Grumert et al. 2015).

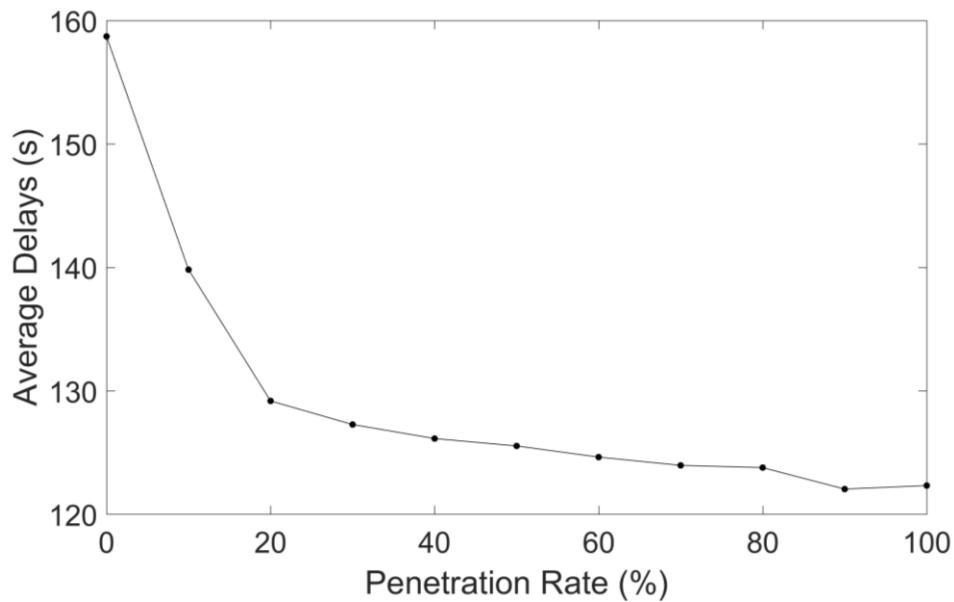
Therefore, in this section, the relationships between the penetration rate of CAVs and communication range of the I2V and control performances are investigated.

The effect of penetration rate is explored by varying it from 0% to 100%, and the VSL control measurements (including TTT, average delays, and average number of stops) with different penetration rates are shown in Figure 7.26(a) through Figure 7.26(c). The freeway capacity increases as the penetration rate of CAVs increases. When the penetration rate is increased by 10%, it is assumed that the bottleneck capacity showed in Table 7.8 is increased by 1% (Wang et al. 2016). The free flow speeds and shock wave speeds are assumed to be the same, and the corresponding critical density and jam density are recalculated. These new hypothetical traffic flow parameters are used as input into the integrated VSL controller. One can see from Figure 7.26 that as the penetration rate increases, the TTT, average delays, and average number of stops all decrease, which indicates that the increasing market penetration rate of CAVs can lead to improvements in freeway mobility and efficiency.

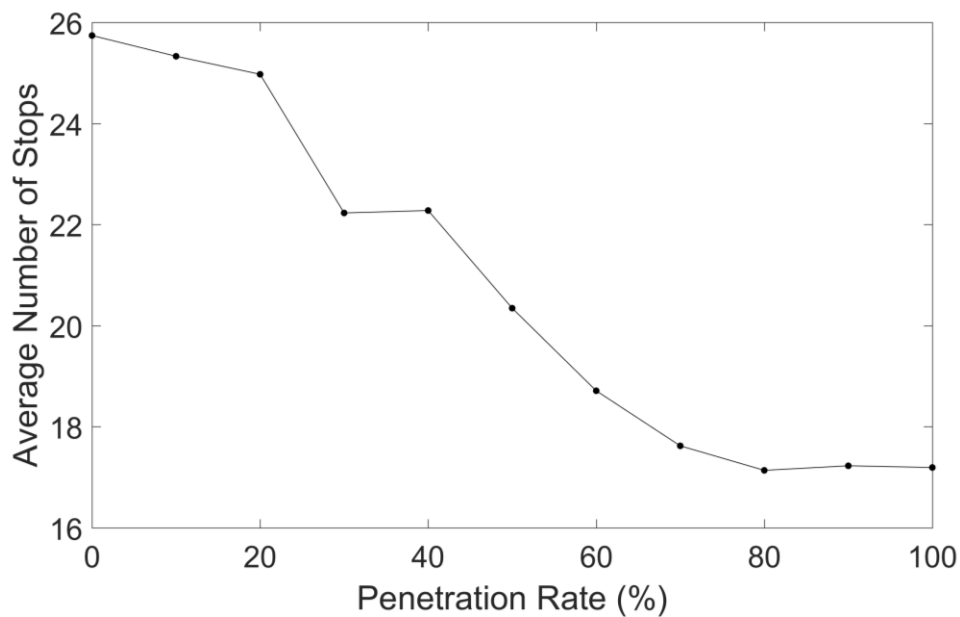


(a) Total Travel Time vs. Penetration Rate

FIGURE 7.26: Simulation Performances vs. Penetration Rate



(b) Average Delays vs. Penetration Rate



(c) Average Number of Stops vs. Penetration Rate

FIGURE 7.26, continued

Finally, the effects of communication range between VSL signs and AVs are also investigated by setting three different distances (328ft (100m), 656ft (200m), and 984ft

(300m)). The corresponding comparison measurements of the integrated VSL control are given in Table 7.9. Six simulation measurements under three scenarios are expected to be better compared to the scenario without I2V communication (i.e., scenario 6 in Table 7.7). This is confirmed in Table 7.9. However, the TTT, average delays, average number of stops, and emissions under these three scenarios do not seem to have a clear relationship with the communication distances (Grumert et al.'s 2015). The reason might be that the distance for AVs to decelerate or accelerate to the displayed speed limit value does not need to be very long during the high-demand period.

TABLE 7.9: Simulation Outputs with Different Communication Range

I2V Range	TTT (veh-h)	Average delay (s)	Average number of stops	Emission (g)			Improvement (%) – Scenario1					
				CO ₂	NOx	Particulate	TTT	Delay	Number of stops	CO ₂	NOx	Particulate
328ft	5251.03	127.93	23.01	600.38	1579.89	1836.16	35.5	68.08	65.95	7.68	8.90	5.89
656ft	5211.97	128.74	23.05	599.63	1576.54	1835.98	35.97	67.88	65.89	7.8	9.09	5.9
984ft	5215.67	127.53	23.57	599.63	1573.07	1835.9	35.93	68.18	65.12	7.8	9.29	5.9

7.6. VSL Control and CAV Platooning

7.6.1. Simulation Results

Using the developed integrated VSL control framework, the speed limit set that minimizes the objective function over a given prediction horizon (i.e., $T_p=5$ min) is recorded. The speed limit changes every minute (i.e., $T_c=1$ min), and the total number of time intervals in this study is $K=180$ (i.e., 180 1-minute time intervals within 3 hours). The discrete time step used in the control model is $T=10$ s. The proposed GA procedure is implemented by using the MATLAB software package. $w_1=0.9$ and $w_2=0.1$ are selected for the simulation.

In order to comprehensive compare different control schemes, nine scenarios are designed. The scenarios and their descriptions are presented in Table II. The first scenario without any control is simulated and used as the reference. Based on scenario 1, the performances of different control strategies (including VSL control, V2V platooning, V2I, and/or I2V etc.) are simulated and compared. It should be pointed out that, since CAVs increase the freeway capacity (Wang et al. 2016; Shladover et al. 2012), under scenario 5 to scenario 9, the study assumes that the bottleneck capacity is increased by 1%. The free flow speed and shock wave speed are assumed to be the same as the computed results in Table 7.10, the critical density and jam density are recalculated. Under scenario 9, the truck platooning is included, and all the trucks are CVs. Since the truck's car-following behavior has not been proposed yet, the study uses the state-of-the-art passenger cars' car-following model in Milanés and Shladover (2014). In order to apply this model for truck platoons, because of the greater length, a much greater time

gap is set for leading truck, i.e., 1.5s (Chen et al. 2017), and the CT for trucks in the platoon is set as 1.0s. The maximum length of truck platoons is assumed to be 5.

TABLE 7.10: Simulation Scenarios and Descriptions

Scenarios	Description
Scenario 1	With 100% human-driven vehicles and without VSL control
Scenario 2	With 10% CAV and without VSL control
Scenario 3	With 10% CAV, V2V platooning, and without VSL control
Scenario 4	With 100% human-driven vehicles and VSL control
Scenario 5	With 10% CAVs and VSL control
Scenario 6	With 10% CAV , V2V platooning, and VSL control
Scenario 7	With 10% CAV, V2V platooning, V2I, and VSL control
Scenario 8	With 10% CAV, V2V platooning, V2I, I2V, and VSL control
Scenario 9	With 10% CAV, V2V platooning, truck platooning, V2I, I2V, and VSL

Simulation results under the nine designed scenarios are presented in Table 7.11.

The operational efficiency (e.g., TTT, average delays and the number of stops) and emission indicators (e.g., CO₂, NO_x, and particulate) are included. Under the scenario without any control, the severe congestion on the selected freeway corridor wastes the travel time of drivers and increases delays. The TTT under scenario 1 is 8140.51 veh-h, and the average delays are 400.76 s. In addition, the severe congestion leads to the so-called stop-and-go traffic conditions, and the average number of stops is 67.58. Huge emission of CO₂, NO_x, and particular can be observed under scenario 1 as well. Under scenario 2 and 3, the CAVs and V2V platooning are incorporated. According to the simulation measurements in Table III, the introduction of CAV and V2V platooning can

slightly improve the mobility and reduce the emission of CO₂, NO_x, and particular. For example, the TTT under scenario 2 and scenario 3 are decreased by 1.87% and 2.31% respectively. The emission of CO₂ is also respectively reduced by 1.34% and 1.51% under scenario 2 and scenario 3.

Under scenario 4 and scenario 5, the developed VSL control strategy is implemented. As can be seen from Table III, both the operational efficiency and emission are considerably improved compared to the scenarios without VSL control. Under scenario 4, the TTT, average delays, and average number of stops are respectively decreased by 34.43%, 60.4%, and 61.91%. Under scenario 5, the percentage decreases are greater than those under scenario 4 due to the CAVs. For example, the emission of CO₂, NO_x, and particular under scenario 5 are respectively reduced by 7.69%, 8.98%, and 5.38% which are all greater than the percentages under scenario 4. In addition, the V2V platooning is integrated with VSL control under scenario 6. As shown in Table III, the integrated control system achieves a greater improvement percentage in the TTT, average delays and number of stops, and emissions compared to scenario 4 and scenario 5.

Under scenario 7 and scenario 8, the V2I and I2V communication are incorporated into the control system. The simulation results under both scenario 7 and scenario 8 are better than those under scenario 6. While under scenario 9, besides the control schemes under scenario 8, the truck platooning is involved. The best performances are yielded under scenario 9 in terms of the improvement percentages. The TTT, average delay, and average number of stops are respectively reduced by 36.02%, 68.42%, and 67.40% under scenario 9 which are all greater than the other scenarios. The percentage decreases of CO₂, NO_x, and particular are the greatest as well.

TABLE 7.11: Performance Comparison under Different Scenarios

Scenario	TTT (veh-h)	Average delays (s)	Average number of stops	Emission (g)			Improvement (%)							
				CO ₂	NOx	Particulate	TTT	Delays	Number of stops	CO ₂	NOx	Particulate		
Scenario 1	8140.51	400.76	67.58	650.33	1734.2	1951	-	-	-	-	-	-	-	-
Scenario 2	7988.12	385.75	61.77	641.59	1730.57	1950.45	1.87	3.75	8.59	1.34	0.21	0.03		
Scenario 3	7952.5	374.19	60.75	640.54	1729.67	1944.08	2.31	6.63	10.11	1.51	0.26	0.35		
Scenario 4	5337.68	158.71	25.74	605	1583.5	1846.12	34.43	60.4	61.91	6.97	8.69	5.38		
Scenario 5	5328.65	139.81	25.33	600.32	1578.54	1838.54	34.54	65.11	62.52	7.69	8.98	5.76		
Scenario 6	5320.49	135.73	24.19	600.05	1577.18	1838.09	34.64	66.13	64.21	7.73	9.05	5.79		
Scenario 7	5219.71	128	23.14	599.43	1576.91	1835.83	35.88	68.06	65.76	7.83	9.07	5.9		
Scenario 8	5210.58	127.53	22.9	598.91	1576.48	1835.32	35.99	68.18	66.11	7.91	9.09	5.93		
Scenario 9	5208.6	126.54	22.03	598	1575.9	1834.21	36.02	68.42	67.4	8.05	9.13	5.99		

The implementation of the V2V platooning, V2I, and I2V can considerably improve the operational efficiency for the selected freeway with multiple bottlenecks. The reduction in TTT and average delays demonstrates that the vehicles' traveling time on the freeway is significantly reduced. The decreased average number of stops suggests that the stop-and-go traffic conditions are greatly relieved due to the control system. Because of the improvement in mobility, the emission is reduced as well. For example, the emission rate of CO₂, NO_x, and particulate under scenario 9 are decreased by about 8.05%, 9.13%, and 5.99%, respectively.

Figure 7.28 illustrates the changes in average speeds from detector 1 to 14 during the whole control time period under scenario 6. The changes in speed limit value are also depicted. As shown in Figure 7.28, the integrated control system proactively and gradually reduces the vehicle speeds upstream of the bottleneck. Compared to the scenario without any control, the speed differences on the same cell between two consecutive time steps and adjacent cells at the same time period are reduced with respect to the constraints, which can reduce the occurrence of rear-end collision. In addition, compared with the speed profiles without any control (see Figure 7.27), due to the VSL control, the speeds at the five bottlenecks are all improved, especially at the third and fourth bottlenecks.

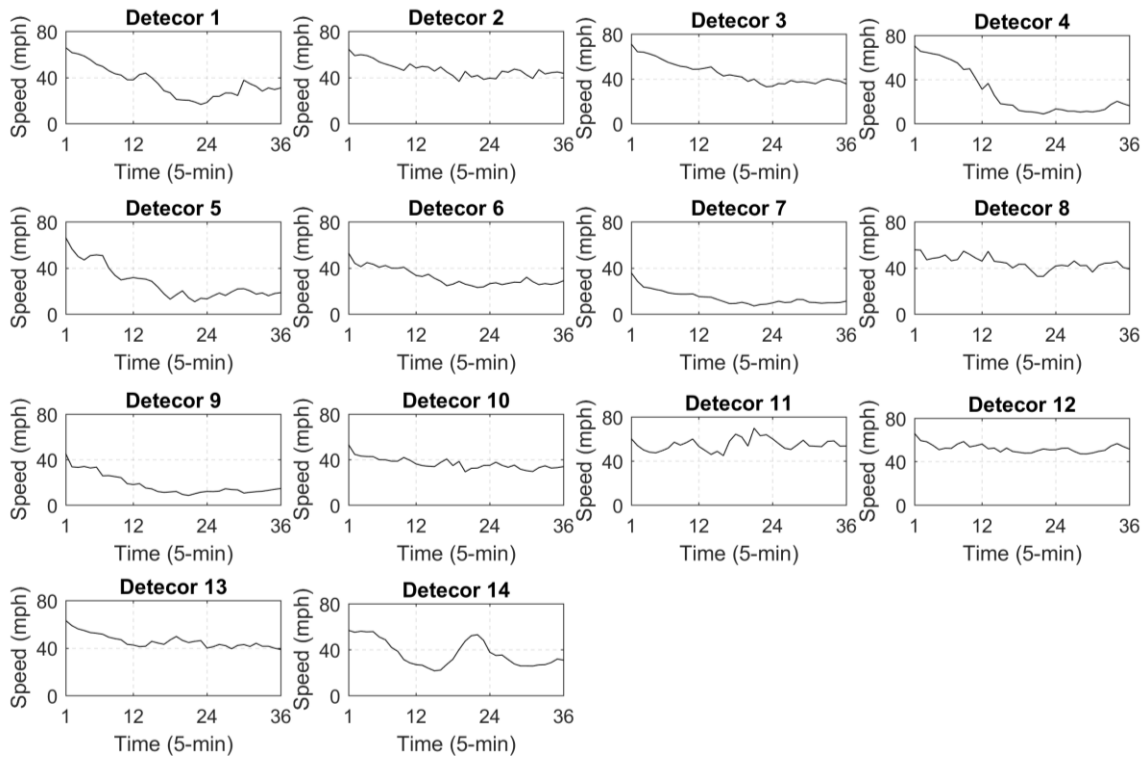


FIGURE 7.27: Speed Profiles without VSL Control

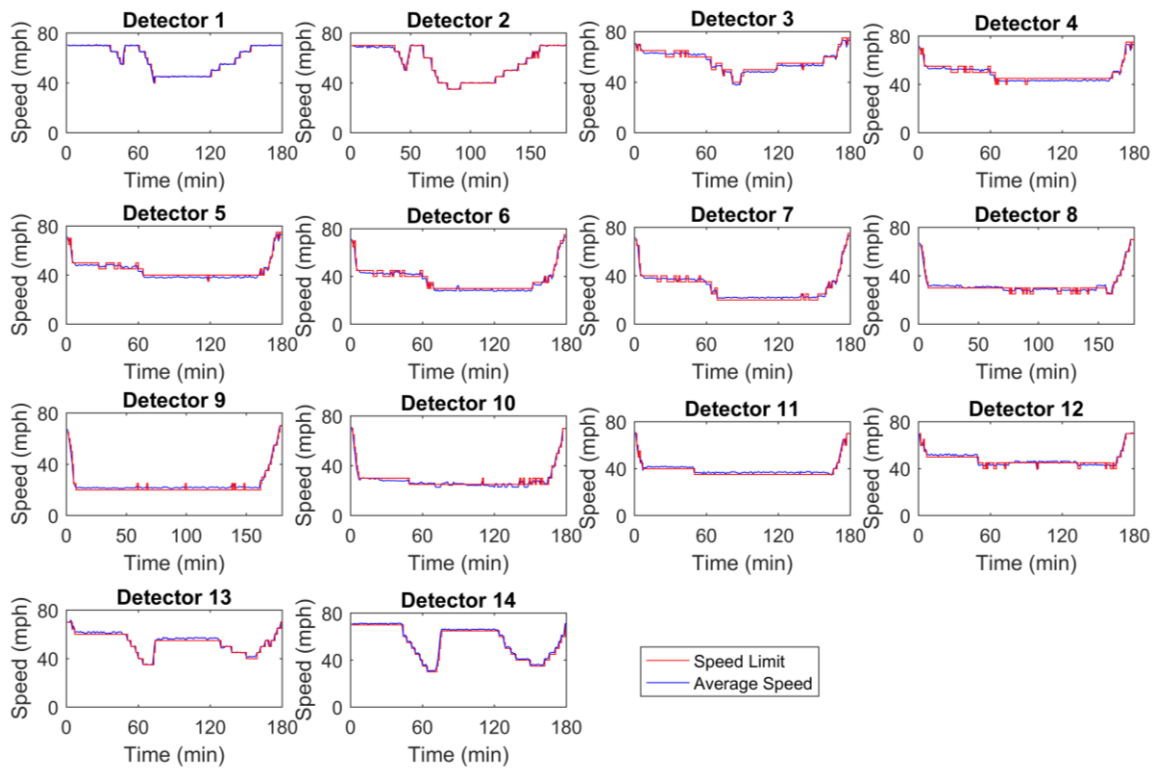


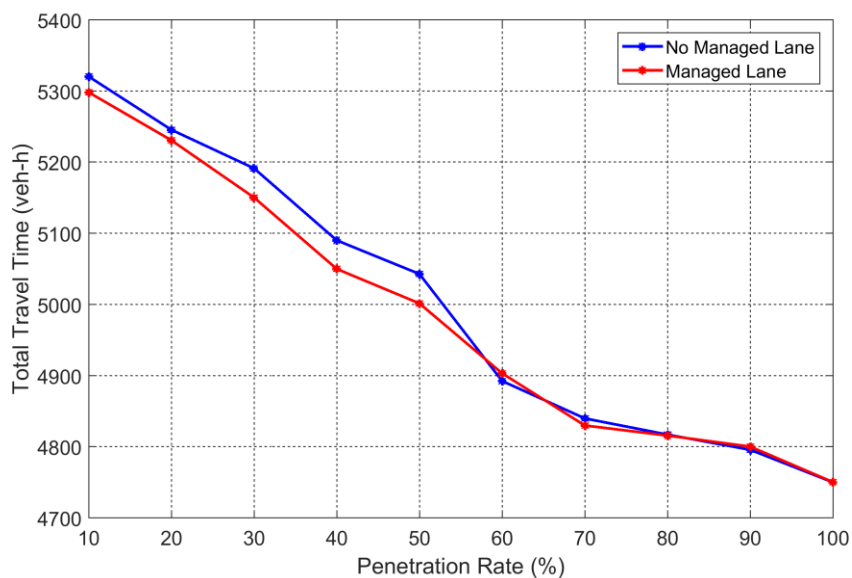
FIGURE 7.28: Speed profile under Scenario 6

7.6.2. Managed Lanes for CAV Platoon

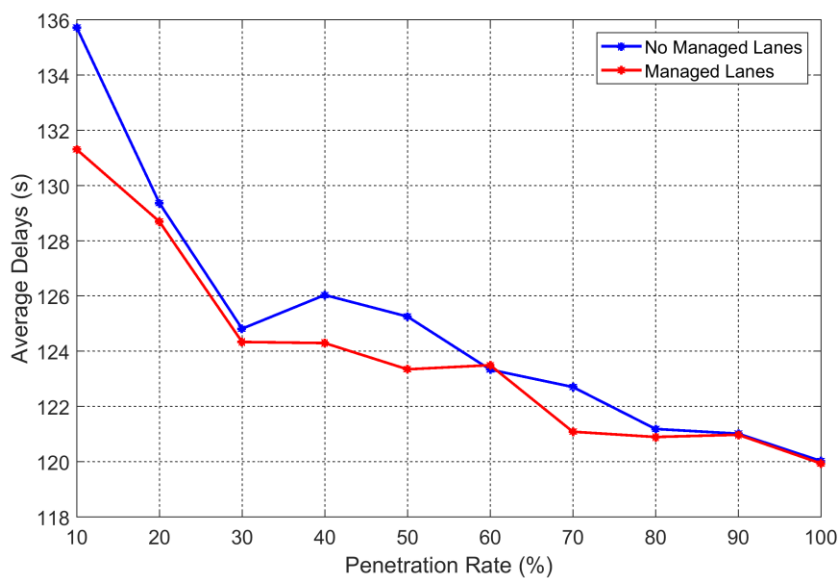
Some researchers have explored the effectiveness of the CAV technology on freeway traffic flow, safety, and mobility with different penetrations of CAVs traveling in all lanes on the selected freeway (Wang et al. 2016; Li et al. 2017). However, the full market penetration of CAVs might not realize in a short period of time. A few researchers have examined the potential benefits of the managed-lanes for CAVs. Rahman and Abdel-Aty studied the CAV platoons in the managed-lane which decreased the crash risk and outperformed all lanes' CAV platoons (Rahman and Abdel-Aty 2017). In this section, the impact of CAV platoons in managed-lane on the operational efficiency on the selected freeway corridor is investigated. The most left lane is set as the managed-lane. Only CAVs are allowed to travel in such lane, and the platoon occurs in the designated lane. Moreover, it has been verified that the market penetration rate of CAVs is a critical factor that affects the efficiency of the control system (Shladover et al. 2012). The sensitivity analysis of the penetration rate is performed under the scenarios without and with the managed CAV lane. It should be pointed out that the bottleneck capacity is assumed to increase by 1% as the penetration rate is increased by 10% (Wang et al. 2016).

The TTT, average delays, and average number of stops at each level of penetration rate are illustrated through Figure 7.29(a) to Figure 7.29(c). As expected, for the scenarios with and without managed-lane, the values of the three indicators decrease with an increase in the CAV penetration rate. Additionally, compared with the scenario without managed CAV lane, the scenario with managed-lane achieves a smaller TTT, average delays, and average number of stops when the penetration rate of CAV is not

very high, e.g. less than 50%. However, with a higher penetration rate, the improvements in these three measurements with managed-lane are not significant compared to the no managed-lane scenario.

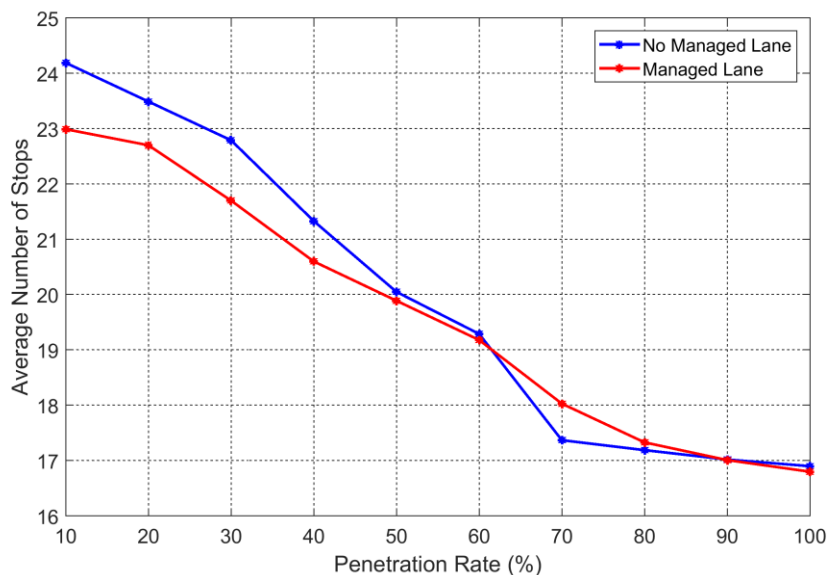


(a) Total Travel Time vs. Penetration Rate



(b) Average Delays vs. Penetration Rate

FIGURE 7.29: Efficiency Measurements vs. Penetration Rate



(c) Average Number of Stops vs. Penetration Rate

FIGURE 7.29, continued

7.6.3. VSL Updating Frequency and Performance

The impact of VSL control configurations (such as the number of VSL signs, speed difference, and updating frequency) on control performances has been explored in some research (Li et al. 2017; Islam et al. 2013). For example, in Islam et al. (2013), VSL updating frequency had a significant influence on traffic collision, but it had no substantial impact on mobility. Proper updating frequency might help obtain better results. As such, this study investigates the effects of VSL updating frequency on the mobility and emission. Five different updating frequencies under scenario 6 are explored, and the simulation results are presented in Table 7.12.

For the developed integrated control system in this study, when the updating frequency is less than or equal to 3 minutes, the improvement percentages of the

operational efficiency (i.e., TTT and average delay and number of stops) and emission (i.e., CO₂, NO_x, and Particulate) are not significantly different. For example, the TTT is reduced by 34.64%, 34.64%, and 34.65% when the updating frequency is 1-min, 2-min, and 3-min, respectively. However, when the updating frequency is greater than 3 minutes (i.e., 4 min and 5 min), in general, the percentage decreases in both the efficiency and emission are less than those with less updating frequency (i.e., 1 min, 2 min, and 3 min). For example, the percentage decreases of TTT, average delay, and average number of stops with 5-min updating frequency are 34.34%, 65.81%, and 62.1%, which are less than those with 1-min updating frequency.

TABLE 7.12: Simulation Outputs with Difference Updating Frequency

Updating Frequency	TTT (veh-h)	Average delay (s)	Average number of stops	Emission (g)			Improvement (%) – Scenario1					
				CO ₂	NOx	Particulate	TTT	Delay	Number of stops	CO ₂	NOx	Particulate
1 min	5320.49	135.73	24.19	600.05	1577.18	1838.09	34.64	66.13	64.21	7.73	9.05	5.79
2 min	5320.89	135.77	24.06	600.53	1577.01	1837.9	34.64	66.12	64.4	7.66	9.06	5.80
3 min	5319.5	135.21	25.72	600.17	1577.44	1838.5	34.65	66.26	61.94	7.71	9.04	5.77
4 min	5325.91	135.44	25.88	601	1578.05	1838.9	34.58	66.2	61.7	7.59	9	5.75
5 min	5345.16	137.03	25.61	601.96	1580.93	1840.92	34.34	65.81	62.1	7.44	8.84	5.64

7.7. Summary

This chapter describes the numerical results of the developed VSL control strategies. Different VSL control strategies are presented. Different control scenarios and control settings are designed and compared. The results demonstrate that the developed VSL controls significantly improve the operational efficiency and reduce the speed variation, particularly in a CAV environment. The potential benefits of V2V platoons, V2I, and I2V on mobility improvement and emission reduction are also examined. In order to achieve a better control performance, the managed-lane strategy with CAV platoons is recommended to be implemented on the basis of the numerical results.

CHAPTER 8: SUMMARY AND CONCLUSIONS

8.1. Introduction

Traffic congestion occurs frequently around the world as freeway demand increases. Traffic congestion is detrimental to vehicle mobility, environmental, and safety. The ATM strategies (including ML, VSL, and RM) which can be used to optimize the existing roadways are receiving more and more attention by the local, state, and federal DOT. Among these ATM strategies, VSL has received increasing attention over the past decades, which can be implemented to improve the freeway mobility and safety and reduce greenhouse gas emissions.

Additionally, with the development of emerging technologies, various novel methods on the basis of intelligent transportation technologies have been developed during recent years. Typically, these new technologies aim to increase the efficiency of the transportation system rather than adding/building more roadways. One of the representative technologies is CAV. Enhanced outcomes can be achieved through integrating VSL control with the V2V, V2I, and/or I2V communications.

The primary objective of this research is to develop VSL control frameworks for mixed traffic flows in a CAV environment. The VSL control framework that takes heavy vehicles into account is formulated. Discrete optimization algorithms (e.g., genetic algorithm and tabu search) are adopted to solve the VSL control problems. In addition, the VSL control framework under left-lane truck lane restriction policy is also evaluated in this dissertation. The integrated VSL control systems in a CAV environment are

developed as well. A real-world freeway corridor is selected as the case study to examine the developed control strategies so that the gaps between the theoretical research and the application of the developed VSL controls can be bridged.

The rest of this chapter is organized as follows. In section 8.2, the principal features of the VSL control are reviewed and a summary of conclusions for the numerical results derived from computational tests is discussed. Section 8.3 presents a brief discussion of the limitations of the current approaches and possible directions for further research are also given.

8.2. Summary and Conclusions

As mentioned, optimal VSL control systems for mixed traffic flows in a CAV environment are developed in this study. The literature describing previous VSL control studies has been reviewed. The benefits of VSL control include improved safety, increased bottleneck throughput, reduced emissions, and resolved traffic breakdown (Lu and Shladover 2014). Existing approaches presented by researchers can be grouped into four categories: MPC, local feedback theory, shock wave theory, and optimal control theory. Among these approaches, The MPC approach has been widely used by the researchers since it was first developed for VSL control by Hegyi et al. (2005).

The shortcomings of previous approaches include the failure to consider mixed traffic flows and failure to consider a system that combines VSL control and truck lane restriction policy. Additionally, with the development of CAV technologies, it is essential to take the CAV into account. Building on previous approaches, the VSL control strategies proposed in this research include the following major features: 1) Mixed traffic

flows (including truck and cars) are taken into account; 2) Discrete optimization algorithms are adopted to optimize the proposed control systems; 3). VSL control systems in a CAV environment which can be used to relieve congestion at multiple bottlenecks are developed; and 4). Integrated VSL control strategies (e.g., combined VSL control with truck lane restriction policy, and combined VSL control with CAV platooning) are formulated.

This dissertation develops and uses the tabu search algorithm to solve the VSL control problem. The objective of a VSL control system is to minimize total value of travel time and total value of speed variation on the selected freeway stretch. Tabu search algorithm frameworks for VSL control are developed and presented. Sensitivity analyses, including the number of iterations and tabu neighbors, are conducted. Different weight sets of objective function are also selected and tested so that the quality solutions could be obtained and compared. The SQP algorithm is used as a benchmark to measure the performance of tabu search algorithm. The results indicate that VSL control, which is solved by tabu search algorithm, outperforms the solutions produced by the SQP algorithm, thereby suggesting that tabu search algorithm can be an effective solution approach for the VSL control. In addition, the presented numerical results indicate that as the number of VSL control segments increases, the total travel time increases but the total speed variation decreases. The relationship between the number of VSL control segments and combined objective function is also presented with different weight sets.

GA-based approach to solving the VSL control for mixed traffic flows including cars and trucks on the selected freeway segments is developed. A multi-objective non-linear integer model is formulated for the VSL control. The SQP is used as a benchmark

to examine the control results of the GA. The results which are optimized by the GA outperform the results from the SQP algorithm. Also, the control results with different driver compliance rates are given and the conclusions are in line with the existing studies. A sensitivity analysis is conducted by varying the truck percentages. The sensitivity analysis results are presented which show that as the truck percentage increases, both the operational efficiency (i.e., TTT) and the level of safety (i.e., TSV and TSD) of VSL control tend to decrease.

To decrease the impact of trucks on cars, the left lane truck restriction policy is integrated with VSL control. The developed non-linear VSL controls are optimized by one of the most widely used derivative-free optimization algorithms. In addition, the control results are compared with another gradient-free algorithm, i.e., SA. A hypothetical freeway stretch is used as the case study. In addition, the relationship between the VSL control performances with different TRPs and truck percentages is explored. An extended METANET model is developed to predict the traffic data in the truck restriction and no truck restriction lanes, respectively. The lane change volume of cars between these two types of lanes is taken into account. The method to compute the lane-changing volume under VSL control is developed. The method to compute the dynamic pce value in the NTR lanes is also given. A multi-objective nonlinear integer model is formulated for the VSL control. In addition, the SA algorithm which has been verified that it can provide a good solution quality for the traffic control problems is selected as the reference. VSL control strategies under different truck lane restriction policies are examined and tested: left one-lane truck restriction and left two-lane truck restriction. Different control scenarios are designed and compared. The simulation results

show that the extended METANET model outperforms the single-class METANET model, and the developed VSL control significantly improves the operational efficiency and reduces the speed variation. In addition, GA provides similar control performances as SA. Also, VSL control increases the utilization of the NTR lanes. The sensitivity analysis is conducted by varying the truck percentages. The sensitivity analysis results demonstrate that as the truck percentage increases, both the operational efficiency and the level of safety of VSL control tend to decrease.

A proof-of-concept study on developing a VSL control strategy in a CAV environment for a freeway corridor is performed. The VSL control is developed on the basis of the extended CTM which considers the capacity drop phenomenon at the bottleneck. The proposed VSL control model takes mixed traffic flows (including human-driven cars, trucks and AVs) into consideration. In addition, the study also discusses how to deploy the proposed VSL control to relieve congestion caused by multiple bottlenecks. The GA is employed to optimize the VSL control. A real-world freeway corridor is selected to examine the developed control strategy. Potential benefits of the AV, V2X, and I2V are also investigated by designing different scenarios. The simulation results demonstrate that the developed VSL control can be used to greatly improve the operational efficiency, freeway mobility, and reduce greenhouse gas emissions. In addition, the control strategies that integrate VSL control with the V2X and I2V outperform the VSL control only. The sensitivity analysis results are presented in this study as well. As the penetration rate of AVs increases, the TTT, average delays, and average number of stops all tend to decrease.

The CAV platooning control is incorporated into the VSL control system. The platooning control which aims to maintain and form a platoon is discussed in detail. The behavior of CAVs is modeled by using the California PATH car-following model. The VSL control system is developed on the basis of the modified CTM which considers the capacity drops at the bottlenecks and mixed traffic flows (including human-driven cars, trucks and AVs). A real-world freeway corridor is selected and used to evaluate and compare the performances under different scenarios. The potential benefits of V2V platoons, V2I, and I2V on mobility improvement and emission reduction are examined. The study also explores and compares the mobility measurements with and without using a managed-lane for CAVs with different market penetration rates. The sensitivity results demonstrate that with a low penetration rate of CAVs, in order to achieve a better control performance, the managed-lane for CAV platoons is recommended to be implemented. Finally, the study also investigates the speed limit updating frequency of the integrated control system.

8.3. Directions for Future Research

In this section, some of the limitations of the developed VSL control frameworks in this dissertation are presented and directions for further research are also discussed.

Typically, the VSL control is always formulated as a discrete-time constrained non-linear optimal control problem. The formulated optimal control problems relying on the macroscopic second-order (e.g., METANET) and first-order mode (e.g., CTM) are often nonlinear and nonconvex, which are hard to solve. In the future, the authors will

aim at formulating the VSL control as an approximate linear optimization problem so that it can be solved in a much more efficient and effective way.

In this study, the intelligent driver model and California PATH car-following model are directly adapted to model the car-following characteristics of CAVs. The lane-changing behavior of CAVs is manipulated using the lane changing model of VISSIM. For CAVs, the effects of lane-changing control should be well studied in the future.

Lastly, communication delays should be considered when formulating the VSL control in a CAV environment. The authors will also explore the stability of the car and truck platoons under different speed limits. The vehicle behavior of CAV platoons before and during lane changes will also be studied.

In the future, with the development of intelligent transportation technologies, an operationally and economically efficient VSL control system will be formulated and implemented, which can be used to decrease air pollution, reduce fuel consumption, and improve highway mobility and safety.

REFERENCES

- Abdalhaq, BK, and MIA Baker. 2014. Using meta heuristic algorithms to improve traffic simulation. *Journal of Algorithms and Optimization* 2(4): 110-128.
- Abdel-Aty M, J Dilmore, and A Dhindsa. 2016. Evaluation of variable speed limits for real-time freeway safety improvement. *Accident Analysis & Prevention* 38: 335 – 345.
- Al-Kaisy A, L Ewan, and D Veneziano. 2012. evaluation of a variable speed limit system for wet and extreme weather conditions: phase I report. FHWA-OR-RD-12-14, Oregon Department of Transportation, Salem, Oregon, June 2012.
http://www.oregon.gov/ODOT/Programs/ResearchDocuments/SPR743_VSL_System.pdf
- Alessandri A, AD Febbraro, A Ferrara, and E Punta. 1999. Nonlinear optimization for freeway control using variable-speed signaling. *IEEE Transactions on Intelligent Transportation Systems* 48(6): 2042 – 2052.
- Allaby P, B Hellinga, and M Bullock. 2007. variable speed limits: safety and operational impacts of a candidate control strategy for freeway applications. *IEEE Transactions on Intelligent Transportation Systems* 8(4): 671 – 680.
- Bagnerini P, and M Rasclé. 2003. A multiclass homogenized hyperbolic model of traffic flow. *SIAM Journal on Mathematical Analysis* 35(4): 949–973.
- Balakrishna R, C Antoniou, M Ben-Akiva, HN Koutsopoulos, and Y Wen. 2007. Calibration of microscopic traffic simulation models methods and application. *Transportation Research Record* 1999: 198–207.
- Bang S, and S Ahn. 2017. Platooning strategy for connected and autonomous vehicles: transition from light traffic. *Transportation Research Record* 2623: 73 – 81.
- Bel G, and J Rosell. 2013. Effects of the 80 km/h and variable speed limits on air pollution in the metropolitan area of Barcelona. *Transportation Research Part D* 23: 90 – 97.
- Bekiaris-Liberis N, L Roncoli, and M Papageorgiou. 2016. Highway traffic state estimation with mixed connected and conventional vehicles. *IEEE Transactions on Intelligent Transportation Systems* 17(12): 3484 – 3497.
- Bertini RL, S Boice, and K Bogenberger. 2006. Dynamics of variable speed limit system surrounding bottleneck on German Autobahn. *Transportation Research Record* 1978: 149–159.
- Chang GL, SY Park, and J Paracha. 2011. Intelligent transportation system field demonstration integration of variable speed limit control and travel time estimation for a recurrently congested highway. *Transportation Research Record* 2243: 55–66.

- Carlson RC, I Papamichail, M Papageorgiou, and A Messmer. 2010a. Optimal motorway traffic flow control involving variable speed limits and ramp metering. *Transportation Science* 44(2): 238 – 253.
- Carlson RC, I Papamichail, M Papageorgiou, and A Messmer. 2010b. optimal mainstream traffic flow control of large-scale motorway networks. *Transportation Research Part C* 18: 193 – 212.
- Carlson RC, I Papamichail, and M Papageorgiou. 2011. Local feedback-based mainstream traffic flow control on motorways using variable speed limits. *IEEE Transactions on Intelligent Transportation Systems* 12(4): 1261-1276.
- Carlson RC, I Papamichail, and M Papageorgiou. 2013. Comparison of local feedback controllers for the mainstream traffic flow on freeways using variable speed limits. *Journal of Intelligent Transportation Systems* 17(4): 268 – 281.
- Cate MA, and T Urbanik II. 2004. Another view of truck lane restrictions. *Transportation Research Record* 1867: 19-24.
- Chanut S, and C Buisson. 2003. Macroscopic model and its numerical solution for two-flow mixed traffic with different speeds and length. *Transportation Research Record* 1852: 209-219.
- Chen D, S Ahn, and A Hegyi. 2014. Variable speed limit control for steady and oscillatory queues at fixed freeway bottlenecks. *Transportation Research Part B* 70: 340 – 358.
- Chen D, and S Ahn. 2015. Variable speed limit control for severe non-recurrent freeway bottlenecks. *Transportation Research Part C* 51: 210 – 230.
- Chen D, S Ahn, M Chitturi, and D Noyce. 2017. Truck platooning on uphill grades under cooperative adaptive cruise control (CACC). *Transportation Research Part C* 94: 50-66.
- Cheu RL, X Jin, KC Ng, YL Ng, and D Srinivasan. 1998. Calibration of FRESIM for Singapore expressway using genetic algorithm. *Journal of Transportation Engineering* 124(6): 526 – 535.
- Chiappone S, O Giuffrè, A Granà, R Mauro, and A Sferlazza. 2016. Traffic simulation models calibration using speed–density relationship: an automated procedure based on genetic algorithm. *Expert Systems with Applications* 44: 147 – 155.
- Cho H, and Y Kim. 2012. Analysis of traffic flow with variable speed limit on highways. *KSCE Journal of Civil Engineering* 16(6): 1048 – 1056.
- Choi S, and C Oh. 2016. Proactive strategy for variable speed limit operations on freeways under foggy weather conditions. *Transportation Research Record* 2551: 29–36.
- Ciuffo B, V Punzo, and V Torrieri. 2008. Comparison of simulation-based and model-

based calibrations of traffic-flow microsimulation models. *Transportation Research Record* 2088: 36–44.

Daganzo CF. 1994. The cell transmission model: a dynamic representation of highway traffic consistent with the hydrodynamic theory. *Transportation Research Part B* 28: 269-287.

DeGaspari M, PJ Jin, WJ Wall, and CM Walton. 2013. The effect of active traffic management on travel time reliability: a case study of I-5 in Seattle. Presented at 92nd Annual Meeting of the Transportation Research Board, Washington, D.C.

Deng Q. 2016. A general simulation framework for modeling and analysis of heavy-duty vehicle platooning. *IEEE Transactions on Intelligent Transportation Systems* 17(11): 3252 – 3262.

Deo P, B De Schutter, and A Hegyi. 2009. Model predictive control for multi-class traffic flows. In *Proc. 12th IFAC Symp. Transp. Sys.* Redondo Beach, CA, USA, Sep., 2009: 25-30.

Dervisoglu G, G Gomes, J Kwan, A Muralidharan, and R Horowitz. 2009. Automatic calibration of the fundamental diagram and empirical observations on capacity. 88th Transportation Research Board Annual Meeting, Transportation Research Board, Washington, DC.

Duret A, S Ahn, and C Buisson. 2012. Lane flow distribution on a three-lane freeway: General features and the effects of traffic controls. *Transportation Research Part C* 24: 157-167.

Elefteriadou L, SS Washburn, Y Yin, Vipul M, and C Letter. 2012. Variable speed limit (VSL) - best management practice. FDOT Contract BDK77 977-11, Florida Department of Transportation, Tallahassee, Florida, July 2012.

http://www.fdot.gov/research/completed_proj/summary_te/fdot_bdk77_977-11_rpt.pdf

Fan W, and L Gong. 2017. Developing a systematic approach to improving bottleneck analysis in North Carolina. FHWA/NC/2016-10, North Carolina Department of Transportation, Raleigh, NC.

<https://connect.ncdot.gov/projects/research/RNAProjDocs/2016-10%20Final%20Report.pdf>

Fan W, and Z Gurmu. 2014. Combined decision making of congestion pricing and capacity expansion: genetic algorithm approach. *Journal of Transportation Engineering*, 140: 04014031-1.

Fan W, and RB Machemehl. 2006. Optimal transit route network design problem with variable transit demand: a genetic algorithm approach. *Journal of Transportation Engineering* 132(1): 40-51.

Fan W, and RB Machemehl. 2008. Tabu search strategies for the public transportation

network optimizations with variable transit demand. *Journal Computer-Aided Civil and Infrastructure Engineering* 23(7): 502-520.

Fang J, M Hadiuzzaman, A Karim, Y Luo, and TZ Qiu. 2014. Variable speed limit control strategy with collision probability assessments based on traffic state prediction. *Transportation Research Record* 2435: 11 – 18.

Federal Highway Administration (FHWA). 2004. Traffic congestion and reliability: linking solutions to problems. July 19.

https://ops.fhwa.dot.gov/congestion_report_04/congestion_report.pdf

Fletcher R. 2007. The sequential quadratic programming method. 77-94.

https://www.math.uh.edu/~rohop/fall_06/Chapter4.pdf

Fountoulakis M, N Bekiaris-Liberis, C Roncoli, I Papamichail, and M Papageorgiou. 2017. Highway traffic state estimation with mixed connected and conventional vehicles: microscopic simulation-based testing. *Transportation Research Part C* 78: 13-33.

Fudala NJ, and MD Fontaine. 2010. Work zone variable speed limit systems: effectiveness and system design issues. FHWA/VTRC 10-R20, Virginia Department of Transportation, Richmond, VA, March 2010.

http://www.virginiadot.org/vtrc/main/online_reports/pdf/10-r20.pdf

Georgia Department of Transportation (GDOT). 2017. Variable speed limits (VSL). <http://www.dot.ga.gov/DriveSmart/SafetyOperation/Pages/VSL.aspx#tab-4> (access on August 25, 2018)

Ghods AH, L Fu, and A Rahimi-Kian. 2010. An efficient optimization approach to real-time coordinated and integrated freeway traffic control. *IEEE Transactions on Intelligent Transportation Systems* 11(4): 873 – 884.

Glover F. 1989. Future paths for integer programming and links to artificial intelligence. *Computers and Operations Research* 13: 533-549.

Glover F. 1990. Artificial intelligence, heuristic frameworks and tabu search. *Managerial and Decision Economics* 11: 365-375.

Grumert E, X Ma, and A Tapani. 2015. Analysis of a cooperative variable speed limit system using microscopic traffic simulation. *Transportation Research Part C* 52: 173-186.

Goatin P, S Göttlich, and O Kolb. 2016. Speed limit and ramp meter control for traffic flow networks. *Engineering Optimization* 48(7): 1121 – 1144.

Gong L, and W Fan. 2017. Applying travel-time reliability measures in identifying and ranking recurrent freeway bottlenecks at the network level. *Journal of Transportation Engineering* 143(8): 04017042

Gong L, and W Fan. 2018. Developing a systematic method for identifying and ranking

freeway bottlenecks using vehicle probe data. *Journal of Transportation Engineering* 144(3): 04017083.

Hadiuzzaman M, and TZ Qiu. 2013. Cell transmission model based variable speed limit control for freeway. *Canadian Journal of Civil Engineering* 40: 46-56.

Hadiuzzaman M, TZ Qiu, and XY Lu. 2013. Variable speed limit control design for relieving congestion caused by active bottlenecks. *Journal of Transportation Engineering* 139(4): 358 – 370.

Hale DK, C Antoniou, M Brackstone, D Michalaka, AT Moreno, and K Parikh. 2015. Optimization-based assisted calibration of traffic simulation models. *Transportation Research Part C* 55:100 – 115.

Hale D, T Phillips, K Raboy, J Ma, P Su, XY Lu, H Rakha, and DJ Dailey. 2016. Introduction of cooperative vehicle-to-infrastructure systems to improve speed harmonization. FHWA, McLean, VA, FHWA-HRT-16-023, Mar. 2016.
<https://www.fhwa.dot.gov/publications/research/operations/16023/16023.pdf>

Han Y, A Hegyi, Y Yuan, S Hoogendoorn, M Papageorgiou, and C Roncoli. 2017. Resolving freeway jam waves by discrete first-order model based predictive control of variable speed limits. *Transportation Research Part C* 77: 405 – 420.

Han Y, D Chen, and S Ahn. 2017. Variable speed limit control at fixed freeway bottlenecks using connected vehicles. *Transportation Research Part B* 98: 113 – 134.

Harbord B, J White, K McCabe, A Riley, and S Tarry. 2006. A flexible approach to motorway control. Presented at 13th World Congress on Intelligent Transport Systems, London, October 13.

Hegyi A. 2004. Model predictive control for integrating traffic control measures. PhD thesis, TRAIL Thesis Series T2004/2. Delft University of Technology, Netherlands, 2004.

Hegyi A, BD Schutter, and J Hellendoorn. 2005. Optimal coordination of variable speed limits to suppress shock waves. *IEEE Transactions on Intelligent Transportation Systems* 6(1): 102 – 112.

Hegyi A, M Burger, BD Schutter, J Hellendoorn, and TJJ van den Boom. 2007. Towards a practical application of model predictive control to suppress shock waves on freeways. *Proceeding of the European Control Conference 2007*, Kos, Greece, July 2-5.

Hegyi A, SP Hoogendoorn, M Schreuder, H Stoelhorst, and F Viti. 2008. SPECIALIST: a dynamic speed limit control algorithm based on shock wave theory. *Proceedings of the 11th International IEEE Conference on Intelligent Transportation Systems*, Beijing, China, October 12-15: 827 - 832.

Hegyi A, SP Hoogendoorn, M Schreuder, and H Stoelhorst. 2009. The expected

effectivity of the dynamic speed limit algorithm SPECIALIST – a field data evaluation method. Proceedings of the European Control Conference 2009, Budapest, Hungary, August 23–26: 1770 - 1775.

Hegy A, BD Netten, M Wang, W Schakel, T Schreiter, Y Yuan, B van Arem, and T Alkim. 2013. A cooperative system based variable speed limit control algorithm against jam waves – an extension of the SPECIALIST algorithm. Proceedings of the 16th International IEEE Annual Conference on Intelligent Transportation Systems (ITSC 2013), Hague, Netherlands, October 6-9: 973 – 978.

Heydecker BG, and JD Addison. 2011. Analysis and modelling of traffic flow under variable speed limits. *Transportation Research Part C* 19: 206 – 217.

Highway Capacity Manual (HCM). 2010. Transportation Research Board, Washington, D.C. <http://trjournalonline.trb.org/doi/book/10.5555/9780309160773>

Hoogendoorn SP, W Daamen, RG Hoogendoorn, and JW Goemans. 2013. Assessment of dynamic speed limits on freeway A20 near Rotterdam, Netherlands. *Transportation Research Record* 2380: 61–71.

Hourdakis J, PG Michalopoulos, and J Kottommannil. 2003. Practical procedure for calibrating microscopic traffic simulation models. *Transportation Research Record* 1852: 130–139.

Iordanidou GR, C Roncoli, I Papamichail, and M Papageorgiou. 2015. Feedback-based mainstream traffic flow control for multiple bottlenecks on motorways. *IEEE Transactions on Intelligent Transportation Systems* 16(2): 610 – 621.

Islam MT, M Hadiuzzaman, J Fang, TZ Qiu, and K El-Basyouny. 2013. Assessing mobility and safety impacts of a variable speed limit control strategy. *Transportation Research Record* 2364: 1 – 11.

Jha M, G Gopalan, A Garms, BP Mahanti, T Toledo, and ME Ben-Akiva. 2004. Development and calibration of a large-scale microscopic traffic simulation model. *Transportation Research Record* 1876: 121–131.

Jia D, and D Ngoduy. 2016. Platoon based cooperative driving model with consideration of realistic inter-vehicle communication. *Transportation Research Part C* 68: 245 – 264.

Jin HY, and WL Jin. 2015. Control of a lane-drop bottleneck through variable speed limits. *Transportation Research Part C* 58: 568-584.

Kang KP, GL Chang, and N Zou. 2004. Optimal dynamic speed-limit control for highway work zone operations. *Transportation Research Record* 1877: 77–84.

Kattan L, B Khondaker, O Derushkina, and E Poosarla. 2014. A probe-based variable speed limit system. *Journal of Intelligent Transportation Systems* 19(4): 339 – 354.

Katz B, J Ma, H Rigdon, K Sykes, Z Huang, and K Raboy. 2017. Synthesis of variable speed limit signs. FHWA-HOP-17-003, U.S. Department of Transportation, Federal Highway Administration, Washington, D.C., May 2017.

<https://ops.fhwa.dot.gov/publications/fhwahop17003/fhwahop17003.pdf>

Kerner BS. 2007. Study of freeway speed limit control based on three-phase traffic theory. *Transportation Research Record* 1999: 30–39.

Khondaker B, and L Kattan. 2015a. Variable speed limit: an overview. *Transportation Letters* 7(5): 264 – 278.

Khondaker B, and L Kattan. 2015b. Variable speed limit: a microscopic analysis in a connected vehicle environment. *Transportation Research Part C* 58: 146 -159.

Kianfar J, P Edara, and C Sun. 2013. Operational analysis of a freeway variable speed limit system - case study of deployment in Missouri. Presented at 92nd Annual Meeting of the Transportation Research Board, Washington, D.C.

Kim SJ, W Kim, and LR Rilett. 2005. Calibration of microsimulation models using nonparametric statistical techniques. *Transportation Research Record* 1935: 111–119.

Knoop VL, A Duret, C Buisson, and B van Arem. 2010. Lane distribution of traffic near merging zones influence of variable speed limits. 13th International IEEE Annual Conference on Intelligent Transportation Systems Madeira Island, Portugal, September 19-22: 485 – 490.

Kockelman K, S Boyles, P Stone, D Fagnant, R Patel, MW Levin, G Sharon, M Simoni, M Albert, H Fritz, R Hutchinson, P Bansal, G Domnenko, P Bujanovic, B Kim, E Pourrahmani, S Agrawal, T Li, J Hanna, A Nichols, and J Li. 2016. An assessment of autonomous vehicles: traffic impacts and infrastructure needs—final report. FHWA/TX-17/0-6847-1, Texas Department of Transportation, Austin, TX, December 2016.

<https://library.ctr.utexas.edu/ctr-publications/0-6847-1.pdf>

Kockelman K, P Avery, P Bansal, SD Boyles, P Bujanovic, T Choudhary, L Clements, G Domnenko, D Fagnant, J Helsel, R Hutchinson, M Levin, J Li, T Li, L Loftus-Otway, A Nichols, M Simoni, and D Stewart. 2016. Implications of connected and automated vehicles on the safety and operations of roadway networks: a final report. FHWA/TX-16/0-6849-1, Texas Department of Transportation, Austin, TX, August 2016.

<https://library.ctr.utexas.edu/ctr-publications/0-6849-1.pdf>

Kononov J, C Durso, D Reeves, and BK Allery. 2012. Relationship between traffic density, speed, and safety and its implications for setting variable speed limits on freeways. *Transportation Research Record* 2280: 1–9.

Kotsialos A, M Papageorgiou, M Mangeas, and H Haj-Salem. 2002. Coordinated and integrated control of motorway networks via non-linear optimal control. *Transportation Research Part C* 10: 65 – 84.

Kwon E, D Brannan, K Shouman, C Isackson, and B Arseneau. 2007. Development and field evaluation of variable advisory speed limit system for work zones. *Transportation Research Record* 2015: 12–18.

Kwon, E, C Park, D Lau, and B Kary. 2011. Minnesota variable speed limit system: adaptive mitigation of shock waves for safety and efficiency of traffic flows. Presented at 92nd Annual Meeting of the Transportation Research Board, Washington, D.C.

Laval JA, and CF Daganzo. 2006. Lane-changing in traffic streams. *Transportation Research Part B* 40: 251-264.

Leclercq L, JA Laval, and N Chiabaut. 2011. Capacity drops at merges: an endogenous model. *Transportation Research Part B* 45: 1302-1313.

Lee JB, and K Ozbay. 2009. New calibration methodology for microscopic traffic simulation using enhanced simultaneous perturbation stochastic approximation approach. *Transportation Research Record* 2124: 233–240.

Lenz H, R Sollacher, and M Lang. 1999. Nonlinear speed-control for a continuum theory of traffic flow. *Proceedings in the 14th World Congress of IFAC, Beijing, China, 5-7 July*: 67–72.

Li Y, C Xu, L Xing, and W Wang. 2017. Integrated cooperative adaptive cruise and variable speed limit controls for reducing rear-end collision risks near freeway bottlenecks based on micro-simulations. *IEEE Transactions on Intelligent Transportation Systems* 18(11): 3157 - 3167.

Li Z, P Liu, W Wang, and C Xu. 2014. Development of a control strategy of variable speed limits to reduce rear-end collision risks near freeway recurrent bottlenecks. *IEEE Transactions on Intelligent Transportation Systems* 15(2): 866 – 876.

Li Z, P Liu, W Wang, and C Xu. 2016. Optimal mainline variable speed limit control to improve safety on large-scale freeway segments. *Computer-Aided Civil and Infrastructure Engineering* 31: 366 – 380.

Liu S, H Hellendoorn, and B De Schutter. 2017. Model predictive control for freeway networks based on multi-class traffic flow and emission models. *IEEE Transactions on Intelligent Transportation Systems* 18(2): 306-320.

Liu S, A Sadowska, JRD Frejo, A Núñez, EF Camacho, H Hellendoorn, and B De Schutter. 2016. Robust receding horizon parameterized control for multi-class freeway networks: a tractable scenario-based approach. *Int. J. Robust Nonlinear Control* 26: 1211-1245.

Liu S, B De Schutter, and H Hellendoorn. 2014. Model predictive traffic control based on a new multi-class METANET model. In *Proc. 19th World Congress Int. Fed. Autom. Control, Cape Town, South Africa. Aug. 2014*: 8781-8786.

- Lownes NE, and RB Machemehl. 2006. Sensitivity of simulated capacity to modification of VISSIM driver behavior parameters. *Transportation Research Record* 1988: 102–110.
- Lu XY, P Varaiya, R Horowitz, D Su, and SE Shladover. 2011. Novel freeway traffic control with variable speed limit and coordinated ramp metering. *Transportation Research Record* 2229: 55–65.
- Lu XY, and SE Shladover. 2014. Review of variable speed limits and advisories: theory, algorithms, and practice. *Transportation Research Record* 2423: 15–23.
- Lu XY, SE Shladover, I Jawad, R Jagannathan, and T Phillips. 2015. Novel algorithm for variable speed limits and advisories for a freeway corridor with multiple bottlenecks. *Transportation Research Record* 2489: 86–96.
- Ma T, and B Abdulhai. Genetic algorithm-based optimization approach and generic tool for calibrating traffic microscopic simulation parameters. *Transportation Research Record* 1800: 6–15.
- Ma J, H Dong, and HM Zhang. 2007. Calibration of microsimulation with heuristic optimization methods. *Transportation Research Record* 1999: 208–217.
- Ma J, X Li, S Shladover, HA Rakha, XY Lu, R Jagannathan, and DJ Dailey. 2016. Freeway speed harmonization. *IEEE Transactions on Intelligent Vehicles* 1(1): 78-89.
- McGuckin T, J Lambert, D Newton, A Pearmine, and E Hubbard. 2017. Leveraging the promise of connected and autonomous vehicles to improve integrated corridor management and operations: a primer. FHWA-HOP-17-001, Federal Highway Administration, U.S. Department of Transportation, Washington, DC, January 2017. <https://ops.fhwa.dot.gov/publications/fhwahop17001/fhwahop17001.pdf>
- Menneni S, C Sun, and P Vortisch. 2008. Microsimulation calibration using speed–flow relationships. *Transportation Research Record* 2088: 1–9.
- Messmer A, and M Papageorgiou. 1990. METANET: a macroscopic simulation program for motorway networks. *Traffic Engineering & Control* 31(9): 466 – 470.
- Milanés V, and SE Shladover. 2014. Modeling cooperative and autonomous adaptive cruise control dynamic responses using experimental data. *Transportation Research Part C* 48: 285 – 300.
- Milanés V, and SE Shladover. 2016. Handling cut-in vehicles in strings of cooperative adaptive cruise control vehicles. *Journal of Intelligent Transportation System* 20(2): 178 – 191.
- Milanés V, SE Shladover, J Spring, C Nowakowski, H Kawazoe, and M Nakamura. 2014. Cooperative adaptive cruise control in real traffic situations. *IEEE Transactions on Intelligent Transportation Systems* 15(1): 296 – 305.

Mirshahi M, J Obenberger, C Fuhs, C Howard, R Krammes, B Kuhn, R Mayhew, M Moore, K Sahebjam, and C Stone. 2007. Active traffic management: The next step in congestion management. FHWA-PL-07-012, U.S. Department of Transportation, Alexandria, VA, July 2007.

https://international.fhwa.dot.gov/pubs/pl07012/atm_eu07.pdf

Müller ER, RC Carlson, W Kraus, and M Papageorgiou. 2015. Microsimulation analysis of practical aspects of traffic control with variable speed limits. *IEEE Transactions on Intelligent Transportation Systems* 16(1): 512 – 522.

Muralidharan A, and R Horowitz. 2015. Computationally efficient model predictive control of freeway networks. *Transportation Research Part C* 8: 532-553.

Newell GF. 1993. A simplified theory of kinematic waves in highway traffic, part I: general theory. *Transportation Research Part B* 27(4): 281-287

Nissan A, and HN Koutsopoulos. 2011. Evaluation of the impact of advisory variable speed limits on motorway capacity and level of service. *Procedia Social and Behavioral Sciences* 16: 100-109.

Nissan A. 2013. Evaluation of recommended variable speed limits for motorway traffic control: the case of E4-Motorway in Stockholm. Presented at 92nd Annual Meeting of the Transportation Research Board, Washington, D.C.

Papageorgiou M, JM Blosseville, and H Hadj-Salem. 1989. Macroscopic modelling of traffic flow on the Boulevard Périphérique in Paris. *Transportation Research Part B* 23(1): 9-47.

Papageorgiou M and A Kotsialos. 2002. Freeway ramp metering: an overview. *IEEE Transactions on Intelligent Transportation Systems* 3(4): 271–280.

Papageorgiou M, E Kosmatopoulos, and I Papamichail. 2008. Effects of variable speed limits on motorway traffic flow. *Transportation Research Record* 2047: 37–48.

Park B, and H Qi. 2005. Development and evaluation of a procedure for the calibration of simulation models. *Transportation Research Record* 1934: 208–217.

Pasquale C, D Anghinolfi, S Sacone, S Siri, and M Papageorgiou. 2016. A comparative analysis of solution algorithms for nonlinear freeway traffic control problems. In *Proc. IEEE 19th Int. Conference Intell. Transp. Sys.*, Rio de Janeiro, Brazil: 1773-1778.

Pasquale C, S Sacone, and S Siri. 2014. Two-class emission traffic control for freeway systems. In *Proc. 19th World Congress Int. Fed. Autom. Control*, Cape Town, South Africa: 936-941.

Pasquale C, I Papamichail, C Roncoli, S Sacone, S Siri, and M Papageorgiou. 2015. Two-class freeway traffic regulation to reduce congestion and emissions via nonlinear optimal control. *Transportation Research Part C* 55: 85-99.

Pasquale C, S Sacone, S Siri, and B De Schutter. 2017. A multi-class model-based control scheme for reducing congestion and emissions in freeway networks by combining ramp metering and route guidance. *Transportation Research Part C* 80: 384 – 408.

Paz A, V Molano, E Martinez, C Gaviria, and C Arteaga. 2015. Calibration of traffic flow models using a memetic algorithm. *Transportation Research Part C* 55: 423 – 443.

Paz A, V Molano, and C Gaviria. 2012. Calibration of CORSIM models considering all model parameters simultaneously. 15th International IEEE Conference on Intelligent Transportation Systems Anchorage, Alaska, USA, September 16-19.

Popov A, A Hegyi, R Babusˇka, and H Werner. 2008. Distributed controller design approach to dynamic speed limit control against shockwaves on freeways. *Transportation Research Record* 2086: 93–99.

Radhakrishnan M, and CG Wilmot. 2009. Impact of left lane truck restriction strategies on multilane highways in Louisiana—a literature review. April 2009.
https://www.ltrc.lsu.edu/pdf/2009/tar_09_1ta.pdf

Roncoli C, M Papageorgiou, and I Papamichail. 2015a. Traffic flow optimization in presence of vehicle automation and communication systems – part I: a first-order multi-lane model for motorway traffic. *Transportation Research Part C* 57: 241 – 259.

Roncoli C, M Papageorgiou, and I Papamichail. 2015b. Traffic flow optimization in presence of vehicle automation and communication systems – part II: optimal control for multi-lane motorways. *Transportation Research Part C* 57: 260 – 275.

Sabawat V, and RK Young. 2013. Control strategy for rural variable speed limit corridor. *Transportation Research Record* 2329: 31–44.

Schreiter T, H van Lint, and S Hoogendoorn. 2011. Multi-class ramp metering: concepts and initial results. Proc. 14th Int. IEEE Conference Intell. Transp. Sys., Washington, DC, USA. Oct.: 885-889.

Shladover SE, J Lappin, RP Denaro, and BW Smith. 2013. Introduction: the transportation research board’s 2013 workshop on road vehicle automation. Stanford University, Calif., July 15–19, 2013.
https://link.springer.com/content/pdf/10.1007%2F978-3-319-05990-7_1.pdf

Shladover SE, D Su, and XY Lu. 2012. Impacts of cooperative adaptive cruise control on freeway traffic flow. *Transportation Research Record* 2324: 63-70.

Shiomi Y, T Yoshii, and R Kitamura. 2011. Platoon-based traffic flow model for estimating breakdown probability at single-lane expressway bottlenecks. *Transportation Research Part B* 45: 1314 – 1330.

Stephens D, T Timcho, T Smith, K Balke, H Charara, and S Sunkari. 2015. Technical report on prototype intelligent network flow optimization (INFLO) dynamic speed

harmonization and queue warning. FHWA-JPO-15-213, USDOT, Washington, D.C., June 19, 2015. https://ntl.bts.gov/lib/55000/55300/55304/100030614-601_Technical_Report_on_Prototype_Intelligent_Network_Flow_Optimization_Final_.pdf

Soriguera F, JM Torne, and D Rosas. 2013. Assessment of dynamic speed limit management on metropolitan freeways. *Journal of Intelligent Transportation Systems* 17(1): 78 – 90.

Talebpour A, HS Mahmassani, and SH Hamdar. 2013. Speed harmonization evaluation of effectiveness under congested conditions. *Transportation Research Record* 2391: 69–79.

Treiber M, A Hennecke, and D Helbing. 2000. Congested traffic states in empirical observations and microscopic simulations. *Phys. Rev. E*. 62: 1805-1824.

Transportation Research Board (TRB). 2015. Automated and connected vehicles. Summary of the 9th university of transportation centers spotlight conference, November 4-5, Washington, D.C. <http://onlinepubs.trb.org/onlinepubs/conf/CPW19.pdf>

TRB Research Needs Statements, 2003. <http://rns.trb.org/dproject.asp?n=15590>

Toledo T, ME Ben-Akiva, D Darda, M Jha, and HN Koutsopoulos. 2004. Calibration of microscopic traffic simulation models with aggregate data. *Transportation Research Record* 1876: 10–19.

U.S. Department of Transportation (USDOT). 2016. 2016 revised value of travel time guidance. Washington D.C. <https://cms.dot.gov/sites/dot.gov/files/docs/2016%20Revised%20Value%20of%20Travel%20Time%20Guidance.pdf>

van Lint JWC., SP Hoogendoorn, and M Schreuder. 2008. FASTLANE: new multiclass first-order traffic flow model. *Transportation Research Record* 2088: 177–187.

Wang M, SP Hoogendoorn, W Daamen, B van Arem, and R Happee. 2015. Game theoretic approach for predictive lane-changing and car-following control. *Transportation Research Part C* 58: 73-92.

Wang M, W Daamen, SP Hoogendoorn, and B van Arem. 2016. Connected variable speed limits control and car-following control with vehicle-infrastructure communication to resolve stop-and-go waves. *Journal of Intelligent Transportation Systems* 20(6): 559-572.

Weikl S, K Bogenberger, and RL Bertini. 2013. Traffic management effects of variable speed limit system on a german autobahn empirical assessment before and after system implementation. *Transportation Research Record* 2380: 48–60.

Wolshon B, S Ishark, Y Qi, M Korhut, X Sun, and C Alecsandru, 2009. Trucker

perceptions of lane restriction and differential speed limit policies on freeways. *Journal of Transportation Safety & Security* 1: 101-120.

Wong GCK, and SC Wong. 2002. A multi-class traffic flow model – an extension of LWR model with heterogeneous drivers. *Transportation Research Part A* 36: 827-841.

Yang H, and WL Jin. 2014. A control theoretic formulation of green driving strategies based on inter-vehicle communications. *Transportation Research Part C* 41: 48-60.

Yang X, Y Lu, and GL Chang. 2015. Exploratory analysis of an optimal variable speed control system for a recurrently congested freeway bottleneck. *Journal of Advanced Transportation* 49: 195 – 209.

Yang X, Y Lu, and Y Lin. 2017. Optimal variable speed limit control system for freeway work zone operations. *Journal of Computing in Civil Engineering* 31(1): 04016044.

Yu M, and W Fan. 2017. Calibration of microscopic traffic simulation models using metaheuristic algorithms. *International Journal of Transportation Science and Technology* 6: 63-77.

Yu M, and W Fan. 2018a. Tabu search strategies for variable speed limit control at a lane drop bottleneck. *Journal of Transportation Engineering, Part A: Systems* 144(7): 04018033.

Yu M, and W Fan. 2018b. Optimal variable speed limit control at a lane drop bottleneck: genetic algorithm approach. *Journal of Computing in Civil Engineering* 32(6): 04018049.

Zackor H. 1991. Speed limitation on freeways: traffic-responsive strategies. In: M. Papageorgiou, ed. *concise encyclopedia of traffic and transportation systems*. Oxford, UK: Pergamon Press: 507–511.

Zegeye SK, BD Schutter, H Hellendoorn, and E Breunese. 2009. Reduction of travel times and traffic emissions using model predictive control. *Proceeding on 2009 American Control Conference Hyatt Regency Riverfront, St. Louis, MO, USA June 10-12.*

Zhang Y, and PA Ioannou. 2017. Combined variable speed limit and lane change control for highway traffic. *IEEE Transactions on Intelligent Transportation Systems* 18(7): 1812 – 1823.